JOÃO MIGUEL MENDES DE ARAÚJO

OPTIMAL DESIGN AND OPERATION OF COMPACT SIMULATED MOVING BED PROCESSES FOR ENANTIOSEPARATIONS

Dissertação apresentada para obtenção do Grau de Doutor em Engenharia Química especialidade Simulação, Optimização e Controlo de Processos pela Universidade Nova de Lisboa, Faculdade de Ciências e Tecnologia

LISBOA

2009

Contraria sunt complementa.
Opposites are complementary.
— Niels Bohr —

Acknowledgements

Arriving at this point a lot could be acknowledged and remembered, it wasn't always nice and easy, but it was a great ride, I had lots of fun and learned a ton along the way. I just want to thank everybody who worked with me and supported me over this years.

First of all I would like to thank Prof. José Paulo Mota, who accepted me as a Ph.D. student in his research group and gave me the opportunity to embrace this extraordinary project and start-up the 'wonderful-world' of Simulated Moving-bed in his group. I am very grateful for the support, guidance, but also freedom he has given me during my research. I also thank him for always challenging me to reach higher goals within research.

The financial support from FCT/MCES (Portugal), through Ph.D. grant SFRH/BD/ 13721 /2003, is gratefully acknowledged.

It was a great pleasure for me to work with Prof. Mário Eusébio during these years. I truly acknowledge is contribution in the development of the process automation system.

Many thanks to my co-worker Rui Rodrigues, that join us during the 'SMB journey'. I am very happy with the work accomplished and pleasant discussions about scientific and nonscientific subjects.

I want also to thank all the nice people I met at FCT/UNL and at all the conferences that I had participated, who made this time very pleasant and joyful.

I must also thank Prof. Isabel Marrucho, the 'sponsor' of my return to *R&D*, for her support and concern during the writing of my thesis.

My sincere gratitude goes to my family, relatives and friends, for all the support, patient and encouragement. For filling my life and make possible every single step of it.

I can not conclude without express my respect and gratefulness toward the sea, I always reborn when riding its ravishing waves.

Ph.inaly **D**.one!!!

Sumário

A técnica cromatográfica de leito móvel simulado (LMS) tem atraído uma atenção crescente devido a sua elevada capacidade para tarefas de separação complexas. Na actualidade, mais de 60% das unidades preparativas de LMS encontram-se instaladas na indústria alimentar e farmacêutica (SDI, *Preparative and Process Liquid Chromatography: The Future of Process Separations, International Strategic Directions, Los Angeles, USA*, 2002. `http://www.strategicdirections.com`). A cromatografia é o método de eleição nestas áreas, uma vez que os produtos farmacêuticos e de química-fina possuem propriedades fisico-químicas que diferem pouca das dos co-produtos, e podem ser termicamente instáveis. Nestes casos, as técnicas de separação standard como a destilação e extracção, não são aplicáveis. A relevância da cromatográfia preparativa, em particular o LMS, como processo de purificação e separação nas indústrias acima mencionadas tem vindo aumentar, devido a sua flexibilidade, eficiência energética e elevada performance relativaemnte a pureza dos produtos.

Consequentemente, um novo paradigma do LMS é necessário devido ao elevado número de aplicações de pequena-escala da tecnologia LMS, que exploram a flexibilidade e versatilidade desta tecnologia. Neste novo paradigma do LMS, inúmeras possibilidades para melhorar a performance do LMS que advêm da variação de parâmetros durante o intervalo de comutação, estão a favorecer a tendência para o uso de unidades com um menor número de colunas, porque uma menor quantidade de fase estacionária é utilizada e consequentemente o *setup* é mais económico. Esta situação é particularmente importante na indústria farmacêutica, onde os LMSs são vistos como uidades multi-tarefas que podem ser aplicadas em diferentes separações em todos os estágios do ciclo de desenvolvimento de formulações farmacêuticas.

De modo a reduzir-se o esforço experimental e consequentemente o custo financeiro associado ao desenvolvimento de processos de separação, modelos de simulação são intensivamente utilizados. Um aspecto importante neste contexto, refere-se a determinação das isotérmicas de adsorção em cromarográfia de LMS. Na qual as separações são usualmente conduzidas em condições fortemente não-lineares, de modo a alcançar produtividades mais elevadas. Um aspecto de fundamental importância para permitir optimizações assistidas-computacionalmente e *scale-up* do processo, é a meticulosa determinação do equilíbrio competitivo de adsorção das espécies enantioméricas.

À escala produtiva o LMS apresenta dois problemas operativos relevantes: a avaliação da qualidade do produto e a manutenção de uma operação estável a longo-termo e controlável. Restrições relativamente a pureza dos produtos, prescritas por entidades reguladoras das actividades farmacêuticas e alimentares, aumentaram drasticamente o controlo de qualidade do produto. A imposição de regulamentação exigente, aumentou a necessidade de desenvolver formulações farmacêuticas opticamente puras. Por isso, a correcta implementação de LMSs implica a aplicação de técnicas robustas de controlo. Estes factores colocam questões fundamentais e desafios tanto a tecnologia LMS como a teoria de controlo.

O objectivo do presente trabalho é o alargamento do conceito de LMS e desenvolvimento de esquemas LMS compactos, que funcionem como uma ponte entre a cromatografia de LMS e a cromatografia descontínua tradicional, na tentativa de trabalhar com o melhor dos 'dois mundos'. Neste contexto dois novos paradigmas de LMS foram concebidos, i.e. o processo LMS de coluna singular com atraso no reciclo (*single-column SMB analog*) e o processo LMS compacto de duas-colunas (*streamlined two-column SMB process*). Além disso, um procedimento geral para a determinação de isotérmicas de adsorção foi desenvolvido e validado, no qual o método inverso é aplicado directamente ao perfil de concentrações do estado estacionário cíclico (EEC) de um processo de LMS para actualizar os parâmetros da isotérmica de adsorção, estimados pela aplicação do método inverso a perfis obtidos no modo de eluição não-linear da mistura racémica. De modo a fornecer uma ferramenta para implementar um controlo do processo apropriado e uma optimização dinâmica do LMS, foi desenvolvido e testado um sistema *on-line* automatizado de análise enantiomérica constituido por um *set-up* HPLC analítico acoplado a dois detectores de UV. As novidades técnicas acima mencionadas são exploradas nas páginas seguintes.

Abstract

Simulated moving bed (SMB) chromatography is attracting more and more attention since it is a powerful technique for complex separation tasks. Nowadays, more than 60% of preparative SMB units are installed in the pharmaceutical and in the food industry [SDI, Preparative and Process Liquid Chromatography: The Future of Process Separations, International Strategic Directions, Los Angeles, USA, 2002. `http://www.strategicdirections.com`]. Chromatography is the method of choice in these fields, because often pharmaceuticals and fine-chemicals have physico-chemical properties which differ little from those of the by-products, and they may be thermally instable. In these cases, standard separation techniques as distillation and extraction are not applicable.

The noteworthiness of preparative chromatography, particulary SMB process, as a separation and purification process in the above mentioned industries has been increasing, due to its flexibility, energy efficiency and higher product purity performance.

Consequently, a new SMB paradigm is requested by the large number of potential small-scale applications of the SMB technology, which exploits the flexibility and versatility of the technology. In this new SMB paradigm, a number of possibilities for improving SMB performance through variation of parameters during a switching interval, are pushing the trend toward the use of units with smaller number of columns because less stationary phase is used and the setup is more economical. This is especially important for the pharmaceutical industry, where SMBs are seen as multipurpose units that can be applied to different separations in all stages of the drug-development cycle.

In order to reduce the experimental effort and accordingly the coast associated with the development of separation processes, simulation models are intensively used. One important aspect in this context refers to the determination of the adsorption isotherms in SMB chromatography, where separations are usually carried out under strongly nonlinear conditions in order to achieve higher productivities. The accurate determination of the competitive adsorption equilibrium of the enantiomeric species is thus of fundamental importance to allow computer-assisted optimization or process scale-up.

Two major SMB operating problems are apparent at production scale: the assessment of product quality and the maintenance of long-term stable and controlled operation. Constraints regarding product purity, dictated by pharmaceutical and food regulatory organizations, have drastically increased the demand for product quality control. The strict imposed regulations are increasing the need for developing optically pure drugs.

Therefore, proper implementation of SMBs in production will require the application of robust control techniques. These features pose fundamental questions and challenges on both SMB technology and control theory.

The aim of this work is to broaden the SMB concept and develop compact SMB schemes, bridging SMB chromatography and batch processes in an attempt to work with the best of 'two worlds'. In this context two new SMB paradigms have been accomplished, i.e. the single-column SMB process with recycle-lag (single-column SMB analog) and the streamlined two-column SMB for chiral separations (two-column open-loop SMB process). Moreover, a general procedure for the determination of the adsorption isotherms has been developed and validated in which the inverse method is applied directly to the cyclic steady-state (CSS) concentration profiles of the running SMB process to update the parameters of the prescribed adsorption isotherm model, estimated by applying the inverse method to the overloaded band profiles of the racemic mixture. To provide a tool to implement a properly process control and dynamic optimization of the SMB, an automated on-line enantiomeric analysis system comprising an analytical HPLC set-up with two UV detectors has been developed and tested. The technical novelties above mentioned are explored in the following pages.

List of Papers

The groundwork of this thesis are the following papers, which are referred to in the text by their Roman numerals I – VII.

I **Single-column simulated-moving-bed process with recycle lag**.
José P.B. Mota, João M.M. Araújo. AIChE J, 51 (2005), 1641-1653.

II **Use of single-column models for efficient computation of the periodic state of a simulated moving-bed process**.
João M.M. Araújo, Rui C.R. Rodrigues, José P.B. Mota. Ind. Eng. Chem. Res., 45 (2006), 5314-5325.

III **Optimal design and operation of a certain class of asynchronous simulated moving bed processes**.
João M.M. Araújo, Rui C.R. Rodrigues, José P.B. Mota. J. Chromatgr. A, 1132 (2006), 76-89.

IV **Single-column simulated-moving bed process with recycle lag: analysis and applications**.
João M.M. Araújo, Rui C.R. Rodrigues, José P.B. Mota. Ads. Sci. Tech., 25 (2007), 647-659.

V **On-line enantiomeric analysis using high-performance liquid chromatography in chiral separation by simulated moving bed**.
João M.M. Araújo, Rui C.R. Rodrigues, Mário F.J. Eusébio, José P.B. Mota. J. Chromatgr. A (2008), 1189, 292-301.

VI **Determination of competitive isotherms of enantiomers by a hybrid inverse method using overloaded band profiles and the periodic state of the simulated moving-bed process**.
João M.M. Araújo, Rui C.R. Rodrigues, José P.B. Mota. J. Chromatgr. A (2008), 1189, 302-313.

VII **Chiral separation by compact two-column, open-loop simulated moving-bed chromatography**.
João M.M. Araújo, Rui C.R. Rodrigues, Mário F.J. Eusébio, José P.B. Mota. J. Chromatogr. A (submitted for publication).

Papers not included in this Thesis

i **Experimental assessment of simulated moving bed and varicol processes using a single-column setup**.
Rui C.R. Rodrigues, João M.M. Araújo, Mário F.J. Eusébio, José P.B. Mota. J. Chromatgr. A (2007), 1142, 69-80.

ii **Optimal design and experimental validation of synchronous, asynchronous and flow-modulated, simulated moving-bed processes using a single-column setup**.
Rui C.R. Rodrigues, João M.M. Araújo, José P.B. Mota. J. Chromatgr. A (2007), 1162, 14-23.

iii **Optimal design of simulated moving-bed processes under flow-rate uncertainty**.
José P.B. Mota, João M.M. Araújo, Rui C. R. Rodrigues. AIChE J. (2007), 53, 2630-2642.

iv **Two-column simulated moving-bed process for binary separation**.
Rui C.R. Rodrigues, Tiago J. S. B. Canhoto, João M.M. Araújo and José P.B. Mota. J. Chromatgr. A (2008), 1180, 42-52.

Table of Contents

Optimal Design and Operation of Compact Simulated Moving Bed Processes for Enantioseparations

Contents

Chapter 1

Single-column Simulated Moving-Bed Process with Recycle Lag

Contents

Chapter 2

Use of Single-column Models for Efficient Computation of the Periodic State of Simulated Moving-Bed Process

Contents

Chapter 3

Optimal Design and Operation of a Certain Class of Asynchronous Simulated Moving-Bed Processes

Contents

Chapter 4

Determination of Competitive Isotherms of Enantiomers by a Hybrid Inverse Method using Overloaded Band Profiles and the Periodic State of the Simulated Moving-Bed Process

Contents

Chapter 5

On-line Enantiomeric Analysis using High-Performance Liquid Chromatography in Chiral Separation by Simulated Moving-Bed

Contents

Chapter 6

Chiral Separation by Compact Two-column, Open-loop Simulated Moving-Bed Chromatography

Contents

Introduction

The trend of purer products and cleaner processes in the agrochemical, biotechnological, food and pharmaceutical industries, due to tight regulations and growing environment concerns, is summoning for fitter separation process technologies. The noteworthiness of preparative chromatography, particulary the Simulated Moving Bed (SMB) process, as a separation and purification process in the above mentioned industries has been increasing, due to its flexibility, energy efficiency and higher product purity performance. Nowadays, the SMB is considered a real production tool in these industries, such as the separation of optical isomers, and it is considered appealing for complex separation tasks, such as separations in the biotechnology industries or multi-separations tasks involving a number of difficult-to-characterize natural compounds.

Consequently, a new SMB paradigm is requested by the large number of potential small-scale applications of the SMB technology, which exploits the flexibility and versatility of the technology. In this new SMB paradigm, a number of possibilities for improving SMB performance through variation of parameters during a switching interval, are pushing the trend toward the use of units with smaller number of columns because less stationary phase is used and the setup is more economical. This is especially important for the pharmaceutical industry, where SMBs are seen as multipurpose units that can be applied to different separations in all stages of the drug-development cycle.

In order to reduce the experimental effort and accordingly the coast associated with the development of separation processes, simulation models are intensively used. One important aspect in this context refers to the determination of the adsorption isotherms in SMB chromatography. In order to achieve higher productivities, enantiomeric separations by SMB chromatography are usually carried out under strongly nonlinear conditions. The accurate determination of the competitive adsorption equilibrium of the enantiomeric species is thus of fundamental importance to allow computer-assisted optimization or process scale-up. This is especially true for the SMB, because its operating conditions cannot be designed conveniently without knowledge of the adsorption isotherms of the feed components.

Two major SMB operating problems are apparent at production scale: the assessment of product quality and the maintenance of long-term stable and controlled operation. Constraints regarding product purity, dictated by pharmaceutical and food regulatory organizations, have drastically increased the demand for product quality control.

The strict imposed regulations are increasing the need for developing optically pure drugs. Therefore, proper implementation of SMBs in production will require the application of robust control techniques. These features pose fundamental questions and challenges on both SMB technology and control theory.

The aim of this work is to broaden the SMB concept and develop compact SMB schemes, bridging SMB and batch chromatography in an attempt to work with the best of 'two worlds':

i SMB chromatography is a powerful tool for chiral separation, because of its many advantages with respect to discontinuous batch chromatography, namely higher product purity, less solvent consumption, and higher productivity per unit stationary phase. Newly developed cyclic operating schemes and column configurations are pushing the trend toward the use of units with fewer columns and more economical set-ups;

ii batch processes, despite the lower productivity and higher solvent consumption, are advantageous in other respects, such as in their simplicity (less design effort is necessary and the scale-up is easier), flexibility (changes in conditions can be easily handled), and versatility (multi- and center-cut separations from multi-component mixtures are easy to implement).

In this context two new SMB paradigms have been accomplished, i.e. the single-column SMB process with recycle-lag (single-column SMB analog) and the streamlined two-column SMB for chiral separations (two-column open-loop SMB process). Moreover, a general procedure for the determination of the adsorption isotherms has been developed and validated in which the inverse method is applied directly to the cyclic steady-state (CSS) concentration profiles of the running SMB process to update the parameters of the prescribed adsorption isotherm model, estimated by applying the inverse method to the overloaded band profiles of the racemic mixture. To provide a tool to implement a properly process control and dynamic optimization of the SMB, an automated on-line enantiomeric analysis system comprising an analytical HPLC set-up with two UV detectors has been developed and tested. The technical novelties above mentioned and explored in this work are outlined below:

♦ In the single-column SMB analog (**paper I**) the periodic state of the simulated-moving-bed (SMB) process is reproduced by a single-column chromatographic process with a recycle lag of $(N-1)\tau$ time units, where N is the number of columns of the equivalent SMB unit and τ is the switching time. The operation of this ideal single-column process is formulated by selecting an arbitrary column of the SMB and following its operation over a complete cycle. To implement the recycle lag in practice, a special type of plug-flow tube has been designed. It includes internal elements to make the flow as close as possible to plug flow, and a piston to compensate for the difference between the inlet and outlet flow rates. This is necessary because the recycle lag is not a multiple of the overall cycle duration. The proposed system is a more compact, less expensive and simpler-to-operate alternative to the SMB. It avoids the problem of packing reproducibility and the total pressure drop is $1/N$th of that of the equivalent SMB. Depending on the efficiency of the recycle tube, our single-column process can achieve the same purities as the analogous SMB unit while keeping the specific productivity constant.
We report some conceptual and numerical results for a single-column chromatograph analogous to an SMB with asynchronous port switching (**paper IV**). It is shown that the requirement of recycling the outlet stream that is not recovered as product back to the column with a lag of $(N-1)\tau$ time units to reproduced the periodic state of the multi-column unit by the one-column chromatograph, holds true regardless of the port configuration, or operating scheme, of the analogous multi-column unit. By upgrading the operation of the single-column chromatograph from the classical synchronous port switching to an optimized asynchronous Varicol mode, it is shown that one can easily compensate for a less perfect operation of the recycle tube.

♦ A mathematical framework for developing efficient methods to calculate the cyclic steady state (CSS) of the simulated moving-bed (SMB) process is established based on single-column models (**paper II**). The formulation and methods presented are equally applicable to recently developed SMB enhancements that vary some of the operating parameters over a switching interval. These include, among others, Varicol, PowerFeed, ModiCon and modulation of solvent strength during process operation. The solution methods can be classified into two major classes: dynamic methods which integrate in time, either truly or artificially, the governing equations over a large number of cycles until CSS is reached, and methods which rely on the direct prediction of the CSS by simultane-

ously discretizing the spatial and temporal coordinates. The performance of each solution method is measured in terms of CPU time, number of cycles to attain CSS, and CPU time per cycle. The various methods are compared for the separation of two binary mixtures that are sufficiently different, in isotherm model and selected operating parameters, for their overall analysis to provide conclusions of general applicability.

♦ In **paper III** a compact representation of the cyclic operation of simulated moving-bed chromatography is established from the governing equations for the analogous single-column model that reproduces the cyclic steady-state (CSS) behavior of the multi-column process. A broad class of physically realizable asynchronous processes is then derived by dropping the integrality condition on the number of columns per zone, which now represents the average over a cycle. The steady periodic solution of the multi-column unit is computed by solving the analogous single-column model using a full-discretization method. The nonlinear algebraic system resulting from the simultaneous discretization of both spatial and temporal coordinates is solved using the gPROMS software. This solution strategy leads to shorter computational times than those previously reported in the literature. Process optimization is handled using single objective functions, to avoid competing effects, which are explicitly constrained by product quality and maximum allowable internal flow rates. The process is optimized for maximum feed throughput, with a possible upper bound on eluent consumption or flow rate, or minimum eluent consumption for a given feed flow rate. The nonlinear programming problem is solved by an external solver while still carrying out the CSS calculations in gPROMS. The feasibility of the approach is demonstrated on the chromatographic separation of an enantiomeric mixture with nonlinear competitive isotherm. Emphasis is given to the benefits that can be gained by upgrading an existing system to asynchronous operation. It is shown that eluent consumption for optimized asynchronous configurations in the higher feed-throughput region can be significantly reduced by modulation of eluent flow rate and selective product withdrawal.

♦ A procedure for determination of adsorption isotherms in simulated moving-bed (SMB) chromatography is presented in **paper VI**. The parameters of a prescribed adsorption isotherm model and rate constants are derived using a hybrid inverse method, which incorporates overloaded band profiles of the racemic mixture and breakthrough

data from a single frontal experiment. The latter are included to reduce the uncertainty on the estimated saturation capacity, due to the dilution of the chromatograms with respect to the injected concentrations. The adsorption isotherm model is coupled with an axially-dispersed flow model with finite mass-transfer rate to describe the experimental band profiles. The numerical constants of the isotherm model are tuned so that the calculated and measured band profiles match as much as possible. The accuracy of the isotherm model is then checked against the cyclic steady state (CSS) of the target SMB process, which is readily and cheaply obtained experimentally on a single-column set-up. This experiment is as expensive and time consuming as just a few breakthrough experiments. If necessary, the isotherm parameters are adjusted by applying the inverse method to the experimental CSS concentration profile. The method is successfully applied to determine the adsorption isotherms of Trögers base enantiomers on Chiralpak AD/methanol system. The results indicate that the proposed inverse method offers a reliable and quick approach to determine the competitive adsorption isotherms for a specific SMB separation.

♦ An automated on-line enantiomeric analysis system comprising an analytical HPLC set-up with two UV detectors sharing the same light source has been employed to monitor the internal composition profile in chiral simulated moving bed chromatography (**paper V**). This monitoring scheme does not use a polarimeter. Using a sampling interface placed between two SMB columns, effluent samples are directed onto a high-efficiency analytical column at a sampling rate faster than the overall dynamics of the preparative unit to achieve on-line enantiomeric analysis of the composition profile. The other UV detector is placed in the SMB loop before the fraction collector to provide instantaneous measurement of the total enantiomeric concentration. The feasibility and effectiveness of the on-line enantimeric monitoring scheme were assessed experimentally on the separation of Tröger's base racemate, using Chiralpak AD as stationary phase and methanol as eluent. It was found that robust monitoring of the concentration profiles of the individual enantiomers is best achieved when the enantiomeric purity obtained from the peak areas of the on-line enantiomer analysis chromatograms is combined with the on-line UV measurement of total enantiomeric concentration. The accuracy and robustness of the proposed on-line enantiomeric monitoring system open up promising perspectives for process control and dynamic optimization of the SMB.

♦ Somewhere in between the SMB and batch chromatography, and in an attempt to work with the best of 'two worlds', a compact two-column open-loop SMB process for enantiomeric separation was designed, which is particularly effective when the resolution is limited (**paper VII**). The chiral separation considered in this work is the separation of reboxetine enantiomers on Chiralpak AD, using a mixture of Hexane-Ethanol-DEA as solvent, for both linear and nonlinear isotherms. This system is one in which there is clearly a lack of resolution between the two components. It is thus difficult to obtain both products with high purity and yield by HPLC for the chosen chromatographic conditions. Reboxetine, (*RS*)-2-[(*RS*)-(2-ethoxyphenoxy)benzyl]-morpholine is an antidepressive NRI drug. Only the (*R,R*)-, (*S,S*)-pair is present as a racemic mixture in the active principle and the commercial formulations. Pharmacological tests have shown that the enantiomers have different pharmacological efficacy; the (*S,S*)-enantiomer is more potent as antidepressant and is responsible for the vasomotor and cardiac side effects of reboxetine.

Chapter 1

Single-column Simulated Moving-Bed Process with Recycle Lag

1 Classical synchronous operation

1.1 Introduction

Simulated-moving-bed (SMB) chromatography has been increasingly applied for the separation of pure substances in the pharmaceutical, fine chemistry, and biotechnology industries, at all production scales, from laboratory to pilot to production scale [1]. The SMB has many advantages with respect to discontinuous batch chromatography [2], such as higher product purity, less solvent consumption, and higher productivity per unit stationary phase [3–5].

Thanks to recent developments in cyclic operation policies, a number of possibilities for improving SMB performance have emerged through variation of parameters during a switching interval. These include, among others, the non-synchronous shift of the inlet and outlet ports within a global switching period [6], modulation of solvent strength during process operation [8], and cyclic modulation of feed flow [9, 10] and feed concentration [11]. These advances are pushing the trend towards the use of units with smaller number of columns [12–14], since less stationary phase is used and the setup is more economic [15].

In many cases it would be advantageous to work with the limiting case of a single column. Because only one column would have to be repacked, switching from one mixture to another would be easier and take less time than with an SMB. This is especially important for the pharmaceutical industry, where SMBs are seen as multipurpose units that can be applied to different separations in all stages of the drug-development cycle [1].

In this line of work, Abunasser et al.[16] have recently developed a one-column chromatographic process with recycle analogous to a four-section SMB, which they termed 'the analog.' The analog has one chromatographic column connected to a number of tanks equal to the number of steps of the SMB cycle. These allow for recycling in a manner that mimics SMB operation. The analog and corresponding SMB were analyzed for the separation of dextran T6–fructose and dextran T6–raffinose mixtures and for the separation of binaphthol enantiomers. Because of mixing in the tanks, lower purities are obtained with the analog than with the SMB for the same productivity and eluent-to-feed, $Q_{\mathrm{E}}/Q_{\mathrm{F}}$, values. The purities can be increased either by dividing the tanks into several smaller ones or by increasing the $Q_{\mathrm{E}}/Q_{\mathrm{F}}$ value.

In a subsequent work [17] both start-up and shut-down analyzes were performed for the analog, which are particularly useful in short campaigns. The authors concluded that correct start-up conditions can reduce the time needed to reach steady-state by fifty percent. Several strategies were suggested to reduce the time and amount of eluent used during shut-down. The concept of the one-column analog was also successfully applied to various three-zone SMB configurations and to the VARICOL process [6].

Inspired by the work of these authors we have developed a novel single-column SMB analog that employs a special type of plug-flow device to implement the appropriate recycle pattern for the process to mimic the corresponding SMB [7] (**paper I**). We first derive the necessary conditions for a single-column chromatographic process to reproduce the periodic state of the SMB. This analysis leads to the concept of an *ideal* single-column analog, i.e. a process which theoretically is indistinguishable from the equivalent SMB, except for the discontinuous use of the inlet/oulet lines. We then discuss how this process can be implemented in practice. Using an enantiomeric separation as a case study, the efficiency of our process is compared with that of the target SMB. For reference, the comparison is also extended to the analog developed by Wankat and coworkers [16, 17]. We show that, depending on the efficiency of the recycle tube, our single-column process can achieve the same purities as the analogous SMB unit while keeping the specific productivity constant.

For brevity of presentation, a single case of enantiomeric separation is analyzed in this study. The conclusions, however, are of general applicability. The selected case study is the separation of binaphthol enantiomers [18], carried out using cellulose triacetate as stationary phase and heptane-isopropanol (72:28) as eluent [19, 20]. The adsorption equilibrium is well-described by a bi-Langmuir competitive isotherm model. The operating conditions and model parameters for this chromatographic separation using SMB are listed in Table 1. The operating parameters have been optimized by Pais et al.[18] and provide a reasonably good separation.

Table 1: Operating conditions and model parameters for the separation of binaphthol enantiomers by SMB chromatography on cellulose triacetate using heptane-isopropanol (72:28) as eluent [18].

Adsorption equilibrium isotherms $(q_{\mathrm{A}}^*, q_{\mathrm{B}}^*) = \frac{(2.69c_{\mathrm{A}}, 3.73c_{\mathrm{B}})}{1 + 0.0336c_{\mathrm{A}} + 0.0466c_{\mathrm{B}}} + \frac{(0.1c_{\mathrm{A}}, 0.3c_{\mathrm{B}})}{1 + c_{\mathrm{A}} + 3c_{\mathrm{B}}}$			
Feed flow rate	$Q_{\mathrm{F}} = 3.64$ mL/min	Porosity ratio	$\phi = 1.5$
Eluent flow rate	$Q_{\mathrm{E}} = 21.45$ mL/min	Column diameter	$d = 2.6$ cm
Raffinate flow rate	$Q_{\mathrm{R}} = 7.11$ mL/min	Péclet number	$\widetilde{\mathrm{Pe}} = v_j L_j / D = 2000$
Extract flow rate	$Q_{\mathrm{X}} = 17.98$ mL/min	LDF coefficients	$k_i = (0.1, 0.1)$ s^{-1}
Recycle flow rate	$Q = 35.38$ mL/min	Feed concentration	$c_i^{\mathrm{F}} = (2.9, 2.9)$ g/L
Zone length	$L_j N/4 = 21.0$ cm	Cycle duration	$N\tau = 24$ min

1.2 Theoretical basis for the single-column SMB analog

First a review of the mathematical basis of the SMB process is presented, since it is a prerequisite for the development and understanding of their single-column analogous processes. Only those aspects that are relevant to the present work are discussed here. More details can be found elsewhere [21, 22].

The classical SMB unit consists of N identical chromatographic columns which are interconnected circularly. By moving the input and withdrawal ports one column ahead (i.e. in the direction of fluid flow) at fixed time intervals, the counter-current contact between the adsorbent and liquid is simulated. The working principle of the SMB is illustrated in Figure 1. At each instant the active ports divide the columns into four sections, each playing a specific role in the separation. The binary mixture to be separated is fed between sections II and III, where the two components are separated. The more-retained species A and the less-retained species B are collected in the extract and raffinate streams, respectively. A desorbent or eluent is fed to section I to regenerate the solid before recycling and the fluid phase is regenerated in turn in section IV.

Assuming that the isothermal operation of the chromatographic columns can be adequately described by an axially dispersed flow model with finite mass-transfer rate described by a linear driving force (LDF) approximation. Although these assumptions are not strictly necessary for the discussion that follows, they provide a reasonable good description of a chromatographic column and were assumed to hold for the simulation results

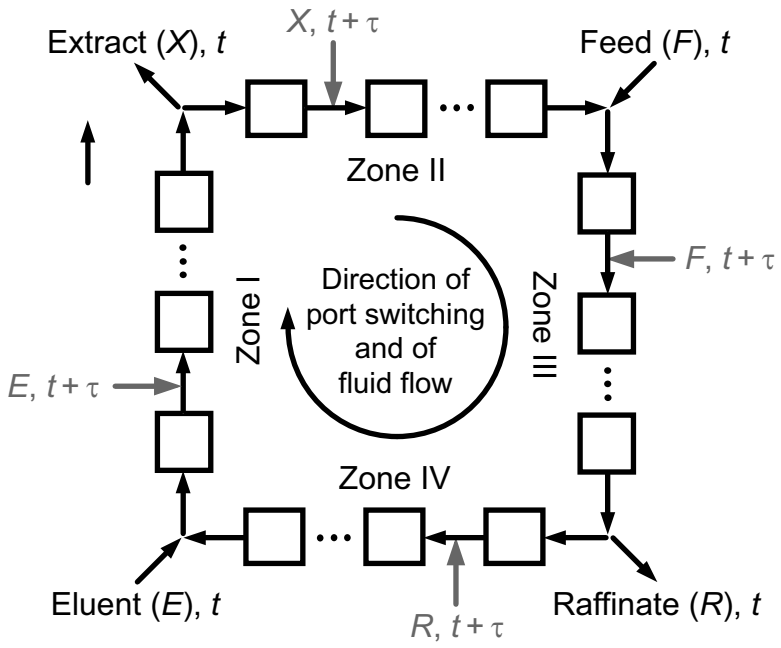

Figure 1: Scheme of the simulated moving bed process. Several chromatographic columns are connected in a loop, the input and withdrawal ports are moved one column ahead every τ time units. The feed, eluent, extract and raffinate streams are denoted by F, E, X and R, respectively.

reported in this work. They are standard practice in SMB modeling [23].

The solute material balance in a differential volume of column j ($j = 1, \ldots, N$) can be written as

$$\frac{\partial c_{ij}}{\partial t} + \phi \frac{\partial q_{ij}}{\partial t} = D_{ij} \frac{\partial^2 c_{ij}}{\partial z^2} - v_j \frac{\partial c_{ij}}{\partial z} \quad (0 < z < L), \tag{1}$$

where $i = \mathrm{A}, \mathrm{B}$ identifies the species in the mixture, $\phi = (1 - \epsilon)/\epsilon$, ϵ is the bed porosity, L is the column length, c is the liquid-phase concentration, q is the adsorbed-phase concentration, v is the interstitial liquid velocity, and D is the axial dispersion coefficient.

The approximation of the adsorption rate by the LDF model leads to

$$\frac{\partial q_{ij}}{\partial t} = k_i (q_{ij}^* - q_{ij}), \quad q_{ij}^* \equiv q_i^*(c_{\mathrm{A}j}, c_{\mathrm{B}j}) \quad (0 \le z \le L), \tag{2}$$

where k_i is the LDF coefficient and $q_i^*(c_\mathrm{A}, c_\mathrm{B})$ is the adsorption isotherm of component i, which relates its equilibrium concentration in the adsorbed phase, q_i^*, with the solute concentrations, c_A and c_B, in the bulk fluid.

Equation 1 is subjected to the following boundary conditions:

$$c_{ij} - \frac{D_{ij}}{v_j} \frac{\partial c_{ij}}{\partial z} = c_{ij}^{\mathrm{in}} \quad \text{for} \quad z = 0, \tag{3}$$

$$\frac{\partial c_{ij}}{\partial z} = 0 \quad \text{for} \quad z = L, \tag{4}$$

where c_{ij}^{in} is the concentration of solute i at the inlet of the jth column. This concentration is determined by the solute material balance at the node between columns $j-1$ and j, which can be expressed as

$$c_{ij}^{\text{in}} = \alpha_j \, c_{i,j-1}^{\text{out}} + (1-\alpha_j) \, c_{ij}^{\text{ex}}, \quad \alpha_j = \frac{\min\{v_{j-1}, v_j\}}{v_j}, \tag{5}$$

where $c_{i,j-1}^{\text{out}}$ is a shorthand for the concentration $c_{i,j-1}(L,t)$ at the outlet of column $j-1$ and c_{ij}^{ex} is the concentration of an external inlet stream (either eluent or feed), if the corresponding port is opened. The nodes can be classified according to the sign of $v_j - v_{j-1}$:

- Connecting node: $v_j = v_{j-1}$ ($\alpha_j = 1$);
- Eluent node: $v_j > v_{j-1}$ ($\alpha_j = v_{j-1}/v_j$), $c_{ij}^{\text{ex}} = 0$;
- Feed node: $v_j > v_{j-1}$ ($\alpha_j = v_{j-1}/v_j$), $c_{ij}^{\text{ex}} = c_i^{\text{F}}$, where c_i^{F} is the feed concentration;
- Extract and raffinate nodes: $v_j < v_{j-1}$ ($\alpha_j = 1$).

Notice that if the feed and eluent ports between columns $j-1$ and j are closed, i.e. $v_j \leq v_{j-1}$, Eq. 37 correctly ignores the value of c_{ij}^{ex} because $\alpha_j = 1$, this eliminates the second term on the right hand side of the equation.

The cyclic operation of an SMB with port configuration NI/NII/NIII/NIV ($N = \sum_{k=\text{I}}^{\text{IV}} N_k$), i.e. NI columns in section I, NII columns in section II etc., is defined by imposing the following time-periodic conditions on v_j and c_{ij}^{ex}:

$$v_j(t) = \begin{cases} v_{\text{I}} & 0 \leq n_j < N\text{I} \\ v_{\text{IV}} & N\text{I} \leq n_j < N\text{I} + N\text{IV} \\ v_{\text{III}} & N\text{I} + N\text{IV} \leq n_j < N - N\text{II} \\ v_{\text{II}} & N - N\text{II} \leq n_j < N \end{cases}, \tag{6}$$

$$c_{ij}^{\text{ex}}(t) = \begin{cases} c_i^{\text{E}} & N\text{I} - 1 \leq n_j < N\text{I} \\ c_i^{\text{F}} & N - N\text{II} - 1 \leq n_j < N - N\text{II} \\ 0 & \text{otherwise} \end{cases}. \tag{7}$$

Here, τ is the switching time (i.e. the time span between the switching of port locations), n_j is defined as

$$n_j = [\, t/\tau + (N+1-j) \,] \bmod N, \quad a \bmod b \equiv a - b \,\text{int}(a/b), \tag{8}$$

and $v_{\mathrm{I}}, \ldots, v_{\mathrm{IV}}$ are the interstitial velocities in each of the four sections. These obey the global node balances

$$v_{\mathrm{I}} = v_{\mathrm{IV}} + Q_{\mathrm{E}}/(A\epsilon), \tag{9}$$

$$v_{\mathrm{II}} = v_{\mathrm{I}} - Q_{\mathrm{X}}/(A\epsilon), \tag{10}$$

$$v_{\mathrm{III}} = v_{\mathrm{II}} + Q_{\mathrm{F}}/(A\epsilon), \tag{11}$$

$$v_{\mathrm{IV}} = v_{\mathrm{III}} - Q_{\mathrm{R}}/(A\epsilon), \tag{12}$$

where A is the cross-sectional area of the columns and the Q's are the inlet/outlet flowrates: eluent (Q_{E}), extract (Q_{X}), feed (Q_{F}), and raffinate (Q_{R}). Since the system has N columns, the duration of the overall cycle, i.e. the time required for each inlet/outlet line to recover its initial position, is $N\tau$.

If the inputs $v_j(t)$ and $c_{ij}^{\mathrm{ex}}(t)$ are constant or time-periodic of period τ, the process converges asymptotically towards a cyclic steady-state (CSS) regime. The definition of the CSS regime depends on the frame of reference. If the observer is stationary, each column is identified according to its fixed position within the unit (or its index number j). In this case, the CSS condition is

$$c_{ij}(z, t + N\tau) = c_{ij}(z, t), \quad q_{ij}(z, t + N\tau) = q_{ij}(z, t) \quad (0 \leq z \leq L), \tag{13}$$

which states that the spatially-distributed concentration profiles at the beginning and at the end of the cycle must be identical.

If the frame of reference moves with the inlet/outlet lines, the CSS condition can be expressed as

$$c_{i,j+1}(z, t + \tau) = c_{ij}(z, t), \quad q_{i,j+1}(z, t + \tau) = q_{ij}(z, t) \quad (0 \leq z \leq L). \tag{14}$$

Equation 14 provides an alternative definition of the CSS for a standard SMB process: the spatially-distributed concentration profiles at the start and at the end of a switching period are identical, apart from a shift of exactly on column. Equation 14 is the basis for a method of directly calculating the CSS regime [24].

The mathematical basis of the SMB process reviewed above establishes the theoretical framework for developing an analogous single-column chromatographic system. At first glance this seems to be a non-trivial exercise. The solution, however, is rather simple as is shown next.

It is convenient to first tackle the problem from a theoretical standpoint and then to discuss how the process model can be realized experimentally. Notice that the former task

requires the development of a mathematical formulation to simulate the behavior of the SMB process using the governing equations of a single chromatographic column. The key to achieve this is noticing that the only equation that references more than one column simultaneously is the solute node balance given by Eq. 37, which besides column j also references column $j-1$. For a single-column process the references to '$j-1$' must be removed from that equation. This is achieved by resorting to the CSS conditions. Looking into past process time we can write

$$\underset{\text{'from Eq. (13)'}}{c_{i,j-1}^{\text{out}}(t)} \;=\; \underset{}{c_{i,j-1}^{\text{out}}(t-N\tau)} \;=\; \underset{\text{'from Eq. (14)'}}{c_{ij}^{\text{out}}(t-N\tau+\tau)} \tag{15}$$

and using Eq. 6 for the velocity:

$$v_{j-1}(t) = v_j(t-N\tau+\tau). \tag{16}$$

Equations 15 and 16 may be used to rearrange Eq. 37 so that it references column j only. The resulting expression is

$$c_i^{\text{in}}(t) = \alpha\, c_i^{\text{out}}(t') + (1-\alpha)\, c_i^{\text{ex}}(t), \quad \alpha = \frac{\min\{v(t'), v(t)\}}{v(t)}, \quad t' = t-(N-1)\tau, \tag{17}$$

where the time dependence is shown explicitly and, for simplicity, the j subscript is omitted because its value is fixed. The periodic conditions imposed on $v(t)$ and $c_i^{\text{ex}}(t)$ for the single-column model are defined by Eqs. 6 and 7, with j set to one of the integer values between 1 and N. The choice is arbitrary; one model with $j = j_1$ behaves similarly to another model with $j = j_2$, except that they are phased out in time one from the other by $|j_2 - j_1|\tau$. We choose $j = N\text{II} + 2$ so that the column is fed at the start of each cycle. Note that in Eq. 17, c_i^{out} is the concentration that left the column $(N-1)\tau$ time units before, whereas in the node balance of the SMB model c_i^{out} is the outlet concentration from the preceding column at the current instant.

Figure 2 compares a complete operating cycle of the simplest four-zone SMB (the one with port configuration 1/1/1/1) with that of the equivalent single-column model. It is seen that the single-column model is obtained by selecting an arbitrary column (shaded area) of the SMB unit and following its operation over a complete cycle. The recycle streams from the other columns of the SMB are replaced by the recycle stream of the single-column at previous times.

In essence, the single-column model can be characterized as follows:

- *The part of its outlet stream that is not recovered as product is recycled to the column with a lag of* $(N-1)\tau$ *time units*;
- *It reproduces the periodic state of the SMB process, because its node balance is obtained from the original SMB node balance by applying the CSS conditions.*

The first point is the critical one from the viewpoint of process design, whereas the second one is precisely the necessary condition for the model to reproduce the behavior of the SMB. Under CSS conditions the two models cannot be discriminated, except for the discontinuous use of the inlet/outlet lines by the single-column model. Under these circumstances the SMB process is equivalent to N identical single-column processes operating in parallel with phase lags of τ time units. One important consequence of this result is that the use of four or more columns is not a necessary condition for simulating the true moving bed process, unless continuous feed and product withdrawal is envisaged.

We end this section with a few notes regarding the use of the single-column model in the context of numerical simulation. Firstly, the theoretical framework described here provides a competitive methodology for calculating the CSS by dynamic simulation. The CSS is established by starting from a given initial condition in the column and simulating the process operation over a sufficiently large number of cycles. However, as opposed to the traditional approach of integrating the equations for all columns, we integrate the equations for just one column and store the outlet concentrations at discrete times in a circular buffer, which is employed to implement the recycle lag. The recycle is reconstructed from the discrete data stored in the buffer using a suitable scheme for data interpolation.

Secondly, it should be noted that the alternative of applying the CSS conditions forward in time was not explored here, because that would not lead to a physically realizable process. From a numerical point of view, however, the resulting model with node balance given by

$$c_i^{\mathrm{in}}(t) = \alpha\, c_i^{\mathrm{out}}(t+\tau) + (1-\alpha)\, c_i^{\mathrm{ex}}(t), \quad \alpha = \frac{\min\{v(t+\tau), v(t)\}}{v(t)}, \tag{18}$$

is the basis for an efficient method of directly computing the CSS. The method consists of discretizing the time coordinate for a single column over a complete cycle ($N\tau$ time units) and directly imposing the periodic boundary conditions given by Eq. 13. The resulting system of algebraic equations, obtained after discretization of the spatial coordinate, is

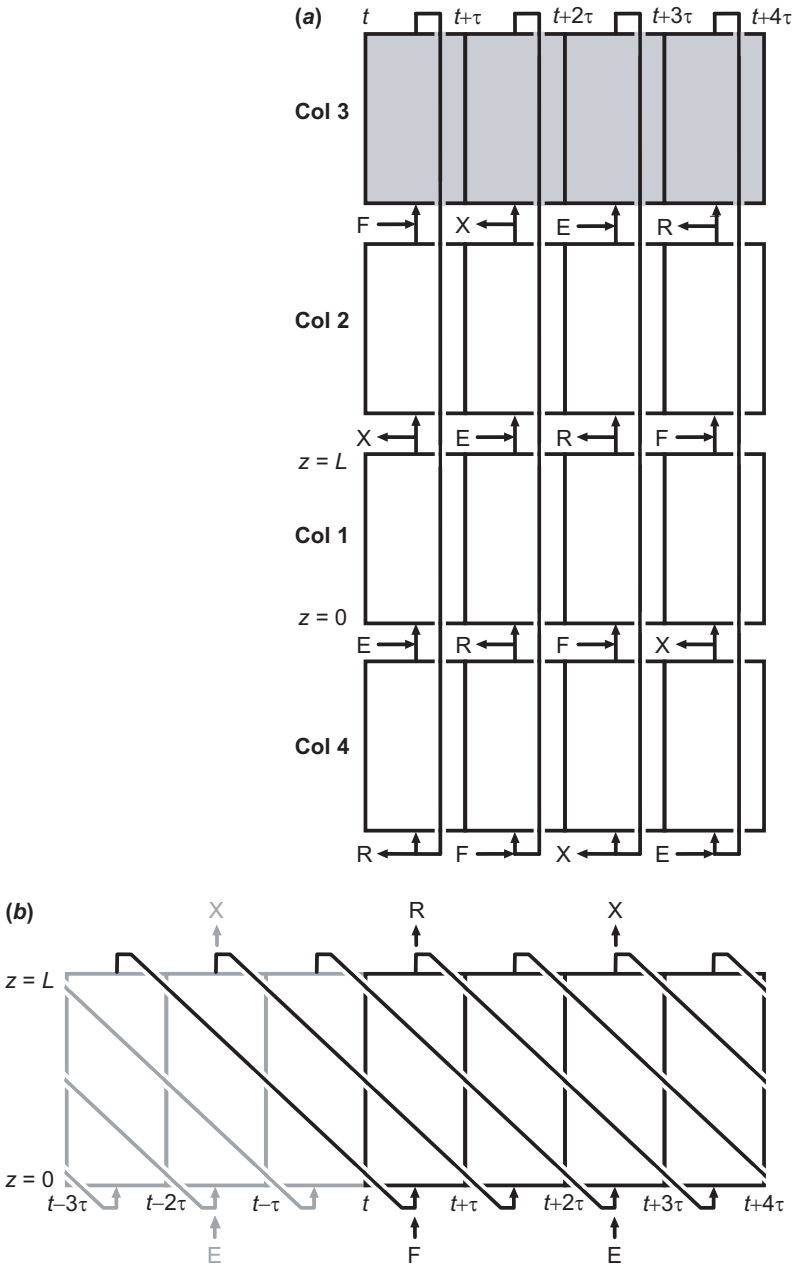

Figure 2: Schematic of operating cycle for (a) an SMB with port configuration 1/1/1/1 and (b) its equivalent single-column system with recycle lag. The latter is obtained by selecting an arbitrary column of the SMB unit (e.g., column 1) and following its operation over a complete cycle (shaded area). The recycle streams from the other nonexistent SMB columns are mimicked by recycling, with a lag of $(N-1)\tau$ time units, the portion of the outlet stream of the column that is not withdrawn as product. The feed, eluent, raffinate and extract streams are identified by letters F, E, R, and X, respectively.

solved directly to compute the CSS solution. Both methods are discussed in detail elsewhere [25].

1.3 Practical implementation of the ideal single-column SMB analog

1.3.1 System with perfectly-mixed tanks

The one-column chromatographic system proposed by Abunasser et al.[16] is one way to implement in practice an approximation to the ideal single-column system described above. In their system several perfectly-mixed tanks are coupled to the chromatographic column for collecting the portion of the outlet stream that is not withdrawn as product and for recycling it to the inlet of the column. The tanks are emptied in the order in which they were filled. This scheme allows for recycling in a manner that mimics the SMB behavior.

The complete cycle for the simplest one-column process developed by Abunasser et al.[16], which is analogous to a four-column SMB, is shown in Figure 3. For this configuration the simplest analog has four tanks. Notice the striking resemblance between Figure 2b and Figure 3.

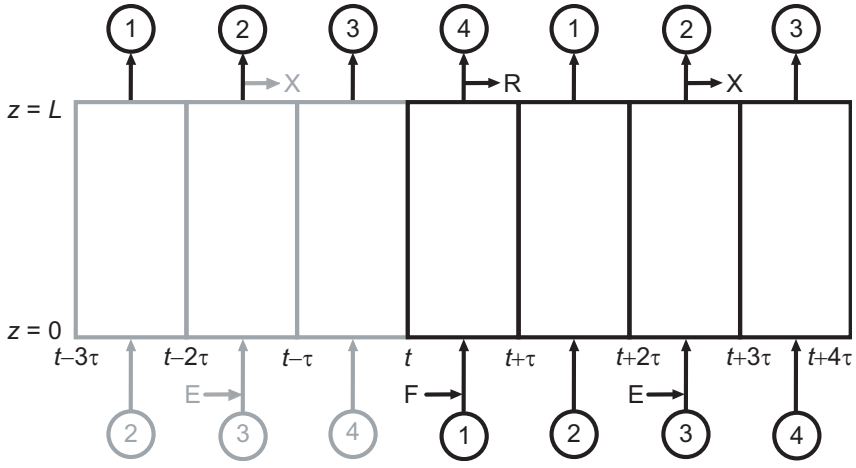

Figure 3: Schematic of complete operating cycle for the simplest version of the one-column process proposed by Abunasser et al.[16], which approximates the operation of an SMB with port configuration 1/1/1/1. In this configuration the analog has four tanks that replace the recycle streams shown in Figure 1b. The feed, eluent, raffinate and extract streams are identified by letters F, E, R, and X, respectively.

The process is well described elsewhere [16, 17]; here, we just add a few notes regarding the analysis of the process and demonstrate that it is indeed an approximation to the ideal single-column process described above. Each tank cannot be filled or emptied in more than

τ time units, otherwise at least one tank would have to be filled and emptied at the same time. This rule sets a minimum number of N tanks for the system to work properly: $N-1$ tanks to collect the recycle stream during $(N-1)\tau$ time units (thereby creating the lag) to be subsequently inputted to the column, and one extra tank to prevent the overlap of filling and emptying operations on the same tank. At each instant, all tanks are filled except for two tanks: the one which is being filled with the portion of the outlet stream of the column that is not withdrawn as product and the other which is providing the recycle stream to the column. In any case, the total liquid volume in the N tanks gives the recycle volume collected during $(N-1)\tau$ time units.

For simplicity of analysis, let us assume that M_τ tanks are filled (emptied) during a switching interval and that the filling (emptying) time, $\tau_m = \tau/M_\tau$, is the same for all tanks. Notice that, although the tanks take the same time to fill (empty), they hold different amounts of liquid because they are filled (emptied) at different rates. Let us also assume that no tank is filled or emptied across a switching interval. These constraints render the analysis simpler but the conclusions hold for the more general case. Under the restrictions considered above, the total number of tanks required for the process to operate properly is $(N-1)M_\tau + 1$. This one-column analog is equivalent to replacing the node balance given by Eq. 17 with

$$c_i^{\text{in}}(t) = \alpha \tilde{c}_i(t) + (1-\alpha) c_i^{\text{ex}}(t), \tag{19}$$

where

$$\tilde{c}_i(t) = \frac{1}{\tau_m} \int_{t^*}^{t^*+\tau_m} c_i^{\text{out}}(\nu)\, d\nu, \quad t^* = \tau_m \,\text{int}(t/\tau_m) - (N-1)\tau. \tag{20}$$

These equations show that the recycle of the ideal single-column system is replaced by a piecewise-constant approximation (staircase concentration profile) $\tilde{c}_i(t)$, where each concentration step is a consequence of the perfectly mixed contents of the tank being emptied. This is nicely exemplified in Figure 4, which compares typical temporal profiles of solute concentration in the recycle stream for the ideal single-column system and for three configurations of the equivalent analog using different number of tanks, when both processes are under CSS conditions. Notice that the concentration profiles of the ideal single-column process are identical to those of the SMB process being mimicked. The simplest analog configuration, the one with four tanks ($M_\tau = 1$), is shown in the top plot of Figure 4; each tank is filled during a complete switching interval ($\tau_m = \tau$). In the middle plot, the number of tanks has been increased to seven ($M_\tau = 2, \tau_m = \tau/2$), and

in the bottom one the number of tanks is ten ($M_\tau = 3, \tau_m = \tau/3$). Figure 4 shows that as the number of tanks is increased, the piecewise-constant concentration profile steadily approaches the profile of the ideal single-column system. From the definition of τ_m and Eq. 20 it is clear that

$$\lim_{M_\tau \to \infty} \tau_m = 0, \quad \lim_{M_\tau \to \infty} \tilde{c}_i(t) = c_i^{\text{out}}(t'), \quad t' = t - (N-1)\tau. \tag{21}$$

This is a formal proof that the analog of Wankat and coworkers [16, 17] approaches the behavior of the SMB process as the number of tanks is increased. It is also clear that this conclusion holds for systems in which the filling time is not the same for all tanks or the charge/discharge of a tank crosses the boundary of a switching interval.

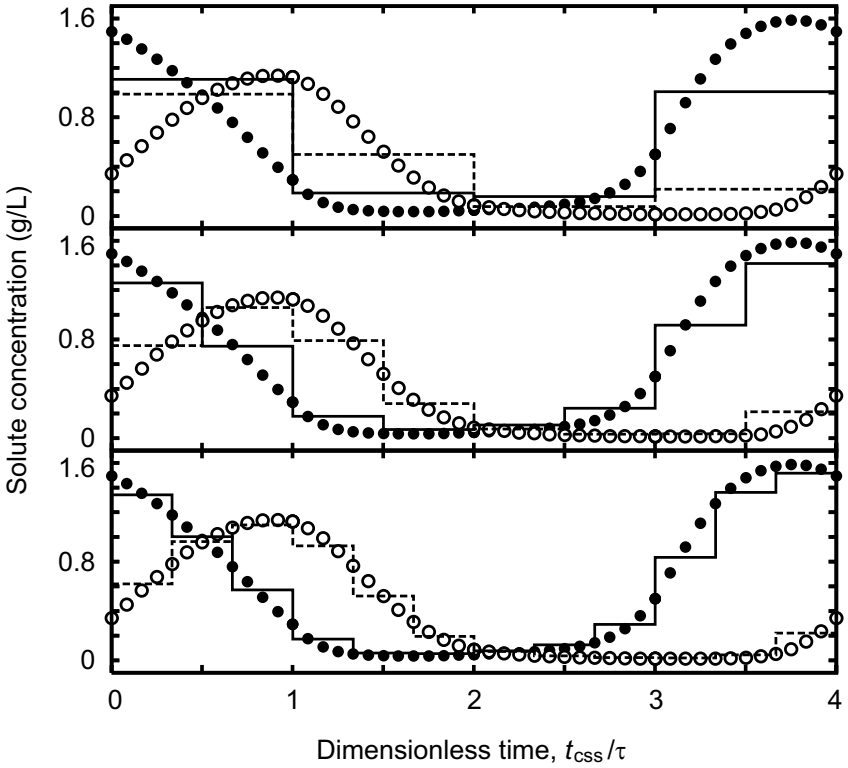

Figure 4: Comparison of the temporal profile of solute concentration in the recycle stream (symbols) that is inputted into the column of the ideal single-column model, i.e. $c_i^{\text{out}}(t')$ in Eq. 17, with the corresponding concentration profile (lines) of the analog developed by Abunasser et al.[16], i.e. $\tilde{c}_i(t)$ in Eq. 19. Both processes are mimicking the operation of a 4-column SMB, the operating conditions and model parameters for the test case considered here are listed in Table 1 (solute A: •, ——; solute B: ○, - - -). The staircase shape of the lines results from the use of several tanks to implement the recycle lag. The number of tanks employed by the analog in each plot is, from top to bottom: 4 ($M_\tau = 1$), 7 ($M_\tau = 2$) and 10 ($M_\tau = 3$). As the number of tanks is increased, the piecewise-constant concentration profile approaches the smooth concentration profile of the ideal single-column system.

This one-column system is conceptually appealing, but can still be improved. Although the system employs a single chromatographic column, the ancillary equipment is not significantly reduced with respect to the analogous SMB. In its simplest configuration it needs at least four tanks, each requiring two valves (inlet and outlet), one relief valve, and probably other ancillary hardware. With regards to the equivalent SMB unit, three chromatographic columns have been replaced by four tanks and the number of two-way valves has been reduced by half. But the biggest drawback is that the purities achieved with the analog are lower than with the SMB for the same productivity and desorbent-to-feed, $Q_{\mathrm{E}}/Q_{\mathrm{F}}$, values. This is because of the loss of separation due to mixing in the tanks, which can only be circumvented by increasing the $Q_{\mathrm{E}}/Q_{\mathrm{F}}$ value or by dividing the tanks into several smaller ones. The former option increases the separation cost, whereas as the latter increases the bulkiness and capital cost of the unit.

1.3.2 New system with plug-flow recycle

Our single-column chromatographic process is more elegant and simpler to implement. Its main strength is that, in principle, it can achieve the same purities as the SMB. The basis for our process is that a recycle lag can be implemented in practice by a plug-flow device with a mean residence time equal to the time lag. This is equivalent to replacing the node balance given by Eq. 17 with

$$c_i^{\mathrm{in}}(t) = \alpha \tilde{c}_i(1,t) + (1-\alpha) c_i^{\mathrm{ex}}(t), \tag{22}$$

where $\tilde{c}_i(x,t)$ is now a spatially distributed concentration that satisfies the plug-flow equation

$$\frac{\partial \tilde{c}_i}{\partial t} + \frac{1}{(N-1)\tau}\frac{\partial \tilde{c}_i}{\partial x} = 0 \quad (0 < x \leq 1), \tag{23}$$

subjected to the inlet boundary condition

$$\tilde{c}_i(0,t) = c_i^{\mathrm{out}}(t). \tag{24}$$

Unfortunately, this simple scheme is still not a practical solution because Eq. 23 assumes that the fluid is fed and withdrawn from the plug-flow device at the same rate. This is not the case for the ideal single-column system, where the flow rate of the portion of the outlet stream of the column for recycling and that of the recycled stream are different during some steps of the cycle. This happens because the recycle lag is not a multiple of the overall cycle duration, $N\tau$.

To solve this problem a more ingenious setup is needed, it is illustrated in Figure 5. The schematic shows the configuration of our single-column system that is analogous to a four-column SMB. The chromatographic column is connected in loop to a plug-flow tube, which has a spring-actuating piston at one end. The spring is continuously pushing the piston against the fluid. The movement of the piston compensates for the difference between the inlet and outlet flow rates. The tube has internal elements, or packing, to breakup the velocity distortion (Poiseuille flow), due to the no-slip of the fluid at the tube wall, and to provide a flow which is as close as possible to plug flow. There are several options to achieve this, such as structured or random inert packing with large void fraction, or corrugated walls. A prototype apparatus is being built to determine the effectiveness of several alternatives. Here, we focus on the conceptual implementation of the process and defer its experimental validation to a subsequent study.

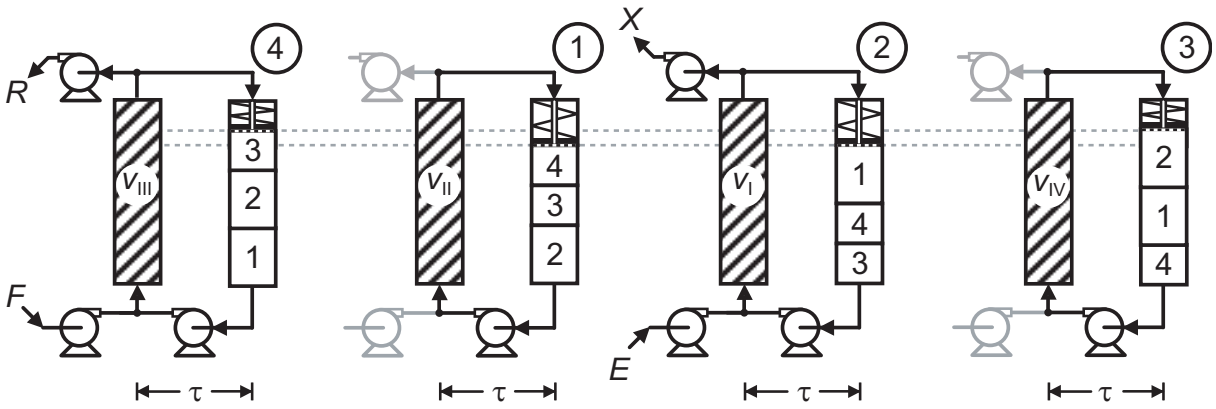

Figure 5: Schematic of the single-column chromatographic process with recycle lag proposed in this work analogous to a four-zone SMB. The chromatographic column is connected to a plug-flow tube with a piston at one end. The tube implements a recycle lag of $(N-1)\tau$ time units. The movement of the piston compensates for the difference in flow rates at the inlet and outlet of the tube which occur during some steps of the cycle. The complete cycle depicted here is for the configuration equivalent to a 4-column SMB unit. The feed, eluent, raffinate and extract streams are identified by letters F, E, R, and X, respectively.

Both the piston placement and pump arrangement shown in the schematic diagram of Figure 5 are not mandatory; the piston can be set opposite to the direction of fluid flow and the recycle pump can be placed at the outlet of the chromatographic column. However, by placing the recycle pump as shown in Figure 5 the recycle tube works at the lowest pressure in the system, whereas the highest pressure value is at the recycle pump outlet. In this configuration the force exerted by the spring is minimized. The use of three pumps provides the easiest implementation. An alternative setup, which saves

one pump, replaces the product withdrawal pump by a ratio-control system that includes a flow meter, a control valve and a flow-rate controller.

The operation of the single-column process shown in Figure 5 deserves a closer look. During the first switching interval of a cycle the column is operating as if it were in section III of the equivalent SMB. The recycle stream is pumped from the tube with flow rate $Q\mathrm{II} = \epsilon v\mathrm{II} A_\mathrm{c}$, where A_c is the cross-sectional area of the chromatographic column, is mixed with the feed, and inputted to the column with interstitial velocity vIII. Part of the outlet stream of the column is collected as raffinate with flow rate $Q_\mathrm{R} = \epsilon(v\mathrm{III} - v\mathrm{IV})A_\mathrm{c}$, the rest is fed to the recycle tube with flow rate $Q\mathrm{IV} = \epsilon v\mathrm{IV} A_\mathrm{c}$. Given that $Q\mathrm{II} > Q\mathrm{IV}$, the piston expands to compensate for the reduction of liquid in the recycle tube.

During the second and fourth switching intervals the chromatographic column is, respectively, in section II and section IV of the equivalent SMB system. In both cases the separation unit operates in closed loop with liquid being fed and withdrawn from the recycle tube at the same rate. The piston is stationary during both switching intervals.

During the third switching interval the column is in section I; part of its outlet stream is withdrawn as product (extract) with flow rate $Q_\mathrm{X} = \epsilon(v\mathrm{I} - v\mathrm{II})A_\mathrm{c}$, the rest is fed to the recycle tube with flow rate QII. Liquid is pumped from the recycle tube with flow rate QIV, diluted with fresh eluent, and fed to the column with interstitial velocity vI. Since $Q\mathrm{II} > Q\mathrm{IV}$, the piston contracts to accommodate the extra liquid that is being accumulated in the recycle tube.

Figure 6 shows the schematic of a complete cycle for the proposed single-column process with configuration analogous to a four-zone SMB unit with two columns per zone (2/2/2/2). The cycle is more complex than that in Figure 5, because it is divided into more steps (the number of columns in the equivalent SMB has doubled and the switching interval has halved), but the operating principle is similar. The piston has now four stop positions (denoted A–D in Figure 6), instead of the previous two, and there are two pairs of consecutive switching intervals during which neither the inlet nor the outlet flow rates of the recycle tube vary. Each one of these pairs of switching intervals can be combined into a single one with twice the duration.

Many of the advantages of using a single-column system have been highlighted elsewhere [16]. The system is a simpler, more flexible, and less expensive alternative to the SMB process, that provides the same specific productivity, i.e.

$$\frac{\text{feed volume processed per cycle}}{\text{amount of stationary phase}}. \tag{25}$$

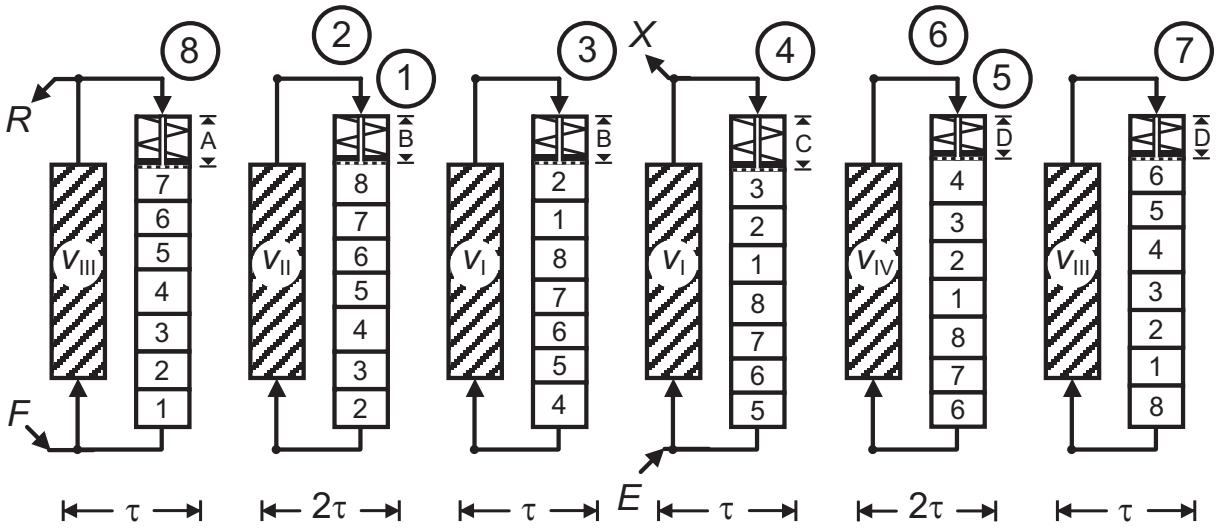

Figure 6: Schematic similar to that of Figure 5, but for the configuration equivalent to a 8-column SMB unit with port configuration 2/2/2/2. Notice that the piston has more intermediate positions than in the scheme of Figure 5. The second and third switching intervals of each cycle can be lumped into a single step of duration 2τ; this is also applicable to the sixth and seventh switching intervals.

Since the process uses a single column, the need to obtain adequate packing reproducibility on several columns is not an issue. Secondly, the total pressure drop is $1/N$th of that of the equivalent SMB process. This may be a big advantage if a particle size smaller than those appropriate for the equivalent SMB is used, since it decreases the mass transfer resistance and allows for higher flow rates in the system. The specific productivity is thus increased. An added advantage is that the hydrodynamic contribution to band broadening in the chromatographic column is reduced because the Péclet number is increased.

The operation of the piston is shown schematically in Figure 7. Liquid is fed to the tube with inlet velocity u_{L} and withdrawn with outlet velocity u_{R}. The tube outlet is at a fixed distance x_{R}, whereas the inlet x_{L} moves with the piston, with velocity equal to $u_{\mathrm{R}} - u_{\mathrm{L}}$, due to the difference between the inlet and outlet velocities. If $u_{\mathrm{R}} > u_{\mathrm{L}}$, the piston reduces the effective length, $x_{\mathrm{R}} - x_{\mathrm{L}}$, of the tube to compensate for the liquid volume that is withdrawn in excess to the feed value. If $u_{\mathrm{R}} < u_{\mathrm{L}}$, the spring contracts to create the necessary space for accommodating the excess liquid into the tube.

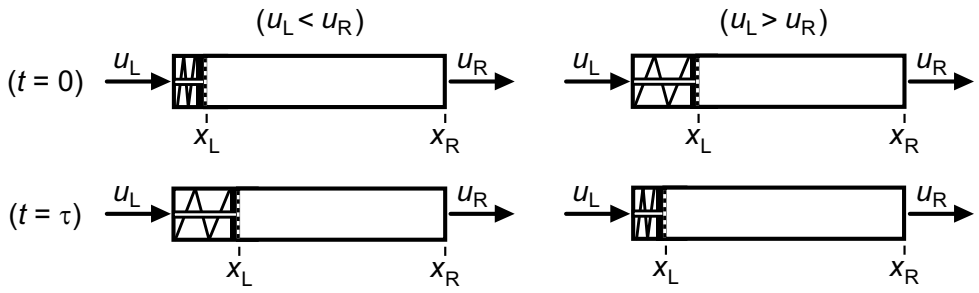

Figure 7: Schematic of the piston movement. Liquid is fed to the recycle tube with velocity u_{L} and withdrawn with velocity u_{R} in the direction shown in the drawing. The spring is constantly pushing the piston against the fluid. If the recycle pump is placed as shown in Figure 5, the tube is at the lowest pressure in the system and the piston can be designed so that the force exerted by the spring is minimum. x_{R} is fixed but x_{L} follows the piston as it moves. At each instant, the effective length of the tube is $x_{\mathrm{R}} - x_{\mathrm{L}}$. If $u_{\mathrm{L}} < u_{\mathrm{R}}$, the spring expands and x_{L} moves in the direction of x_{R}; the opposite happens when $u_{\mathrm{L}} > u_{\mathrm{R}}$.

As a first approximation, the transport of solute through the recycle tube is described by an axially dispersed flow model,

$$\frac{\partial \tilde{c}_i}{\partial t} + u_{\mathrm{R}} \frac{\partial \tilde{c}_i}{\partial x} - \tilde{D} \frac{\partial^2 \tilde{c}_i}{\partial x^2} = 0 \quad (x_{\mathrm{L}} < x \leq x_{\mathrm{R}}), \tag{26}$$

subjected to the boundary conditions

$$\tilde{c}_i = c_i^{\mathrm{out}} \quad \text{for} \quad x = x_{\mathrm{L}}, \quad \frac{dx_{\mathrm{L}}}{dt} = u_{\mathrm{R}} - u_{\mathrm{L}}; \tag{27}$$

$$\frac{\partial \tilde{c}_i}{\partial x} = 0 \quad \text{for} \quad x = x_{\mathrm{R}}. \tag{28}$$

Notice that Eq. 27 is a moving boundary condition. The dispersion coefficient $\tilde{D}$ accounts for the spread of the concentration profiles by the presence of molecular diffusion and velocity distortion (hydrodynamic dispersion) that is not fully eliminated by the internal elements of the tube.

We define a Péclet number, $\widetilde{\mathrm{Pe}}$, for hydrodynamic dispersion in the tube, as

$$\widetilde{\mathrm{Pe}} = \frac{u_{\mathrm{R}}[x_{\mathrm{R}} - x_{\mathrm{L}}(0)]}{\tilde{D}}. \tag{29}$$

Here, $\widetilde{\mathrm{Pe}}$ is used as a general parameter to account for deviations from perfect plug flow in the tube, and to demonstrate the practical need for an efficient plug-flow device for the system to work correctly. In actual engineering work, $\widetilde{\mathrm{Pe}}$ would be a sizing or design parameter. When designing a new unit, $\widetilde{\mathrm{Pe}}$ would provide an estimate of the maximum admissible value of $\tilde{D}$ (which is directly related to the characteristics of the internal elements of the recycle tube) for product purity to be kept, within a given tolerance, near to that of the equivalent SMB. For an existing unit, $\widetilde{\mathrm{Pe}}$ would be an extra parameter to

be taken into account when determining the operating conditions (the appropriate flow rates for each step of the cycle) to obtain a desired separation performance. It should be pointed out that Eqs. 26–28 provide a reasonable description of the flow through random or structured inert packing, but may very well be inadequate to describe the impact of other types of internals on the flow field.

Equation 26 is easier to solve numerically if the moving boundary condition is replaced by a stationary one. To achieve this we introduce a change of variable that maps the spatial domain $x^{\text{in}}[x_{\text{L}}, x_{\text{R}}]$ onto a dimensionless domain $\xi^{\text{in}}[0, 1]$, of fixed length, through the transformation

$$\xi = (x - x_{\text{L}})/(x_{\text{R}} - x_{\text{L}}). \tag{30}$$

Using the chain rule we get

$$\frac{\partial \tilde{c}_i(\xi, t)}{\partial t} = \frac{\partial \tilde{c}_i(x, t)}{\partial t} + \frac{\partial \tilde{c}_i(x, t)}{\partial x} \frac{\partial x(\xi, t)}{\partial t}, \tag{31}$$

which allows us to rewrite Eqs. (26–28) for $\tilde{c}_i(\xi, t)$ as

$$\frac{\partial \tilde{c}_i}{\partial t} + \frac{\tilde{u}_{\text{R}} - (\tilde{u}_{\text{R}} - \tilde{u}_{\text{L}})(1 - \xi)}{1 - (\tilde{u}_{\text{R}} - \tilde{u}_{\text{L}})t} \frac{\partial \tilde{c}_i}{\partial \xi} - \frac{\tilde{u}_{\text{R}}/\widetilde{\text{Pe}}}{[1 - (\tilde{u}_{\text{R}} - \tilde{u}_{\text{L}})t]^2} \frac{\partial^2 \tilde{c}_i}{\partial \xi^2} = 0 \quad (0 < \xi \leq 1), \tag{32}$$

$$\tilde{c}_i(0, t) = c_i^{\text{out}}(t), \qquad \left.\frac{\partial \tilde{c}_i}{\partial x}\right)_{x_{\text{R}}} = 0, \tag{33}$$

where $\tilde{u} = u/[x_{\text{R}} - x_{\text{L}}(0)]$. The convective term can also be rewritten in conservative form as

$$\frac{\dfrac{\partial}{\partial \xi}\Big\{[\tilde{u}_{\text{R}} - (\tilde{u}_{\text{R}} - \tilde{u}_{\text{L}})(1 - \xi)]\tilde{c}_i\Big\} - (\tilde{u}_{\text{R}} - \tilde{u}_{\text{L}})\tilde{c}_i}{1 - (\tilde{u}_{\text{R}} - \tilde{u}_{\text{L}})t}. \tag{34}$$

Notice that $1/\tilde{u}_{\text{R}}$ is the average residence time of a fluid particle in the tube if its length is fixed at $x_{\text{R}} - x_{\text{L}}(0)$. Details of the numerical method for solving these equations, and its validation, are given in an appendix.

It is straightforward to determine the amount of liquid in the recycle tube, or its effective length, at the beginning of a given step of the cycle. Each slice of liquid, indexed in both Figures 5 and 6, is fed to the recycle tube and withdrawn from it with the same velocity, although it will travel along the tube with varying velocity as the steps change. Since a slice of liquid, say the jth one, is fed and withdrawn in τ time units, its volume is $u^{(j)} A_{\text{t}} \tau$, where $u^{(j)}$ is its feed velocity and A_{t} is the cross-sectional area of the tube; the length of tube taken by that slice of fluid is simply $u^{(j)}\tau$. Thus, the effective length of the tube at the beginning of the step in which slice j is inputted is

$$\tau \textstyle\sum_{k=1, k\neq j}^{N} u^{(k)}, \tag{35}$$

and the corresponding values of $\tilde{u}_{\mathrm{L}}$ and $\tilde{u}_{\mathrm{R}}$ are

$$\{\tilde{u}_{\mathrm{L}}, \tilde{u}_{\mathrm{R}}\} = \frac{\{u^{(j)}, u^{(j+1)}\}}{\tau \sum_{k=1,k\neq j}^{N} u^{(k)}}. \tag{36}$$

Since $\tilde{u}_{\mathrm{L}}$ and $\tilde{u}_{\mathrm{R}}$ are actually a ratio of u's, and each one of these is proportional to one of the interstitial velocities $v\mathrm{I}, \ldots, v\mathrm{IV}$, the ratio of the latter can be used instead. Table 2 lists the main input parameters governing each step of a full cycle of the proposed single-column process for a configuration analogous to a four-section SMB with one column per section; those for a configuration analogous to a SMB with two columns per section are listed in Table 3.

Table 2: Main input parameters for each step of a full cycle of the proposed single-column chromatographic process. The configuration mimics the behavior of a four-section SMB with one column per section. The node balance is: $c_i^{\mathrm{in}} = \alpha \tilde{c}_i^{\mathrm{out}} + (1-\alpha) c_i^{\mathrm{ex}}$.

Switching interval	v	α	c_i^{ex}	$\tilde{u}_{\mathrm{L}}\tau$	$\tilde{u}_{\mathrm{R}}\tau$	c_i^{R}	c_i^{X}
1	v_{III}	$\frac{v_{\mathrm{II}}}{v_{\mathrm{III}}}$	c_i^{F}	$\frac{v_{\mathrm{IV}}}{2v_{\mathrm{II}}+v_{\mathrm{IV}}}$	$\frac{v_{\mathrm{II}}}{2v_{\mathrm{II}}+v_{\mathrm{IV}}}$	c_i^{out}	–
2	v_{II}	1	–	$\frac{v_{\mathrm{II}}}{v_{\mathrm{II}}+2v_{\mathrm{IV}}}$	$\frac{v_{\mathrm{II}}}{v_{\mathrm{II}}+2v_{\mathrm{IV}}}$	–	–
3	v_{I}	$\frac{v_{\mathrm{IV}}}{v_{\mathrm{I}}}$	c_i^{E}	$\frac{v_{\mathrm{II}}}{v_{\mathrm{II}}+2v_{\mathrm{IV}}}$	$\frac{v_{\mathrm{IV}}}{v_{\mathrm{II}}+2v_{\mathrm{IV}}}$	–	c_i^{out}
4	v_{IV}	1	–	$\frac{v_{\mathrm{IV}}}{2v_{\mathrm{II}}+v_{\mathrm{IV}}}$	$\frac{v_{\mathrm{IV}}}{2v_{\mathrm{II}}+v_{\mathrm{IV}}}$	–	–

Table 3: Main input parameters for each step of a complete cycle of the proposed single-column chromatographic process. The configuration mimics the behavior of a four-section SMB with two columns per section. The node balance is: $c_i^{\mathrm{in}} = \alpha \tilde{c}_i^{\mathrm{out}} + (1-\alpha) c_i^{\mathrm{ex}}$.

Switching interval	v	α	c_i^{ex}	$\tilde{u}_{\mathrm{L}}\tau$	$\tilde{u}_{\mathrm{R}}\tau$	c_i^{R}	c_i^{X}
1	v_{III}	$\frac{v_{\mathrm{II}}}{v_{\mathrm{III}}}$	c_i^{F}	$\frac{v_{\mathrm{III}}}{v_{\mathrm{I}} + 3v_{\mathrm{II}} + 3v_{\mathrm{IV}}}$	$\frac{v_{\mathrm{II}}}{v_{\mathrm{I}} + 3v_{\mathrm{II}} + 3v_{\mathrm{IV}}}$	–	–
2 & 3	v_{II}	1	–	$\frac{v_{\mathrm{II}}}{v_{\mathrm{I}} + 2v_{\mathrm{II}} + v_{\mathrm{III}} + 3v_{\mathrm{IV}}}$	$\frac{v_{\mathrm{II}}}{v_{\mathrm{I}} + 2v_{\mathrm{II}} + v_{\mathrm{III}} + 3v_{\mathrm{IV}}}$	–	–
4	v_{I}	1	–	$\frac{v_{\mathrm{II}}}{v_{\mathrm{I}} + 2v_{\mathrm{II}} + v_{\mathrm{III}} + 3v_{\mathrm{IV}}}$	$\frac{v_{\mathrm{I}}}{v_{\mathrm{I}} + 2v_{\mathrm{II}} + v_{\mathrm{III}} + 3v_{\mathrm{IV}}}$	c_i^{out}	–
5	v_{I}	$\frac{v_{\mathrm{IV}}}{v_{\mathrm{I}}}$	c_i^{E}	$\frac{v_{\mathrm{I}}}{3v_{\mathrm{II}} + v_{\mathrm{III}} + 3v_{\mathrm{IV}}}$	$\frac{v_{\mathrm{IV}}}{3v_{\mathrm{II}} + v_{\mathrm{III}} + 3v_{\mathrm{IV}}}$	–	–
6 & 7	v_{IV}	1	–	$\frac{v_{\mathrm{IV}}}{v_{\mathrm{I}} + 3v_{\mathrm{II}} + v_{\mathrm{III}} + 2v_{\mathrm{IV}}}$	$\frac{v_{\mathrm{IV}}}{v_{\mathrm{I}} + 3v_{\mathrm{II}} + v_{\mathrm{III}} + 2v_{\mathrm{IV}}}$	–	–
8	v_{III}	1	–	$\frac{v_{\mathrm{IV}}}{v_{\mathrm{I}} + 3v_{\mathrm{II}} + v_{\mathrm{III}} + 2v_{\mathrm{IV}}}$	$\frac{v_{\mathrm{III}}}{v_{\mathrm{I}} + 3v_{\mathrm{II}} + v_{\mathrm{III}} + 2v_{\mathrm{IV}}}$	–	c_i^{out}

Figure 8 compares raffinate and extract purities for the single-column process proposed in this work, the SMB analog of Abunasser et al.[16] and the equivalent four-section SMB. Note that the purities of the SMB are identical to those of the ideal single-column process described in the previous section, and are achieved by our process for $\widetilde{\mathrm{Pe}} \to \infty$ and by the analog of Abunasser et al.[16] when $M_\tau \to \infty$. The analysis is carried out for three different port configurations: one column per section (1/1/1/1), six columns (1/2/2/1), and two columns per section (2/2/2/2).

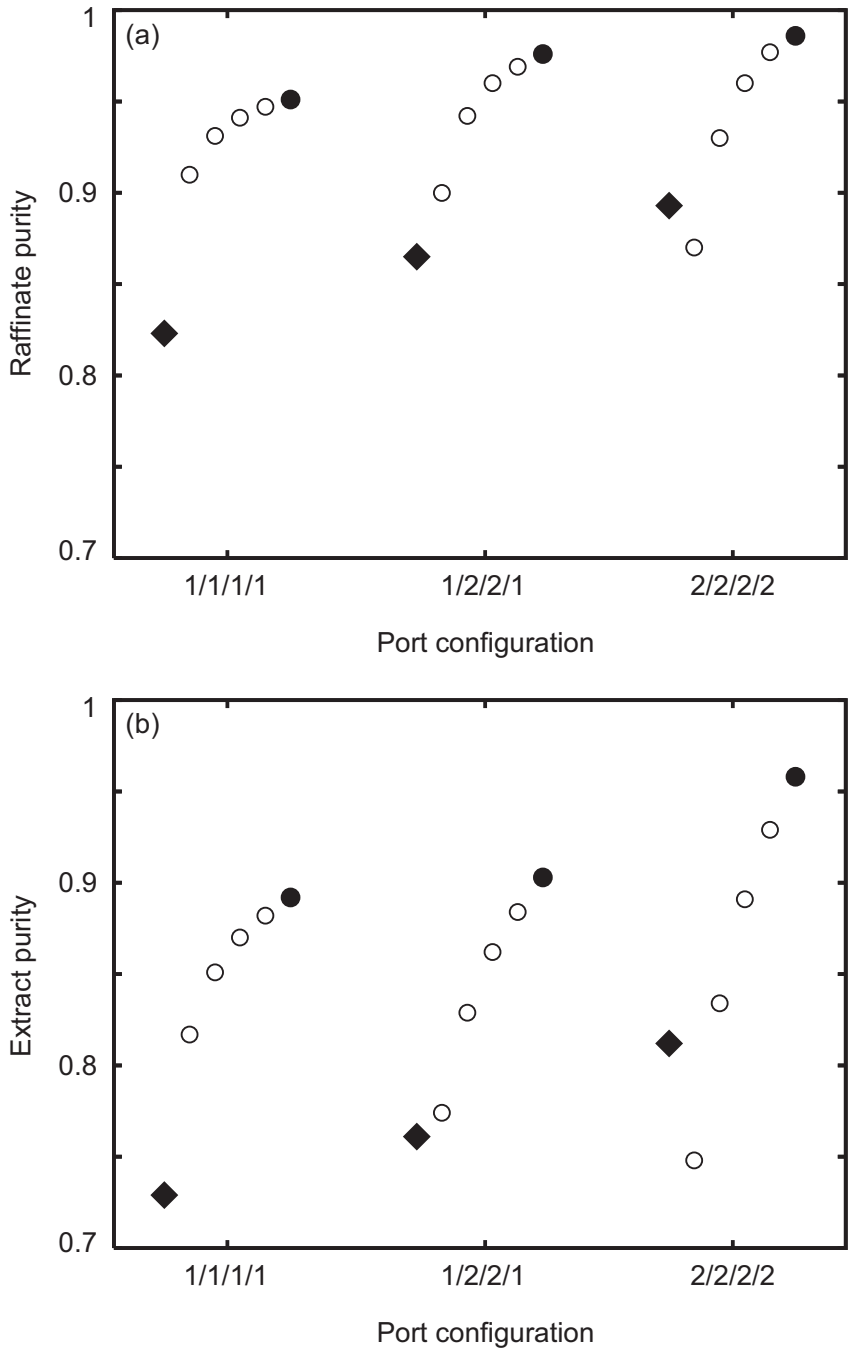

Figure 8: Comparison of raffinate (a) and extract (b) purities for the analog developed by Abunasser et al.[16] ($\diamond$), the single-column process proposed here ($\circ$; the value of $\widetilde{\mathrm{Pe}}$ is, from left to right, 500, 1000, 2000, and 5000), and the equivalent four-section SMB ($\bullet$). Note that the closed circles also denote purities for the proposed the single-column process when $\widetilde{\mathrm{Pe}} \to \infty$. The results are presented for three different port configurations: one column per section (1/1/1/1), six columns (1/2/2/1), and two columns per section (2/2/2/2). The operating conditions and model parameters for the test case considered here are listed in Table 1.

The results show that, as the value of $\widetilde{\mathrm{Pe}}$ is increased, the purities of our single-column process approach those of the equivalent SMB. The analog of Abunasser et al.[16] provides lower purities than our process for the range of $\widetilde{\mathrm{Pe}}$ values tested. The performance of their process improves with increasing number of columns of the analogous SMB. There are two reasons for this: the purities of the SMB are better when the sections are divided into more columns, but mostly because, as demonstrated in Figure 4, there is less loss of separation due to mixing in the tanks when their number is increased. This analysis is roughly equivalent to tracking the purities of our process by increasing both the number of columns of the analogous SMB and the value of $\widetilde{\mathrm{Pe}}$.

For a given configuration, the influence of $\widetilde{\mathrm{Pe}}$ on product purity is as expected. The results are, however, less obvious when different configurations are compared for the same $\widetilde{\mathrm{Pe}}$ value. For example, for $\widetilde{\mathrm{Pe}} = 500$ better purities are obtained with the configuration analogous to a four-column SMB than with the other two configurations. For $\widetilde{\mathrm{Pe}} = 1000$, the 1/2/2/1 configuration gives the best raffinate purity, whereas the highest extract purity is still obtained with the 1/1/1/1 configuration. For $\widetilde{\mathrm{Pe}} = 2000$ and above, the purities follow the expected trend of improving with increasing number of columns of the equivalent SMB configuration. Thus, the impact of $\widetilde{\mathrm{Pe}}$ on product purity appears to be more severe when the number of columns of the analogous SMB configuration is larger. It should be pointed out that the results presented here are for a fixed set of operating conditions. No attempt was made to adjust the flow rates to optimize the separation performance for each $\widetilde{\mathrm{Pe}}$ value. Note also that the results have some embedded numerical diffusion, an inevitability of every spatial discretization scheme, that increases the value of the simulated Péclet number.

Figures 9–12 provide some insight into the mechanism by which $\widetilde{\mathrm{Pe}}$ influences product purity. The first two figures show the spatial profiles of solute concentration in the liquid phase that would be observed over the four sections of the SMB mimicked by the single-column process. Figure 9 is for the analog to a SMB with one column per section, whereas Figure 10 is for the analog to a SMB with two columns per section. The data plotted in both figures were obtained after the system attained cyclic steady state. To construct each spatial concentration profile, we took several snapshots of the profile in the column of the analog with a sampling period equal to τ (as indicated in the respective graphic) and then plotted them sequentially. For a given $\widetilde{\mathrm{Pe}}$ value, band broadening is more pronounced for the 8-column analog than for the 4-column analog. Dispersion tends to reduce solute

concentration where it is higher and increase it where it is lower. This has a double negative effect on product purity, since it decreases the concentration of the target solute near its withdrawal point and increases that of the impurity. Since the spatial concentration profile is bell shaped and is constrained by the global material balance, it crosses another profile for a different $\widetilde{\mathrm{Pe}}$ value twice along the four sections. For the less-retained component this happens near the feed point and half-way in section IV. The profiles for the more retained component cross others near the extract and feed points.

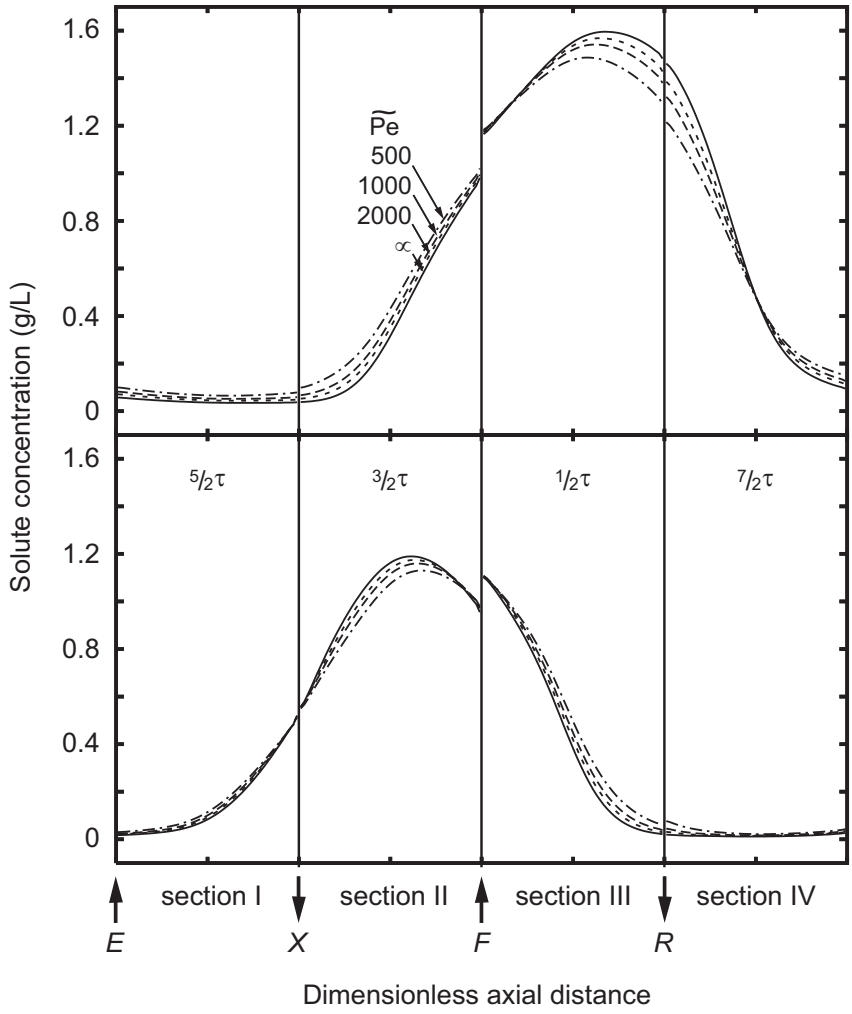

Figure 9: Spatial concentration profiles of less-retained (top plot) and more-retained component (bottom plot) in the middle of a switching interval, for the proposed single-column process analogous to a four-section SMB with one column per section. The results are given for various values of the hydrodynamic Péclet number in the recycle tube, $\widetilde{\mathrm{Pe}}$, and were obtained after the process attained CSS conditions. Note that the results obtained for $\widetilde{\mathrm{Pe}} \to \infty$ are identical to those of the ideal single-column process and reproduce those of the equivalent SMB. To construct the spatial concentration profile spanning the four sections of the equivalent SMB, four snapshots of the profile in the column were taken with a sampling period equal to τ (as indicated in the graphic). The operating conditions and model parameters for the test case considered here are listed in Table 1.

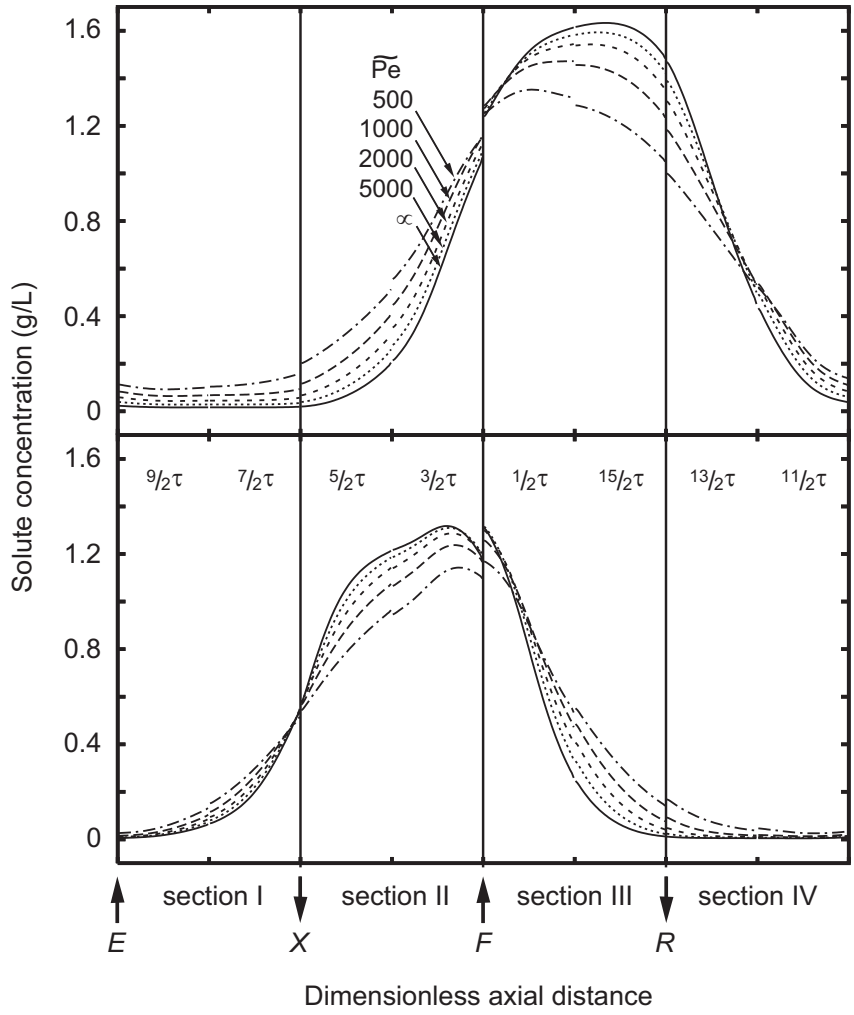

Figure 10: Plot similar to that of Figure 9, but for a configuration analogous to a four-section SMB with two columns per section. Notice that the number of snapshots of the spatial concentration profile require to construct the profile spanning the four sections of the equivalent SMB has doubled.

Figures 11 and 12 show temporal profiles of solute concentration at the outlet of the chromatographic column under CSS conditions for the two configurations analyzed in Figures 9 and 10. Again, it is seen that small values of $\widetilde{\mathrm{Pe}}$ smooth the solute concentration profile, diluting it where it is higher and increasing its polluting effect where it is lower. Overall, these results demonstrate the practical need for an efficient plug-flow device for the system to work efficiently.

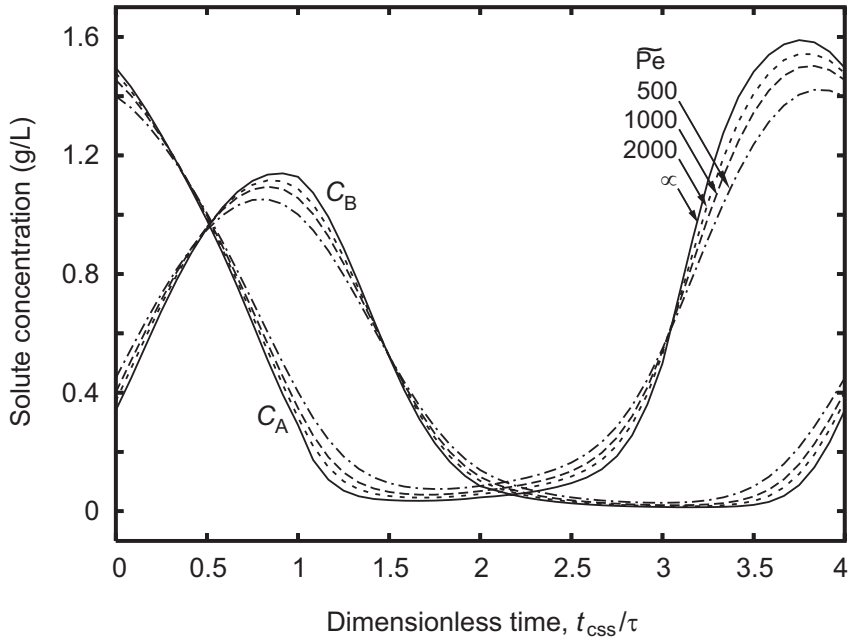

Figure 11: Temporal profiles of solute concentration at the outlet of the proposed single-column process for a configuration analogous to a four-section SMB with one column per section. The results are given for various values of the hydrodynamic Péclet number in the recycle tube, $\widetilde{\mathrm{Pe}}$, and were obtained after the process attained CSS conditions. Note that the results obtained for $\widetilde{\mathrm{Pe}} \to \infty$ are identical to those of the ideal single-column process and reproduce those of the equivalent SMB. The operating conditions and model parameters for the test case considered here are listed in Table 1.

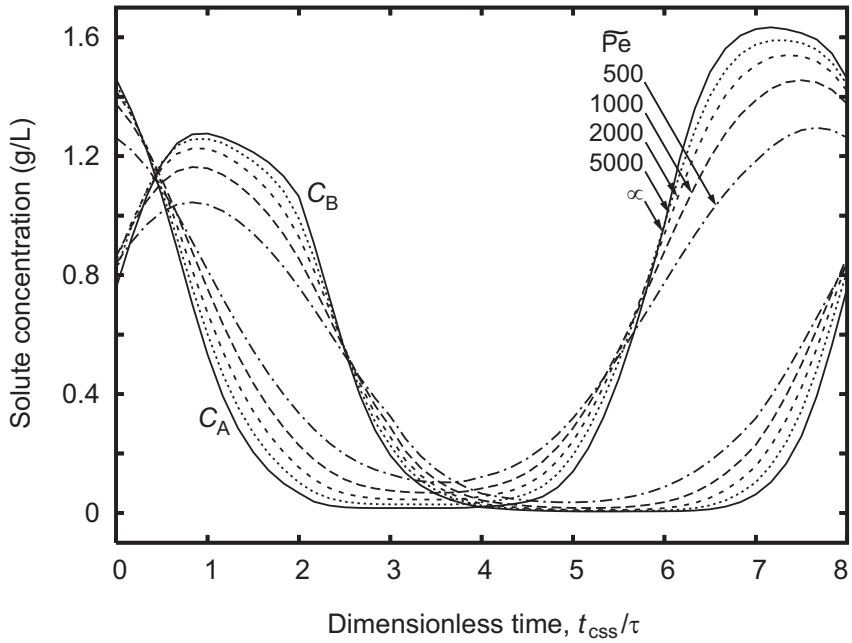

Figure 12: Plot similar to that of Figure 11, but for a configuration analogous to a four-section SMB with two columns per section.

1.4 Conclusions

In this work it has been demonstrated that the periodic state of the SMB can be reproduced by a single-column chromatographic process with a recycle lag of $(N-1)\tau$ time units. To implement the recycle lag in practice, a special type of plug-flow tube has been designed. It includes internal elements to provide a flow which is as close as possible to plug flow, and a piston to compensate for the difference between the inlet and outlet flow rates. This is necessary because the recycle lag is not a multiple of the overall cycle duration. Our system is a more compact, less expensive and simpler-to-operate alternative to the SMB that can potentially achieve the same purities while keeping the specific productivity constant.

It is clear that the presented single-column chromatographic process can be easily applied to other SMB configurations besides those considered in this work (e.g., three-zone ones). The numerous possibilities for improving SMB performance, through variation of parameters during a switching interval, are readily applicable to our single-column analog. A detailed analysis of the application of the VARICOL concept [6] to the disclosed single-column system is presented ahead in the next sections. These recently developed novel cycles add extra flexibility to the acquainted process and the improved performance obtained with them can compensate for a less perfect operation of the recycle tube.

2 Optimized asynchronous operation

2.1 Introduction

It has been recently shown that SMB performance can be significantly improved through variation of parameters during a switching interval. These include, among others, the asynchronous shift of the inlet and outlet ports [6], modulation of solvent strength [8], and cyclic modulation of feed flow [9, 10] and feed concentration [11]. These advances are pushing the trend towards the use of units with smaller number of columns [12–14], since less stationary phase is used and the setup is more economic [15].

In several applications of SMB technology it would be advantageous to work with the limiting case of a single column. Because only one column would have to be repacked, switching from one mixture to another would be easier and take less time than with SMB. This is especially important for the pharmaceutical industry, where SMBs are seen as multipurpose units that can be applied to different separations in all stages of the drug-development cycle [1]. It has been recently shown that this can be achieved by one-column analogous processes [7, 16, 17, 25, 32, 33], which mimic the operation of an SMB with a single chromatographic column.

The theory of single-column chromatography with recycle analogous to SMB has only recently been developed [7, 25]. In particular it has been demonstrated that the periodic state of the SMB is reproduced by a single-column chromatographic process with a plug-flow device to implement a recycle lag of $(N-1)\tau$ time units, where N is the number of columns of the equivalent SMB process and τ is the switching interval. Theoretically, this single-column process is indistinguishable from the analogous SMB, except for the discontinuous use of the inlet/outlet lines. It has been shown that, depending on the efficiency of the plug-flow device, the developed single-column process can achieve the same purities as the analogous SMB unit while keeping the specific productivity constant.

The numerous possibilities for improving SMB performance, through variation of parameters during a switching interval, are readily applicable to our single-column analog. A detailed analysis of the application of the VARICOL concept [6] to the single-column system disclosed in the previous sections is presented ahead [34] (**paper IV**). These recently developed novel cycles add extra flexibility to the acquainted process and the improved performance obtained with them can compensate for a less perfect operation of the recycle tube.

2.2 Theoretical basis for the single-column chromatograph analogous to SMB

The SMB is a practical way of implementing a counter-current chromatographic process. The system consists of N identical chromatographic columns connected in series to build a closed loop. By moving the input and withdrawal ports one column ahead (i.e. in the direction of fluid flow) at fixed intervals, the counter-current contact between the adsorbent and liquid is simulated. A schematic diagram of a typical four-section SMB is shown in Figure 1. More details can be found elsewhere [7, 21, 22, 25].

The theoretical framework for establishing the necessary conditions for a single-column chromatographic process to reproduce the periodic state of the SMB is reviewed here.

Figure 13 shows the schematic representation of a generic node connecting two consecutive columns, say $j-1$ and j, of an SMB unit. The notation employed is as follows: Q is the liquid flow rate, $c^{\text{out}}_{i,j-1}$ is the concentration of solute i at the outlet of column $j-1$ and c^{in}_{ij} is the corresponding solute concentration at the inlet of column j. The solute concentration and flow rate of the external inlet/outlet lines are identified by scripts E (eluent), X (extract), F (feed), and R (raffinate).

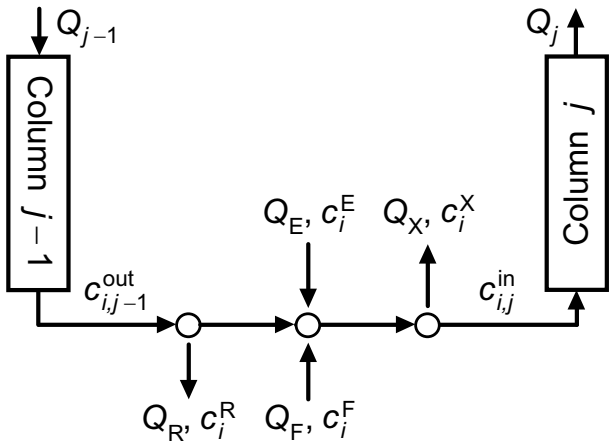

Figure 13: Schematic representation of the node connecting columns $j-1$ and j of an SMB unit. The concentration of solute i in liquid phase is c_i and Q is the volumetric flow rate. Scripts E, X, F, and R denote eluent, extract, feed and raffinate lines, respectively.

The individual node balance for solute i between two adjacent SMB columns, can be written as

$$\begin{cases} Q_{\text{III}}\, c^{\text{in}}_{ij} = \; Q_{\text{II}}\, c^{\text{out}}_{i,j-1} + (Q_{\text{III}} - Q_{\text{II}})\, c^{\text{F}}_i & \text{(feed node)} \\ Q_{\text{I}}\, c^{\text{in}}_{ij} = Q_{\text{IV}}\, c^{\text{out}}_{i,j-1} + (Q_{\text{I}} - Q_{\text{IV}})\, c^{\text{E}}_i & \text{(eluent node)}\,, \\ c^{\text{in}}_{ij} = \quad c^{\text{out}}_{i,j-1} & \text{(otherwise)} \end{cases} \tag{37}$$

where $Q_{\mathrm{I}}, \dots Q_{\mathrm{IV}}$ are the flow rates in the four sections of the SMB, and are determined by the global node balances:

$$Q_{\mathrm{I}} = Q_{\mathrm{IV}} + Q_{\mathrm{E}}, \tag{38}$$

$$Q_{\mathrm{II}} = Q_{\mathrm{I}} - Q_{\mathrm{X}}, \tag{39}$$

$$Q_{\mathrm{III}} = Q_{\mathrm{II}} + Q_{\mathrm{F}}, \tag{40}$$

$$Q_{\mathrm{IV}} = Q_{\mathrm{III}} - Q_{\mathrm{R}}. \tag{41}$$

Because of the circular arrangement of the columns and the periodic nature of the inputs ($Q_{\mathrm{I}}, \dots Q_{\mathrm{IV}}$; c_i^{F}; c_i^{E}), the process converges asymptotically towards a cyclic steady-state (CSS) regime. The definition of the CSS regime depends on the reference frame. If the observer is stationary, each column is identified according to its fixed position within the unit (or its index number j). In this case, the CSS condition is

$$c_{ij}(z, t + N\tau) = c_{ij}(z, t), \quad q_{ij}(z, t + N\tau) = q_{ij}(z, t) \quad (0 \le z \le L), \tag{42}$$

which states that in every column the spatially-distributed concentration profiles distanced by $N\tau$ time units must be identical.

If the frame of reference moves with the inlet/outlet lines, the CSS condition can be expressed as

$$c_{i,j+1}(z, t + \tau) = c_{ij}(z, t), \quad q_{i,j+1}(z, t + \tau) = q_{ij}(z, t) \quad (0 \le z \le L). \tag{43}$$

Eqn (43) provides an alternative definition of the CSS for a standard SMB process: the spatially-distributed concentration profiles distanced by τ time units are identical, apart from a shift of exactly one column.

Using the CSS conditions to look into past process time we can write

$$c_{i,j-1}^{\mathrm{out}}(t) = c_{ij}^{\mathrm{out}}(t - N\tau + \tau), \quad Q_{j-1}(t) = Q_j(t - N\tau + \tau). \tag{44}$$

The resulting solute node balance, which references a single column, is

$$\begin{cases} Q_{\mathrm{III}}\, c_i^{\mathrm{in}}(t) = Q_{\mathrm{II}}\, c_i^{\mathrm{out}}(t') + (Q_{\mathrm{III}} - Q_{\mathrm{II}})\, c_i^{\mathrm{F}} & \text{(feed mode)} \\ Q_{\mathrm{I}}\, c_i^{\mathrm{in}}(t) = Q_{\mathrm{IV}}\, c_i^{\mathrm{out}}(t') + (Q_{\mathrm{I}} - Q_{\mathrm{IV}})\, c_i^{\mathrm{E}} & \text{(eluent mode)} \\ c_i^{\mathrm{in}}(t) = c_i^{\mathrm{out}}(t') & \text{(otherwise)} \end{cases}, \tag{45}$$

where $t' = t - (N-1)\tau$ and, for simplicity, the j subscript is omitted because its value is fixed (we are tracking the dynamic behavior of a fixed column of the SMB unit). Clauses

'feed mode' and 'eluent mode' apply to the interval of the cycle during which the column is in the leftmost position of zone I and zone III, respectively. The choice of the value for j is arbitrary because all columns are assumed to be identical and undergo the same cycle. Eqn (45) defines a single-column batch chromatographic system that has the same CSS dynamics as a fixed column of the equivalent multi-column chromatographic process. The time lag of $(N-1)\tau$ is a consequence of the circular column arrangement and periodic nature of the process operation [7]. Note that in eqn (45) c_i^{out} is the concentration that left the column $(N-1)\tau$ time units before, whereas in the node balance of the SMB model, i.e. eqn (37), c_i^{out} is the outlet concentration from the preceding column at the current instant.

Figure 14 provides a block diagram of eqn (45), where it is show that by applying the CSS condition, backward in time, to the solute node balance the periodic state of the SMB process is reproduced by the single-column chromatographic model whose node balance is given by eqn (45).

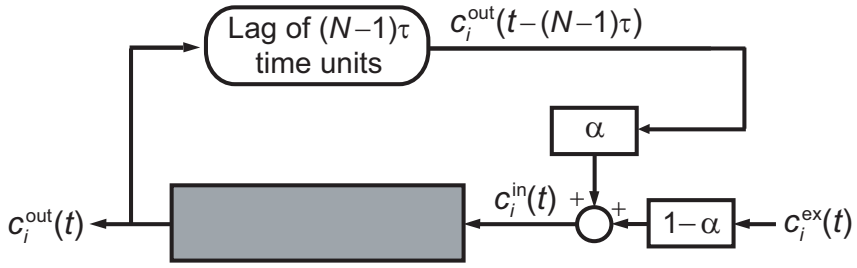

Figure 14: Block diagram of node balance for the ideal single-column chromatographic model analogous to an SMB process. $\alpha = Q_{\text{II}}/Q_{\text{III}}$, $c_i^{\text{ex}} = c_i^{\text{F}}$ (feed mode); $\alpha = Q_{\text{IV}}/Q_{\text{I}}$, $c_i^{\text{ex}} = c_i^{\text{E}}$ (eluent mode); $\alpha = 1$, $c_i^{\text{ex}} = 0$ (otherwise).

A comparison between the complete operating cycle of the simplest four-zone SMB (the one with port configuration 1/1/1/1) with that of the equivalent single-column model is highlighted in Figure 2. It is seen that the single-column model is obtained by selecting an arbitrary column (shaded area) of the SMB unit and following its operation over a complete cycle. The recycle streams from the other columns of the SMB are replaced by the recycle stream of the single-column at previous times. Under CSS conditions the two models cannot be discriminated, except for the discontinuous use of the inlet/outlet lines by the single-column model. Under these circumstances the SMB process is equivalent to N identical single-column processes operating in parallel with phase lags of τ time units.

2.3 Practical implementation of the single-column chromatograph with recycle lag

The implementation of our single-column chromatographic process with recycle lag, which mimics an SMB with port configuration 1/1/1/1 is illustrated in Figure 15. The chromatographic column is connected in loop to a plug-flow tube, which has a spring-actuating piston at one end. The spring is continuously pushing the piston against the fluid. The movement of the piston compensates for the difference between the inlet and outlet flow rates. The tube has internal elements, or packing, to breakup the velocity distortion (Poiseuille flow), due to the no-slip of the fluid at the tube wall, and to provide a flow which is as close as possible to plug flow.

The operation of the single-column process shown in Figure 15 is as follows. During the first switching interval of a cycle the column is operating as if it were in section III of the equivalent SMB. The recycle stream is pumped from the tube with flow rate $Q\mathrm{II} = \epsilon v\mathrm{II}A_\mathrm{c}$, where A_c is the cross-sectional area of the chromatographic column, is mixed with the feed, and inputted to the column with interstitial velocity $v\mathrm{III}$. Part of the outlet stream of the column is collected as raffinate with flow rate $Q_\mathrm{R} = \epsilon(v\mathrm{III} - v\mathrm{IV})A_\mathrm{c}$, the rest is fed to the recycle tube with flow rate $Q\mathrm{IV} = \epsilon v\mathrm{IV}A_\mathrm{c}$. Given that $Q\mathrm{II} > Q\mathrm{IV}$, the piston expands to compensate for the reduction of liquid in the recycle tube. During the second and fourth switching intervals the chromatographic column is, respectively, in section II and section IV of the equivalent SMB system. In both cases the separation unit operates in closed loop with liquid being fed and withdrawn from the recycle tube at the same rate. The piston is stationary during both switching intervals. During the third switching interval the column is in section I; part of its outlet stream is withdrawn as product (extract) with flow rate $Q_\mathrm{X} = \epsilon(v\mathrm{I} - v\mathrm{II})A_\mathrm{c}$, the rest is fed to the recycle tube with flow rate $Q\mathrm{II}$. Liquid is pumped from the recycle tube with flow rate $Q\mathrm{IV}$, diluted with fresh eluent, and fed to the column with interstitial velocity $v\mathrm{I}$. Since $Q\mathrm{II} > Q\mathrm{IV}$, the piston contracts to accommodate the extra liquid that is being accumulated in the recycle tube.

The proposed single-column process can be equally applied to asynchronous operation and parameter modulation over the switching interval. To better understand the concept and operation of our single-column process, the operation of an SMB, Varicol, and analogous single-column models, are illustrated schematically in Figure 16 over two switching intervals. The Varicol process is based on an asynchronous shift of the inlet and outlet ports; this is in contrast to the SMB process which employs a synchronous

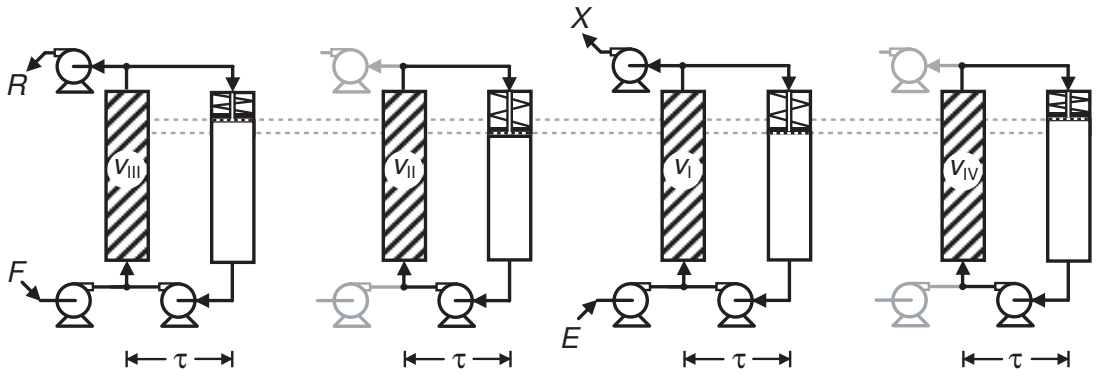

Figure 15: Schematic of the single-column chromatographic process with recycle lag proposed in this work analogous to a four-zone SMB. The chromatographic column is connected to a plug-flow tube with a piston at one end. The tube implements a recycle lag of $(N-1)\tau$ time units. The movement of the piston compensates for the difference in flow rates at the inlet and outlet of the tube which occur during some steps of the cycle. The complete cycle depicted here is for the configuration equivalent to a 4-column SMB unit. The feed, eluent, raffinate and extract streams are identified by letters F, E, R, and X, respectively.

shift of the inlet/outlet lines. For the two-subinterval VARICOL process shown in Figure 16, the column configuration changes from 1/1/2/1, over the first half of the switching interval, into 1/2/1/1, over the second half of the switching interval, by shifting the feed port forward by one column, and finally returning to the original configuration of 1/1/2/1 by shifting the eluent, extract and raffinate ports one column forward. As a result, in this two-subinterval VARICOL process, there are two different column configurations during a switching interval due to the local shifting of the ports. The number of columns in one zone varies with time within a switching interval, but the number of columns in each zone returns to the starting value at the end of the switching interval. In terms of average number of columns per zone this corresponds to a 1/1.5/1.5/1 configuration. The asynchronous port switching of a VARICOL system adds extra degrees of freedom that can be optimized for enhanced productivity or reduced solvent consumption. This leads to a mixed integer nonlinear problem, whose solution procedure is in general quite complex [35]. For example, a port may shift more than once during a switching interval and can temporarily move back. As a result, VARICOL processes have a very large number of column configurations.

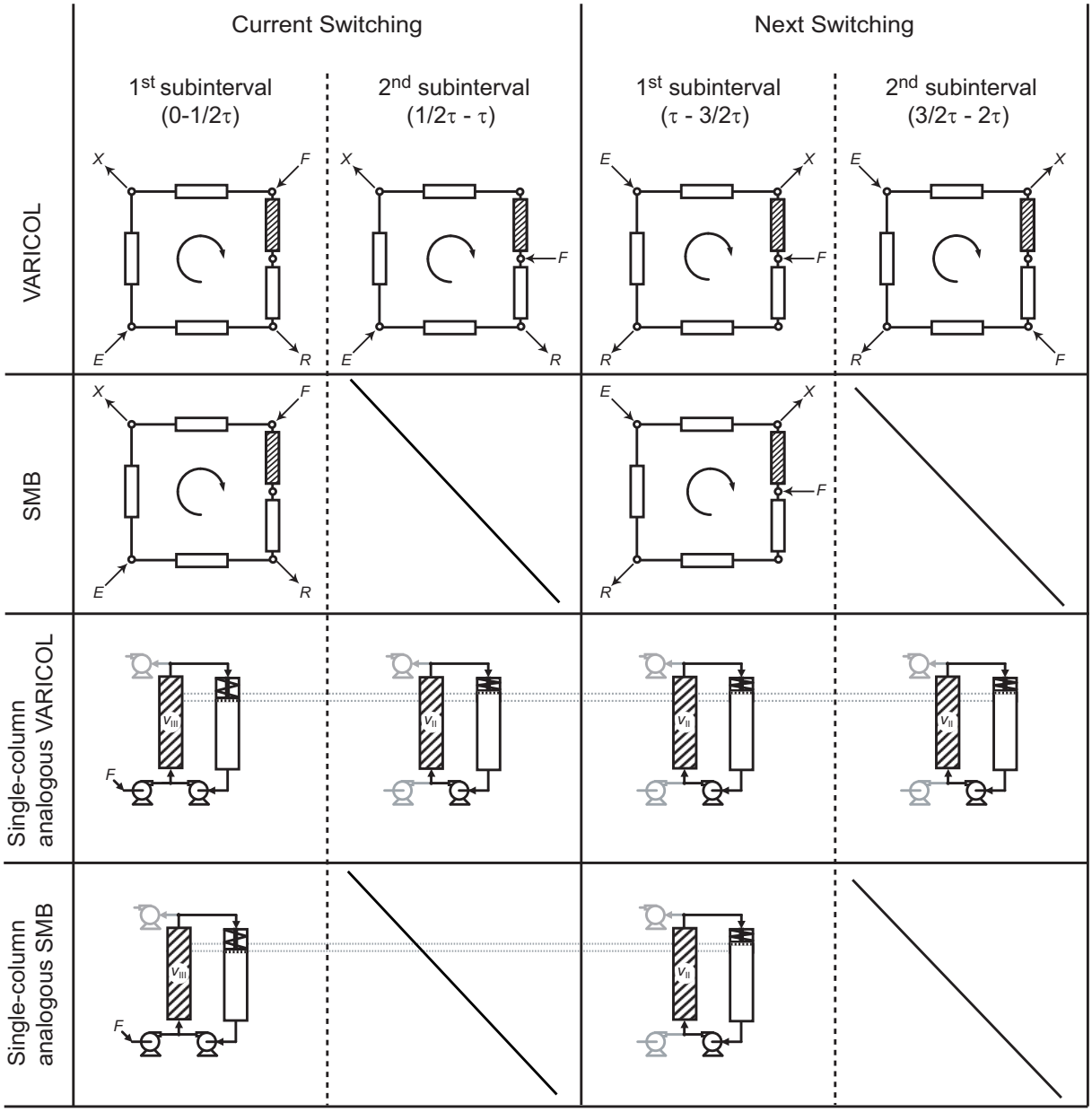

Figure 16: Principle of operation of SMB and two-subinterval VARICOL system and respectives single-column analogs for two switching intervals. The five-column SMB and VARICOL configurations are respectively 1/1/2/1 and 1/1.5/1.5/1. The single-column models are obtained by selecting an arbitrary column (outlined area) of the SMB and VARICOL unit respectively, and following its operation over the two switching intervals.

The analogous single-column models are obtained by selecting the outlined column in Figure 16 of the SMB and VARICOL process respectively. The operation of the single-column process analogous VARICOL show in Figure 16 is as follow. During the first subinterval of the current switching $(0 - \frac{1}{2}\tau)$ the column is operating as if it were in section III of the equivalent VARICOL process. The recycle stream is pumped from the tube with flow rate QII and is mixed with the feed, and inputted to the column with interstitial velocity vIII. The outlet stream of the column is fed to the recycle tube with flow rate QIII. Given that QIII $>$ QII, the piston contracts to accommodate the extra

liquid that is being accumulated in the recycle tube. During the second subinterval of the current switching ($\frac{1}{2}\tau - \tau$) and the first ($\tau - \frac{3}{2}\tau$) and second ($\frac{3}{2}\tau - 2\tau$) subintervals of the next switching the column is operating as if it were in section II of the equivalent VARICOL system. In the three cases the separation unit operates in closed loop with liquid being fed and withdrawn from the recycle tube at the same rate. The piston is stationary during the three subintervals.

2.4 Analysis, applications and results

For brevity of presentation, a single case of chromatographic separation is analyzed here. The conclusions however, are of general applicability. The selected case study is the binary separation of binaphthol enantiomers on cellulose triacetate using heptane-isopropanol (72:28) as eluent [18]. The adsorption equilibrium is well described by a bi-Langmuir competitive isotherm model [36].

The analysis is carried out for four different SMB port configurations: one (1/1/1/1) and two (2/2/2/2) columns per section, five columns (1/2/1/1), six columns (1/2/2/1), and seven columns (2/2/2/1). The analysis is also extended to three different VARICOL port configurations: five columns (1/1.5/1.5/1), six columns (1.5/1.5/1.5/1.5), and seven columns (1.5/2/1.5/2).

A suitable set of operating parameters was obtained by minimizing the flow ratio $Q_{\mathrm{E}}/Q_{\mathrm{F}}$ for two SMB port configurations with one (1/1/1/1) and two (2/2/2/2) columns per section. The operating parameters for the other SMB configurations were adapted from the four-column SMB (1/1/1/1), while maintaining the same flow rates and the cycle duration ($N\tau$ time units) and scaling switching interval by a factor of $4/N$. The operating parameters for the VARICOL configurations were obtained from the 4-column SMB, by scaling the overall switching interval by a factor of $4/N$ and then dividing it into two sub-switching intervals of equal size. The model parameters and operating conditions for the binary separation are listed in Table 4.

The objective of the present work is not to report a full process optimization study. Our aim is to demonstrate the applicability of our single-column process to asynchronous operation and show the benefits obtained by adopting this operating scheme.

We define a Péclet number, $\widetilde{\mathrm{Pe}}$, for hydrodynamic dispersion in the plug-flow tube, as

$$\widetilde{\mathrm{Pe}} = u_{\mathrm{t}} L_{\mathrm{t}} / \tilde{D}, \tag{46}$$

where u_{t} is the velocity at which the fluid is withdrawn from the tube and L_{t} is the

Table 4: Model parameters and operating conditions for the test case of binary separation of binapthol enantiomers by SMB chromatography.

Zone length, $L_j N/4$ (cm)	21.0	Péclet number, Pe	$\widetilde{\mathrm{Pe}} = v_j L_j / D = 2000$
Column diameter, d (cm)	2.6	LDF coeficients, k_i (s^{-1})	0.1, 0.1
Porosity, ϵ	0.4	Feed concentration, c_i^{F} (g/l)	2.9, 2.9
Bi-Langmuir isotherm, q_i^* (g/l)		$\dfrac{2.69c_{\mathrm{A}},\ 3.73c_{\mathrm{B}}}{1+0.0336c_{\mathrm{A}}+0.0466c_{\mathrm{B}}} + \dfrac{0.1c_{\mathrm{A}},\ 0.3c_{\mathrm{B}}}{1+c_{\mathrm{A}}+3c_{\mathrm{B}}}$	

Flow rate (ml/min)	SMB 1/1/1/1	SMB 2/2/2/2
Feed, Q_{F}	7.31	3.30
Eluent, Q_{E}	22.70	12.23
Raffinate, Q_{R}	9.36	5.26
Extract, Q_{X}	16.65	10.27
Recycle, Q	28.87	21.30

Port configuration	τ (min)
SMB 1/1/1/1	6.69
SMB 1/2/1/1	$\frac{4}{5} \times 6.69$
SMB 1/2/2/1	$\frac{4}{6} \times 6.69$
SMB 2/2/2/1	$\frac{4}{7} \times 6.69$
VARICOL 1/1.5/1.5/1	$\frac{4}{10} \times 6.69$
VARICOL 1.5/1.5/1.5/1.5	$\frac{4}{12} \times 6.69$
VARICOL 1.5/2/2/1.5	$\frac{4}{14} \times 6.69$
SMB 2/2/2/2	4.78

average effective length of the tube (as measured from the piston to the other end of the tube). The dispersion coefficient $\tilde{D}$ accounts for the spread of the concentration profiles by the presence of molecular diffusion and velocity distortion (hydrodynamic dispersion). Here, $\widetilde{\mathrm{Pe}}$ is used as a general parameter to account for deviations from perfect plug flow in the tube, and to demonstrate the practical need for an efficient plug-flow device for the system to work correctly.

The purity results are summarized in Figure 17, where it is shown that, as the value of $\widetilde{\mathrm{Pe}}$ is increased, the purities of our single-column process approach those of the equivalent SMB and VARICOL processes.

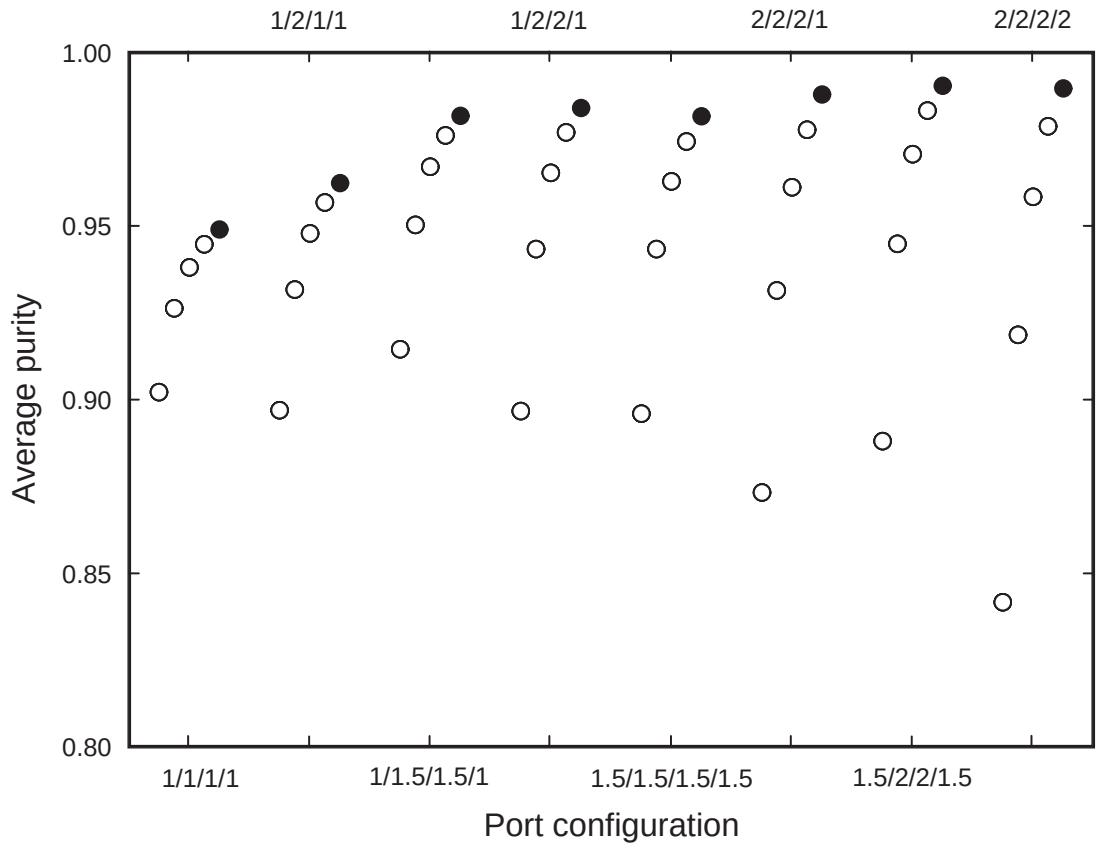

Figure 17: Average purity for the single-column process proposed here (∘; the value of $\widetilde{\mathrm{Pe}}$ is, from left to right, 500, 1000, 2000, and 5000), and the equivalent four-section SMB and VARICOL (•) processes. Note that the closed circles also denote purities for the proposed single-column process when $\widetilde{\mathrm{Pe}} \to \infty$.

Figure 18 shows the spatial profile of solute concentration in the liquid phase over the four sections of the SMB mimicked by the single-column process for two port configurations: (a) 1/2/1/1 and (b) VARICOL 1/1.5/1.5/1. This figure gives some insight into the mechanism by which $\widetilde{\mathrm{Pe}}$ influences product purity.

The data plotted in Figure 18 were obtained at CSS. To generate each spatial concentration profile, we took several snapshots of the profile in the column of the analog with a sampling period equal to τ (as indicated in the respective graphic) and them plotted them sequentially. Notice that the number of snapshots of the spatial concentration profile require to construct the profile spanning the four sections of the equivalent VARICOL (1/1.5/1.5/1) is the double of the snapshots of the SMB (1/2/1/1), because the VARICOL is obtained by dividing the switch interval (τ) of the SMB in two sub-switch intervals.

Dispersion tends to reduce solute concentration where it is higher and increase it where it is lower. This has a double negative effect on product purity, since its decrease the concentration of the target solute near its withdrawal point and increases that of the impurity. These results demonstrate the practical need for an efficient plug-flow device

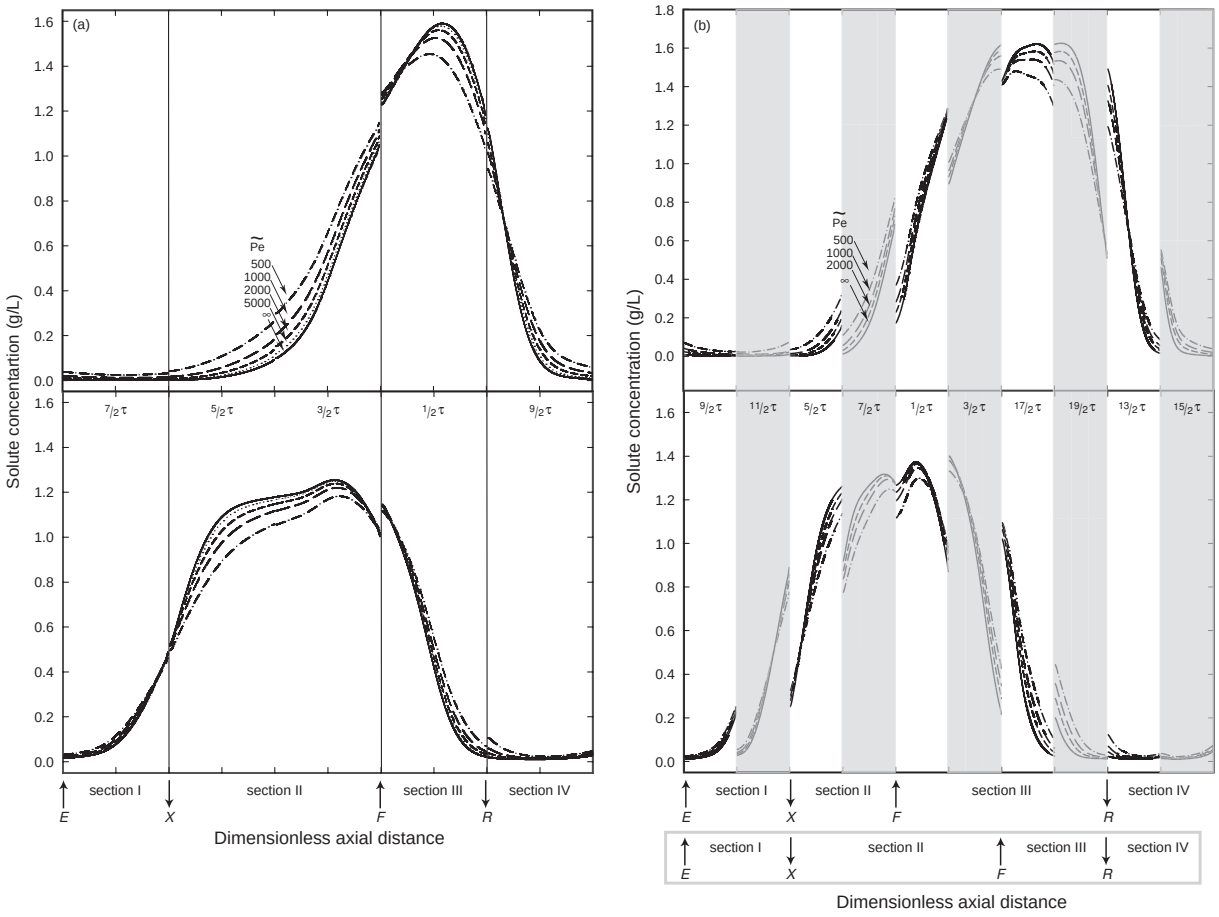

Figure 18: Spatial concentration profiles of less-retained (top plot) and more-retained component (bottom plot) at the middle of a switch interval, for the proposed single-column process analogous to (a) four section SMB with port configuration 1/2/1/1 and (b) four section VARICOL with port configuration 1/1.5/1.5/1. The results are given for various values of the hydrodynamic Péclet number in the recycle tube, $\widetilde{\mathrm{Pe}}$, and were obtained after the system attained CSS conditions. To construct the spatial concentration profile spanning the four sections of the equivalent SMB (a), five snapshots of the profile in the column were taken with a sampling period equal to τ (as indicated in the graphics). Notice that the number of snapshots of the spatial concentration profile required to construct the profile spanning the four sections of the equivalent VARICOL (b) is the double of the snapshots of the SMB (a), because the VARICOL is obtained by dividing the switch interval (τ) of the SMB in two sub-switch intervals.

for the system to work efficiently. Deviations from plug flow in the recycle tube can be compensated by performance improvements obtained through numerous possibilities of parameter variation during a switch interval. These novels cycles add extra flexibility to our process and the improvement performance obtained compensates for a less perfect operation of the recycle tube. For example, it is seen in Figure 17 that the purities obtained with our single-column process mimicking the 1/1.5/1.5/1 and 1.5/2/2/1.5 VARICOL configurations are higher, for all the values of $\widetilde{\mathrm{Pe}}$, than the corresponding five- and seven-columns SMB configurations.

Figure 19 shows chronograms of port switching for the two different five columns configurations disclosed in Figure 18. The top chronogram reproduces the five columns SMB process (1/2/1/1), and the bottom chronogram describes the asynchronous port switching for a five columns VARICOL process with average number of columns per zone 1/1.5/1.5/1.

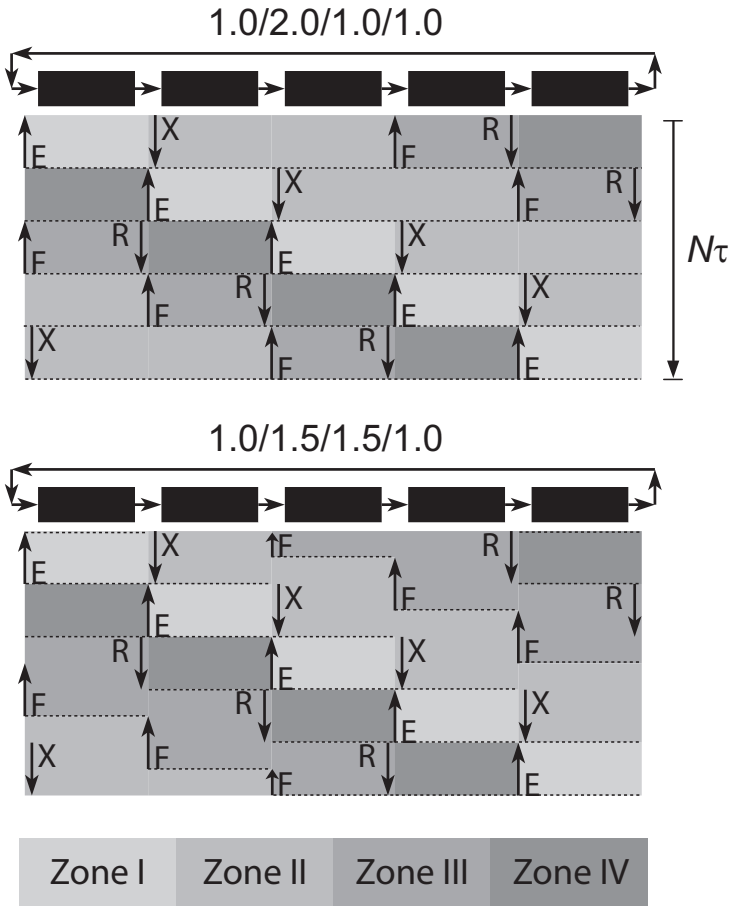

Figure 19: Chronograms of port switching for the SMB with port configuration 1/2/1/1 and VARICOL with port configuration 1/1.5/1.5/1 referred in figure 18.

2.5 Conclusions

The single-column system proposed in this work is a more compact, less-expensive, and simpler to operate alternative to the SMB that can potentially achieve the same purities while keeping the same specific productivity. Because the process uses a single column, the need to obtain adequate packing reproducibility on several columns is not an issue.

The versatility of our single-column process allows the application of numerous possibilities for improving the SMB performance, through variation of parameters during the switch interval. The implementation of the VARICOL concept to our system improved its performance, compensating for a less perfect operation the recycle tube. This advantage is retained when other cyclic operations policies, such as Power-Feed [10] or ModiCon [37], are applied to our single-column process.

Appendix

The purpose of this appendix is to briefly describe the numerical method employed to solve Eq. 32. We demonstrate the validity of Eq. 32 to describe the axially dispersed flow in the recycle tube, and adequacy of the numerical procedure, by solving some test problems for which the analytical solution is easily derived. Since the same basic flow mechanism is assumed to govern solute transport in the chromatographic column, it is not surprising that the same numerical method was used to solve the governing equations for the chromatographic column.

We employ the method-of-lines approach [26] to solve the conservation equations. The control-volume method [27] is applied to the spatial domain to convert the partial differential equations into a large system of differential-algebraic equations (DAEs) to which an efficient DAE solver is applied. In order to prevent non-physical oscillations of the solution, the convective terms were discretized by the van Leer harmonic flux-limited scheme, implemented in the form advocated by Waterson and Deconinck [28]. The chromatographic column and the recycle tube are divided into 50 and 200 equally-sized control volumes, respectively. The resulting DAEs, together with additional constraints (node balance) introduced to characterize the interactions between sub-models of the process, are solved using gPROMS (general PROcess Modelling System), a software package for the modeling and simulation of processes with combined discrete and continuous characteristics (Process Systems Enterprise, http://www.psenterprise.com). Inside gPROMS, the DAE system is integrated over time using the DASOLV code [29] with absolute and relative tolerances of 10^{-5}. We note that gPROMS also allows the direct modelling of systems described by partial differential equations; the numerical discretization is applied automatically to these equations reducing them to DAEs. However, the package does not currently implement the control-volume method with flux-limited correction, which we favor over other discretization methods. More information on the package can be found elsewhere [30, 31].

In the first numerical experiment (Figure 20), we simulate the injection of a rectangular pulse of tracer at infinite Péclet number ($\widetilde{\mathrm{Pe}} = \infty$), under conditions where the outlet flow rate is twice that of the inlet ($\tilde{u}_{\mathrm{R}}/\tilde{u}_{\mathrm{L}} = 2$). In this case the piston reduces the effective length of the tube to compensate for the liquid that is withdrawn in excess to the feed value. Since the exit flow rate is twice that of the feed, the width of the outputted pulse is reduced to half of that of the injected pulse (top plot of Figure 20).

At dimensionless instant $\tilde{u}_{\mathrm{R}}t = 0.9$ (bottom plot of Figure 20), the right side of the pulse is located at $\xi = (0.9 - 0.9/2)/(1 - 0.9/2) = 0.82$, and the left side is positioned at $\xi = (0.5/2+(0.9-0.5)-0.9/2)/(1-0.9/2)$. It is seen that there is good agreement between the numerical and analytical solutions, although the former introduces some numerical dispersion.

Figure 21 summarizes the results obtained in the second test, which simulates the dispersive transport at low Péclet number ($\widetilde{\mathrm{Pe}} = 500$) of a rectangular profile of tracer. Again, the flow rates are such that $\tilde{u}_{\mathrm{R}}/\tilde{u}_{\mathrm{L}} = 2$. Since at the initial instant the rectangular profile is fully contained within the tube, and sufficiently distant from the piston, its dispersive transport is not affected by the movement of the piston. Thus, the problem can be solved using Eq. 26 on a fixed grid and the results subsequently mapped onto the dimensionless coordinate ξ. The numerical solution obtained by this approach is in perfect agreement with the solution obtained by solving Eq. 32.

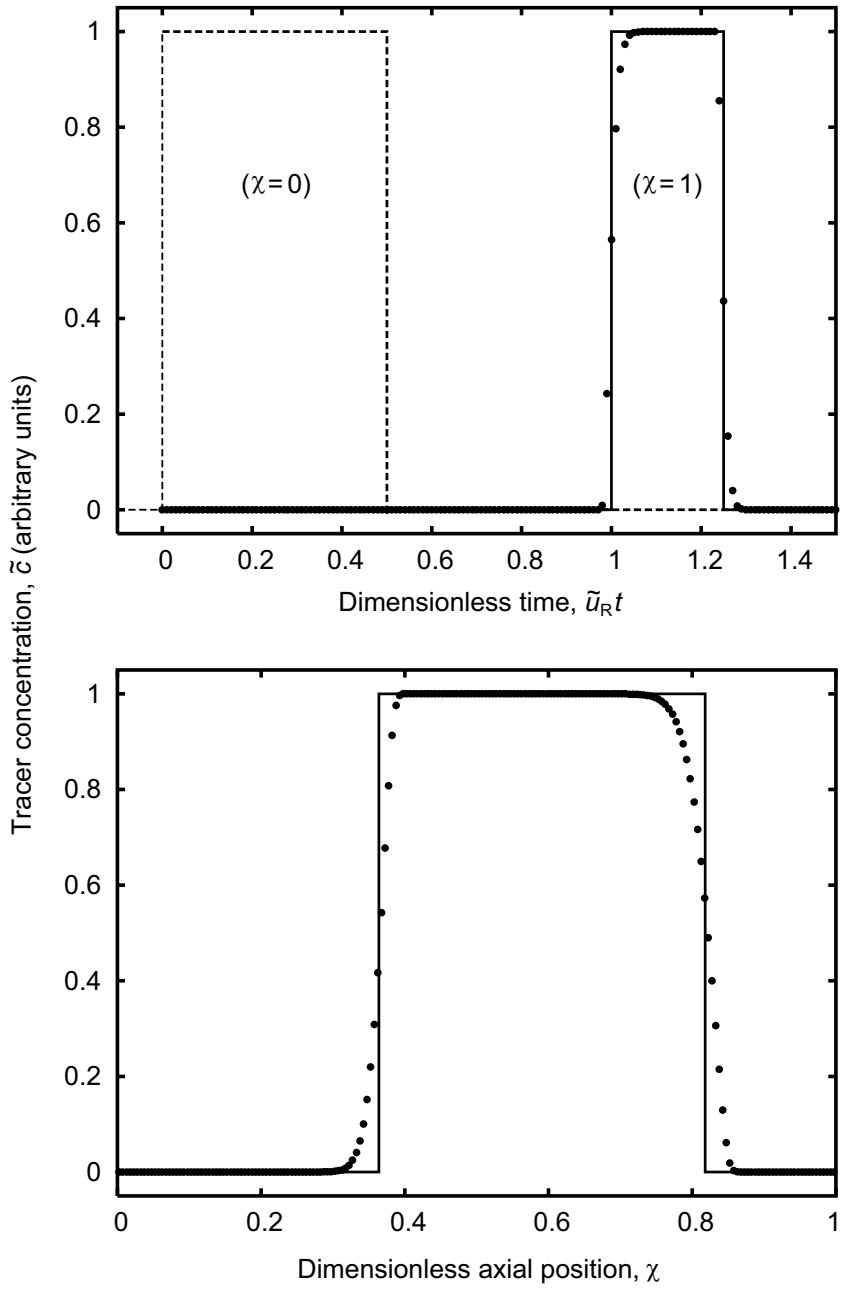

Figure 20: The first of a pair of numerical experiments to validate Eq. 32 and the numerical method for solving it. This test simulates the injection of a rectangular pulse of tracer (dashed line) at infinite Péclet number (no hydrodynamic dispersion) under conditions where $\tilde{u}_R/\tilde{u}_L = 2$, i.e. liquid is withdrawn with flow rate which is twice that of the feed. The symbols are the numerical solution of the corresponding breakthrough curve (top plot) and spatial profile at dimensionless time $\tilde{u}_R t = 0.9$ (bottom plot); both are in very good agreement with the analytical solution (solid lines).

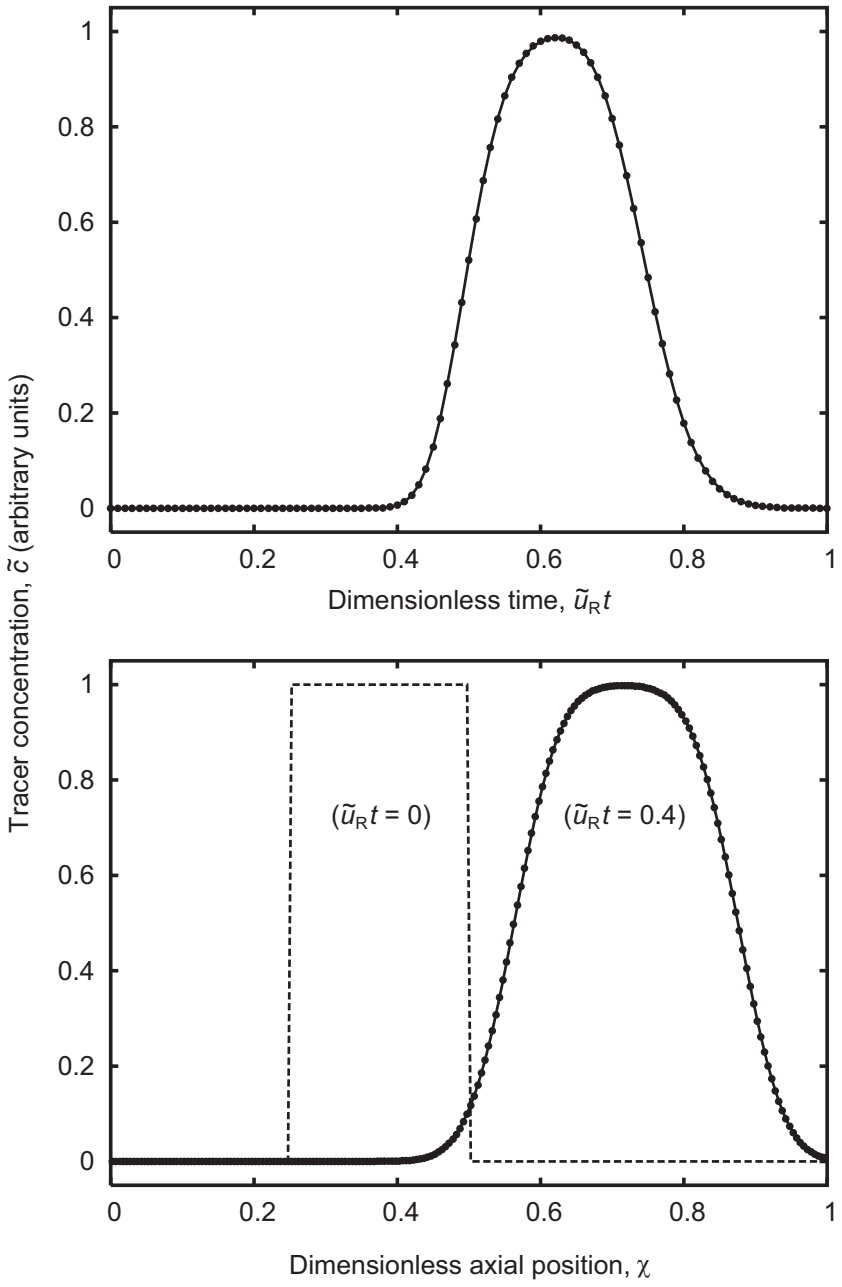

Figure 21: The second of a pair of numerical experiments to validate Eq. 32 and the numerical method for solving it. This test simulates the dispersive transport ($\widetilde{\mathrm{Pe}} = 500$) of a rectangular profile of tracer (dashed line) initially contained within the tube. Again, the flow rates are such that $\tilde{u}_\mathrm{R}/\tilde{u}_\mathrm{L} = 2$. Since the inlet boundary condition for the tracer concentration is simply $\tilde{c}_i(0,t) = 0$, the problem can also be solved using Eq. 26 in a fixed grid provided that the internal tracer profile is adjusted to the true length of the tube. The symbols are the numerical solution of the corresponding breakthrough curve (bottom plot) and spatial profile at dimensionless time $\tilde{u}_\mathrm{R} t = 0.4$ (top plot) using Eq. 32; both are in excellent agreement with the numerical solution of Eq. 26 obtained in a fixed grid (solid lines).

Nomenclature

A	column cross-sectional area (cm^2)
c	solute concentration (g/l)
d	column diameter (cm)
D	axial dispersion coefficient (cm^2/min)
$\widetilde{D}$	axial dispersion coefficient in recycle tube (cm^2/min)
k	LDF coefficient (s^{-1})
L	column length (cm)
M_τ	tanks filled/emptied during switching interval
N	number of columns/tanks
$\widetilde{\mathrm{Pe}}$	Péclet number
q	adsorbed concentration (g/l)
Q	flow rate (cm^3/min)
t	time (min)
t'	time (min) which references a single-column, $t-(N-1)\tau$
u	liquid velocity in recycle tube (cm/min)
v	interstitial fluid velocity (cm/min)
x	axial position in recycle tube (cm)
z	axial position in column (cm)

Greek letters

α	interstitial velocity ratio
ϵ	total porosity
ϕ	porosity ratio, $(1-\epsilon)/\epsilon$
τ	switching interval (min)
τ_m	tank filling/empting time (min)
θ	dimensionless time, t/τ
ξ	dimensionless axial position in recycle tube, $(x-x_\mathrm{L})/(x_\mathrm{R}-x_\mathrm{L})$

Subscripts and superscripts

E	eluent
ex	external inlet stream
F	feed
i	solute index
I,...,IV	zone index

in	column inlet
j	column index
(j)	slice of liquid in recycle tube index
out	column outlet
R	raffinate
t	recycle tube
X	extract
$\tilde{}$	discrete value

List of Tables

List of Figures

Bibliography

[1] M. Juza, M. Mazzotti, M. Morbidelli, Trends in Biotech. 18 (2000) 108.

[2] R.M. Nicoud, LC-GC 5 (1992) 43.

[3] A. Jupke, A. Epping, H. Schmidt-Straub, J. Chromatogr. A 944 (2002) 93.

[4] J. Strube, S. Haumreisser, H. Schmidt-Traub, M. Schulte, R. Ditz, Org. Proc. Res. Devel. 2 (1998) 305.

[5] P.C. Wankat, Rate-Controlled Separations, Kluwer, Amsterdam, 1990.

[6] O. Ludemann-Hombouger, R.M. Nicoud, M. Bailly, Sep. Purif. Techn. 35 (2000) 1829.

[7] J.P.B. Mota, J.M.M. Araújo, AIChE J. 51 (2005) 1641.

[8] D. Antos, A. Seidel-Morgenstern, Chem. Eng. Sci. 56 (2000) 6667.

[9] Y. Zang, P.C. Wankat, Ind. Eng. Chem. Res. 41 (2002) 2504.

[10] Z.Y. Zhang, M. Mazotti, M. Morbidelli, J. Chromatogr. A 1006 (2003) 87.

[11] H. Schramm, M. Kaspereit, A. Kienle, A. Seidel-Morgenstern, Chem. Eng. Sci 58 (2003) 5217.

[12] S. Lehoucq, D. Verhève, A.V. Wouwer, E. Cavoy, AIChE J. 46 (2000) 247.

[13] R.M. Nicoud, R.E. Majors, LC-GC 18 (2000) 680.

[14] L.S. Pais, A.E. Rodrigues, J. Chromatogr. A. 1006 (2003) 33.

[15] O. Ludemann-Hombourger, M. Bailly, R.M. Nicoud, Sep. Sci. Techn. 35 (2000) 1285.

[16] N. Abunasser, P.C. Wankat, Y.S. Kim, Y.M. Koo, Ind. Eng. Chem. Res. 42 (2003) 5268.

[17] N. Abunasser, P.C. Wankat, Ind. Eng. Chem. Res. 43 (2004) 5291.

[18] L.S. Pais, J.M. Loureiro, A.E. Rodrigues, Sep. Purif. Techn. 20 (2003) 67.

[19] L.S. Pais, J.M. Loureiro, A.E. Rodrigues, Chem. Eng. Sci. 52 (1997) 245.

[20] L.S. Pais, J.M. Loureiro, A.E. Rodrigues, J. Chromatogr. A. 769 (1997) 25.

[21] D.M. Ruthven, C.H. Ching, Chem. Eng. Sci. 44 (1989) 1011.

[22] C. Migliorini, A. Gentilini, M. Mazotti, M. Morbidelli, Ind. Eng. Chem. Res. 38 (1999) 2400.

[23] D.M. Ruthven, C.B. Ching, In: Ganetsos G., Barker P. E. Preparative and Production Scale Chromatography. New York: Marcel Dekker, 1993:629.

[24] E. Kloppenburg, E.D. Gilles, Chem. Eng. Technol. 22 (1990) 10.

[25] J.M.M. Araújo, R.C.R. Rodrigues, J.P.B. Mota, Ind. Eng. Chem. Res. 45 (2006) 5314.

[26] W.E. Schiesser, The Numerical method of lines. New York: Academic Press, 1991.

[27] S.V. Patankar, Numerical Heat Transfer and Fluid Flow. New York: McGraw-Hill, 1980.

[28] N.P. Waterson, H. Deconinck, A unified approach to the design and application of bounded higher-order convection schemes. In: Taylor C, Durbetaki P. Numerical Methods in Laminar and Turbulent Flow. Swansea, UK: Pineridge Press, 1995:203.

[29] R.B. Jarvis, C.C. Pantelides, DASOLV—a differential-algebraic equation solver. Technical report, Center for Process Systems Engineering, Imperial College, 1992.

[30] P.I. Barton, C.C. Pantelides, AIChE J. 40 (1994) 966.

[31] M. Oh, C.C. Pantelides, Comp. Chem. Eng. 20 (1996) 611.

[32] N. Abunasser, P.C. Wankat, Sep. Sci. Technol. 40 (2005) 3239.

[33] N. Abunasser, P.C. Wankat, AIChE J. 52 (2006) 2461.

[34] J.M.M. Araújo, R.C.R. Rodrigues, J.P.B. Mota, Ads. Sci. Tech. 25 (2006) 647.

[35] J.M.M. Araújo, R.C.R. Rodrigues, J.P.B. Mota, J. Chromatogr. A 1132 (2006) 76.

[36] R.M. Nicoud, A. Seidel-Morgenstern, Adsorption isotherms: experimental determination and application to preparative chromatography, in R.M Nicoud (ed.), Simulated Moving Bed Basics and Applications, INPL, Nancy, France, 1993.

[37] H. Schramm, M. Kaspereit, A. Kienle, A. Seidel-Morgenstern, Chem. Eng. Technol. 25 (2002) 1151.

Chapter 2

Use of Single-column Models for Efficient Computation of the Periodic State of Simulated Moving-Bed Process

1 Introduction

Simulated moving bed (SMB) chromatography has been increasingly applied for the separation of pure substances in the pharmaceutical, fine chemistry, and biotechnology industries, at all production scales, from laboratory to pilot to production scale [1]. The SMB has many advantages with respect to discontinuous batch chromatography [2], such as higher product purity, less solvent consumption, and higher productivity per unit stationary phase [3–5].

The SMB is a practical way of implementing a counter-current chromatographic process. The system consists of N identical chromatographic columns connected in series to build a closed loop. By moving the input and withdrawal ports one column ahead (i.e. in the direction of fluid flow) at fixed intervals, the counter-current contact between the adsorbent and liquid is simulated. A schematic diagram of a typical four-section SMB is shown in Fig. 1.

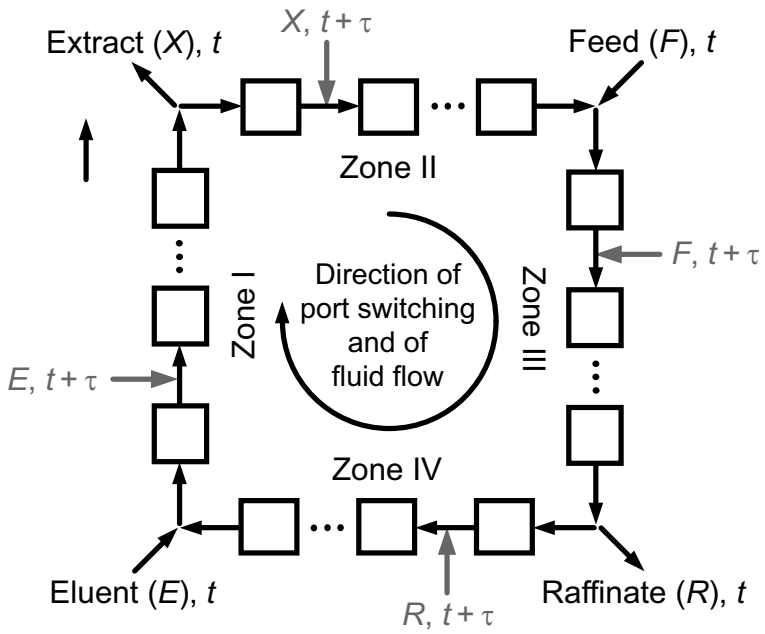

Figure 1: Schematic diagram of a four-section SMB unit. Several chromatographic columns are interconnected circularly, the input and withdrawal ports are moved one column ahead every τ time units. The feed, eluent, extract and raffinate streams are denoted by F, E, X and R, respectively.

Thanks to recent developments in cyclic operation policies, a number of possibilities for improving SMB performance have emerged through variation of parameters during a switching interval. These include, among others, the non-synchronous shift of the inlet and outlet ports within a global switching period [6, 7], modulation of solvent strength during

process operation [8–11], and cyclic modulation of feed flow [12–16] and feed concentration [17, 18]. These advances are pushing the trend toward the use of units with smaller number of columns, since less stationary phase is used and the setup is more economic. In many cases it would be advantageous to work with the limiting case of a single column. Because only one column would have to be repacked, switching from one mixture to another would be easier and take less time than with an SMB. It has been recently shown that this can be achieved by one-column analog processes [19–21], which mimic the operation of an SMB with a single chromatographic column.

The optimal design and selection of optimal operating parameters are essential to realize the economic potential of nonstandard SMB operating modes and their successful implementation on industrial scale. These call for the use of advanced optimization procedures coupled with a detailed dynamic model of process dynamics. The complexity of the optimization problem is increased further by the intrinsic dynamic nature of the process, which approaches a cyclic steady state after a sufficiently long period of time. This is due to the circular arrangement of the columns and the periodic nature of the port switching. For process design the initial transient behavior is of little interest, but only the fully established periodic state. In most cases, the latter has been computed by direct dynamic simulation of the whole process unit. Often, the hypothetical true moving-bed (TMB) process is used as a simplified model for the SMB. The TMB model is continuous and has a stationary state which can be computed easily. However, if a small number of columns is used, or the operating parameters are varied during a switching interval, the system behavior deviates significantly from the classical SMB process and precludes the application of the TMB analogy.

A detailed SMB process model is computationally expensive. While for exploratory or small parametric studies the computing time is not an issue, that may no longer the case for rigorous model-based optimization [3, 22–25], especially when the number of optimization variables is increased by the extra degrees of freedom in the operating conditions of nonstandard SMB processes [26–28]. It is thus apparent that the increasing complexity of the optimization problems addressed in preparative chromatography calls for efficient methods to compute the periodic state. However, with a few exceptions [22, 29], little has been published on this issue. The present work is concerned with establishing a rigorous mathematical framework for this task.

The current work [30] (**paper II**) establish a general mathematical formulation of all single-column chromatographic processes that replicate the equivalent SMB operation, and use it to develop efficient methods to calculate the periodic state. The formulation and methods presented are equally applicable to the nonstandard SMB processes discussed above. Since the models employ a single chromatographic column, their numerical solution is easy to implement and is computationally cheap. The solution methods can be classified into two major classes: dynamic methods which integrate in time, either truly or artificially, the governing equations over a large number of cycles until CSS is reached, and methods which rely on the direct prediction of the CSS by simultaneously discretizing the spatial and temporal coordinates, thereby transforming the model into a large sparse system of nonlinear algebraic equations.

The various solution methods are compared for the separation of two different binary mixtures. The first case is an enantiomeric separation; the corresponding isotherms are of the bi-Langmuir type. The second case is derived from the first one by fitting a linear isotherm model to a series of simulated band profiles of the bi-Langmuirian binary mixture. These two cases are sufficiently different, in terms of isotherm model and selected operating parameters, for their overall analysis to provide conclusions of general applicability. The performance of each solution method is measured in terms of CPU time, number of cycles to attain CSS, and CPU time per cycle.

2 Mathematical formulation

In the notation employed here the columns are numbered sequentially in the direction of liquid flow. Because they are connected circularly, and in order not to overload the notation, throughout this paper the column index is implicitly defined modulo N. Thus, $j = 0$ actually means column N, whereas $j = N + 1$ is the same as referring to column 1.

Let us consider the node between two consecutive columns, say $j-1$ and j, of an SMB unit, as depicted in Fig. 2. The notation employed is as follows: v is the interstitial liquid velocity, $c^{\text{out}}_{i,j-1}(t)$ is the concentration of solute i at the outlet of column $j-1$, $c^{\text{in}}_{ij}(t)$ is the corresponding solute concentration at the inlet of column j, and $c^{\text{ex}}_{ij}(t)$ is the solute concentration in the external inlet stream (either eluent or feed), if the corresponding port is opened.

The individual solute material balance at the node expresses c_{ij}^{in} as a weighted average of $c_{i,j-1}^{\text{out}}$ and c_{ij}^{ex}:

$$c_{ij}^{\text{in}} = \alpha_j \, c_{i,j-1}^{\text{out}} + (1 - \alpha_j) \, c_{ij}^{\text{ex}}, \quad \alpha_j = \frac{\min\{v_{j-1}, v_j\}}{v_j}, \tag{1}$$

where $\alpha_j(t)$ is the dynamic weighting factor.

At each instant the node can be in one of four states, which can be discriminated according to the sign of $v_j - v_{j-1}$ and to the value of c_{ij}^{ex}:

- Connecting node: $v_j = v_{j-1}$ ($\alpha_j = 1$);
- Eluent node: $v_j > v_{j-1}$ ($\alpha_j = v_{j-1}/v_j$) and $c_{ij}^{\text{ex}} = c_i^{\text{E}}$, where c_i^{F} is the solute concentration in the eluent stream (usually, $c_i^{\text{E}} = 0$);
- Feed node: $v_j > v_{j-1}$ ($\alpha_j = v_{j-1}/v_j$) and $c_{ij}^{\text{ex}} = c_i^{\text{F}}$, where c_i^{F} is the solute concentration in the feed stream;
- Extract and raffinate nodes: $v_j < v_{j-1}$ ($\alpha_j = 1$).

Notice that when both the feed and eluent ports are closed, i.e. $v_j \leq v_{j-1}$, Eq. (1) becomes independent of c_{ij}^{ex} because $\alpha_j = 1$ and $(1 - \alpha_j) \, c_{ij}^{\text{ex}}$ is equal to zero regardless of the value of c_{ij}^{ex}.

The cyclic operation of the SMB process is achieved by moving the input and withdrawal ports one column ahead (i.e. in the direction of fluid flow) every τ time units, where τ is the switch interval. Mathematically, this can be expressed as

$$v_j(t) = v(\theta_j), \quad c_{ij}^{\text{ex}}(t) = c_i^{\text{ex}}(\theta_j), \quad \theta_j = [t - (j-1)\tau] \bmod N\tau, \tag{2}$$

where $v(t)$ and $c_i^{\text{ex}}(t)$ are $N\tau$-periodic input functions and 'mod' defines the usual modulo operator: $a \bmod b \equiv a - b \, \text{int}(a/b)$. Note that Eq. (2) implies

$$v_{j+1}(t + \tau) = v_j(t), \quad c_{i,j+1}^{\text{ex}}(t + \tau) = c_{ij}^{\text{ex}}(t). \tag{3}$$

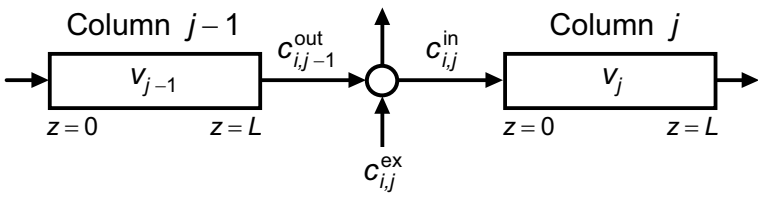

Figure 2: Schematic of node connecting columns $j-1$ and j of a SMB unit; $i = 1, 2$ is the solute index, $c(t)$ is the solute concentration in liquid phase, $v(t)$ is the interstitial fluid velocity, and $c^{\text{ex}}(t)$ is the concentration of an external inlet stream (either eluent or feed), if the corresponding port is opened.

The periodic operation of the classical SMB with column configuration $N_{\mathrm{I}}/N_{\mathrm{II}}/N_{\mathrm{III}}/N_{\mathrm{IV}}$ ($N = \sum_{k=\mathrm{I}}^{\mathrm{IV}} N_k$), i.e. N_{I} columns in section I, N_{II} columns in section II etc., is defined by the following piecewise constant periodic inputs:

$$v(\theta) = \begin{cases} v_{\mathrm{I}} & 0 \leq \theta < N_{\mathrm{I}} \\ v_{\mathrm{IV}} & N_{\mathrm{I}} \leq \theta < N_{\mathrm{I}} + N_{\mathrm{IV}} \\ v_{\mathrm{III}} & N_{\mathrm{I}} + N_{\mathrm{IV}} \leq \theta < N - N_{\mathrm{II}} \\ v_{\mathrm{II}} & N - N_{\mathrm{II}} \leq \theta < N \end{cases}, \quad c_{ij}^{\mathrm{ex}}(\theta) = \begin{cases} c_i^{\mathrm{E}} & N_{\mathrm{I}} - 1 \leq \theta < N_{\mathrm{I}} \\ c_i^{\mathrm{F}} & N - N_{\mathrm{II}} - 1 \leq \theta < N - N_{\mathrm{II}} \\ 0 & \text{otherwise} \end{cases}, \tag{4}$$

where $\theta = (t/\tau) \bmod N$, and $v_{\mathrm{I}}, \ldots, v_{\mathrm{IV}}$ are the interstitial velocities in the four sections of the SMB. These obey the global node balances

$$v_{\mathrm{I}} = v_{\mathrm{IV}} + Q_{\mathrm{E}}/(A\epsilon), \tag{5}$$

$$v_{\mathrm{II}} = v_{\mathrm{I}} - Q_{\mathrm{X}}/(A\epsilon), \tag{6}$$

$$v_{\mathrm{III}} = v_{\mathrm{II}} + Q_{\mathrm{F}}/(A\epsilon), \tag{7}$$

$$v_{\mathrm{IV}} = v_{\mathrm{III}} - Q_{\mathrm{R}}/(A\epsilon), \tag{8}$$

where A is the cross-sectional area of the columns and the Q's are the inlet/outlet flowrates: eluent (Q_{E}), extract (Q_{X}), feed (Q_{F}), and raffinate (Q_{R}). Because the system has N columns, the duration of the overall cycle, i.e. the time required for each inlet/outlet line to recover its initial position, is $N\tau$.

Note that in our analysis the operating parameters $N_{\mathrm{I}}, \ldots, N_{\mathrm{IV}}$, $v_{\mathrm{I}}, \ldots, v_{\mathrm{IV}}$, c_i^{E} and c_i^{F} are allowed to be τ-periodic input functions in order for the mathematical formulation presented above to encompass other cyclic operation schemes besides that of the conventional SMB process. For example, processes that vary the flow rates to improve the separation performance [12–16] change some, or all, of the flow rates Q_{E}, Q_{X}, Q_{F}, and Q_{R}, from continuous constant flow to τ-periodic flow, while still satisfying the global constraint $Q_{\mathrm{E}} + Q_{\mathrm{F}} = Q_{\mathrm{X}} + Q_{\mathrm{R}}$. Similarly, in the ModiCon process [17, 18], which is based on the concept of cyclic modulation of the feed concentration, c_i^{F} is changed to a piecewise-constant τ-periodic function. The VARICOL process [6, 7, 26–28, 31], which implements an asynchronous shift of the inlet/outlet lines resulting in a variation of column configuration, fits into the formulation presented above provided that one is able to define a global switching interval τ as the time required for all positions to be switched by one column. This allows us to define the asynchronous shift of the inlet/outlet lines over time in compact notation by converting the column-configuration parameters $N_{\mathrm{I}}, \ldots, N_{\mathrm{IV}}$

into integer vectors and introducing a vector of subdivisions of the switching interval:

$$N_{\mathrm{I}} = (N_{\mathrm{I}}^1, \ldots, N_{\mathrm{I}}^{n_{\mathrm{s}}})^T, \quad \ldots, \quad N_{\mathrm{IV}} = (N_{\mathrm{IV}}^1, \ldots, N_{\mathrm{IV}}^{n_{\mathrm{s}}})^T, \quad \tau = (\tau_1, \ldots, \tau_{n_{\mathrm{s}}})^T, \tag{9}$$

where n_{s} is the number of subdivisions of the switching interval, and $N_{\mathrm{I}}^k/N_{\mathrm{II}}^k/N_{\mathrm{III}}^k/N_{\mathrm{IV}}^k$ is the column configuration during the kth subinterval, whose duration is τ_k. The Varicol process can thus be seen as an operating scheme that changes the column-configuration parameters $N_{\mathrm{I}}, \ldots, N_{\mathrm{IV}}$ from fixed values to piecewise-constant τ-periodic integer functions, where $\tau = \sum_{i=k}^{n_{\mathrm{s}}} \tau_k$ is the global switching interval.

Because of the circular arrangement of the columns and the periodic nature of the inputs operating parameters, after a sufficiently long period of time the process approaches a cyclic steady-state (CSS) regime. This cyclic steady behavior is attained when all state variable that characterize the chromatographic columns show the same time periodicity as that expressed by Eq. (3) for $v_j(t)$ and $c_i^{\mathrm{ex}}(t)$. For the classical SMB process, the CSS condition can be written as

$$c_{i,j+1}(z, t+\tau) = c_{ij}(z,t), \quad q_{i,j+1}(z, t+\tau) = q_{ij}(z,t) \quad (0 \le z \le L), \tag{10}$$

where z is the axial spatial coordinate along the column, L is the column length, and q_i is the solute concentration in adsorbed phase. Thus, under CSS conditions the spatially-distributed concentration profiles distanced by τ time units are identical, apart from a shift of exactly one column. This is what an observer moving with the inlet/outlet lines would observe. Note that the CSS condition, as expressed by Eq. (10), must be extended to the other state variables that characterize the chromatographic process of more complex cyclic operation schemes (e.g., eluent strength in the case of gradient-eluent SMB operation, temperature profile if the columns are dynamically heated, etc.).

By applying Eq. (10) recursively N times, a more relaxed CSS condition is obtained:

$$c_{ij}(z, t+N\tau) = c_{ij}(z,t), \quad q_{ij}(z, t+N\tau) = q_{ij}(z,t) \quad (0 \le z \le L), \tag{11}$$

which states that in every column the spatially-distributed concentration profiles distanced by $N\tau$ time must be identical. Notice, however, that this condition is less rich in information about the periodic state of the SMB process than Eq. (10) because one cannot deduce Eq. (10) from Eq. (11) without resorting to supplementary information about the process.

For process design the initial transient SMB behavior is of little interest, except for unusually short campaigns. The CSS regime is the relevant period of process operation,

except for unusually short campaigns, and for the classical SMB process is usually attained after a moderate number of cycles (each cycle is $N\tau$ long). There is evidence that all memory of the initial condition is lost when CSS is attained, since multiple periodic states have never been reported for this process. This is in contrast to more complex cyclic adsorption processes, such as pressure- and temperature-swing adsorption.

We now proceed to develop single-column processes that reproduce the periodic state of the multi-column SMB process. To achieve this, all references to column $j-1$ must be removed from the the solute node balance given by Eq. (1), so that after rearrangement the node references a single column. This must be done by resorting exclusively to the CSS conditions in order to preserve the periodic state of the SMB process.

From Eq. (2) and Eq. (10), respectively, one can write

$$v_{j-1}(t) = v_j(t-(N-1)\tau) = v_j(t+\tau), \tag{12}$$

$$c^{\text{out}}_{i,j-1}(t) = c^{\text{out}}_{ij}(t-(N-1)\tau) = c^{\text{out}}_{ij}(t+\tau). \tag{13}$$

Using these relations the individual solute material balance at the node can be rewritten as (Figure 3):

$$c^{\text{in}}_i(t) = \alpha\, c^{\text{out}}_i(t') + (1-\alpha)\, c^{\text{ex}}_i(t), \quad \alpha = \frac{\min\{v(t), v(t')\}}{v(t)}, \quad t' = \begin{cases} t-(N-1)\tau \\ \text{or} \\ t+\tau \end{cases}, \tag{14}$$

where the time dependence is shown explicitly and, for simplicity, the j subscript is omitted because its value is fixed. The choice of the value for j is arbitrary because all columns are assumed to be identical and undergo the same cycle; one model with $j = j_1$ behaves similarly to another model with $j = j_2$, except for a simple phase difference of $|j_2 - j_1|\tau$. We choose $j = 1$ so that v_j and c^{ex}_{ij} coincide with $v(t)$ and $c^{\text{ex}}_i(t)$.

Figure 3 provides a block diagram of (14), where it is shown that by applying the CSS conditions, either backward or forward in time, to the solute node balance the periodic state of the SMB process is reproduced by two different single-column chromatographic models whose node balance is given by Eq. (14).

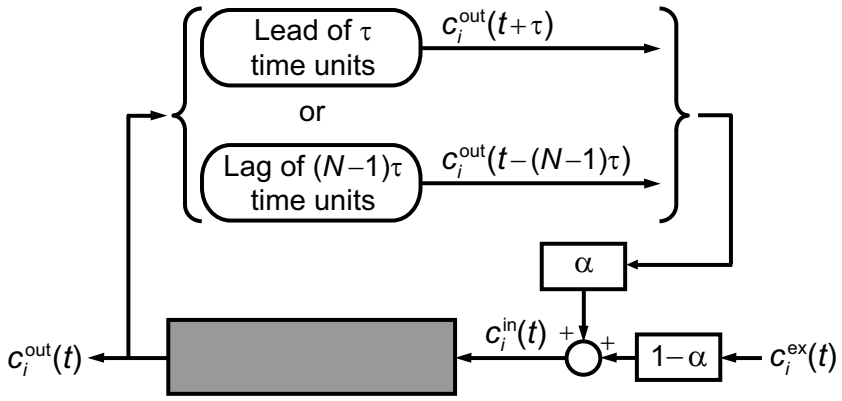

Figure 3: Block diagram of node balance for the two ideal single-column chromatographic models analogous to a SMB process.

- A process model in which the part of its outlet stream that is not recovered as product is recycled to the column with a time lag of $(N-1)\tau$:

$$t' = t - (N-1)\tau; \tag{15}$$

- Another process model in which the part of its outlet stream that is not recovered as product is recycled to the column with a time lead of τ:

$$t' = t + \tau. \tag{16}$$

Both single-column processes are obtained by selecting an arbitrary column of the SMB unit (e.g., column 1 in Figure 4) and following its operation over a complete cycle. The recycle streams from the nonexisting columns are mimicked by recycling, with a time lag of $(N-1)\tau$ or time lead of τ, the portion of the outlet stream of the column that is not withdrawn as product.

These two process models establish a rigorous mathematical framework for all single-column chromatographic processes that replicate the equivalent SMB operation. Since the models employ a single chromatographic column, their numerical solution is easy to implement and is computationally cheap. Therefore, these models are the basis for efficient methods to calculate the periodic state of the SMB process, which can be employed in process design and optimization. It is shown next that this is indeed the case.

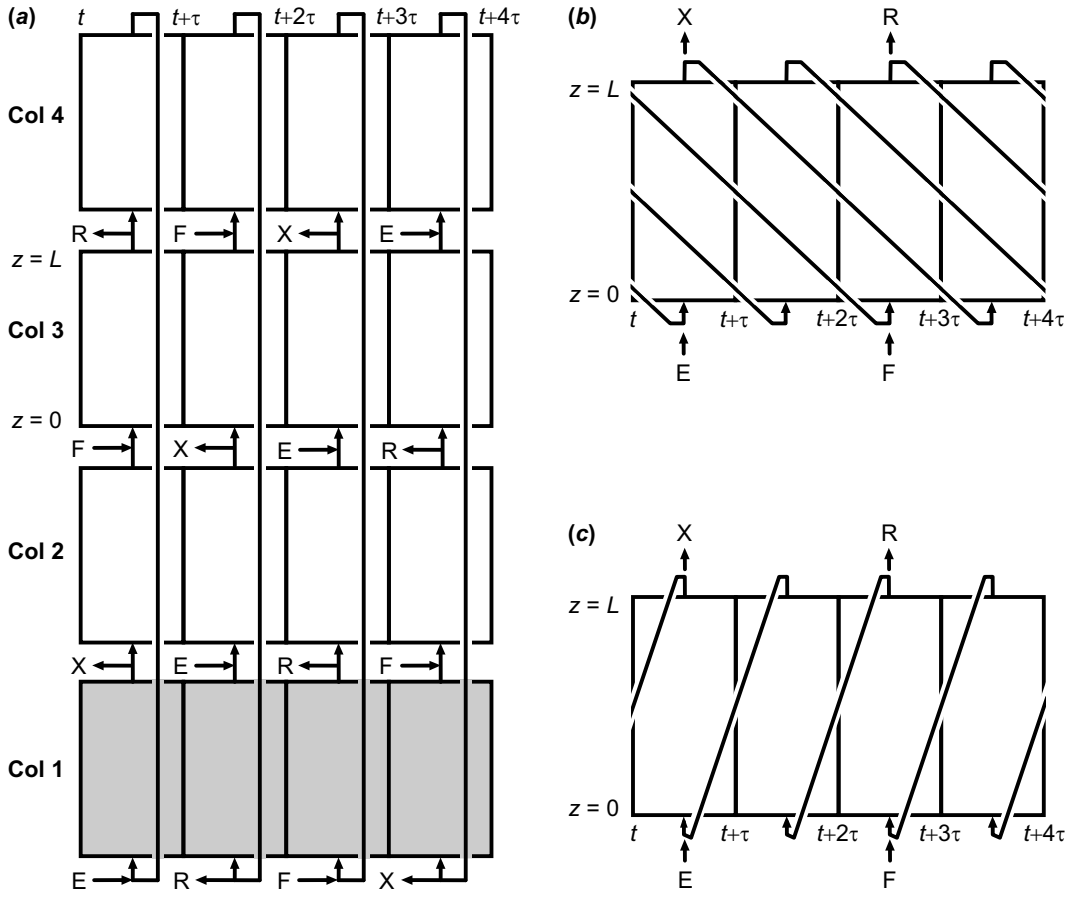

Figure 4: Schematic of operating cycle for (a) classical SMB with port configuration 1/1/1/1, (b) its single-column analog with recycle lag, and (c) its single-column analog with recycle lead. Both single-column processes are obtained by selecting an arbitrary column of the SMB unit (e.g., column 1) and following its operation over a complete cycle. The recycle streams from the nonexisting columns are mimicked by recycling, with a time lag of $(N-1)\tau$ or time lead of τ, the portion of the outlet stream of the column that is not withdrawn as product.

3 Numerical implementation

3.1 Single-column model with recycle lag

This process model is the basis for methods that integrate, either truly or artificially, the governing equations over a sufficiently large number of cycles until CSS is reached. These methods follow the method-of-lines approach [32, 33], which basically consists of discretizing the spatial derivatives to obtain a set of ordinary differential equations (ODE's), or more generally a differential-algebraic equation (DAE) system, for which robust and computationally efficient software is widely available to generate a numerical solution. However, contrary to the traditional approach of integrating the equations for the N columns comprising the SMB unit, here we integrate the equivalent set of equations for

just one column.

Note that this approach requires the numerical implementation of a lag in the recycled value of the outlet concentration $c_i^{\text{out}}(t)$. Most of the general purpose DAE solvers currently available, such as DAEPACK [34], DASPK [35], DDASAC [36], and DASOLV [37], are based on the backward differentiation formulas (BDF). These codes employ an interpolant to compute the solution at points which are not necessarily at the time steps chosen by the code. This capability is needed not only for output purposes, but also for root finding and state event location. By keeping track of the interpolant coefficients for c_i^{out}, it is possible to evaluate $c_i^{\text{out}}(t-(N-1)\tau)$ in a way which is consistent with the integration method employed by the solver. This is the most efficient and accurate method of keeping track of the lagged value of c_i^{out}. Obviously, this is only possible if one has access to the DAE solver code and has some knowledge of its internal workings. For this to be feasible, one must have access to the solver code and have some knowledge of its internal workings.

The numerical work reported here was carried out using gPROMS, a software package for the modeling and simulation of lumped and distributed-parameter process models with combined discrete and continuous characteristics. More information on the package can be found in [38, 39]. Because the code of the standard DAE solvers built into gPROMS (DASOLV or SRADAU) cannot be modified by the user, alternative approaches to implement the concentration lag were developed and tested.

In the first scheme, a discrete buffer is employed to store values of $c_i^{\text{out}}(t)$ and, possibly dc_i^{out}/dt, sampled at regular intervals over a period of $(N-1)\tau$. The contents of the buffer is updated periodically, and the oldest data stored in the buffer are interpolated to compute a continuous approximation of the lagged value of c_i^{out}. Let n_{b} denote the number of discrete values $\tilde{c}_i^{(k)}(k=1,\ldots,n_{\text{b}})$ stored in the buffer at any time and τ_b the sampling interval of the buffer, i.e. the time interval between successive samples of $c_i^{\text{out}}(t)$. The n_{b} values of solute concentration stored in the buffer are updated as follows: every τ_b time units the first value $\tilde{c}_i^{(1)}$ is discarded, the other $n_{\text{b}}-1$ values are shifted by one position, i.e. $\tilde{c}_i^{(k+1)} \rightarrow \tilde{c}_i^{(k)}$, and the last concentration $\tilde{c}_i^{(n_b)}$ is replaced by the current value of $c_i^{\text{out}}(t)$. Note that this shifting operation does not introduce any numerical error; the only source of error is the interpolation of $\tilde{c}_i^{(k)}$ to compute the lagged value of c_i^{out}. The interpolation error depends on the order of the interpolant, which is roughly proportional to the number $\tilde{n}$ of points $\tilde{c}_i^{(k)}$ $(k=1,\ldots,\tilde{n})$ employed by the interpolant, and on the value of τ_b.

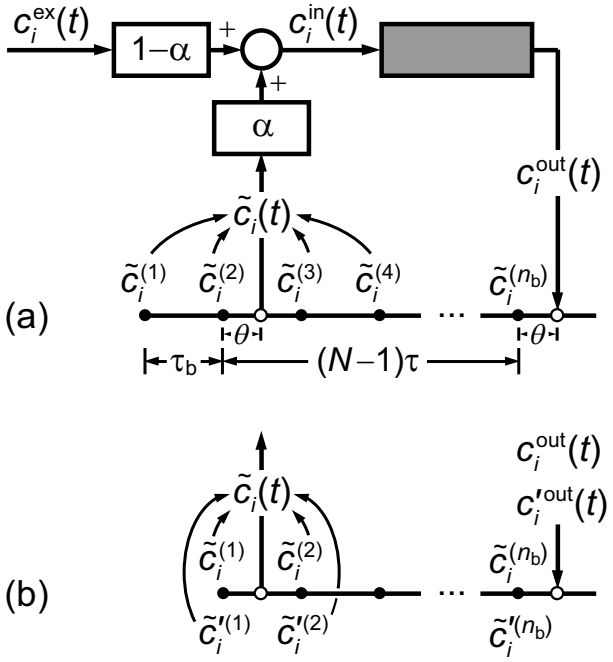

Figure 5: Schematic of discrete buffer and polynomial interpolation schemes for numerical implementation of the recycle lag: (a) third-order polynomial interpolation, (b) cubic Hermite polynomial interpolation.

We have implemented and tested two different polynomial interpolants to evaluate the lagged value of c_i^{out}, a schematic diagram of their use in the node balance is shown is Figure 4.

- Piecewise-cubic polynomial interpolation:

$$\tilde{c}_i(t) = \tilde{c}_i^{(1)} + (\theta+1)\left\{\tilde{c}_i^{(2)} - \tilde{c}_i^{(1)} + \theta\left[\frac{\tilde{c}_i^{(3)} - 2\tilde{c}_i^{(2)} + \tilde{c}_i^{(1)}}{2} + (\theta-1)\frac{\tilde{c}_i^{(4)} - 3\tilde{c}_i^{(3)} + 3\tilde{c}_i^{(2)} - \tilde{c}_i^{(1)}}{6}\right]\right\}, \quad (17)$$

  where $\theta = (t \bmod t_{\text{b}})/t_{\text{b}} = (t/t_{\text{b}} \bmod 1)$ and $\tau_b = (N-1)\tau/(n_{\text{b}}-2)$. Note that to minimize the interpolation error, the buffer holds discrete data sampled over a period of $(N-1)\tau + \tau_{\text{b}}$, so that $0 < \theta < 1$ (see Fig. 4a).

- Piecewise-cubic Hermite interpolation:

$$\tilde{c}_i(t) = \tilde{c}_i^{(1)} + \theta\,\tilde{c}_i'^{(1)} + \theta^2\left[3\tilde{c}_i^{(2)} - \tilde{c}_i'^{(2)} - 3\tilde{c}_i^{(1)} - 2\tilde{c}_i'^{(1)}\right] + \theta^3\left[\tilde{c}_i'^{(2)} - 2\tilde{c}_i^{(2)} + 2\tilde{c}_i^{(1)} + \tilde{c}_i'^{(1)}\right], \quad (18)$$

  where $\tau_b = (N-1)\tau/(n_{\text{b}}-1)$ and $\tilde{c}_i'^{(k)} (k = 1, \ldots, n_{\text{b}})$ are the discrete values of the time derivative dc_i^{out}/dt stored in the buffer. This interpolant requires the sampling

of the discrete values of time derivative, besides those of the concentration, over a period of $(N-1)\tau$.

Note that, strictly speaking, the piecewise-cubic polynomial interpolant has a discontinuous derivative at each sampling instant $t_k = \tau_b k$ $(k = 1, 2, \ldots)$. Since piecewise-cubic Hermite interpolation gives rise to a C^1 interpolant, it does not suffer from this drawback. In practice, however, this apparent deficiency of the third-order polynomial interpolant does not seem to have any detrimental impact on the numerical solution. In fact, both interpolants have similar computational efficiencies and accuracies, and we cannot objectively favor one over the other.

Another option is to model the recycle lag by a plug-flow equation with a residence time equal to the time lag. In this approach, the node balance defined by Eq. (14) with $t' = t - (N-1)\tau$ is replaced by

$$c_i^{\text{in}}(t) = \alpha\, \tilde{c}_i(1,t) + (1-\alpha)\, c_i^{\text{ex}}(t), \tag{19}$$

where $\tilde{c}_i(x,t)$ is now a spatially distributed concentration governed by

$$\frac{\partial \tilde{c}_i}{\partial t} + \frac{1}{(N-1)\tau}\frac{\partial \tilde{c}_i}{\partial x} = 0 \quad (0 < x \leq 1) \quad \text{s.t.} \quad \tilde{c}_i(0,t) = c_i^{\text{out}}(t). \tag{20}$$

It is straightforward to demonstrate using the Laplace transform that $\tilde{c}_i(1,t) = c_i^{\text{out}}(t - (N-1)\tau)$. The computational efficiency of this scheme is heavily dependent on the selection of an appropriate spatial discretization method for Eq. (20). In particular, the adopted numerical method must be highly accurate and dispersion free.

For completeness, we also discuss a shooting method proposed by other authors [40–43] for pressure swing adsorption models, and recently enhanced by Jiang et al. [44]. Basically, the method consists of approximating the steady periodic profile of $c_i^{\text{out}}(t)$ over a single cycle $(0 \leq t \leq N\tau)$ by a suitable profile parameterization,

$$c_i^{\text{out}}(t) = \tilde{c}(u_i; t), \tag{21}$$

defined by a set of parameters $u_i = [u_i^{(1)}, \ldots, u_i^{(n_u)}]$. These can be, e.g., the values of c_i^{out} at n_u prescribed discrete points distributed over the cycle, together with a suitable interpolation scheme (polynomial or spline) to generate a continuous profile between nodal values. Alternatively, the profile can be approximated by a truncated series expansion or an analytical expression with sufficient flexibility to approximate the shape of c_i^{out} over the cycle. Note that the profile parameterization should preferably depend on a small set

of parameters and exploit the time-periodic behavior of $c_i^{\text{out}}(t)$ at CSS, i.e. n_u should be small and $\tilde{c}(u_i;t)$ should be a continuous and smooth $N\tau$-periodic function of time:

$$\tilde{c}(u_i;t) = \tilde{c}(u_i;t-N\tau) = \tilde{c}(u_i;t+N\tau). \tag{22}$$

Then, $c_i^{\text{out}}(t')$ is replaced by $\tilde{c}_i(u_i;t')$ in the solute node balance given by Eq. (14) and the dynamic simulation is converted into a dynamic optimization problem which can be expressed as

$$\min_{u_1,u_2} \phi^{\text{CSS}} = \int_0^{N\tau} \sum_{i=1}^{2} ||c_i^{\text{out}}(t) - \tilde{c}(u_i;t)||\,\mathrm{d}t, \tag{23}$$

where the residual function $||\Delta c||$ can be, e.g., $(\Delta c)^2$ or $|\Delta c|$ (the only requirement is that the minimum value of $||\Delta c||$ be obtained for $\Delta c = 0$). The parameters u_i are now regarded as control variables to be determined so as to minimize the objective function ϕ^{CSS}. Note that ϕ^{CSS} is a measure of system deviation from CSS, and attains its minimum value at CSS.

The optimization solver integrates the DAE system of the discretized single-column model over a single cycle along with sensitivity information for the solution. The sensitivities are then used to determine a new estimate of the control variables u_i in an attempt to minimize the value of ϕ^{CSS}. The new estimate is later used for integration of a new cycle and this iterative process is repeated until the CSS condition is satisfied. A good optimization code can achieve quadratic or superlinear convergence rates and require far fewer interations than the dynamic simulation approach. However, extra computation time is needed to calculate the Jacobian.

Strictly speaking, the dynamic optimization problem expressed above is incomplete because the spatial concentration profiles at the start of the cycle, $c_i(z,0)$ and $q_i(z,0)$, are undefined. In fact, for completeness they should also be parameterized and their periodicity condition added as a constraint. To be more specific, suppose that $c_i(z,0)$ and $q_i(z,0)$ are approximated by parameterizations $\tilde{c}(u_i^c;z)$ and $\tilde{q}(u_i^q;z)$, respectively, which depend on the sets of parameters u_i^c and u_i^q. The original set of control variables should be augmented with u_i^c and u_i^q and the dynamic optimization problem be subjected to the initial condition and periodicity constraint:

$$c_i(z,0) = \tilde{c}(u_i^c;z), \quad q_i(z,0) = \tilde{q}(u_i^q;z); \tag{24}$$

$$c_i(z,N\tau) = c(u_i^c;z), \quad q_i(z,N\tau) = q(u_i^q;z). \tag{25}$$

However, if one is only evaluating CSS solutions which yield good separation and the initial port configuration is correctly chosen, the extra parameterization can be avoided.

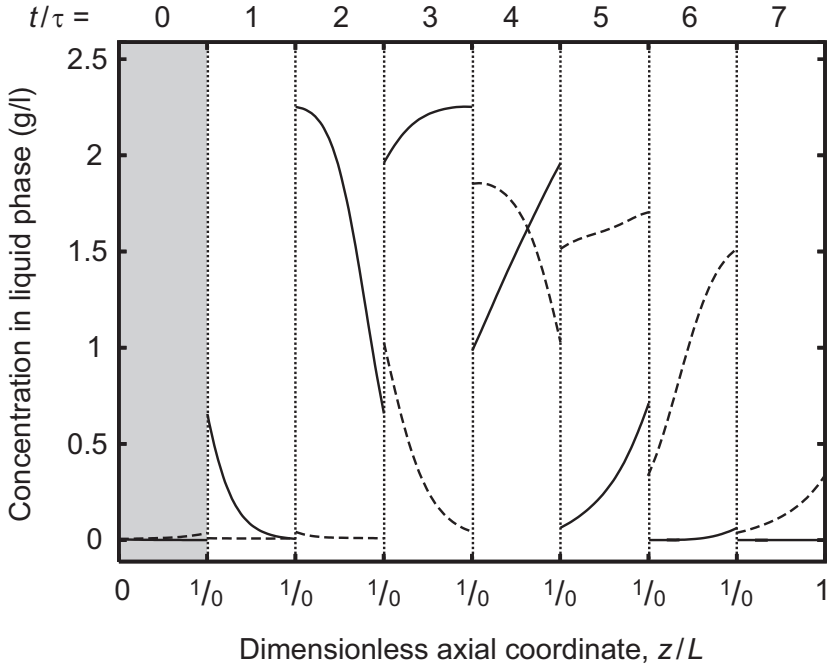

Figure 6: Simulated axial profiles of solute concentration in liquid phase at the beginning of each switch interval of the cycle for the single-column model analogous to the 2/2/2/2 nonlinear SMB process defined in Table 1. Results were obtained under CSS conditions. The cycle starts after eluent addition, raffinate is withdrawn during the 3rd switch interval, the system is fed during the 4th switch interval and extract is obtained on the 7th switch interval. Because the operating conditions yield good separation, the state of the column at the start of the cycle (shaded area) is nearly solute free and is well approximated by that of a clean column.

For operating conditions that achieve high separation performances, the state of the column at the end of the switch interval during which it was partially fed with eluent (as exemplified by the shaded area in Fig. 6) is very well approximated by that of a clean column. The port configuration for the next switch interval is, therefore, the preferred one for start-up of the cycle, because at CSS the state of the column after eluent addition is very close to that of a clean column:

$$c_i(z,0) = c_i(z,N\tau) \approx 0, \quad q_i(z,0) = q_i(z,N\tau) \approx 0 \quad \text{at CSS.} \tag{26}$$

In fact, this reasoning is the basis for an efficient procedure to experimentally assess SMB performance using a single-column setup [45]. Thus, the extra parameterization can be discarded and it suffices to add to the dynamic optimization problem the initial condition

$$c_i(z,0) = 0 \quad q_i(z,0) = 0. \tag{27}$$

Nevertheless, it is always good to check afterwards that

$$c_i(z,N\tau) \approx 0, \quad q_i(z,N\tau) \approx 0. \tag{28}$$

Perhaps the most appealing characteristic of this approach is that it can easily incorporate optimization goals and design specifications, say

$$\min_{d} f \quad \text{s.t.} \quad h(d) = 0, \quad g(d) \geq 0, \tag{29}$$

where f is the objective function (e.g., the flow ratio $Q_{\mathrm{E}}/Q_{\mathrm{F}}$), d is the set of design variables (flow rates, switch interval, etc.), h is a vector of equality constraints and g is a vector of inequality constraints (e.g., purity constraints).

Two approaches can be adopted to incorporate the CSS condition expressed by Eq. (23) into the optimization problem define above. In the first approach, the CSS condition is directly added to the optimization function:

$$\min_{d,u_1,u_2} f + \mu\phi^{\mathrm{CSS}} \quad \text{s.t.} \quad h(d) = 0, \quad g(d) \geq 0, \tag{30}$$

where μ is a penalty constant with a large positive value. Alternatively, Eq. (23) can be converted into a constraint:

$$\min_{d} f \quad \text{s.t.} \quad h(d) = 0, \quad g(d) \geq 0, \quad \phi^{\mathrm{CSS}} \leq \delta, \tag{31}$$

where δ is a small CSS tolerance.

Either way, CSS convergence is achieved only at the optimal solution and the CSS convergence loop is eliminated. This is in essence the simultaneous tailored approach proposed by Biegler and coworkers [44, 46, 47] for simulation and optimization of pressure-swing adsorption processes. Based on the results presented below, it is unlikely that for standard SMB processes this method can compete against the successive substitution methods discussed above or the complete discretization method given below. The reason for this is that, contrary to other cyclic adsorption processes, the SMB process usually requires a moderate number of cycles to attain the CSS. This may not be the case, however, if SMB operation is rendered more complex, e.g. by dynamically heating the columns or changing eluent strength.

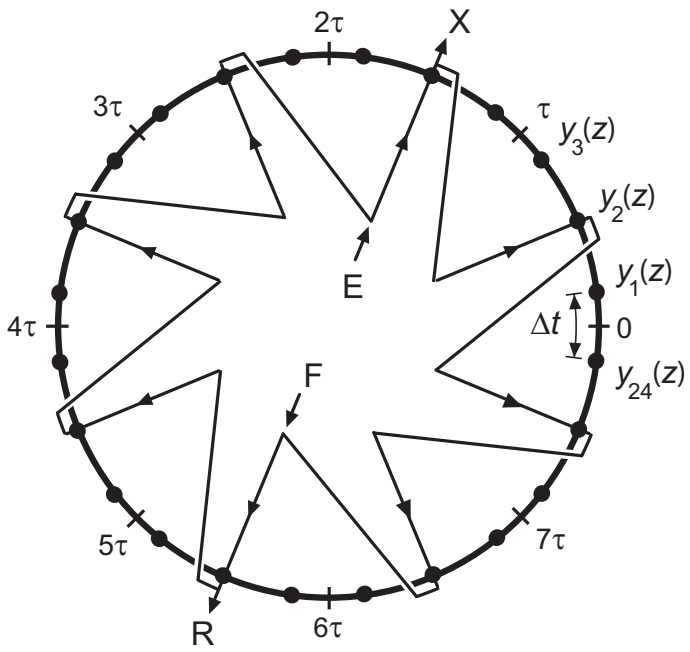

Figure 7: Schematic of temporal domain and periodic boundary conditions for the complete discretization method applied to the single-column model with recycle lead. In this particular example, the SMB port configuration is 2/2/2/2 and the resolution of the temporal mesh is $\Delta t = \tau/n_\tau$ with $n_\tau = 3$ (the grid nodes are identified by solid circles). Note that $y_k(z) \equiv \{c_1(z), c_2(z), q_1(z), q_2(z)\}_{t=t_k}$.

3.2 Single-column model with recycle lead

This single-column model is also the basis for an efficient method of directly computing the CSS. The method consists of discretizing the time coordinate for the single-column model over a complete cycle ($N\tau$ time units) and directly imposing the CSS condition expressed by Eq. (11). This replaces the original dynamic system by a set of partial differential equations, which depend on the spatial coordinate only and in which the periodic boundary condition is implicitly defined. This system is then converted to a (large) sparse system of nonlinear algebraic equations by applying an appropriate discretization scheme to the spatial derivatives. The resulting algebraic system is solved using a suitable nonlinear algebraic equation solver appropriate for sparse systems. This method, termed complete or simultaneous discretization method, was proposed by Nilchan and Pantelides [48, 49] for pressure swing adsorption systems and also tested by other authors on similar [46, 47] or related problems [50, 51].

Figure 7 shows a schematic of the temporal mesh for directly computing the periodic state of a classical 2/2/2/2 SMB unit. In practice, each switch interval is divided into n_τ smaller time intervals, each one with duration $\Delta t = \tau/n_\tau$. Given that the overall cycle duration is $N\tau$, the total number of temporal discretization points is $n_\tau N$. The solution

is calculated at the time instants

$$t_k = \Delta t(k - 0.5), \quad k = 1, \ldots, n_\tau N, \tag{32}$$

which are purposively staggered with respect to the switch times in order to avoid handling the discontinuous jump of the inputs $v(t)$ and $c_i^{\text{ex}}(t)$ when the status of the inlet port changes. The partial derivatives of solute concentration with respect to time, $\partial y/\partial t$, where $y \equiv \{c_1(z,t), c_2(z,t), q_1(z,t), q_2(z,t)\}$, are replaced by a third-order backward differencing formula:

$$\left.\frac{\partial y(z,t)}{\partial t}\right|_{t_k} = \frac{2y(z,t_{k+1}) + 3y(z,t_k) - 6y(z,t_{k-1}) + y(z,t_{k-2})}{6\Delta t}, \quad k = 1, \ldots, n_\tau N. \tag{33}$$

This discretization scheme was found to be much more efficient than the usual second-order differencing formula

$$\left.\frac{\partial y(z,t)}{\partial t}\right|_{t_k} = \frac{3y(z,t_k) - 4y(z,t_{k-1}) + y(z,t_{k-2})}{2\Delta t}, \quad k = 1, \ldots, n_\tau N. \tag{34}$$

In fact, the use of Eq. (34) gives rise to a solution method that is not competitive against the dynamic solution methods described in the previous section.

Taking into account the periodic boundary condition $y(t - N\tau) = y(t) = y(t + N\tau)$, it is straightforward to eliminate the external nodes, which appear in the differencing formulae for the time instants t_1, t_2 and $t_{n_\tau N}$, by noting that

$$y_{-1} \equiv y_{n_\tau N - 1}, \quad y_0 \equiv y_{n_\tau N}, \quad y_{n_\tau N + 1} \equiv y_1. \tag{35}$$

Also, the discrete analog of the node balance given by Eq. (14) is

$$c_i^{\text{in}}(t_k) = \alpha_k c_i^{\text{out}}(t_{k'}) + (1 - \alpha_k) c_i^{\text{ex}}(t_k), \quad \alpha_k = \frac{\min\{v(t_k), v(t_{k'})\}}{v(t_k)}, \tag{36}$$

where

$$k' = \begin{cases} k + n_\tau, & k \leq n_\tau(N-1) \\ k + n_\tau - n_\tau N, & k > n_\tau(N-1) \end{cases}. \tag{37}$$

To summarize, the discretization of the time coordinate replaces the original dynamic system by a set of partial differential equations

$$F_z(y) = 0, \quad y(z) = [y_1(z), \ldots, y_{n_\tau N}(z)], \tag{38}$$

which depends on the spatial coordinate z only, and in which the periodic boundary condition is implicitly defined. In Eq. (38), $y_k(z)$ represents the solute concentration profiles $y(z, t_k)$ at time instant t_k. This system is then converted to a (large) sparse system of nonlinear algebraic equations by applying an appropriate discretization scheme to the spatial derivatives. The resulting algebraic system is solved using a suitable nonlinear algebraic equation solver appropriate for sparse systems.

Table 1: Model parameters and operating conditions for the two test cases of binary separation by SMB. In both cases the SMB port configuration is 2/2/2/2.

Column length, L (cm)	11.0	Péclet number, Pe	1000
Column diameter, d (cm)	2.6	LDF coeficients, k_i (s^{-1})	0.1, 0.1
Porosity, ϵ	0.4	Feed concentration, c_i^F (g/l)	2.9, 2.9

Linear isotherm, q_i^* (g/l)	$2.72c_A$, $3.86c_B$
Bi-Langmuir isotherm, q_i^* (g/l)	$\frac{2.69c_A,\ 3.73c_B}{1+0.0336c_A+0.0466c_B}+\frac{0.1c_A,\ 0.3c_B}{1+c_A+3c_B}$

Flow rate (ml/min)	Linear isotherm	Bi-Langmuir isotherm
Feed, Q_F	4.65	2.78
Eluent, Q_E	15.77	9.93
Raffinate, Q_R	8.19	4.52
Extract, Q_X	12.23	8.19
Recycle, Q	23.00	15.93
τ (min)	4.56	6.22

4 Results and discussion

For brevity of presentation, only two binary separations are analyzed in this study. Nevertheless, they are sufficiently different, in terms of isotherm model and selected operating parameters, for their overall analysis to provide conclusions of general applicability. The nonlinear case, governed by a bi-Langmuir competitive isotherm model, was adapted from [52–54] and provides a reasonably good description of the separation of binaphthol enantiomers on cellulose triacetate using heptane-isopropanol (72:28) as eluent. The linear isotherm case was derived from the nonlinear one by fitting a linear isotherm model to a series of simulated band profiles of the bi-Langmuirian binary mixture. For both cases, a suitable set of operating parameters was obtained by minimizing the flow ratio Q_E/Q_F subjected to a minimum purity constraint of 0.99. The model parameters and operating conditions for the two test cases are listed in Table 1.

It is assumed that the isothermal operation of the chromatographic columns can be adequately described by an axially dispersed flow model with finite mass-transfer rate described by a linear driving force (LDF) approximation. These assumptions provide a reasonable good description of a chromatographic column and are assumed to hold for the

simulation results reported in this work. They are standard practice in SMB modeling [55].

The solute material balance in a differential volume of the column can be written as

$$\frac{\partial c_i}{\partial t} + \frac{1-\epsilon}{\epsilon}\frac{\partial q_i}{\partial t} = v \quad \left(\frac{L}{\mathrm{Pe}}\frac{\partial^2 c_i}{\partial z^2} - \frac{\partial c_i}{\partial z}\right) \quad (0 < z < L), \tag{39}$$

where $i = 1, 2$ identifies the species in the mixture, ϵ is the bed porosity, L is the column length, v is the interstitial liquid velocity, $\mathrm{Pe} = vL/D$ is the Péclet number and D is the axial dispersion coefficient.

The approximation of the adsorption rate by the LDF model leads to

$$\frac{\partial q_i}{\partial t} = k_i(q_i^* - q_i), \quad q_i^* \equiv q_i^*(c_1, c_2) \quad (0 \le z \le L), \tag{40}$$

where k_i is the LDF coefficient and $q_i^*(c_1, c_2)$ is the adsorption isotherm of component i, which relates its equilibrium concentration in the adsorbed phase, q_i^*, with the solute concentrations, c_1 and c_2, in the bulk fluid.

Equation 39 is subjected to the following boundary conditions:

$$c_i - \frac{L}{\mathrm{Pe}}\frac{\partial c_i}{\partial z} = c_i^{\mathrm{in}} \quad \text{for} \quad z = 0, \tag{41}$$

$$\frac{\partial c_i}{\partial z} = 0 \quad \text{for} \quad z = L. \tag{42}$$

The discretization scheme and grid resolution for each solution method were chosen so that all methods give identical results, to within a purity tolerance level of 0.001. With one exception, the choice of spatial discretization scheme was limited to those already built into gPROMS (orthogonal collocation on finite elements and various finite differencing schemes).

In every case, the spatial derivatives in Eq. (39) were discretized using third-order orthogonal collocation on 4 equally-sized finite elements [56, 57]. This scheme gives rise to a spatial mesh with 13 collocation points where the solution is computed. After some preliminary testing, this choice of spatial discretization was found to give an accurate solution with a minimum number of collocation points. As we shall demonstrate, the mesh resolution is not critical for dynamic simulation methods, but it plays an important role in the success or failure of the complete discretization approach. If an overly fine mesh is used to discretize the column the method is likely to be computationally prohibitive.

To implement the recycle lag, the discrete buffer was updated every $\tau_{\mathrm{b}} = \tau/5$ time units ($n_{\mathrm{b}} = 37$) and the lagged value of c_i^{out} was evaluated using the piecewise-cubic polynomial interpolant given by Eq. (17). The discrete buffer can be implemented efficiently

in gPROMS by resorting to some of the more advanced features of the software package. The trick is to avoid an unnecessary reinitialization of the DAE solver at every sampling interval τ_{b}. The interested reader is referred to the appendix for a detailed description of the coding.

The plug flow model, defined by Eq. (20), was discretized using third-order orthogonal collocation on 40 equally-sized finite elements. This method was found to be more efficient than the second-order backward finite difference method also available in gPROMS. We also tested a control-volume method with flux-limited correction [21], which prevents the appearance of artificial oscillations in the numerical solution of strongly hyperbolic problems. However, the small oscillations observed on the lagged value of c_i^{out} obtained by orthogonal collocation are completely damped inside the column and, thus, have little impact on the solution. For this reason the flux-limited scheme is less efficient because the elimination of artificial oscillations comes at the expense of a nonlinear formula in the interpolated variables and a corresponding increase in computational effort. However, this cannot be taken as a general conclusion because the LDF coefficients used in our tests are relatively large. Under these conditions the column operation shifts from equilibrium towards a more dispersed solution. If the LDF coefficients were smaller, more elements would be needed to get an accurate solution and the orthogonal collocation method would be less competitive.

The temporal grid resolution employed in the full domain discretization method is defined by $\Delta t = \tau/7$ ($n_\tau = 7$); thus, the total number of temporal grid points is $n_\tau N = 56$. Lower values of n_τ gave rise to numerical solutions that did not satisfy the prescribed purity tolerance level. Note that in our current implementation, $\tau/\Delta t$ must be an integer number and this constrains the grid size to be an integer multiple of N. In a more complex implementation, unconstrained by the aforementioned restriction, a more optimized temporal grid could be employed.

In the dynamic simulation methods, the integration is stopped when the temporal profile of solute concentration in a cycle is identical, within a given tolerance, to that in the previous cycle. This can be expressed mathematically as

$$\frac{1}{N\tau c_i^{\mathrm{F}}} \int_{N\tau(k-1)}^{N\tau k} |c_i^{\mathrm{out}}(t) - c_i^{\mathrm{out}}(t - N\tau)| \, \mathrm{d}t < 2.5 \times 10^{-4}, \quad k = 2, 3, \ldots . \tag{43}$$

For computational efficiency, this stop criterium is not applied at every step of the cycle, but only at those steps where the product streams are obtained.

The values of solute concentration in the accumulated withdrawn fluid of each product

stream during a switch interval are defined as

$$\left\langle c_i^{\mathrm{X}}, c_i^{\mathrm{R}} \right\rangle = \frac{\displaystyle\int_t^{t+\tau} \{c_i^{\mathrm{X}} Q_{\mathrm{X}}, c_i^{\mathrm{R}} Q_{\mathrm{R}}\}\, dt'}{\displaystyle\int_t^{t+\tau} \{Q_{\mathrm{X}}, Q_{\mathrm{R}}\}\, dt'}. \tag{44}$$

These are easily determined in the context of dynamic simulation by solving a few extra ODEs. Taking the extract stream as an example, the relevant equations are

$$\frac{d\left\langle C_i^{\mathrm{X}} \right\rangle}{dt} = c_i^{\mathrm{X}} Q_{\mathrm{X}}, \quad \frac{d\left\langle Q_{\mathrm{X}} \right\rangle}{dt} = Q_{\mathrm{X}}, \tag{45}$$

where $\left\langle C_i^{\mathrm{X}} \right\rangle$ and $\langle Q_{\mathrm{X}} \rangle$ are auxiliary variables which must be reset at the beginning of every switch interval by setting

$$\left\langle C_i^{\mathrm{X}} \right\rangle = 0, \quad \langle Q_{\mathrm{X}} \rangle = 0. \tag{46}$$

The values of these auxiliary variables at the end of every switch interval can then be used to compute the desired integral value of concentration:

$$\left\langle c_i^{\mathrm{X}} \right\rangle = \left\langle C_i^{\mathrm{X}} \right\rangle / \left\langle Q_{\mathrm{X}} \right\rangle. \tag{47}$$

In the case of the complete discretization method, the integral value of concentration in the accumulated fluid during a switch interval must be computed using a quadrature rule. The formula employed in this work is

$$\langle c \rangle = \frac{17c_1 - 7c_2 + 2c_3}{24n_\tau} + \frac{c_1 + 4c_2 + 2c_3 + \cdots + 4c_{n_\tau - 1} + c_{n_\tau}}{3n_\tau} + \frac{2c_{n_\tau - 2} - 7c_{n_\tau - 1} + 17c_{n_\tau}}{24n_\tau}, \tag{48}$$

which is Simpson's rule applied to the interval $[\Delta t/2, \tau - \Delta t/2]$ plus a three-point semi-open quadrature for the end intervals $[0, \Delta t/2]$ and $[\tau - \Delta t/2, \tau]$. Equation (48) is applicable to the first switch interval of the cycle; for other intervals the node index must be shifted accordingly. Note also that, for simplicity, we have assumed that the flow rate during the switch interval is kept constant and, therefore, can be removed from the integrals in Eq. (44).

Figure 8 displays the solute concentration field in liquid phase, $c_i(z,t)$, at cyclic steady state, for the binary separation governed by the bi-Langmuir competitive isotherm model. The plotted data can be obtained by any of the methods discussed above. The concentration field is most conveniently represented as an annular plot because of the periodicity condition at CSS. The radial coordinate of each annular plot represents the axial coordinate along the column, whereas the tangential coordinate represents the time coordinate

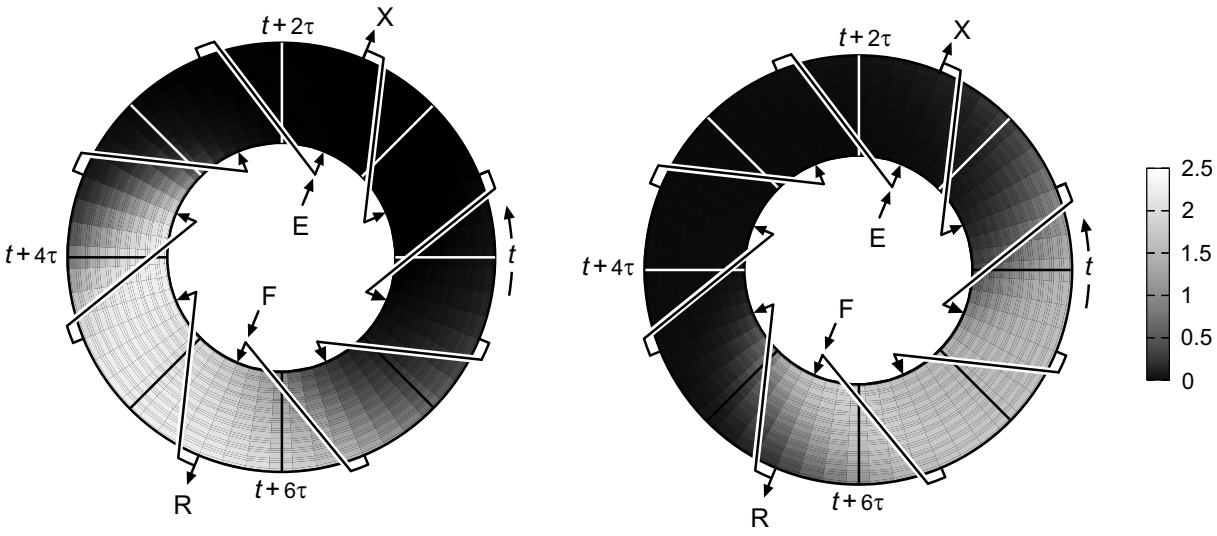

Figure 8: Solute concentration field in liquid phase $c_i(z,t)$, at cyclic steady state, for the nonlinear enantiomeric separation defined in Table 1 (solutes 1 and 2 are displayed in the left and right plots, respectively).

which spans a whole cycle of operation, i.e. $N\tau$ time units. Thus, the annular domain represented in each plot is coincident with the computational domain handled by the complete discretization method. The inner radius represents the column inlet, $c_i(z=0,t)$, whereas the outer radius represents the column outlet, $c_i(z=L,t)$. Arrows are superposed on the each plot to show the recycle pattern as well as to identify the intervals during which feed or eluent is added to the column and raffinate or extract is withdrawn. The recycle with a time lead of τ is easily seen in the plots, but, given the $N\tau$ periodicity of the concentration profiles at CSS, it is also equivalent to a time lag of $(N-1)\tau$.

Note that the annular slice defined by the time interval $(j-1)\tau < t < j\tau$ gives the state of column j of the equivalent SMB unit over the interval $0 < t < \tau$. In fact, for any state variable or external input, ϕ, the following equivalence holds:

$$\underset{(j-1)\tau<t_j<j\tau}{\phi(t_j)} \quad = \quad \underset{0<t<\tau}{\phi_j(t)} \ , \tag{49}$$

where the l.-h.-s. refers to the single-column model and the r.-h.-s. denotes the jth column of the N-column model. This shows that solving the single-column model with recycle lead over $N\tau$ time units using the complete discretization method is the same as solving for N identical columns interconnected circularly over a single switch interval using the periodicity condition given by Eq. (10). Thus, our complete discretization method turns out to be identical to the method proposed in [22] for direct computation of periodic SMB states.

The performance of each solution method discussed above is measured in terms of

Table 2: Computational effort (CPU time in seconds) of the various methods for CSS determination of SMB process. The benchmark test for each isotherm model is a sequence of 11 CSS calculations for increasing values of the switch interval from 0.9τ to 1.1τ in steps of 0.02τ. Numbers report the CPU time spent on each run when its initial estimate/condition was the solution obtained from the previous run. The numbers in parenthesis, however, were obtained when null initial condition/estimate was imposed, i.e. the system was initially solute free.

Linear isotherm			
Method	$\langle$CPU time$\rangle$/run	$\langle N_{\mathrm{cyc}}\rangle$/run	$\langle$CPU time$\rangle$/cycle
N columns	4.6 (5.5)	10.7 (12.9)	0.431
One column with recycle lag			
Discrete buffer	3.1 (4.2)	48.8 (66.8)	0.063
Plug-flow, Eq. (20)	12.8 (17.6)	48.8 (66.8)	0.263
One column with recycle lead	1.0 (1.0)	—	—
Nonlinear isotherm			
Method	$\langle$CPU time$\rangle$/run	$\langle N_{\mathrm{cyc}}\rangle$/run	$\langle$CPU time$\rangle$/cycle
N columns	5.8 (7.4)	11.9 (15.2)	0.485
One column with recycle lag			
Discrete buffer	3.7 (5.2)	52.1 (74.0)	0.071
Plug-flow, Eq. (20)	13.0 (19.3)	52.1 (74.0)	0.261
One column with recycle lead	12.4 (19.0)	—	—

CPU time, number of cycles to attain CSS, and CPU time per cycle. For reference, the computer hardware employed was an Intel 1.7 GHz Pentium IV with 512 MB RAM. The benchmark test for each isotherm model is a sequence of 11 CSS calculations for increasing values of the switch interval from 0.9τ to 1.1τ in steps of 0.02τ. By using as initial estimate/condition for each run the solution obtained from the previous run, the benchmark test mimics (although somewhat grossly) the typical sequence of intermediate evaluations performed by an optimization code. For completeness, the results reported here also include the computational effort of the various methods when null initial condition/estimate is imposed, i.e. the system is initially solute free. The results are summarized in Table 2.

Our benchmark tests show that the dynamic simulation of the single-column model is more efficient than the traditional dynamic simulation of the full N-column model when the recycle lag is implemented using the discrete buffer. The gain in computational performance is about 35% and is independent of the isotherm model. As expected, the

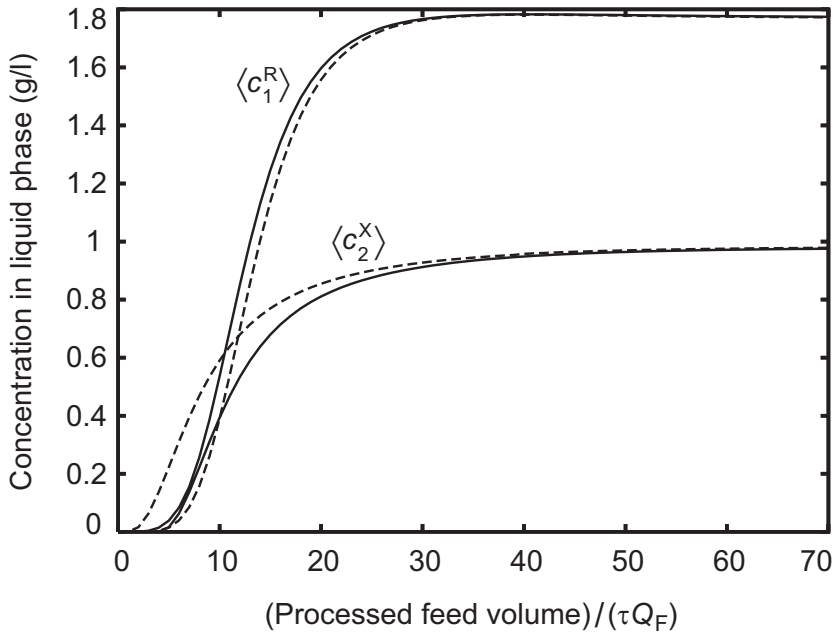

Figure 9: Simulated average solute concentration in the accumulated withdrawn fluid during a switch interval as a function of processed feed volume for the nonlinear SMB process (solid lines) defined in Table 1 and its analogous single-column model with recycle lag (dashed lines).

performance gain does not increase N fold because the single-column model is fed only $1/N$th per cycle. The computational gain is due not only to the more compact numerical representation of the process provided by the single-column model, but also to the somewhat different paths followed by the two models to reach the same CSS solution. This is exemplified in Figure 9 for the nonlinear case, where the simulated average solute concentration in the accumulated withdrawn fluid during a switch interval is plotted as a function of processed feed volume for each process model. The two curves for the raffinate stream are similar (but do not completely overlap), which implies that the two models behave similarly in terms of raffinate response. However, the product concentration in the extract stream of the single-column model reaches its CSS value faster than that of the SMB model. In fact, from the data listed in the third column of Table 2 one concludes that CSS is attained 45% faster by the single-column model for both test cases. We believe this value to be a reasonable estimate of the upper limit on performance gain which would be obtained by the single-column model with a dedicated code.

The models are solved faster when the solution obtained from a run is used as initial estimate for a subsequent run with small changes in the operating parameters. This is because less cycles are required to attain the fully established periodic state. For the benchmark tests considered in this study the number of cycles taken by the N-column

model is reduced by about 20%, this value is further reduced to 28% for the single-column process with recycle lag. The impact of the initial estimate is even more effective on the efficiency of the complete discretization method, which is improved by 35%. The performance gain for the bi-Langmuirian mixture is slightly better than for the linear isotherm case. Note that the efficiency of the complete discretization method for linear isotherms is independent of the initial estimate because the discretized model is linear and gPROMS uses a direct linear solver.

The dynamic simulation of the single-column model is not competitive when the recycle lag is implemented by means of a classical discretization of Eq. (20). A good estimate of the computational overhead incurred by adding the plug-flow equation is obtained by subtracting the third row of Table 2 from the fourth one. Roughly $(12.8-3.1)/12.8 = 76\%$ (linear isotherm) and $(13.0-3.7)/13.0 = 72\%$ (nonlinear case) of computer time is spent on the solution of the plug-flow equation. The reason for this overhead is that a large number of discretization points is required to obtain an accurate and dispersion free solution of the plug-flow equation. In this sense, the discrete-buffer approach can be viewed as a very efficient and accurate scheme of solving Eq. (20) for $\tilde{c}_i(1,t)$.

The numerical solution of the single-column model using the complete discretization method is very fast when the isotherm model is linear. It is three times faster than the best dynamic-solution method of the single-column model and almost five times faster than the traditional dynamic simulation of the N-column model. Because the isotherm is linear, and both the spatial and time discretization schemes employ linear stencils, the overall discretized model is a sparse system of linear algebraic equations that is solved in a single iteration by the nonlinear equation solver built into gPROMS. This is because the current version of gPROMS (2.3.1) employs a direct LU-factorisation algorithm designed for large, sparse, asymmetric systems of linear equations. This may change in future versions.

When the isotherm model is nonlinear, the complete discretization approach is less competitive than the dynamic simulation methods. Assuming that the CPU time to solve the linear-isotherm model is a reasonable estimate of the time spent per iteration of the nonlinear algebraic solver, one can estimate that the latter requires 10–12 iterations to solve the nonlinear-isotherm problem. We believe that the direct calculation of the periodic state is heavily penalized by the inefficiency of the general-purpose solvers built into gPROMS for this particular problem . Tables 3 and 4 support our statement. These tables show the influence of temporal and spatial discretizations on the CPU time required

Table 3: Influence of temporal discretization resolution, as measured by the value of n_τ, on the computational effort (CPU time in seconds) of the complete discretization method for solving the single-column model with recycle lead. The benchmark tests are the same as those for Table 2, with as initial estimate for each run the solution obtained from the previous run. The exponent β of the power dependence of computational effort on temporal resolution, i.e. CPU time $\propto (n_\tau)^\beta$, is also listed.

n_τ	Linear isotherm	Nonlinear isotherm
5	0.5	4.7
7	1.0	12.5
9	3.4	20.6
11	6.4	33.5
β	3.3	2.5

Table 4: Influence of spatial discretization resolution, as measured by the number of finite elements (n_{FE}), on the computational effort (CPU time in seconds) of the two best single-column methods for CSS determination of SMB process. The benchmark tests are the same as those for Table 2, with as initial estimate/condition for each run the solution obtained from the previous run. The recycle-lag method employs a discrete buffer with $n_{\mathrm{b}} = 37$ ($\tau_{\mathrm{b}} = \tau/5$). The complete discretization method applied to the recycle-lead model uses $n_\tau = 7$. The exponent β of the power dependence of computational effort on spatial resolution, i.e. CPU time $\propto (n_{\mathrm{FE}})^\beta$, is also listed.

	Linear isotherm					Nonlinear isotherm				
n_{FE}	4	5	6	7	β	4	5	6	7	β
Lag	3.0	3.4	3.9	4.4	0.7	3.6	4.0	4.7	5.3	0.7
Lead	1.0	2.4	3.5	6.4	3.1	12.3	22.9	37.2	74.3	3.1

by the complete discretization method. The exponent β of the power dependence of CPU time on temporal mesh resolution, i.e. CPU time $\propto (n_\tau)^\beta$, where n_τ is the number of divisions of the switch interval, is $\beta = 3.3$ for the linear separation problem and $\beta = 2.5$ for the nonlinear one. The CPU time spent in evaluating and factorizing the Jacobian matrix, which happens only once for the linear problem but several times for the nonlinear one, scales better with n_τ than the forward-backward substitution steps of the LU algorithm. This explains why the value of β for the nonlinear-isotherm problem is slightly smaller than that for the linear separation problem. Nevertheless, the values of β show a strong superlinear dependence of CPU time on temporal mesh resolution and demonstrate the inability of the LU-factorization algorithm to efficiently solve the linear systems generated

by the nonlinear solver for the particular algebraic systems generated by the complete discretization method.

Table 4 shows the exponent β of the power dependence of CPU time on spatial mesh resolution, i.e. CPU time $\propto (n_{\mathrm{FE}})^{\beta}$, where n_{FE} is the number of finite elements along the the length of the column. The dynamic simulation method exhibits a mild dependence on spatial mesh resolution ($\beta = 0.7$), but the complete discretization method shows again an undesirable strong superlinear dependence ($\beta = 3.1$).

This suggests that a Newton-type nonlinear algebraic equation solver with an embedded LU-factorization algorithm is not the best choice for the complete discretization method, and that the direct linear solver should be replaced by an iterative solver suitable for sparse linear systems. Krylov methods [58, 59] are the most obvious candidates for this task. These methods (such as GMRES or conjugate gradient squared method) solve the linear system $Ax = b$ by repeatedly performing matrix-vector multiplications involving matrix A and, possibly also the conjugate transpose of A (the latter includes methods like Lanczos biorthogonalization, QMR, and biconjugate gradient methods). We believe that the correct choice of the linear solver would substantially reduce the computing time and render the complete discretization method more competitive for nonlinear problems.

Note also that the benchmark tests reported here are representative of the computational effort spent by stochastic optimization codes which require only function evaluations, not derivatives. These methods, such as genetic algorithms [60], adaptive random search [61] and simulated annealing [62–64], are robust and less sensitive to non-convexities in both the objective function and constraints as compared with gradient based methods. They have been recently applied with success for the optimization of the isocratic SMB process [65, 66], Varicol [26, 27, 66], and gradient SMB process [67].

On the other hand, there are many powerful optimization algorithms, such as sequential quadratic programming (SQP) [68, 69], which additionally require the values of the partial derivatives (sensitivities) of the objective function and constraints with respect to the design variables. These methods are less robust when handling the minimization or maximization of nonlinear, non-smooth objective functions. However, if a preliminary parameter study is performed in order to find initial values close to optimum before the optimization problem is solved, these methods require far less function evaluations to converge than stochastic methods [3, 22–25, 28]. If a gradient-based methods is selected, the derivatives are easier to compute (and require less computational effort) from the al-

gebraic solution of the complete discretization method than from the dynamic simulation of the single-column model. For a review of efficient sensitivity calculation methods for large-scale differential-algebraic systems, see Li et al. [70].

The current version of gPROMS imposes restrictions on model formulation for dynamic optimization. For example, it is easy to implement the operating procedure for cyclic operation of the SMB or Varicol processes by means of the elementary tasks and hierarchical sub-task decomposition capability available in the gPROMS language. However, this functionality of the language is lost when the dynamic model is employed for optimization. In this case, the operating procedure must be implemented by means of binary variables, or the equivalent CASE statement built into the language. Furthermore, control over the time horizon required to achieve CSS is lost, and the easiest way to tackle this constraint is to fix the time horizon at a sufficiently large value to guarantee that CSS is always achieved for any set of values of the design variables. Alternatively, one can adopt the simultaneous tailored approach proposed in refs [44, 46, 47] and described in section 3.1.

On the other hand, it is relatively easy to interface the model obtained by the complete discretization method with gOPT, the optimization solver built into gPROMS which is based on a SQP algorithm. However, the optimization of the model obtained by the complete discretization method using gOPT does not appear to be robust and many of our attempts often led to divergence. In fact, the optimized operating parameters listed in Table 1 we obtained by a continuous simulated annealing global optimization algorithm described in ref [71], as implemented and modified by Goffe et al.[72]. CSS calculations for the operating points generated by the optimizer for the linear separation problem were performed using the complete discretization method, whereas for the nonlinear case we resorted to the dynamic simulation method applied to the single-column model.

5 Conclusions

A mathematical framework for developing efficient methods to calculate the periodic state of the SMB process based on single-column models is established. The solution methods are classified into two major classes: dynamic methods which integrate in time, either truly or artificially, the governing equations over a large number of cycles until CSS is reached, and methods which rely on the direct prediction of the CSS by simultaneously discretizing the spatial and temporal coordinates, thereby transforming the model into a

large sparse system of nonlinear algebraic equations.

Our benchmark tests using gPROMS show that the dynamic simulation of the single-column model is more efficient than the traditional dynamic simulation of the full N-column model. The complete discretization approach is the most efficient method when the isotherm model is linear but loses competitiveness for nonlinear isotherm models. This is due to the inefficiency of the general-purpose solver built into gPROMS in solving the nonlinear algebraic system generated by the complete discretization method. This suggests that a Newton-type nonlinear algebraic equation solver with an embedded LU-factorization algorithm is not the best choice for the complete discretization method. We believe that if the direct LU-factorization algorithm is replaced by a Krylov-type iterative linear solver, the computing time is substantially reduced and the complete discretization method becomes more competitive for nonlinear problems. On the other hand, it should be pointed out that the efficiency of the dynamic simulation approach might also be improved by using methods to accelerate cyclic steady-state convergence, such as AItken, Muller, and Broyden based updating schemes [73].

Appendix

In this appendix we describe an efficient method for implementing the discrete buffer in gPROMS. We start by noting that the concentrations comprising the contents of the buffer, $\tilde{c}_i^{(k)}$ $(k = 1, \ldots, n_\mathrm{b})$, are merely auxiliary variables in the simulation. Though they are subjected to a discontinuity every τ_b time units, the key output variable $\tilde{c}_i(t)$ obtained by piecewise-cubic polynomial interpolation is a smooth function of time. Therefore, an explicit periodic update of the contents of the buffer, which involves discarding the oldest concentration value, shifting the other values by one position and updating the newest concentration value, forces an unnecessary reinitialization of the DAE solver every τ_b time units. The trick for an efficient implementation of the buffer is to avoid these unnecessary reinitializations of the DAE solver.

To achieve this the buffer is implemented outside the scope of the simulation module by using the facilites provided by gPROMS[74] for exchanging data with external software (Figure 10). The *foreign process interface* provides a general mechanism for sending information from the executing gPROMS simulation. This communication takes place at discrete time points throughout the duration of the simulation. The user is entirely free to determine the frequency and content of the exchanges. We use this feature to send the value of $c_i^{\mathrm{out}}(t)$ to the external module at every sampling interval . This operation does not have any impact on the simulation (except for forcing an interpolation of the solution at a point which is not necessarily at the time step chosen by the DAE solver). The external module updates the buffer contents in response to the newly received value of c_i^{out}.

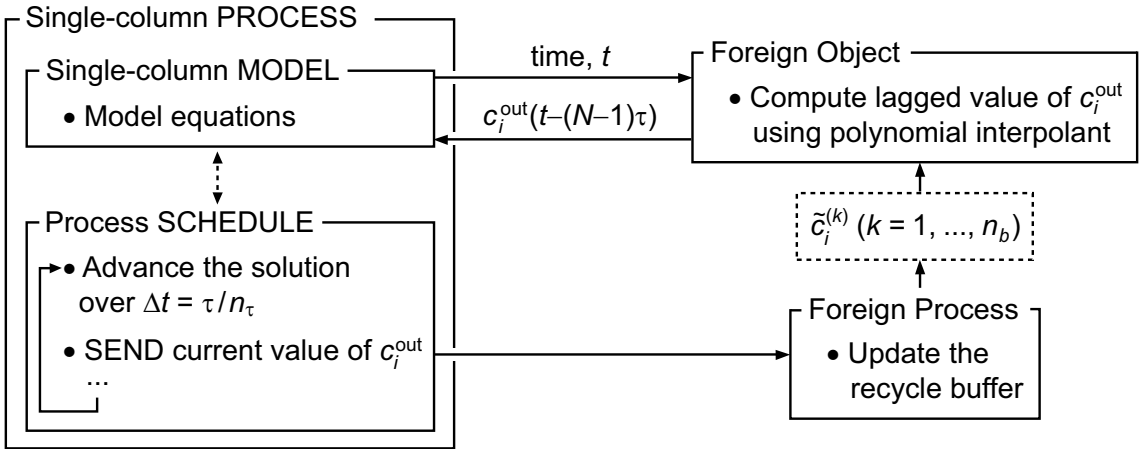

Figure 10: Flowsheet of numerical implementation of the discrete buffer in gPROMS.

Whenever requested, the current value of $\tilde{c}_i(t)$ is returned to gPROMS by means of a *foreign object* which implements the polynomial interpolant. A foreign object is an

external piece of software which provides a gPROMS simulation or optimization run with computational services during run time. This foreign object is defined as having the time variable as single input and $\tilde{c}_i(t)$ as output. gPROMS assumes $\tilde{c}_i(t)$ to be a smooth function of time and, as desired, sees no need to reinitialize the DAE solver every sampling interval.

Nomenclature

A	column cross-sectional area (cm^2)
c	solute concentration (g/l)
d	column diameter (cm)
D	axial dispersion coefficient (cm^2/min)
k	LDF coefficient (s^{-1})
L	column length (cm)
N	number of columns
n_{b}	discrete values solute concentration stored in the buffer
n_{FE}	spatial discretization resolution
n_{s}	number of subdivisions of the switching interval
n_τ	temporal discretization resolution
Pe	Péclet number
q	adsorbed concentration (g/l)
Q	flow rate (cm^3/min)
t	time (min)
t'	modified time (min) for both single-column processes (lag and lead)
v	interstitial fluid velocity (cm/min)
x	axial position in recycle tube (cm)
z	axial position in column (cm)

Greek letters

α	dynamic weighting factor
ϵ	total porosity
τ	switching interval (min)
τ_b	sampling interval of the buffer
θ	dimensionless time

Subscripts and superscripts

E	eluent
ex	external inlet stream
F	feed
i	solute index
I,...,IV	zone index
in	column inlet

j	column index
k	switching interval subinterval index
out	column outlet
R	raffinate
X	extract
$\tilde{}$	discrete value

List of Tables

List of Figures

Bibliography

[1] M. Juza, M. Mazzotti, M. Morbidelli, Trends in Biotech. 18 (2000) 108.

[2] R.M. Nicoud, LC-GC 5 (1992) 43.

[3] A. Jupke, A. Epping, H. Schmidt-Straub, J. Chromatogr. A 944 (2002) 93.

[4] J. Strube, S. Haumreisser, H. Schmidt-Traub, M. Schulte, R. Ditz, Org. Proc. Res. Devel. 2 (1998) 305.

[5] P.C. Wankat, Rate-Controlled Separations. Kluwer: Amsterdam, 1990.

[6] O. Ludemman-Hombourger, R.M. Nicoud, M. Bailly, Sep. Sci. Technol. 35 (2000) 1829.

[7] O. Ludemman-Hombourger, G. Pigorini, R.M. Nicoud, D.S. Ross, G. Terfloth, J. Chromatogr. A 947 (2002) 59.

[8] T.B. Jensen, T.G.P. Reijns, H.A.V. Billiet, L.A.M. van der Wielen, J. Chromatogr. A 873 (2000) 149.

[9] D. Antos, A. Seidel-Morgenstern, Chem. Eng. Sci. 56 (2001) 6667.

[10] S. Abel, M. Mazzotti, M. Morbidelli, J. Chromatogr. A 944 (2002) 23.

[11] J. Houwing, T.B. Jensen, S.H. van Hateren, H.A.H. Billiet, L.A.M. van der Wielen, AIChE J. 49 (2003) 665.

[12] M.M. Kearney, K.L. Hieb, US Patent, 5, 102, 1992.

[13] Y. Zang, P.C. Wankat, Ind. Eng. Chem. Res. 41 (2002) 2504.

[14] Y. Zang, P.C. Wankat, Ind. Eng. Chem. Res. 41 (2002) 5283.

[15] Z. Zhang, M. Mazzotti, M. Morbidelli, J. Chromatogr. A 1006 (2003) 87.

[16] Z. Zhang, M. Mazzotti, M. Morbidelli, AIChE J. 50 (2004) 625.

[17] H. Schramn, M. Kaspereit, A. Kienle, A. Seidel-Morgenstern, Chem. Eng. technol. 25 (2002) 1151.

[18] H. Schramn, M. Kaspereit, A. Kienle, A. Seidel-Morgenstern, J. Chromatogr. A 1006 (2003) 77.

[19] N. Abunasser, P.C. Wankat, Y.S. Kim, Y.M. Koo, Ind. Eng. Chem. Res. 42 (2003) 5268.

[20] N. Abunasser, P.C. Wankat, Ind. Eng. Chem. Res. 43 (2004) 5291.

[21] J.P.B Mota, J.M.M. Arajo, AIChE J. 51 (2005) 1641.

[22] E. Kloppenburg, E.D. Gilles, Chem. Eng. Technol. 22 (1999) 313.

[23] K.U. Klatt, G. Dunnebier, S. Engell, F. Hanisch, Comput. Chem. Eng. 24 (2000) 1119.

[24] A. Toumi, F. Hanisch, S. Engell, Ind. Eng. Chem. Res. 41 (2002) 4328.

[25] A. Toumi, S. Engell, F. Hanisch, Chem. Ing. Tech. 10 (2002) 1483.

[26] Z. Zhang, K. Hidajat, A.K. Ray, M. Morbidelli, AIChE J. 48 (2002) 2800.

[27] Z. Zhang, M. Mazzotti, M. Morbidelli, J. Chromatogr. A 989 (2003) 95.

[28] A. Toumi, S. Engell, O. Ludemann-Hombourger, R.M. Nicoud, M. Bailly, J. Chromatogr. A 1006 (2003) 15.

[29] M. Minceva, L.S. Pais, A.E. Rodrigues, Chem. Eng. Processing 40 (2003) 93.

[30] J.M.M. Araújo, R.C.R. Rodrigues, J.P.B. Mota, Ind. Eng. Chem. Res. 45 (2006) 5314.

[31] L.S. Pais, A.E. Rodrigues, J. Chromatogr. A 1006 (2003) 33.

[32] M.B. Carver, Method-of-lines solution of differential equations—Fundamental principles and recent extensions, Foundations of Computer-Aided Process Design, R.S.H. Mah and W.D. Seider (Eds.); Engineering Foundation, pp. 369-402, New York, NH, 1981.

[33] W.E. Schiesser, The numerical method of lines; Academic Press, New York, 1991.

[34] W. Feehery, J. Tolsma, P. Barton, Appl. Numer. Math. 25 (1997) 41.

[35] S. Li, L. Petzold, Design of new DASPK for Sensitivity Analysis. Technical Report, University of California: Santa Barbara, CA, 1999.

[36] W.E. Stewart, M. Caracotsios, J.P. Sorensen, DDASAC software package documentation, Chemical Engineering Department, University of Wisconsin—Madison: WI, 1995.

[37] R.B. Jarvis, C.C. Pantelides, DASOLV—a differential-algebraic equation solver. Technical report, Center for Process Systems Engineering, Imperial College: London, U.K., 1992.

[38] P.I. Barton, C.C. Pantelides, AIChE J. (40) (1994) 966.

[39] M. Oh, C.C. Pantelides, Comput. Chem. Eng. 20 (1996) 611.

[40] O.J. Smith, A.W. Westerberg, Chem. Eng. Sci. 46 (1991) 2967.

[41] O.J. Smith, A.W. Westerberg, Ind. Eng. Chem. Res. 31 (1992) 1569.

[42] D.T. Croft, M.D. LeVan, Chem. Eng. Sci. 49 (1994) 1821.

[43] Y. Ding, M.D. LeVan, Chem. Eng. Sci. 56 (2001) 5217.

[44] L. Jiang, L.T. Biegler, V.G. Fox, AIChE J. 49 (2003) 1140.

[45] J.M.M. Araújo, R.C.R. Rodrigues, M.F.J. Eusbio, J.P.B. Mota, Presentation P-229 at PREP-2005 Symposium, Philadelphia, Pennsylvania, May 2005.

[46] D. Ko, I. Moon, Ind. Eng. Chem. Res. 41 (2002) 93.

[47] D. Ko, R. Siriwardane, L.T. Biegler, Ind. Eng. Chem. Res. 42 (2003) 329.

[48] S. Nilchan, The optimization of periodic adsorption processes, PhD Diss., Imperial College: London, 1997.

[49] S. Nilchan, C.C. Pantelides, Adsorption 4 (1998) 113.

[50] Cheng, Y. S.; Abi, C. F.; Kershenbaum, L. S. Comput. Chem. Eng. 20 (1996) S793.

[51] I. Yongsunthon, E. Alpay, Comp. Chem. Eng. 22 (1998) S733.

[52] L.S. Pais, J.M. Loureiro, A.E. Rodrigues, Chem. Eng. Sci. 52 (1997) 245.

[53] L.S. Pais, J.M. Loureiro, A.E. Rodrigues, J. Chromatogr. A 769 (1997) 25.

[54] L.S. Pais, J.M. Loureiro, A.E. Rodrigues, Sep. Purif. Technol. 20 (2000) 67.

[55] D.M. Ruthven, B.D. Ching, In: Ganetsos, G., Barker, P. E., eds. Preparative and Production scale chromatography. New York, NY: Marcel Dekker, 629, 1993.

[56] G.F. Carey, B.A. Finlayson, Chem. Eng. Sci. 30 (1975) 587.

[57] B.A. Finlayson, Nonlinear Analysis in Chemical Engineering. McGraw-Hill: New York, 1980.

[58] Y. Saad, Iterative Methods for Sparse Linear Systems. PWS Publishing Company: Boston, 1996.

[59] H.A. van der Vorst, Iterative Krylov Methods for Large Linear Systems. Cambridge Monographs on Applied and Computational Mathematics, No. 13. Cambridge University Press: New York, 2003.

[60] G. Mitsuo, C. Runwei, Genetic Algorithms and Engineering Optimization. John Wiley: New York, 2000.

[61] R. Salcedo, Ind. Eng. Chem. Res. 31 (1992) 262.

[62] R.H.J.M. Otten, L.P.P.P van Ginneken, The annealing algorithm. Kluwer: Boston, 1989.

[63] M. Cardoso, R. Salcedo, S. de Azevedo, D. Barbosa, Comput. Chem. Eng. 21 (1997) 1349.

[64] R. Faber, T. Jockenhovel, G. Tsatsaronis, Comput. Chem. Eng. 29 (2005) 273.

[65] Z. Zhang, K. Hidajat, A.K. Ray, Ind. Eng. Chem. Res. 41 (2002) 3213.

[66] H.J. Subramani, K. Hidajat, A.K. Ray, Comput. Chem. Eng. 27 (2003) 1883.

[67] G. Ziomek, K. Kaspereit, J. Jeyzowski, A. Seidel-Morgenstern, D. Antos, J. Chromatogr. A, 1070 (2005) 111.

[68] D.J. Ternet, L.T. Biegler, Comput. Chem. Eng. 22 (1998) 963.

[69] P.T. Boggs, J.W. Tolle, J. Comput. Appl. Math. 124 (2000) 123.

[70] S. Li, L. Petzold, W. Zhu, Appl. Numer. Math. 32 (2000) 161.

[71] A. Corana, M. Marchesi, C. Martini, S. Ridella, ACM Trans. Math. Soft. 13 (1987) 262.

[72] W.L. Goffe, G.D. Ferrier, J. Rogers, J. Econometrics 60 (1994) 65.

[73] Kvamsdal, H. M.; Hertzberg, T. Comput. Chem. Eng. 21 (1997) 819.

[74] gPROMS advanced user guide, release 2.3; Process Systems Enterprise Ltd; London, U.K., 2004.

Chapter 3

Optimal Design and Operation of a Certain Class of Asynchronous Simulated Moving-Bed Processes

1 Introduction

Simulated moving bed (SMB) chromatography has been increasingly applied for the separation of pure substances in the pharmaceutical, fine chemistry, and biotechnology industries, at all production scales, from laboratory to pilot to production scale [1]. The SMB has many advantages with respect to discontinuous batch chromatography [2], such as higher product purity, less solvent consumption, and higher productivity per unit stationary phase [3–5].

The SMB is a practical way of implementing a counter-current chromatographic process. The system consists of N identical chromatographic columns connected in series to build a closed loop. By moving the input and withdrawal ports one column ahead (i.e. in the direction of fluid flow) at fixed intervals, the counter-current contact between the adsorbent and liquid is simulated. A schematic diagram of a typical four-section SMB is shown in Fig. 1.

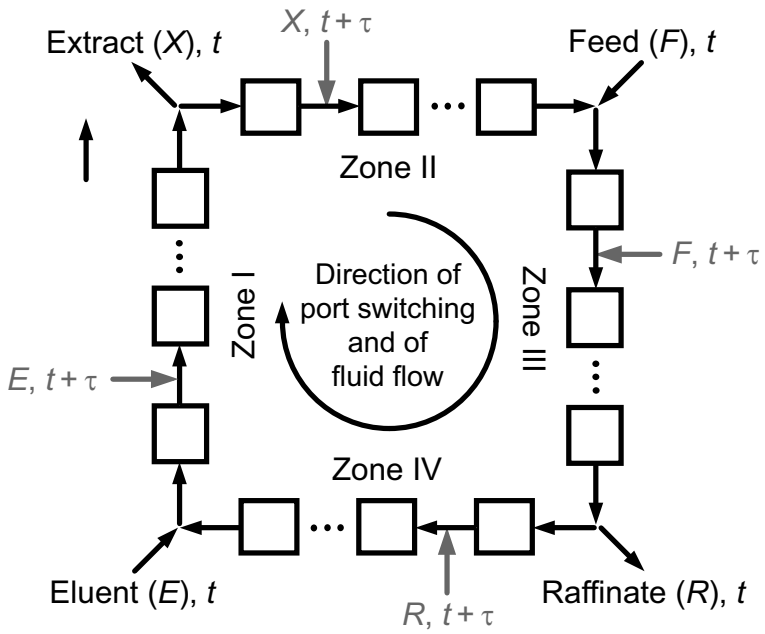

Figure 1: Schematic diagram of a four-section SMB unit. Several chromatographic columns are interconnected circularly, the input and withdrawal ports are moved one column ahead every τ time units. The feed, eluent, extract and raffinate streams are denoted by F, E, X and R, respectively.

Thanks to recent developments in cyclic operation schemes, a number of possibilities for improving SMB performance have emerged through variation of parameters during a switching interval. These include, among others, the asynchronous shift of the inlet and outlet ports [6, 7], modulation of solvent strength [8–11], and cyclic modulation of feed

flow [12–16] and feed concentration [17, 18]. These advances are pushing the trend toward the use of units with a small number of columns, since less stationary phase is used and the setup is more economic.

The optimal design and selection of optimal operating parameters are essential to realize the economic potential of nonstandard SMB operating modes and their successful implementation on industrial scale. These call for the use of advanced optimization procedures coupled with a detailed model of process dynamics. The complexity of the optimization problem is increased further by the intrinsic dynamic nature of the process, which approaches a cyclic steady state after a sufficiently long period of time. For process design the initial transient behavior is of little interest, but only the fully established periodic state. In most cases, the latter has been computed by direct dynamic simulation of the whole process unit. Often, the hypothetical true moving-bed (TMB) process is used as a simplified model for the SMB. The TMB model is continuous and has a stationary state which can be computed easily. However, if a small number of columns is used, or the operating parameters are varied during a switching interval, the system behavior deviates significantly from the classical SMB process and precludes the application of the TMB analogy.

A detailed SMB process model is computationally expensive and becomes an issue for rigorous model-based optimization [19–24], especially when the number of optimization variables is increased by the extra degrees of freedom in the operating conditions of nonstandard SMB processes. Stochastic approaches, as well as gradient-based approaches, have been proposed to tackle the complex optimization problem of continuous chromatographic processes. Stochastic optimization methods, such as genetic algorithms [25], adaptive random search [26] and simulated annealing [27–29], are robust and less sensitive to non-convexities in both the objective function and constraints as compared with gradient-based methods. They have been recently applied with success for the optimization of the isocratic SMB process [30, 31], Varicol [31–34], PowerFeed [34], and gradient SMB process [35]. Gradient-based methods additionally require the values of the partial derivatives (sensitivities) of the objective function and constraints with respect to the design variables. However, if a preliminary parameter study is performed in order to find initial values close to optimum before the optimization problem is solved, these methods require far less function evaluations to converge than stochastic methods [19–24].

In this work [36] (**paper III**), it is firstly establish the cyclic operation of the SMB

process from the necessary conditions for a single-column model to reproduce the cyclic steady-state (CSS) behaviour of the multi-column process. By extending the valid range of number of columns per zone from integer to rational domain, it is shown that a physically realizable class of asynchronous processes is readily obtained from the same set of governing equations. Secondly, it is briefly described an optimization strategy that relies on simultaneous temporal and spatial discretization to directly compute the CSS solution at every step of the optimization procedure. This is shown to be very efficient for chromatography optimization. The feasibility of this approach is demonstrated on the separation of an enantiomeric mixture with nonlinear isotherm. Units with a small number of columns, between three and five, are considered, since they look more promising for future applications of SMB and related technologies. The results presented here, as well as those of other authors, show that significant performance improvements can be achieved by varying some of the operating parameters during the switching interval. It is further shown that eluent consumption for some of the optimized asynchronous configurations can be significantly reduced by modulation of eluent flow rate partial product withdrawal.

2 Mathematical formulation

In the notation employed here the N columns are numbered sequentially in the direction of liquid flow. Because they are connected circularly, the column index is implicitly defined modulo N. Thus, $j = 0$ actually means column N, whereas $j = N + 1$ is the same as referring to column 1.

Figure 2 shows the schematic of a generic node between two consecutive columns, say $j - 1$ and j. The notation employed is as follows: Q is the liquid flow rate, $c^{\text{out}}_{i,j-1}$ is the concentration of solute i at the outlet of column $j - 1$ and c^{in}_{ij} is the corresponding solute concentration at the inlet of column j. The solute concentration and flow rate of the external inlet/outlet lines are identified by scripts E (eluent), X (extract), F (feed), and R (raffinate).

Note that in the node schematic of Fig. 2 the sequence in which the inlet/outlet lines are connected to the node is such that it allows certain zones to cease to exist temporarily, while avoiding mixing issues and occurrence of short-cut streams. In particular, the asynchronous port switching explored in this work can temporarily suppress zone I and zone IV. In the former case eluent is added and extract is withdrawn simultaneously

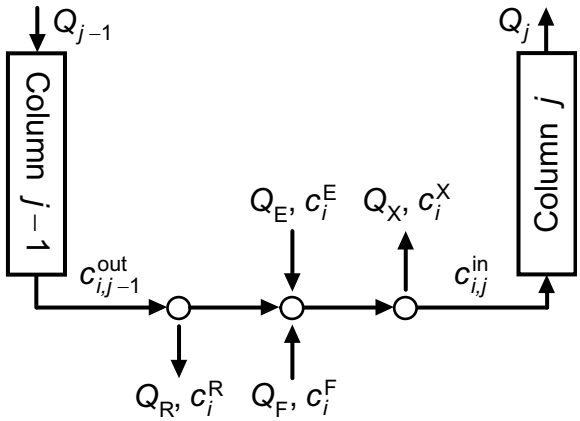

Figure 2: Schematic of node connecting columns $j-1$ and j of an SMB unit. The concentration of solute i in liquid phase is c_i and Q is the volumetric flow rate. Scripts E, X, F, and R denote eluent, extract, feed and raffinate lines, respectively.

on the same node, whereas in the latter case raffinate is withdrawn from the node into which eluent is being simultaneously introduced. The two remaining options, suppression of zones II or III, are not taken into consideration in the node schematic of Fig. 2, because they are unlikely to occur in practice. The purpose of these zones is to prevent the contamination of the extract and raffinate streams with the undesired component; product purity would be affected if they ceased to exist. Note, however that the equations given below are of general applicability provided that lines do not cross each other and that adjacent zones do not cease to exist simultaneously.

Under the assumptions discussed above, the solute node balance can be written as

$$\begin{cases} Q_{\mathrm{III}}\, c_{ij}^{\mathrm{in}} = \ Q_{\mathrm{II}}\, c_{i,j-1}^{\mathrm{out}} + (Q_{\mathrm{III}} - Q_{\mathrm{II}})\, c_i^{\mathrm{F}}, & \text{feed node} \\ Q_{\mathrm{I}}\, c_{ij}^{\mathrm{in}} = Q_{\mathrm{IV}}\, c_{i,j-1}^{\mathrm{out}} + \ (Q_{\mathrm{I}} - Q_{\mathrm{IV}})\, c_i^{\mathrm{E}}, & \text{eluent node}, \\ c_{ij}^{\mathrm{in}} = \qquad c_{i,j-1}^{\mathrm{out}}, & \text{otherwise} \end{cases} \tag{1}$$

where $Q_{\mathrm{I}}, \ldots Q_{\mathrm{IV}}$ are the flow rates in the four sections of the SMB. These obey the global node balances

$$Q_{\mathrm{I}} = Q_{\mathrm{IV}} + Q_{\mathrm{E}}, \quad Q_{\mathrm{II}} = Q_{\mathrm{I}} - Q_{\mathrm{X}}, \quad Q_{\mathrm{III}} = Q_{\mathrm{II}} + Q_{\mathrm{F}}, \quad Q_{\mathrm{IV}} = Q_{\mathrm{III}} - Q_{\mathrm{R}}. \tag{2}$$

The cyclic operation of the SMB process is achieved by moving the inlet and outlet ports one column downstream (i.e. in the direction of fluid flow) every τ time units, where τ is the switching interval. Mathematically, this can be expressed as

$$\Omega_j(t) = \Omega(t_j), \quad t_j = [t - (j-1)\tau] \bmod N\tau, \tag{3}$$

where Ω_j denotes the set of input variables for column j, which includes Q_j and the state (opened or closed) of the four inlet/outlet lines connected to its inlet node; 'mod' defines

the usual modulo operator: $a \bmod b \equiv a - b\,\mathrm{int}(a/b)$. Note that Eq. (3) imposes a $N\tau$ periodicity on $\Omega_j(t)$ and that

$$\Omega_{j-1}(t) = \Omega_j(t+\tau). \tag{4}$$

For the classical SMB process Ω and c_i^{F} are constant, but in the present analysis they are allowed to be τ-periodic input functions so that the mathematical formulation presented here can encompass other cyclic operation schemes. For example, processes that vary the flow rates to improve the separation performance [12–16] change some, or all, of the flow rates from continuous constant flow to τ-periodic flow, while still satisfying the global constraint $Q_{\mathrm{E}} + Q_{\mathrm{F}} = Q_{\mathrm{X}} + Q_{\mathrm{R}}$. Similarly, in the ModiCon process [17, 18], which is based on the concept of cyclic modulation of the feed concentration, c_i^{F} is changed to a piecewise-constant τ-periodic function. The VARICOL process [6, 7, 21, 22], which implements an asynchronous port switching resulting in a variation of column configuration, fits into our formulation provided that one is able to define a global switching interval as the time required for each of the inlet/outlet lines to be shifted by one column.

Because of the circular column arrangement and periodic nature of the operating parameters, after a sufficiently long period of time the process approaches a cyclic steady-state (CSS) regime. This cyclic steady behavior is attained when all state variables that characterize the chromatographic columns have the same time periodicity as that expressed by Eq. (3) for $\Omega_j(t)$. Following Eq. (4), the CSS condition for the SMB process can be written as

$$c_{i,j-1}(z,t) = c_{ij}(z,t+\tau), \quad q_{i,j-1}(z,t) = q_{ij}(z,t+\tau) \quad (0 \le z \le L), \tag{5}$$

where z is the axial spatial coordinate along each column, L is the column length, and q_i is the solute concentration in adsorbed phase. Eq. (5) states that under CSS conditions the spatially-distributed concentration profiles distanced by τ time units are identical, apart from a shift of one column. Note that the CSS condition, as expressed by Eq. (5), must be extended to the other state variables that characterize column behavior for more complex cyclic operation schemes (e.g., eluent strength in the case of gradient-eluent SMB operation [8–11], temperature profile if the columns are dynamically heated [37], etc.).

For process design the CSS regime is the relevant period of process operation, except for unusually short campaigns, and for the classical SMB process it is usually attained after a moderate number of cycles (each cycle is $N\tau$ long). By applying the CSS condition [Eq. (5)] to the solute node balance, either backward or forward in time, we have recently

demonstrated [38, 39] that the periodic state of the SMB process is reproduced by two different single-column chromatographic models. The one of interest to the present work is obtained by replacing every occurrence of $c_{i,j-1}^{\text{out}}(t)$ in Eq. (1) by $c_{ij}^{\text{out}}(t+\tau)$, so that all references to column $j-1$ are removed from the node balance. Figure 3 shows a block diagram of the resulting single-column chromatographic model. Hereafter, we employ this model as a convenient tool for specifying cyclic operation schemes, efficient CSS evaluation, and process optimization.

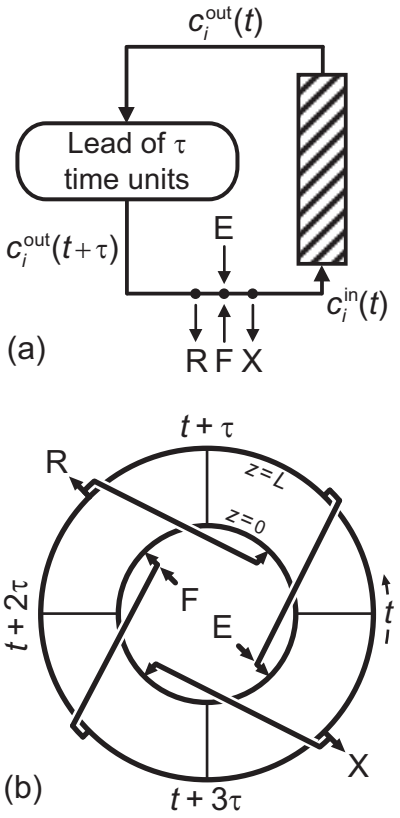

Figure 3: (a) Block diagram of single-column chromatographic model with recycle lead, which is a discontinuous replica of the periodic state of the SMB process, and (b) schematic of $N\tau$-periodic cycle when the model simulates a classical 4-column SMB. The radial coordinate of the annular plot represents the axial position along the column, whereas the angular coordinate represents the time coordinate over a complete cycle of operation.

To establish the periodic operation of an SMB process one has to specify the time interval during which each clause of the node balance [Eq. (1)] applies, the profile of liquid flow-rate through the column, and the time intervals during which the two product streams are collected. To do this, it is convenient to define a dimensionless time coordinate

$\theta = t/\tau$ and introduce the auxiliary parameters

$$\begin{cases} \theta_4 = N_{\mathrm{IV}} \\ \theta_3 = N_{\mathrm{III}} + \theta_4 = N_{\mathrm{IV}} + N_{\mathrm{III}} \\ \theta_2 = N_{\mathrm{II}} + \theta_3 = N_{\mathrm{IV}} + N_{\mathrm{III}} + N_{\mathrm{II}} \\ \theta_1 = N_{\mathrm{I}} + \theta_2 = N_{\mathrm{IV}} + N_{\mathrm{III}} + N_{\mathrm{II}} + N_{\mathrm{I}} = N \end{cases}, \tag{6}$$

which are related to the chosen column configuration $N_{\mathrm{I}}/N_{\mathrm{II}}/N_{\mathrm{III}}/N_{\mathrm{IV}}$, where $N_{\mathrm{I}}, \ldots, N_{\mathrm{IV}}$ are the number of columns in sections I, ..., IV, of the SMB unit, respectively.

The solute node balance can then be written as

$$\begin{cases} Q_{\mathrm{III}}\, c_i^{\mathrm{in}}(\theta) = Q_{\mathrm{II}}\, c_i^{\mathrm{out}}(\theta+1)' + (Q_{\mathrm{III}} - Q_{\mathrm{II}})\, c_i^{\mathrm{F}}, & \theta_3 - 1 < \theta' < \theta_3 \\ Q_{\mathrm{I}}\, c_i^{\mathrm{in}}(\theta) = Q_{\mathrm{IV}}\, c_i^{\mathrm{out}}(\theta+1)' + (Q_{\mathrm{I}} - Q_{\mathrm{IV}})\, c_i^{\mathrm{E}}, & \theta_1 - 1 < \theta' < \theta_1 \\ c_i^{\mathrm{in}}(\theta) = c_i^{\mathrm{out}}(\theta+1)', & \text{otherwise} \end{cases}, \tag{7}$$

where $\theta' = \theta \bmod N$ and, for simplicity, the j subscript is omitted because its value is fixed (we are tracking the dynamics of a fixed column of the SMB unit). The choice of the value for j is arbitrary because all columns are assumed to be identical and undergo the same cycle; one model with $j = j_1$ behaves similarly to another model with $j = j_2$, except for a simple phase difference of $|j_2 - j_1|\tau$.

The temporal profile of liquid flow-rate through the column is piecewise-constant because the column changes zone over time, and is given by

$$Q(\theta) = \begin{cases} Q_{\mathrm{IV}}, & 0 < \theta' < \theta_4 \\ Q_{\mathrm{III}}, & \theta_4 < \theta' < \theta_3 \\ Q_{\mathrm{II}}, & \theta_3 < \theta' < \theta_2 \\ Q_{\mathrm{I}}, & \theta_2 < \theta' < \theta_1 \end{cases}. \tag{8}$$

Finally, the solute concentrations in product streams are expressed as

$$Q_{\mathrm{I}}\, c_i^{\mathrm{X}} = \begin{cases} Q\, c_i^{\mathrm{out}} + (Q_{\mathrm{I}} - Q)\, c_i^{\mathrm{E}}, & \theta_2 < \theta' < \theta_2 + 1 \\ 0, & \text{otherwise} \end{cases} \quad (N_{\mathrm{I}} \geq 1) \tag{9}$$

$$Q_{\mathrm{I}}\, c_i^{\mathrm{X}} = \begin{cases} Q\, c_i^{\mathrm{out}} + (Q_{\mathrm{I}} - Q)\, c_i^{\mathrm{E}}, & 0 < \theta' < \theta_2 + 1 - \theta_1 \\ & \text{and } \theta_2 < \theta' < \theta_1 \\ 0, & \text{otherwise} \end{cases} \quad (N_{\mathrm{I}} < 1) \tag{10}$$

$$Q_{\mathrm{III}}\, c_i^{\mathrm{R}} = \begin{cases} Q\, c_i^{\mathrm{out}} + (Q_{\mathrm{III}} - Q)\, c_i^{\mathrm{F}}, & \theta_4 < \theta' < \theta_4 + 1 \\ 0, & \text{otherwise} \end{cases} \tag{11}$$

One advantage of this formulation is that by extending the range of valid values for N_{I}, ..., N_{IV} from integer to rational domain, one can generate a whole class of asynchronous port switching schemes univocally defined by the four rational numbers N_{I}, ..., N_{IV} (provided that $N = \sum N_j$ is still an integer), which now define the average number of columns per zone. The continuous chromatographic processes generate by this procedure have the following properties with respect to the movement of the input/output lines:

- the lines do not cross each other;
- the lines only move downstream;
- each line is moved only once every τ time units.

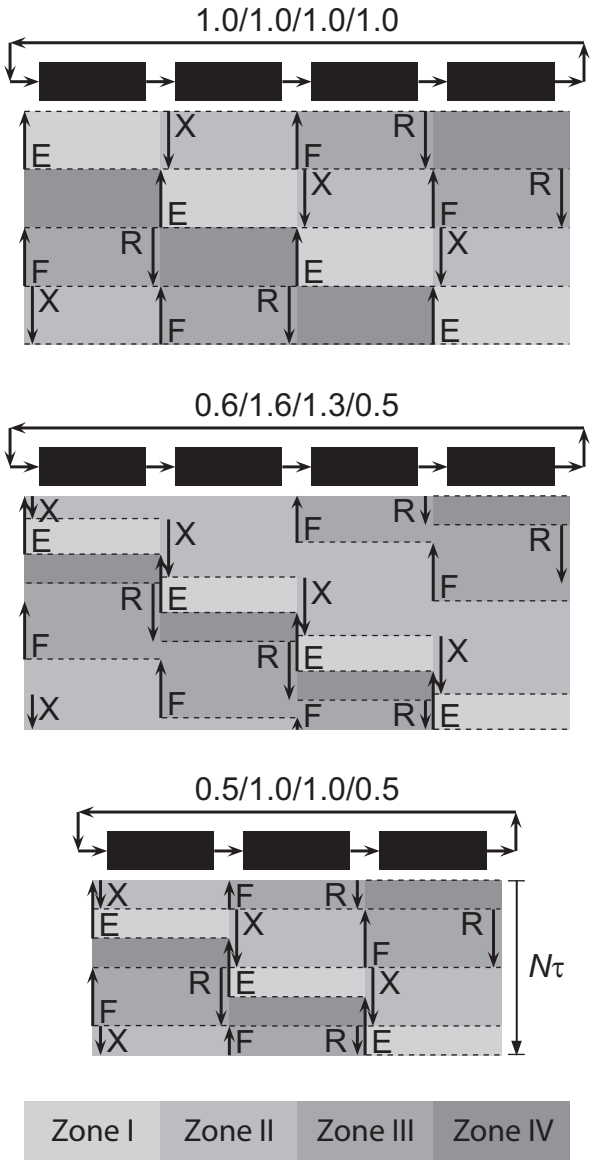

Figure 4: Chronograms of port switching obtained from Eqs. (6)–(11) for 3 different choices of $N_{\mathrm{I}}/N_{\mathrm{II}}/N_{\mathrm{III}}/N_{\mathrm{IV}}$.

Figure 4 shows chronograms of port switching obtained by the aforementioned formulation for three different choices of $N_{\mathrm{I}}/N_{\mathrm{II}}/N_{\mathrm{III}}/N_{\mathrm{IV}}$. The top chronogram reproduces the classical four-column SMB process with one column per zone. The middle chronogram describes the asynchronous port switching for a 4-column Varicol process with average number of columns per zone 0.6/1.6/1.3/0.5; the bottom chronogram is a representative example of a 3-column Varicol process (0.5/1.0/1.0/0.5). Although a 4-zone SMB cannot

be operated with 3 columns, this is made possible by desynchronizing the port switching. Notice that the inlet node of the rightmost column ($j = N$) of each configuration plotted in Fig. 4 is governed by Eqs. (7)–(11); the nodes of the other columns are governed by the same set of equations but with the appropriate time shifts according to Eq. (4).

The average number of columns per zone must be constrained in order to obtain physically realizable processes. Obviously, $N_j > 0$ and $\sum N_j = N$. But more subtle constraints arise when the system is analyzed in more detail. Firstly, we do not allow raffinate and extract to be simultaneously withdrawn from the same column. Therefore, the intersection of the time periods $\Delta\theta_{\mathrm{R}} = [\theta_4, \theta_4 + 1]$ and $\Delta\theta_{\mathrm{X}} = [\theta_2, \theta_2 + 1]$ must be void, which leads to the inequalities $\theta_4 + 1 \leq \theta_2$ and $\theta_2 + 1 \leq \theta_1 + \theta_4$. These can be expressed in terms of average number of columns per zone as

$$N_{\mathrm{II}} + N_{\mathrm{III}} \geq 1 \quad \text{and} \quad N_{\mathrm{I}} + N_{\mathrm{IV}} \geq 1. \tag{12}$$

Secondly, feed and eluent are not allowed to be added simultaneously on the same node. This means that the time periods $\Delta\theta_{\mathrm{F}} = [\theta_3 - 1, \theta_3]$ and $\Delta\theta_{\mathrm{E}} = [\theta_1 - 1, \theta_1]$ cannot overlap, i.e. $\theta_3 \geq 1$ and $\theta_1 - 1 \geq \theta_3$. This restriction reduces to

$$N_{\mathrm{I}} + N_{\mathrm{II}} \geq 1 \quad \text{and} \quad N_{\mathrm{III}} + N_{\mathrm{IV}} \geq 1. \tag{13}$$

Overall, these constraints force every two adjacent zones of the unit to span at least one column on average.

3 CSS evaluation

In a recent paper [39] we have compared efficient methods to calculate the periodic state of the SMB process. The solution methods investigated can be classified into two major classes: dynamic methods which integrate in time, either truly or artificially, the governing equations over a large number of cycles until CSS is reached, and methods which rely on the direct CSS prediction by simultaneously discretizing the spatial and temporal coordinates, thereby transforming the model into a large sparse system of nonlinear algebraic equations.

As in previous work, the results reported here were obtained using gPROMS, a software package for the modeling and simulation of lumped and distributed-parameter process models with combined discrete and continuous characteristics [40, 41]. In [39] our benchmark tests led us to conclude that the full-discretization approach is the most efficient method when the isotherm model is linear but loses competitiveness for nonlinear

isotherm models. This conclusion was based on a gPROMS implementation of the fully discretized model which included an unnecessary large number of auxiliary variables. Furthermore, the tests were only done for an 8-column SMB configuration. However, recent benchmark tests for lower number of columns using a newly implemented version of the full-discretization method with a minimum number of variables favor the complete discretization approach over dynamic simulation, even for nonlinear isotherm models.

The full-discretization method is detailed elsewhere [39], and only a brief description is presented here for clarity. In essence, the method consists of discretizing the time coordinate for the single-column model over a complete cycle ($N\tau$ time units) and directly imposing the periodic condition

$$c_{ij}(z, t + N\tau) = c_{ij}(z, t), \quad q_{ij}(z, t + N\tau) = q_{ij}(z, t) \quad (0 \leq z \leq L). \tag{14}$$

This replaces the original dynamic system by a set of partial differential equations, which depend only on the spatial coordinate and in which the periodic boundary condition is implicitly defined. This system is then converted to a (large) sparse system of nonlinear algebraic equations by applying an appropriate discretization scheme to the spatial derivatives. The resulting algebraic system is solved using a suitable nonlinear algebraic equation solver appropriate for sparse systems. This approach has been referred to in the literature as full-, global-, or simultaneous-discretization method, and first proposed for cyclic adsorption processes by Nilchan and Pantelides [42, 43] who applied it to a pressure swing adsorption process. It has also been tested by other authors on similar [44, 45] or related problems [46, 47].

In our implementation of the method, each switching interval is divided into n_τ smaller time intervals of dimensionless length $\Delta\theta = 1/n_\tau$. Given that the overall duration of the cycle is $N\tau$, the total number of temporal discretization points is $n_\tau N$. The solution is calculated at the dimensionless time instants

$$\theta_k = \Delta\theta(k - 0.5), \quad k = 1, \ldots, n_\tau N, \tag{15}$$

which are purposively staggered with respect to the switching intervals in order to avoid handling the step change on the value of the input variables $\Omega(t)$ when the inlet/outlet ports are commuted. The partial derivatives of solute concentration with respect to time, $\partial y/\partial\theta$, where $y \equiv \{c_1(z, \theta), c_2(z, \theta), q_1(z, \theta), q_2(z, \theta)\}$, are replaced by a third-order back-

ward differencing formula:

$$\left.\frac{\partial y(z,\theta)}{\partial t}\right|_{\theta_k} = \frac{2y(z,\theta_{k+1}) + 3y(z,\theta_k) - 6y(z,\theta_{k-1}) + y(z,\theta_{k-2})}{6\Delta\theta}, \qquad k = 1,\ldots,n_\tau N. \tag{16}$$

Taking into account the periodic condition $y(z,\theta - N) = y(z,\theta) = y(z,\theta + N)$, it is straightforward to eliminate the external nodes, which appear in the differencing formulae for the time instants θ_1, θ_2 and $\theta_{n_\tau N}$, by noting that

$$y(z,\theta_{-1}) \equiv y(z,\theta_{n_\tau N-1}), \quad y(z,\theta_0) \equiv y(z,\theta_{n_\tau N}), \quad y(z,\theta_{n_\tau N+1}) \equiv y(z,\theta_1). \tag{17}$$

The discretization of Eqs. (6)–(11) with respect to the time coordinate is summarized next. First, the θ's are converted to their nearest integers. In practice it is more convenient to work with

$$k_j = \text{nint}\{\, n_\tau \theta_j \,\}, \quad j = 1,\ldots,4, \tag{18}$$

where $\text{nint}\{\,\cdot\,\}$ is the round-to-integer function, i.e. it rounds its argument to the nearest whole number.

The discretization of the node balance given by Eq. (7) can be written in generic form as

$$\begin{cases} Q^{\text{in}}(\theta_k)\, c_i^{\text{in}}(\theta_k) = [Q^{\text{in}}(\theta_k) - Q^{\text{out}}(\theta_k)]\, c_i^{\text{ex}}(\theta_k) + Q^{\text{out}}(\theta_k)\, c_i^{\text{out}}(\theta_{k+n_\tau}), & k \le k_1 - n_\tau \\ Q^{\text{in}}(\theta_k)\, c_i^{\text{in}}(\theta_k) = [Q^{\text{in}}(\theta_k) - Q^{\text{out}}(\theta_k)]\, c_i^{\text{ex}}(\theta_k) + Q^{\text{out}}(\theta_k)\, c_i^{\text{out}}(\theta_{k+n_\tau-k_1}), & k > k_1 - n_\tau \end{cases} \tag{19}$$

where

$$(Q^{\text{in}}, Q^{\text{out}}, c_i^{\text{ex}}) = \begin{cases} (Q_{\text{III}}, Q_{\text{II}}\ , c_i^{\text{F}}), & k_3 - n_\tau < k \le k_3 \\ (\ Q_{\text{I}}\ , Q_{\text{IV}}, c_i^{\text{E}}), & k_1 - n_\tau < k \le k_1 \\ (\ 1\ \ ,\ \ 1\ \ ,\ 0\ ), & \text{otherwise} \end{cases} . \tag{20}$$

The temporal profile of liquid flow rate in the column, written in discrete form, is

$$Q(\theta_k) = \begin{cases} Q_{\text{IV}}, & 1 \le k \le k_4 \\ Q_{\text{III}}, & k_4 < k \le k_3 \\ Q_{\text{II}}, & k_3 < k \le k_2 \\ Q_{\text{I}}, & k_2 < k \le k_1 \end{cases} \tag{21}$$

Finally, the solute concentration in product streams is obtained as follows:

$$Q_{\text{I}}\, c_i^{\text{X}}(k) = \left\{ \begin{cases} Q(\theta_k)\, c_i^{\text{out}}(\theta_k) + \ [Q_{\text{I}} - Q(\theta_k)]\, c_i^{\text{E}}, & k_2 < k \le k_2 + n_\tau \\ 0, & \text{otherwise} \end{cases} \right\} \ (N_{\text{I}} \ge 1) \tag{22}$$

$$Q_{\text{I}}\, c_i^{\text{X}}(k) = \left\{ \begin{cases} Q(\theta_k)\, c_i^{\text{out}}(\theta_k) + \ [Q_{\text{I}} - Q(\theta_k)]\, c_i^{\text{E}}, & 1 \le k \le k_2 + n_\tau - k_1 \\ & \text{and} \ \ k_2 < k \le k_1 \\ 0, & \text{otherwise} \end{cases} \right\} \ (N_{\text{I}} < 1) \tag{23}$$

$$Q_{\text{III}}\, c_i^{\text{R}}(\theta_k) = \begin{cases} Q(\theta_k)\, c_i^{\text{out}}(\theta_k) + [Q_{\text{III}} - Q(\theta_k)]\, c_i^{\text{F}}, & k_4 < k \le k_4 + n_\tau \\ 0, & \text{otherwise} \end{cases} \tag{24}$$

To summarize, the discretization of the time coordinate replaces the original dynamic system by a set of partial differential equations

$$F_z(y) = 0, \quad y(z) = [y(z, \theta_1), \ldots, y(z, \theta_{n_\tau N})], \tag{25}$$

which depend only on the spatial coordinate z, and in which the periodic condition is implicitly defined. This system is then converted to a (large) sparse system of nonlinear algebraic equations by applying an appropriate discretization scheme to the spatial derivatives. The resulting algebraic system is solved using a suitable nonlinear algebraic equation solver appropriate for sparse systems.

4 Optimization strategy

In the most general case, the task of finding the optimal design and operation of a chromatographic process for a given separation is the minimization of the separation costs [48]. A realistic cost calculation must take into account the costs of stationary phase, mobile phase and solvent recovery, personnel, plant, and product upgrading and losses [3, 49]. For a new separation some of these contributions may be only approximately known, and their relative weight may change from from laboratory to pilot to production scale. In other cases, the cost considerations can be simplified. For example, the overall cost of production-scale enantiomeric separation depends mostly on the costs of stationary and mobile phases [49]. But even in this simpler case, maximization of productivity and minimization of solvent requirement are competing objectives and can only be conciliated through a detailed cost analysis of the two contributions. In some cases the solvent is inexpensive, but the energy necessary for evaporation in product upgrading can contribute significantly to the total cost calculation.

Here, we follow the simpler approach of focusing on the benefits that can be gained by upgrading an existing system to asynchronous operation. We note that this is only possible in practice if the the port switching is not implemented by means of a single rotary valve, as in the original UOP process. This analysis only requires single objective functions, to avoid competing effects, which have no specific cost coefficients and are explicitly constrained by product quality. The column length and particle diameter are important design parameters [50, 51], but are not treated as adjustable parameters in this work. Inequality constraints are imposed on product purity (and/or recovery) and on flow rate in zone I. The later constraint is an approximate way of specifying a maximum

admissible pressure drop in the unit. The objective function is either the maximization of feed throughput (Q_{F}) or minimization of eluent flow rate (Q_{E}) for a given feed throughput. The former objective function can be constrained by either fixing eluent consumption ($Q_{\mathrm{E}}/Q_{\mathrm{F}}$) or its flow rate ($Q_{\mathrm{E}}$).

The most natural design parameters are the flow rates of eluent (Q_{E}), extract (Q_{X}), feed (Q_{F}) and recycle (Q_{IV}), and the switching interval (τ). To also optimize the asynchronous port switching, the average lengths of three among the four sections must be added to the set of design parameters (N_{I}–N_{III} are allowed to vary in the present work; N_{IV} is obtained from the relation $\sum N_j = N$). The optimization problem can thus be formulated with 5 or 8 degrees of freedom, depending on whether the port configuration is specified or optimized. However, as pointed out previously in the literature [19, 21, 22], the choice of the flow rates of inlet and outlet streams as degrees of freedom results in an ill-conditioned optimization problem. A less coupled optimization problem can be obtained if the above-mentioned optimization variables are replaced by the key design parameters for the equivalent true counter-current unit as determined by equilibrium theory:

$$Q_{\mathrm{s}} = \frac{(1-\epsilon)V}{\tau}, \quad m_j = \frac{Q_j}{Q_{\mathrm{s}}} - \frac{\epsilon}{1-\epsilon} \quad (j = \mathrm{I}, \ldots, \mathrm{IV}). \tag{26}$$

Here, V is the column volume, Q_{s} is the apparent volumetric solid flow rate, Q_j is the volumetric flow rate in section j of the SMB unit and m_j is the corresponding net flow-rate ratio. The m-factors, which were introduced by the group of Mazzotti and Morbidelli in their well-known triangle theory [52–56], reflect the fact that in a counter-current process, the absolute value of the flow rates is unimportant, but only their values relative to the apparent solid movement [57].

If one of the inlet flow rates is fixed (i.e. $Q_{\mathrm{F}} = Q_{\mathrm{F}}^{\mathrm{fix}}$ or $Q_{\mathrm{E}} = Q_{\mathrm{E}}^{\mathrm{fix}}$), Q_{s} is removed from the set of optimization variables and determined as follows:

$$Q_{\mathrm{s}} = \frac{Q_{\mathrm{E}}^{\mathrm{fix}}}{m_{\mathrm{I}} - m_{\mathrm{IV}}} \quad \text{or} \quad Q_{\mathrm{s}} = \frac{Q_{\mathrm{F}}^{\mathrm{fix}}}{m_{\mathrm{III}} - m_{\mathrm{II}}}. \tag{27}$$

The nonlinear programming problem (NLP) is summarized in Table 1, and in our current implementation is handled by solver SolvOpt [58]. One reason for not employing the default NLP solver of gPROMS 2.3.7 are restrictions imposed on model formulation for optimization purposes. For example, it is easy to implement the operating procedure for asynchronous cyclic operation by means of the elementary tasks and hierarchical sub-task decomposition capability available in the gPROMS language. However, this functionality of the language is lost when the process model is employed for optimization. In this

Table 1: Outline of optimization problem.

Optimization variables
$\{Q_\mathrm{s}, m_\mathrm{I}, \ldots, m_\mathrm{IV}\}$ or $\{Q_\mathrm{s}, m_\mathrm{I}, \ldots, m_\mathrm{IV}, N_\mathrm{I}, N_\mathrm{II}, N_\mathrm{III}\}$
Objective function
$\max\{Q_\mathrm{F} : \text{fixed } \phi \in (\varnothing, Q_\mathrm{E}, Q_\mathrm{E}/Q_\mathrm{F})\}$ or $\min\{Q_\mathrm{E} : \text{fixed } \phi \in (Q_\mathrm{F}, Q_\mathrm{E}/Q_\mathrm{F})\}$
Basic constraints
$Q_\mathrm{s} > 0, \quad Q_\mathrm{I} < Q_\mathrm{I}^\mathrm{max}$
Purity requirements
$P_{\mathrm{R},1} = \dfrac{\int_0^{\theta_1} Q_\mathrm{R} c_1^\mathrm{R}\,\mathrm{d}\theta}{\int_0^{\theta_1} Q_\mathrm{R}(c_1^\mathrm{R} + c_2^\mathrm{R})\,\mathrm{d}\theta} \geq P_\mathrm{R}^\mathrm{min}, \quad P_{\mathrm{X},2} = \dfrac{\int_0^{\theta_1} Q_\mathrm{X} c_2^\mathrm{X}\,\mathrm{d}\theta}{\int_0^{\theta_1} Q_\mathrm{X}(c_1^\mathrm{X} + c_2^\mathrm{X})\,\mathrm{d}\theta} \geq P_\mathrm{X}^\mathrm{min}$
Recovery requirements
$R_{\mathrm{R},1} = \dfrac{\int_0^{\theta_1} Q_\mathrm{R} c_1^\mathrm{R}\,\mathrm{d}\theta}{\int_0^{\theta_1} Q_\mathrm{F} c_1^\mathrm{F}\,\mathrm{d}\theta} \geq R_\mathrm{R}^\mathrm{min}, \quad R_{\mathrm{X},2} = \dfrac{\int_0^{\theta_1} Q_\mathrm{X} c_2^\mathrm{X}\,\mathrm{d}\theta}{\int_0^{\theta_1} Q_\mathrm{F} c_2^\mathrm{X}\,\mathrm{d}\theta} \geq R_\mathrm{X}^\mathrm{min}$
Feasibility constraints on m-factors
$m_\mathrm{I} > m_\mathrm{IV} > 0$, $(Q_\mathrm{E} > 0)$ $\quad m_\mathrm{I} > m_\mathrm{II}$, $(Q_\mathrm{X} > 0)$ $\quad m_\mathrm{III} > m_\mathrm{II} > 0$, $(Q_\mathrm{F} > 0)$ $\quad m_\mathrm{III} > m_\mathrm{IV}$ $(Q_\mathrm{R} > 0)$
Feasibility constraints on section length
$N_\mathrm{I} + N_\mathrm{II} \geq 1, \quad N_\mathrm{II} + N_\mathrm{III} \geq 1, \quad N_\mathrm{III} + N_\mathrm{IV} \geq 1, \quad N_\mathrm{I} + N_\mathrm{IV} \geq 1$

case, the operating procedure must be implemented by means of binary variables, or the equivalent CASE statement built into the language. Furthermore, the default NLP solver of gPROMS is not a feasible path solver. These reasons led us to handle the optimization problem using an external NLP solver while still carrying out the CSS calculations within gPROMS.

SolvOpt minimizes or maximizes nonlinear, possibly non-smooth objective functions and solves nonlinear programming problems taking into account constraints by the so-called method of exact penalization. The implemented method is a version of Shor's minimization method with space dilation [59]. This algorithm seems to be one of the most efficient methods for the minimization of non-smooth (i.e., almost-differentiable) functions. This is one of the reasons for selecting SolvOpt, since the purity constraints have a non-smooth dependence on the N_j's due to the full-discretization method adopted.

SolvOpt is a gradient-based NLP solver and, therefore, requires the gradient of the objective function as well as the gradient of the constraint with maximal residual at a point. Note that the objective function and all but one of the constraints do not depend on the solution of the CSS model and are computed at no cost. In fact, the only component of the optimization problem which is dependent on the CSS solution are the inequality constraints on product purity or recovery. The same applies to the gradients of the objective function and constraints, which are computed analytically except for those of the purity (or recovery) constraints. These are evaluated using first-order forward differencing:

$$\frac{\partial g}{\partial \phi_i} = \frac{g(\phi_i + \delta\phi_i) - g(\phi_i)}{\delta\phi_i} \tag{28}$$

The values of the optimization variables are iteratively updated according to SolvOpt's NLP algorithm. Whenever the purity (or recovery) constraints, or their gradients, are required by the optimization procedure, the values of Q_s and m_j's are converted into flow rates and switching interval and, together with the values of N_I–N_IV, sent to gPROMS for computing the corresponding CSS solution. Upon completion, gPROMS returns the node values of $c_i^\mathrm{out}(\theta_k)$ and CPU execution is switched back to the optimization code.

The integral values of concentration in the accumulated fluid during a switch interval, which are required to determine purity or recovery, are evaluated by integrating the cubic-spline interpolant of the node values of c_i^out or by using a quadrature rule. In particular, we have observed that the extended midpoint rule,

$$\int_0^{\theta_1} c_i^\mathrm{out}(\theta)\,\mathrm{d}\theta = \Delta\theta[c_i^\mathrm{out}(\theta_1) + \ldots + c_i^\mathrm{out}(\theta_{k_1})] + O(\Delta\theta^2), \tag{29}$$

gives nearly the same results as the spline interpolant.

5 Results and discussion

The feasibility of our approach is demonstrated on the separation of an enantiomeric mixture which exhibits a nonlinear multicomponent adsorption behavior. The adsorption isotherm, adapted from [60–62], is governed by a bi-Langmuir competitive isotherm model and provides a reasonably good description of the separation of binaphthol enantiomers on cellulose triacetate using heptane-isopropanol (72:28) as eluent. The model parameters and operating conditions are listed in Table 2.

It is assumed that the isothermal operation of the chromatographic column can be adequately described by an axially dispersed flow model with finite mass-transfer rate

Table 2: Model parameters and operating conditions for the enantiomeric separation.

Column length, L (cm)	10.0	Péclet number, Pe	950
Column diameter, d (cm)	2.6	LDF coeficients, k_i (min^{-1})	6.0, 6.0
Porosity, ϵ	0.4	Feed concentration, c_i^{F} (g/l)	2.9, 2.9
Bi-Langmuir isotherm, q_i^* (g/l)		$\dfrac{2.69c_1,\ 3.73c_2}{1+0.0336c_1+0.0466c_2}+\dfrac{0.1c_1,\ 0.3c_2}{1+c_1+3c_2}$	

described by a linear driving force (LDF) approximation. These assumptions provide a reasonable good description of the behavior of a chromatographic column and are assumed to hold for the simulation results reported in this work. They are standard practice in SMB modeling [57].

The solute material balance in a differential volume of the column can be written as

$$\frac{\partial c_i}{\partial \theta}+\left(\frac{1-\epsilon}{\epsilon}\right)\frac{\partial q_i}{\partial \theta}=\frac{\tau Q}{\epsilon V}\left(\frac{1}{\text{Pe}}\frac{\partial^2 c_i}{\partial x^2}-\frac{\partial c_i}{\partial x}\right)\quad (0<x<1), \tag{30}$$

where $x=z/L$ is the dimensionless axial position along the column, ϵ is the bed porosity, V is the column volume, $\text{Pe}=vL/D$ is the Péclet number and D is the axial dispersion coefficient.

The approximation of the adsorption rate by the LDF model leads to

$$\frac{\partial q_i}{\partial \theta}=\tau k_i(q_i^*-q_i),\quad q_i^*\equiv q_i^*(c_1,c_2)\quad (0\le x\le 1), \tag{31}$$

where k_i is the LDF coefficient and $q_i^*(c_1,c_2)$ is the adsorption isotherm of component i, which relates its equilibrium concentration in the adsorbed phase, q_i^*, with the solute concentrations, c_1 and c_2, in the bulk fluid.

Equation 30 is subjected to the following boundary conditions:

$$c_i-\frac{1}{\text{Pe}}\frac{\partial c_i}{\partial x}=c_i^{\text{in}}\quad \text{for}\quad x=0, \tag{32}$$

$$\frac{\partial c_i}{\partial x}=0\quad \text{for}\quad x=1. \tag{33}$$

The spatial derivatives in Eq. (30) were discretized using third-order orthogonal collocation on 4 uniform finite elements [63, 64]. This scheme gives rise to a spatial mesh with 13 collocation points where the solution is computed. After some preliminary testing, this choice of spatial discretization was found to give an accurate solution with a minimum number of collocation points.

The grid spacing on the time coordinate is $\Delta\theta = n_\tau$, with $n_\tau = 7$, which gives a total number of $n_\tau N = 56$ nodes. The numerical solutions computed on this grid are very close to those obtained by dynamic simulation using the standard differential-algebraic equation solver built into gPROMS. Note that in our current implementation of the full-discretization method the grid size must be an integer multiple of N. In a more advanced implementation, unconstrained by the aforementioned restriction, a more optimized temporal grid could be employed.

Because the solution is computed on a temporal mesh with dimensionless grid spacing $\Delta\theta = 1/n_\tau$, the optimal values of N_j are determined with an uncertainty of $\pm 0.5/n_\tau$. This is not a serious drawback, however, because in the present case the uncertainty on average zone length is only 5% of column length. Also, one is forced to set the perturbation of N_j for gradient estimation by first-order differencing equal to $\Delta\theta$. Although this might not be the optimum value of the perturbation parameter for a solution computed by dynamic simulation, the restriction imposed by the complete discretization approach does not seem to have a detrimental impact on the robustness or accuracy of the optimization procedure. After some preliminary testing, the other perturbation parameters were fixed at $\delta_{Q_s} = \delta_m = 0.005$.

For reference, the computer hardware employed is an Intel 1.7 GHz Pentium IV with 512 MB RAM running Microsoft Windows XP. To reduce the CPU time spent on each optimization, the initial estimate for each CSS calculation is the solution obtained from the previous calculation [39]. The average CPU time per CSS calculation was only 3.1 secs, which is a remarkably small value, especially if the unavoidable computational overhead of the interpretative machine of gPROMS is taken into account. A compiled code would perform even better. Such low computation time for a CSS calculation demonstrates the superiority of the full-discretization method over dynamic simulation for the combination of isotherm model, number of separation plates, and number of columns studied here. Overall, each optimization run was completed in less than one hour. Computational times of this order of magnitude for rigorous model-based optimization are perfectly acceptable in industrial practice and are much shorter than most previously reported in the literature [19–22].

In many cases, the SMB operating parameters of an optimized solution could be slightly improved by performing a second optimization with the average zone lengths N_j fixed at their previously optimized values. This is not surprising because the numerical

CSS solution is a smooth function of the SMB parameters but changes stepwise with N_j due to the discretization of the time domain. It should also be noted that the optimization algorithm used in this work does not perform a global optimization. Depending on the starting point, the algorithm may converge toward a local minimum. In order to check whether or no that has happened, the optimization can be restarted from different initial points.

Table 4 lists the results of the more representative optimizations carried out in this work. The table includes the optimized values of port configuration and SMB operating parameters used as degrees of freedom, the corresponding values of switching interval and flow rates, and eluent consumption ($Q_{\mathrm{E}}/Q_{\mathrm{F}}$). Since the purity constraints were always satisfied within the allowed tolerance of 5×10^{-4}, the table also includes the purity values obtained by dynamic simulation as a check for consistency between the two solution methods. A small caption at the bottom of the table gives further information on the objective function and constraints.

The reference case is a 4-column SMB unit (SMB4) for which the feed throughput was maximized ($\max Q_{\mathrm{F}}$) for minimal extract and raffinate purities of 98%. Its operating parameters are listed in the first row of Table 4. For the same number of columns, the port switching and SMB parameters were subsequently optimized for different operating objectives related to the reference case: maximization of feed throughput for the same eluent flow rate (case 2) or eluent consumption (case 4) as in the SMB4 case [i.e. $Q_{\mathrm{E}} = Q_{\mathrm{E}}^{\mathrm{SMB4}}$ or $Q_{\mathrm{E}}/Q_{\mathrm{F}} = (Q_{\mathrm{E}}/Q_{\mathrm{F}})^{\mathrm{SMB4}}$], and minimization of eluent consumption for specified feed flow rate $Q_{\mathrm{F}} = Q_{\mathrm{F}}^{\mathrm{SMB4}}$ (case 3).

Invariably, the asynchronous port switching enhances process performance significantly, as demonstrated by either the increase of 120% in feed throughput for the same solvent consumption (case 4) or the eluent savings of 44% (case 3) for the same feed throughput. The temporal profiles of solute concentration at column outlet and in raffinate and extract streams, for a complete cycle under CSS conditions, are plotted in Fig. 5 for the 4 optimized configurations. The shaded areas show the intervals during which extract and raffinate are withdrawn from the system during a cycle. The profiles are reported for the single-column model, which is the basis for the CSS solution method, and are in phase with those for the last column of the multi-column unit to get fresh eluent every cycle (as are the rightmost columns of Fig. 4). The concentration profiles for the other columns are identical to those plotted in Fig. 5, but shifted in time according to

Table 3: Optimization runs for minimum purity requirement of 0.98 on both product streams. In all cases the purity requirements, as determined by the full-discretization method, are met with a maximum tolerance of 5×10^{-4}. For reference, P_{R} and P_{X} are the values of raffinate and extract purity, respectively, determined by dynamic simulation. Flow rates are expressed in ml/min and τ in min.

Case	$N_{\mathrm{I}}/N_{\mathrm{II}}/N_{\mathrm{III}}/N_{\mathrm{IV}}$	Q_s	m_1	m_2	m_3	m_4	τ	Q_{IV}	Q_{E}	Q_{F}	Q_{X}	Q_{R}	$Q_{\mathrm{E}}/Q_{\mathrm{F}}$	P_{R}	P_{X}
1	1.0/1.0/1.0/1.0	2.26	4.44	2.81	3.20	2.43	14.09	7.00	4.54	0.86	3.67	1.73	5.27	98.0	98.0
2	0.6/1.5/1.3/0.6	1.78	4.61	2.44	3.12	2.07	17.87	4.87	4.54	1.22	3.88	1.88	3.72	97.8	97.7
3	0.6/1.3/1.3/0.8	1.25	4.36	2.44	3.12	2.33	25.40	3.76	2.55	0.86	2.41	1.00	2.96	97.8	97.7
4	0.6/1.4/1.4/0.6	3.06	5.13	2.53	3.15	1.89	10.40	7.83	9.94	1.89	7.97	3.86	5.27	97.7	97.7
5	0.5/1.6/1.4/0.5	4.99	8.13	2.64	3.14	1.14	6.39	9.03	34.86	2.49	27.40	9.95	13.99	97.7	97.8
6	0.3/1.0/1.0/0.7	1.75	6.52	2.85	3.21	2.19	18.17	4.95	7.65	0.62	6.43	1.84	12.28	98.0	98.1
7	0.5/1.0/1.0/0.5	1.35	5.28	2.76	3.18	1.92	23.52	3.51	4.54	0.57	3.41	1.71	7.91	98.1	98.1
8	1.0/2.0/1.0/1.0	3.88	5.10	2.57	3.01	2.30	8.20	11.53	10.89	1.73	9.83	2.76	6.30	98.0	97.7

$\sum N_j = 4$ (cases 1–5), 3 (cases 6 & 7), 5 (case 8). Cases 1 (SMB4) & 8 (SMB5): $\max Q_{\mathrm{F}}$, fixed N_j; cases 2 & 7: $\max Q_{\mathrm{F}}$, $Q_{\mathrm{E}} = Q_{\mathrm{E}}^{\mathrm{SMB4}}$; case 3 : $\min Q_{\mathrm{E}}$, $Q_{\mathrm{F}} = Q_{\mathrm{F}}^{\mathrm{SMB4}}$; case 4 : $\max Q_{\mathrm{F}}$, $Q_{\mathrm{E}}/Q_{\mathrm{F}} = (Q_{\mathrm{E}}/Q_{\mathrm{F}})^{\mathrm{SMB4}}$; cases 5 & 6: $\max Q_{\mathrm{F}}$.

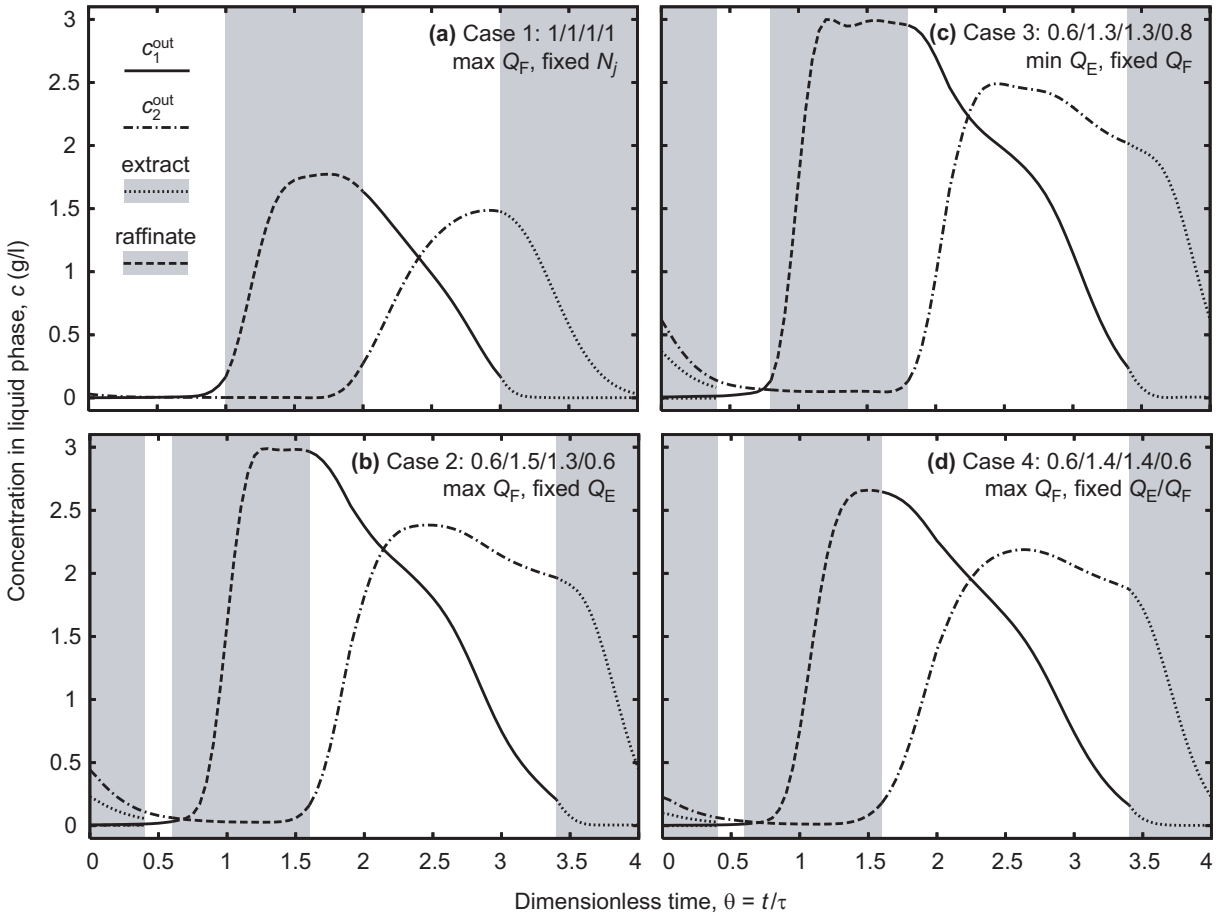

Figure 5: Temporal profiles of solute concentration at column outlet (c_i^{out}) and in product streams (c_i^{X} and c_i^{R}), under CSS conditions, for the first four optimized solutions listed in Table 4.

Eq. (5). The corresponding axial concentration profiles along the columns, taken at half switching interval, are displayed in Fig. 6. Because a single-column model is employed, and in order to construct a spatial concentration profile spanning all columns, snapshots of the profile for the single-column model were taken at instants 0.5τ, 1.5τ, ..., $(N-0.5)\tau$ of the cycle, and then plotted sequentially according to the Eq. (5).

In agreement with other authors [21, 22], the optimization of asynchronous port switching increases the length of zones II and III, and reduces that of zones I and IV to the smallest required for regeneration of the adsorbent and recycling of clean eluent, respectively. By increasing the length of zones II and III, the system can withstand more heavily loaded columns (the average solute concentration is increased) with steeper concentration fronts squeezed inside the narrower zones I and IV. Notice that for cases 2 and 3, the axial concentration profile of less retained solute surpasses slightly the feed concentration at the edge between zones III and IV. Overall, this solute is recovered at high concentration in the raffinate stream (Fig. 5). The more retained solute is recovered in the extract at a

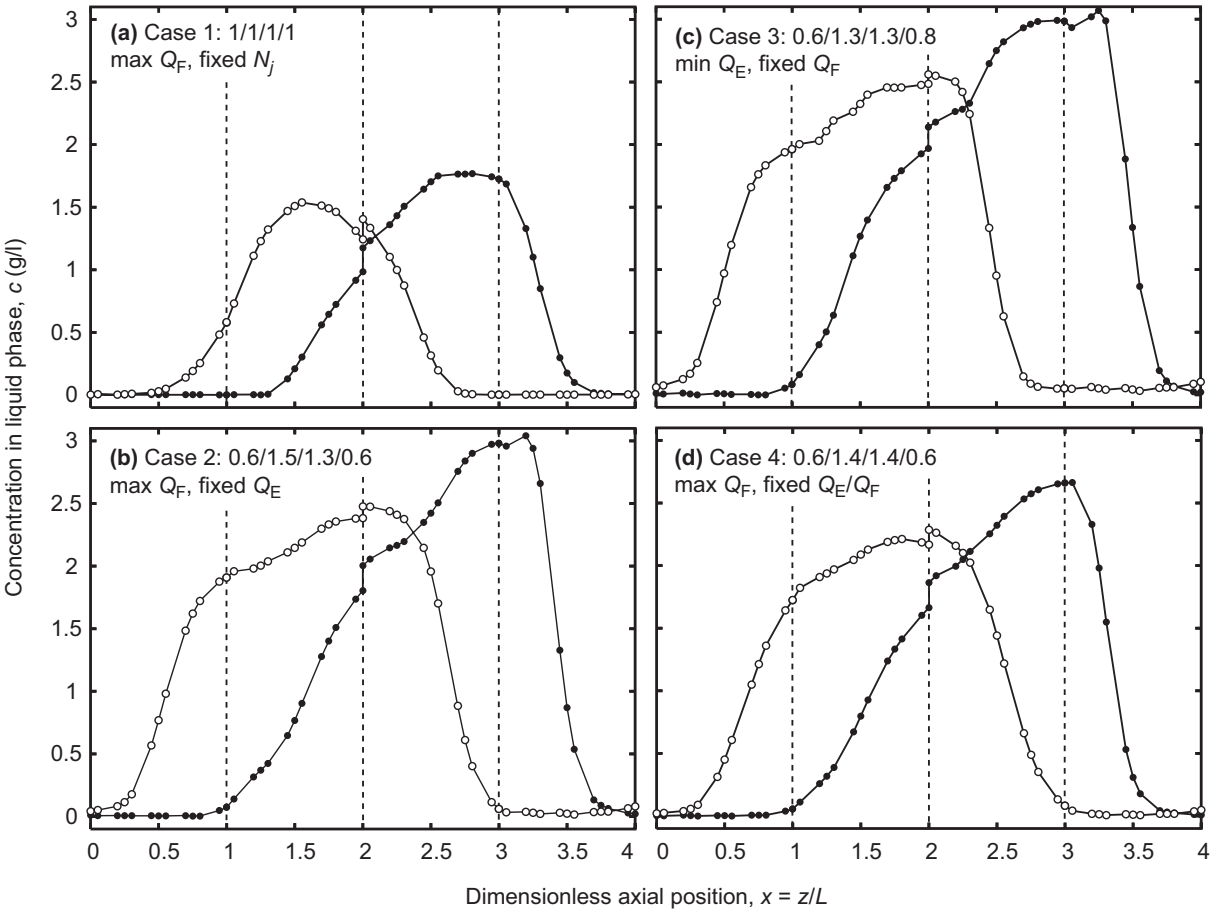

Figure 6: Axial profiles of solute concentration in liquid phase (c_1, —●—; c_2, —○—), taken at half switching interval under CSS conditions, for the first four optimized solutions listed in Table 4.

lower concentration, but still only moderately diluted. Because recovery is high for both solutes, but the dilution rate is larger for extract than for raffinate, the extract flow rate is higher than that of the raffinate. Since the average length of zone IV is smaller than column length ($N_{\mathrm{IV}} < 1$), the liquid that is not collected as product during an initial phase of raffinate withdrawal ($N_{\mathrm{IV}} < \theta < 1$) is diluted with fresh eluent before being fed to the next column. Notice that $c_i^{\mathrm{out}}(\theta)$ and $c_i^{\mathrm{R}}(\theta)$ are superposable, because the dilution occurs after product withdrawal. On the other hand, because $N_{\mathrm{I}} < 1$ the liquid stream at the column outlet is diluted with fresh eluent before being collected as product during a final phase of extract withdrawal ($0 < \theta < 1 - N_{\mathrm{I}}$). Since the dilution takes place before product is collected, $c_i^{\mathrm{out}}(\theta) > c_i^{\mathrm{X}}(\theta)$. This is only visually noticeable in Fig. 5 for the more retained solute because the other solute is present in very small concentration in order to satisfy the purity requirement.

The 5th optimized case the optimal port configuration and operating parameters that provide the highest feed throughput for a 4-column system, $Q_{\mathrm{F}} = 2.49$ ml/min. This value

is nearly three times larger than the maximum value obtained for the optimized 4-column SMB (case 1). Cases 6 and 7 are optimized solutions for a 3-column configuration. As stated above, a 4-zone SMB cannot be operated with 3 columns, but this is made possible by desynchronizing the port switching. In case 6 feed throughput is maximized without any further restrictions, whereas in case 7 the eluent flow rate is fixed at the valued obtained in case 1 (SMB4). The optimized 3-column processes perform reasonably well, particularly if the 25% reduction in amount of stationary phase is taken into account. Furthermore, the specific productivity, Q_{F}/N, for case 6 is identical to that obtained for the optimized 4-column SMB (case 1). Eluent consumption appears to increase considerably when one column is removed, but it can be substantially reduced through modulation of its flow rate. This procedure is discussed below. Finally, the bottom row of table 4 gives the optimized results for the best 5-column SMB configuration. This system doubles the feed throughput with respect to SMB4, but at the cost of adding one more column (25% increase in amount of stationary phase) and increasing eluent consumption by 20%.

Unlisted in Table 4 are the results of a series of optimized 4-column configurations for which eluent consumption was minimized for intermediate values of Q_{F} between that of SMB4 (case 1) and the highest achievable value for a 4-column configuration (case 5). The obtained $Q_{\mathrm{E}}/Q_{\mathrm{F}}$ values, as well as those for the 8 cases listed in Table 4, are plotted as a function of Q_{F} in Fig. 7 .

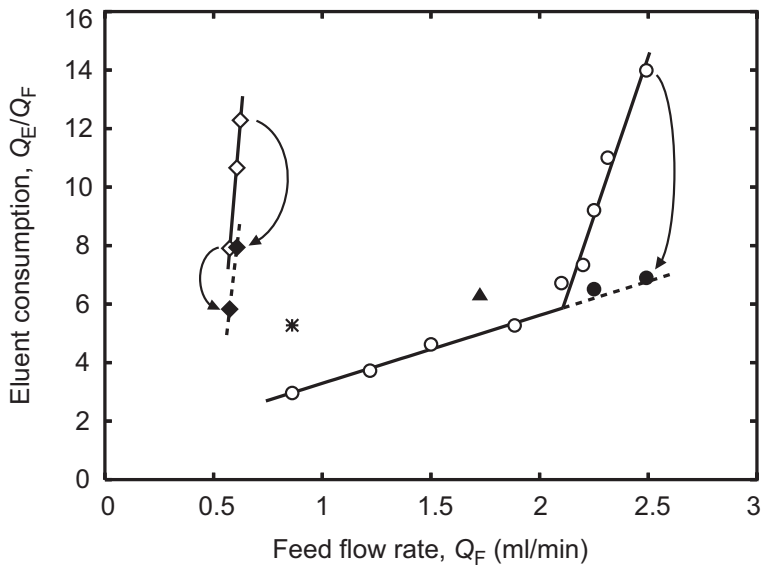

Figure 7: Eluent consumption as a function of feed throughput for the optimized processes analyzed in this work. ⋇, SMB4 (case 1); ∘, 4-column asynchronous processes (cases 2–5 and others not listed in Table 4); ◊, 3-column configurations (cases 6 and 7); ▲, 5-column SMB (case 8); •, ⧫, same as corresponding cases denoted by open symbols, but with modulation of eluent flow.

By optimizing the asynchronous port switching, the feed throughput of the 4-column SMB unit is more than doubled for the same eluent consumption. Figure 7 shows that the productivity can be increased or the separation cost can be reduced by simply updating the control software to handle the asynchronous port switching. Other uses for asynchronous operation are to reduce the inventory of expensive stationary phases or to increase the potential market for compact chromatographic units with a small number of columns [16, 65, 66]. For example, our results show that a 4-column process with optimized asynchronous port switching performs better than a classical 5-column SMB process. This has already been highlighted by other authors [6, 7, 21, 22, 32]. For the separation under study, eluent consumption is reduced by 22% or feed throughput is increased by 24%.

Figure 7 shows that solvent consumption for the 4-column asynchronous configurations increases linearly with feed throughput at moderate rate up to $Q_{\mathrm{F}} \approx 2.1$ ml/min. At higher feed flow rates the trend is still linear, but with a much larger slope, which means that an increase in feed throughput is obtained at the expense of much larger eluent consumption than in the low feed-throughput region. Apparently, it becomes prohibitively expensive to operate the 4-column unit above $Q_{\mathrm{F}} > 2.1$ ml/min because of the required high solvent consumption. This is misleading, however, because eluent consumption for those configurations can be substantially reduced through an intuitive modulation of its flow rate. The procedure works as a corrective adjustment to an optimized configuration obtained by the methodology described above. To show how this is done, we examine in detail the optimized solution that gives the highest achievable value of Q_{F} for a 4-column configuration.

Figure 8 shows the axial profiles of solute concentration in liquid phase, taken at the beginning, middle and end of the switching interval, under CSS conditions, for the asynchronous configuration of case 5. These profiles are considered to be of major importance to optimize the process [6] and in practice are measured experimentally by monitoring the concentration over time at the inlet or outlet of a fixed column in the loop. This procedure is basically the same as using Eq. (5) to generate the axial profiles of Fig. 6 from the corresponding temporal profiles plotted in Fig. 5. The internal concentration profile is the closest analogy to the equivalent true counter-current process, which is probably why it is used so often. However, if the operating parameters are varied during a switching interval, the internal concentration profile deviates significantly from a stationary profile circulating around the multi-column loop. For this reason, a concentration plot such as

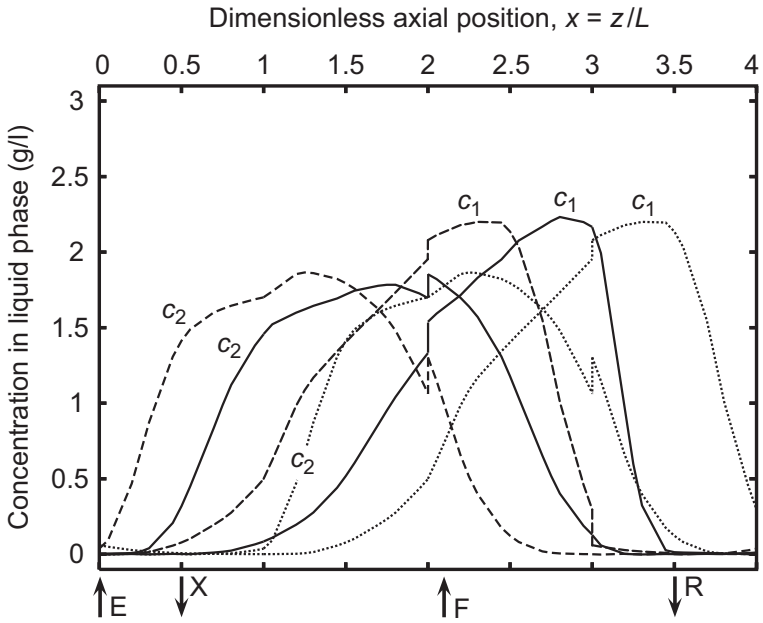

Figure 8: Axial profiles of solute concentration in liquid phase, taken at the beginning (– – –), middle (——) and end (- - -) of the switching interval, under CSS conditions, for the asynchronous configuration of case 5 listed in Table 4.

that of Fig. 8 is less useful as diagnostic tool for the recently emerged cyclic operation policies that vary parameters during a switching interval. For example, it is difficult to assess from the profiles of Fig. 8 why solvent consumption is much higher for this case than for the cases considered in Fig. 6, and what are the required changes, if any, to the operating parameters for improving the $Q_{\mathrm{R}}/Q_{\mathrm{F}}$ ratio. In this case, the examination of how the internal concentration changes over time at the outlet of a fixed column is more important to optimize the process.

The bottom graph of Figure 9 shows the temporal solute concentration profiles at column outlet, $c_i^{\mathrm{out}}(\theta)$, for case 5. A closer inspection of these profiles reveals that during the first 0.9τ time units of the cycle the liquid exiting the column is nearly clean of solute. But during this interval the same liquid is partially withdrawn as product from the system. More precisely, the last 50% of extract collected every switching interval are withdrawn during $0 < \theta < 0.5$ and the first 40% of collected raffinate are taken during $0.5 < \theta < 0.9$. Furthermore, during the first τ time units fresh eluent is being added to the system via the eluent line connected at the column outlet. This can be inferred from the flow-rate profiles for the node placed at column outlet, which are plotted in the top graph of Figure 9. Thus, for $0 < \theta < 0.5$ the liquid exiting the column (which is nearly solute free) is mixed with fresh eluent, and a fraction of that mixed stream is collected as extract. During the next 0.4τ time units ($0.5 < \theta < 0.9$), the fraction of liquid that is not

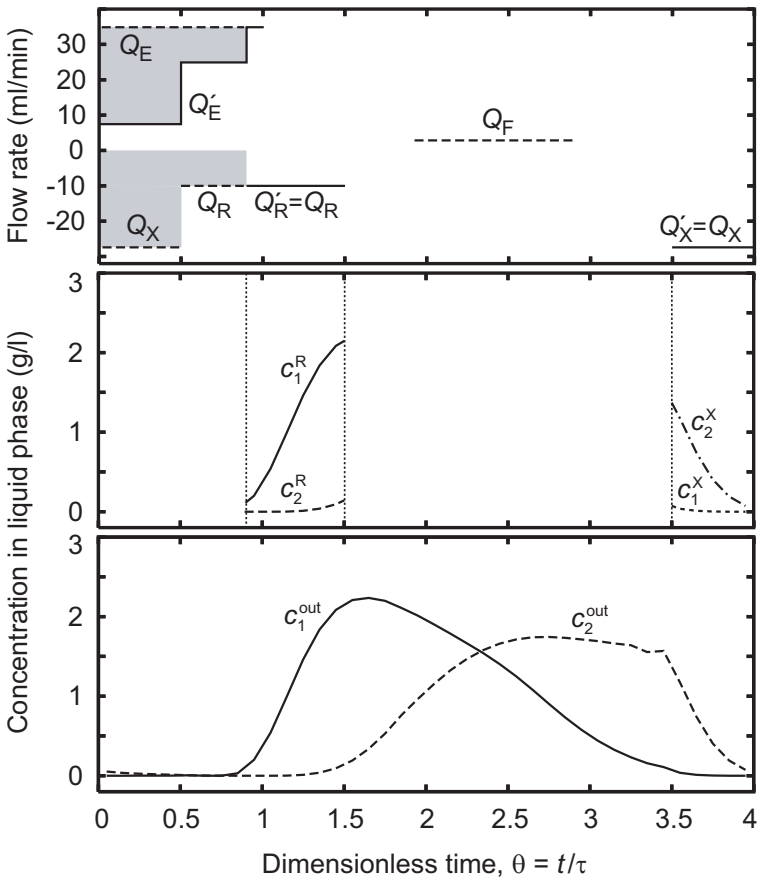

Figure 9: Solute concentration profiles at column outlet (c_i^{out}) and in extract (c_i^{X}) and raffinate (c_i^{R}) streams, and flow-rate profiles of eluent (Q_{E}), feed (Q_{F}), extract (Q_{X}) and raffinate (Q_{R}), for the node located at column outlet, over a complete cycle under CSS conditions, for the asynchronous configuration listed as case 5 in Table 4. Note that $c_i^{\text{R}}(\theta)$ and $c_i^{\text{X}}(\theta)$ are the concentration profiles for selective raffinate and extract withdrawal when the eluent flow rate is modulated.

withdrawn as raffinate is mixed with fresh eluent before being introduced into the next column. Note that this portion of the raffinate has very little solute.

From the discussion above, it is apparent how to reduce solvent consumption without affecting product purity nor productivity. During $0 < \theta < 0.5$ of every switching interval, extract is no longer withdrawn from the system and eluent is added at a lower flow rate, $Q'_{\text{E}} = Q_{\text{E}} - Q_{\text{X}}$. During the next 0.4τ time units of the switching interval, the raffinate port is kept closed and the eluent flow rate is reduced to $Q'_{\text{E}} = Q_{\text{E}} - Q_{\text{R}}$. During the remaining 0.1τ units of the switching interval, the eluent flow rate is increased to its original value Q_{E}. Like the desynchronization of port switching, this operating scheme only requires the updating of the control software that drives the pump flow rates. The original and modified chronograms of port switching are compared in Fig. 10. The solvent flow rate is reduced from 34.86 ml/min to an average value of $34.86-(0.5)(27.40)-(0.4)(9.95) = 17.18$ ml/min, which corresponds to a solvent consumption $Q_{\text{E}}/Q_{\text{F}} = 6.9$. As shown by the rightmost

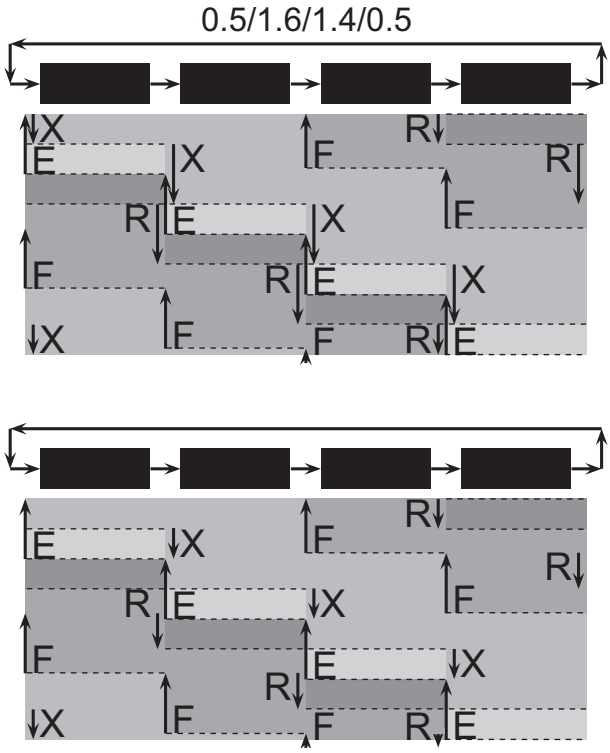

Figure 10: Chronogram of port switching for the 5th optimization case listed in Table 4 (top) and the required changes for reducing its solvent consumption (bottom).

solid circle in Fig. 7, this value is on the linear trend line that fits the Q_E/Q_F values for lower feed throughputs. By applying the same procedure to other cases with feed throughputs between 2.1 ml/min and 2.49 ml/min, their solvent consumptions are reduced to values which are in agreement with the trend line for Q_F values below 2.1 ml/min. As shown by the filled and opened lozenges in Fig. 7, the same operating scheme can be applied to the 3-column configurations in order to reduce their solvent consumption considerably.

Note that this operating policy combines two operating modes—asynchronous port switching and flow-rate modulation—in the same process to improve its performance. The same concept has been recently investigated by other authors [34] using a multiobjective optimization approach with genetic algorithms, who demonstrated that the combination of two operating modes, e.g. Varicol & PowerFeed, Varicol & ModiCon, or PowerFeed & ModiCon, gives better performance than is achievable with either of the two operating modes alone. However, the improvement is not as significant as that obtained in the present work. Note also that our procedure is one way of tackling a multi-objective optimization problem with conflicting objectives using a sequential single-objective optimization approach. In fact, what we have done is to assign a different set of degrees

of freedom to each objective function and then determine their optimal values sequentially. First, Q_s, m_j and N_j are optimized to obtain the maximum feed throughput for a given eluent flow rate. Then, eluent consumption for the optimized configuration is minimized by changing the inlet/outlet flow rates from continuous constant flow to an optimal piecewise-constant τ-periodic flow.

6 Conclusions

In this work, we have derived a physically realizable set of asynchronous SMB processes which are uniquely defined by four parameters representing the average number of columns per zone. To optimize the operating parameters and port configuration we have developed an optimization strategy that relies on a fully discretized single-column model for directly computing the CSS solution at every step of the optimization procedure. This is shown to be very efficient for chromatography optimization. Process optimization is handled using single objective functions, which are explicitly constrained by product quality and maximum pressure drop. These are maximization of feed throughput, with a possible upper bound on eluent consumption or flow rate, and minimization of solvent consumption for a given feed flow rate. The feasibility of our approach has been demonstrated on the separation of an enantiomeric mixture with a nonlinear competitive isotherm. Only units with a small number of columns, between three and five, have been considered, since they look more promising for future applications of SMB and related technologies. The results presented here, as well as those of other authors, show that significant performance improvements can be achieved by varying some of the operating parameters during the switching interval. It is shown that eluent consumption for optimized asynchronous configurations in the higher feed-throughput region can be significantly reduced by modulation of eluent flow rate and selective product withdrawal. This hybrid operating scheme can be viewed as a combination of two operating modes governed by distinct control parameters, which are optimized sequentially with respect to a different objective function.

Nomenclature

c	solute concentration (g/l)
d	column diameter (cm)
D	axial dispersion coefficient (cm^2/min)
k	LDF coefficient (s^{-1})
L	column length (cm)
N	number of columns
n_τ	temporal discretization resolution (subintervals of the switching interval)
Pe	Péclet number
q	adsorbed concentration (g/l)
Q	flow rate (cm^3/min)
t	time (min)
v	interstitial fluid velocity (cm/min)
V	column volume (cm^3)
x	dimensionless axial position, z/L
z	axial position in column (cm)

Greek letters

ϵ	total porosity
Ω	set input variables for column j
τ	switching interval (min)
θ	dimensionless time, t/τ

Subscripts and superscripts

E	eluent
ex	external inlet stream
F	feed
i	solute index
I,...,IV	zone index
in	column inlet
j	column index
k	switching interval subinterval index
out	column outlet
R	raffinate
X	extract

$\tilde{}$ discrete value

List of Tables

List of Figures

Bibliography

[1] M. Juza, M. Mazzotti, M. Morbidelli, Trends in Biotech. 18 (2000) 108.

[2] R.M. Nicoud, LC-GC 5 (1992) 43.

[3] J. Strube, S. Haumreisser, H. Schmidt-Traub, M. Schulte, R. Ditz, Org. Proc. Res. Devel. 2 (1998), 305.

[4] P.C. Wankat, Large Scale Adsorption and Chromatography, CRC Press, Boca Raton, 1986.

[5] A. Jupke, A. Epping, H. Schimdt-Traub, J. Chromatogr. A 944 (2002) 93.

[6] O. Ludemman-Hombourger, R.M. Nicoud, M. Bailly, Sep. Sci. Technol. 35 (2000) 1829.

[7] O. Ludemman-Hombourger, G. Pigorini, R.M. Nicoud, D.S. Ross, G. Terfloth, J. Chromatogr. A 947 (2002) 59.

[8] T.B. Jensen, T.G.P. Reijns, H.A.V. Billiet, L.A.M. van der Wielen, J. Chromatogr. A 873 (2000) 149.

[9] D. Antos, A. Seidel-Morgenstern, Chem. Eng. Sci. 56 (2001) 6667.

[10] S. Abel, M. Mazzotti, M. Morbidelli, J. Chromatogr. A 944 (2002) 23.

[11] J. Houwing, T.B. Jensen, S.H. van Hateren, H.A.H. Billiet, L.A.M. van der Wielen, AIChE J. 49 (2003) 665.

[12] M.M. Kearney, K.L. Hieb, US Pat. 5102553, 1992.

[13] Y. Zang, P.C. Wankat, Ind. Eng. Chem. Res. 41 (2002) 2504.

[14] Y. Zang, P.C. Wankat, Ind. Eng. Chem. Res. 41 (2002) 5283.

[15] Z. Zhang, M. Mazzotti, M. Morbidelli, J. Chromatogr. A 1006 (2003) 87.

[16] Z. Zhang, M. Mazzotti, M. Morbidelli, AIChE J. 50 (2004) 625.

[17] H. Schramn, M. Kaspereit, A. Kienle, A. Seidel-Morgenstern, Chem. Eng. Technol. 25 (2002) 1151.

[18] H. Schramn, M. Kaspereit, A. Kienle, A. Seidel-Morgenstern, J. Chromatogr. A 1006 (2003) 77.

[19] G. Dünnebier, K.-U. Klatt, Comput. Chem. Eng. 23 (1999) S189.

[20] G. Dünnebier, J. Fricke, K.-U. Klatt, Ind. Eng. Chem. Res. 39 (2000) 2290.

[21] A. Toumi, F. Hanisch, S. Engell, Ind. Eng. Chem. Res. 41 (2002) 4328.

[22] A. Toumi, S. Engell, O. Ludemann-Hombourger, R.M. Nicoud, M. Bailly, J. Chromatogr. A 1006 (2003) 15.

[23] E. Kloppenburg, E.D. Gilles, Chem. Eng. Technol. 22 (1999) 313.

[24] K.-U. Klatt, F. Hanisch, G. Dunnebier, S. Engell, Comput. Chem. Eng. 24 (2000) 1119.

[25] G. Mitsuo, C. Runwei, C. Runwei, Genetic Algorithms and Engineering Optimization, John Wiley, New York, 2000.

[26] R. Salcedo, R. Solving Nonconvex Nonlinear-Programming and Mixed-Integer Nonlinear- Programming Problems with Adaptive Random Search. Ind. Eng. Chem. Res. 31 (1992) 262.

[27] R.H.J.M. Otten, L.P.P.P. van Ginneken, The annealing algorithm. Kluwer, Boston, 1989.

[28] M. Cardoso, R. Salcedo, S. de Azevedo, D. Barbosa, Comput. Chem. Eng. 21 (1997) 1349.

[29] R. Faber, T. Jockenhovel, G. Tsatsaronis Comput. Chem. Eng. 29 (2005) 273.

[30] Z. Zhang, K. Hidajat, A.K. Ray, Ind. Eng. Chem. Res. 41 (2002) 3213.

[31] H.J. Subramani, K. Hidajat, A.K. Ray, Comput. Chem. Eng. 27 (2003) 1883.

[32] Z. Zhang, K. Hidajat, A.K. Ray, M. Morbidelli, AIChE J. 48 (2002) 2800.

[33] Z. Zhang, M. Mazzotti, M. Morbidelli, J. Chromatogr. A 989 (2003) 95.

[34] Z. Zhang, M. Mazzotti, M. Morbidelli, Korean J. Chem. Eng. 21 (2004) 454.

[35] G. Ziomek, K. Kaspereit, J. Jeyzowski, A. Seidel-Morgenstern, D. Antos, J. Chromatogr. A 1070 (2005) 111.

[36] J.M.M. Araújo, R.C.R. Rodrigues, J.P.B. Mota, J. Chromatogr. A 1132 (2006) 76.

[37] J.K. Kim, N. Abunasser, P.C. Wankat, Adsorption 11 (2005) 579.

[38] J.P.B. Mota, J.M.M. Araújo, AIChE J. 51 (2005) 1641.

[39] J.M.M. Araújo, R.C.R. Rodrigues, J.P.B. Mota, Ind. Eng. Chem. Res. 45 (2005) 5314.

[40] P.I. Barton, C.C. Pantelides, AIChE J. 40 (1994) 966.

[41] M. Oh, C.C. Pantelides, Comput. Chem. Eng. 20 (1996) 611.

[42] S. Nilchan, The Optimization of Periodic Adsorption Processes, PhD Diss., Imperial College, London, 1997.

[43] S. Nilchan, C.C. Pantelides, Adsorption 4 (1998) 113.

[44] D. Ko, I. Moon, Ind. Eng. Chem. Res. 41 (2002) 93.

[45] D. Ko, R. Siriwardane, L.T. Biegler, Ind. Eng. Chem. Res. 42 (2003) 329.

[46] Y.S. Cheng, C.F. Abi, L.S. Kershenbaum, Comput. Chem. Eng. 20 (1989), S793.

[47] I. Yongsunthon, E. Alpay, Comp. Chem. Eng. 22 (1998), S733.

[48] G. Guiochon, A. Felinger, J. Chromatogr. A 752 (1996) 31.

[49] J.E.A. Bauer, A comprehensive look at scaling-up SMB chiral separations from the Lab to commercial production, ChiraTech Symposium Proceedings, Philadelphia, P.A. 1997.

[50] F. Charton, R.-M. Nicoud, J. Chromatogr. A 702 (1995) 97.

[51] O. Ludemann-Hombourger, M. Bailly, R.-M. Nicoud, Sep. Sci. Technol. 35 (2000) 1285

[52] G. Storti, M. Mazzotti, M. Morbidelli, S. Carr, AIChE J. 39 (1993) 471.

[53] M. Mazzotti, G. Storti, M. Morbidelli, AIChE J. 40 (1994) 1825.

[54] M. Mazzotti, G. Storti, M. Morbidelli, AIChE J. 42 (1996) 2784.

[55] M. Mazzotti, G. Storti, M. Morbidelli, J. Chromatogr. A 769 (1997) 3.

[56] A. Gentilini, C. Migliorini, M. Mazzotti, M. Morbidelli, J. Chromatogr. A 805 (1998) 37.

[57] D.M. Ruthven, C.B. Ching, Chem. Eng. Sci. 44 (1989) 1011.

[58] A. Kuntsevich, F. Kappel, SolvOpt 1.1: The Solver For Local Nonlinear Optimization Problems, Institute for Mathematics, Karl-Franzens University of Graz, 1997.

[59] N.Z. Shor, Minimization Methods for Non-Differentiable Functions, Springer Series in Computational Mathematics, Vol. 3, Springer-Verlag, Berlin, 1985.

[60] L.S. Pais, J.M. Loureiro, A.E. Rodrigues, Chem. Eng. Sci. 52 (1997) 245.

[61] L.S. Pais, J.M. Loureiro, A.E. Rodrigues, J. Chromatogr. A 769 (1997) 25.

[62] L.S. Pais, J.M. Loureiro, A.E. Rodrigues, Sep. Purif. Technol. 20 (2000) 67.

[63] G.F. Carey, B.A. Finlayson, Orthogonal collocation on finite elements, Chem. Eng. Sci. 30 (1975) 587.

[64] B.A. Finlayson, Nonlinear Analysis in Chemical Engineering, McGraw-Hill, New York, 1980.

[65] S. Lehoucq, D. Verhève, A.V. Wieckhusen, E. Cavoy, AIChE J. 46 (2000) 155.

[66] J. Blehault, W. Hauck, R.M. Nicoud, Seminar on Batch and SMB Design and Applications, AIChE Meeting, Chicago, IL, March 2001.

Chapter 4

Determination of Competitive Isotherms of Enantiomers by a Hybrid Inverse Method using Overloaded Band Profiles and the Periodic State of the Simulated Moving-Bed Process

1 Introduction

The production of pure enantiomers is one of the major fields of application of preparative chromatography in the pharmaceutical industry, which is subject to tight constrains regarding product purity dictated by pharmaceutical and food regulatory organizations, lead by the American FDA [1].

Batch chromatography is usually the preferred method when amounts from a few mg up to about 100 g of purified enantiomer are needed. When larger amounts are required, ranging from several hundred grams to kilograms, the simulated moving-bed (SMB) is often a more efficient alternative [2]. During the last decade, SMB chromatography has been increasingly applied for the separation of pure substances in the pharmaceutical, fine chemistry, and biotechnological industries, at all production scales [3]. The SMB is now considered a real production tool for the separation of optical isomers. Daicel chemicals and UCB pharma have been reportedly operating SMB units since 1998 for the annual production of several tons of pure enantiomers of two different chiral drugs [4].

Enantiomeric separations are carried out on chiral stationary phases (CSP) that frequently have a relatively low saturation capacity. The CSPs are mostly composed of silica gel with only a few chiral elements that rapidly overload. Therefore, these separations are usually carried out under strongly nonlinear conditions. The accurate determination of the competitive adsorption equilibrium of the enantiomeric species is thus of fundamental importance to allow computer-assisted optimization or process scale-up. This is especially true for the SMB, because its operating conditions cannot be designed conveniently without knowledge of the adsorption isotherms of the feed components.

Several methods are available to determine equilibrium isotherms by chromatography, though some of them can only be applied for the determination of single-component isotherms. The more frequently employed methods are frontal analysis (FA), elution by characteristic point (ECP), frontal analysis by characteristic point (FACP), and perturbation methods (PM) [5].

These methods can be grouped into two categories: pulse methods (ECP and FACP) that derive isotherm data from the elution chromatogram of a single, large-size pulse, and plateau methods (FA and PM) that derive isotherm data from events taking place on concentration pulses. The methods of the first type consume less chemicals than the latter ones, because with plateau methods the determination of each isotherm point requires a separate experiment and this demands large amounts of sample and solvent.

As an alternative, the inverse method of isotherm determination is becoming popular as a quick procedure for estimation of the adsorption equilibrium data necessary for designing SMB separations [6–8]. This method is relatively recent [9–13]. It derives the isotherm from overloaded band profiles of individual solutes or of their mixture. As opposed to the direct problem of chromatography, which consists on the calculation of the band profiles of the components involved from their equilibrium isotherms, in the inverse method the adsorption isotherms are determined by numerically solving a suitable chromatographic model and by tuning the values of the isotherm parameters to minimize the difference between the calculated and measured band profiles. In a recent study [12], reporting a comparison of frontal analysis and inverse methods, it is concluded that the inverse method gives accurate estimates of the competitive isotherm parameters up to the maximum elution concentration of the overloaded bands. However, it is only moderately accurate from the maximum elution concentration up to the injected concentration. A summary of the methods used to estimate isotherms is illustrated in Fig. 1.

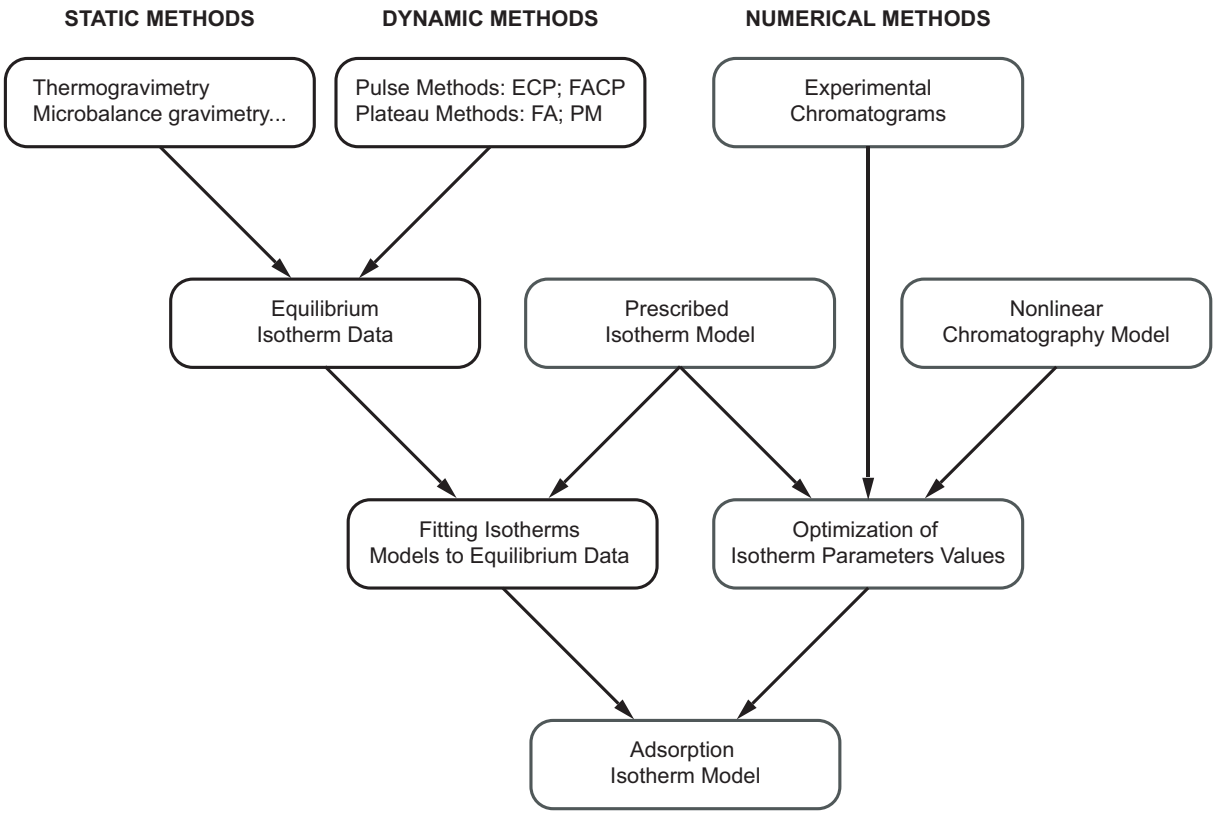

Figure 1: Adsorption isotherm estimation methods.

The objective of the present work [14] (**paper VI**) is to demonstrate that competitive isotherms can be estimated with good accuracy using the inverse method from the band profiles of the feed mixture obtained in the overloaded elution mode, without measuring

any of the single-component chromatograms. The rate parameters are also determined using the same procedure, without resorting to additional experiments.

The proposed method incorporates breakthrough data from a single frontal analysis to minimize the uncertainty on the estimated saturation capacity, due to dilution of the chromatographic bands with respect to the injected concentration. The set of estimated parameters is then validated against the cyclic steady state (CSS) of the target SMB process, and if necessary recomputed by applying the inverse method to the experimental CSS concentration profiles. The CSS is readily and cheaply obtained experimentally on a single-column setup [15], which has been recently developed by our group. This system is able to experimentally reproduce the steady periodic behavior of the multicolumn process with a single column in just 2 or 3 cycles [15–17]. Therefore, the experimental run is not more expensive nor time consuming than a few breakthrough experiments.

The applicability of the propounded method is demonstrated on the determination of the competitive adsorption isotherms of Tröger's base enantiomers on Chiralpak AD using pure methanol as mobile phase.

2 Chromatographic column model

The isothermal operation of a chromatographic column is adequately described by a dispersed plug-flow model with linear-driving-force approximation for mass transfer. These assumptions are standard practice in preparative chromatography and SMB modeling [18]. The lumped solid-diffusion version of the model can be written as

$$\frac{\partial c_i}{\partial \theta} + \beta \frac{\partial q_i}{\partial \theta} = \frac{\tau v}{L} \left(\frac{1}{\mathrm{Pe}} \frac{\partial^2 c_i}{\partial x^2} - \frac{\partial c_i}{\partial x} \right) \quad (0 < x < 1), \tag{1}$$

$$\frac{\partial q_i}{\partial \theta} = \tau k_i (q_i^* - q_i), \tag{2}$$

where subscript i is the solute index, $\theta = t/\tau$ and $x = z/L$ are the dimensionless temporal and axial coordinates, respectively, $\beta = (1-\epsilon)/\epsilon$ is the phase ratio, L is the column length, v is the linear velocity of the mobile phase, $\mathrm{Pe} = vL/D_\mathrm{L}$ is the Péclet number, D_L is the dispersion coefficient, $q_i^*(c_\mathrm{A}, c_\mathrm{B})$ is the adsorption isotherm for solute i, and k_i is the linear-driving-force (LDF) coefficient for mass transfer. The reference time, τ, to render the time coordinate dimensionless is chosen to be equal to the switching interval of the SMB process.

Equation (1) is subject to the usual boundary conditions

$$c_i - \frac{1}{\mathrm{Pe}}\frac{\partial c_i}{\partial x} = c_i^{\mathrm{in}} \quad \text{for} \quad x = 0, \tag{3}$$

$$\frac{\partial c_i}{\partial x} = 0 \quad \text{for} \quad x = 1, \tag{4}$$

where c_i^{in} is the inlet concentration of solute i.

In the working range of fluid velocity used in preparative or process-scale chromatography, the contribution of axial molecular diffusion is negligible [19] and the Péclet number is independent of v. Furthermore, adsorption kinetics is usually governed by intraparticle diffusion rather than by external film resistance, which means that k_i can also be considered as being independent of v.

3 Calculation of band profiles

When the column is subjected to a pulse experiment, the initial condition for the chromatographic model given above is $c_i(x, 0) = 0$, which states that the column is initially equilibrated with pure mobile phase. As a first approximation, we assume that the sample is injected into the column as a rectangular pulse. Assuming that the concentration of component i in the sample is c_i^{o} and that the duration of the sample injection is t_{p}, then c_i^{in} is given by

$$c_i^{\mathrm{in}} = \begin{cases} c_i^{\mathrm{o}} & \text{for} \quad 0 < \theta < t_{\mathrm{p}}/\tau \\ 0 & \text{for} \quad \theta > t_{\mathrm{p}}/\tau \end{cases}. \tag{5}$$

To determine the outlet concentration profiles, $\{c_i^{\mathrm{out}}(\theta)\}^{\mathrm{sim}} \equiv \{c_i(x = 1, \theta)\}^{\mathrm{sim}}$, the governing equations of the chromatographic column model are solved numerically using gPROMS, a software package for the modeling and simulation of lumped and distributed-parameter process models with combined discrete and continuous characteristics [20, 21].

3.1 Experimental set-up for producing large rectangular pulses

Experimentally, one of the main requirements for the successful application of the inverse method is that the boundary condition, or injection profile [i.e. Eq. (5)], must be accurately known. This condition should approximate as much as possible a rectangle, although, in practice, significant deviations from this profile are often observed [22]. The main problem is that as the volume of the injection loop in the chromatograph is increased, to vary the injected pulse width, the rectangular front remains sharp but its rear part becomes more diffusive. Rather than changing the sample volume, the feed concentration can be changed instead, but this only works up to the solubility limit of the racemate mixture.

To minimize the experimental uncertainty in producing wide-plug injections, the experimental set-up depicted in Fig. 2 is employed. Besides the chromatographic column, the main equipment comprises two HPLC pumps, an electrically-actuated 6-port 2-position valve, and an UV detector to monitor the total enantiomeric concentration profile at the column outlet, $\{c^{\text{out}}\}^{\text{exp}} = \{c_{\text{A}}^{\text{out}} + c_{\text{B}}^{\text{out}}\}^{\text{exp}}$. The whole setup if fully automated.

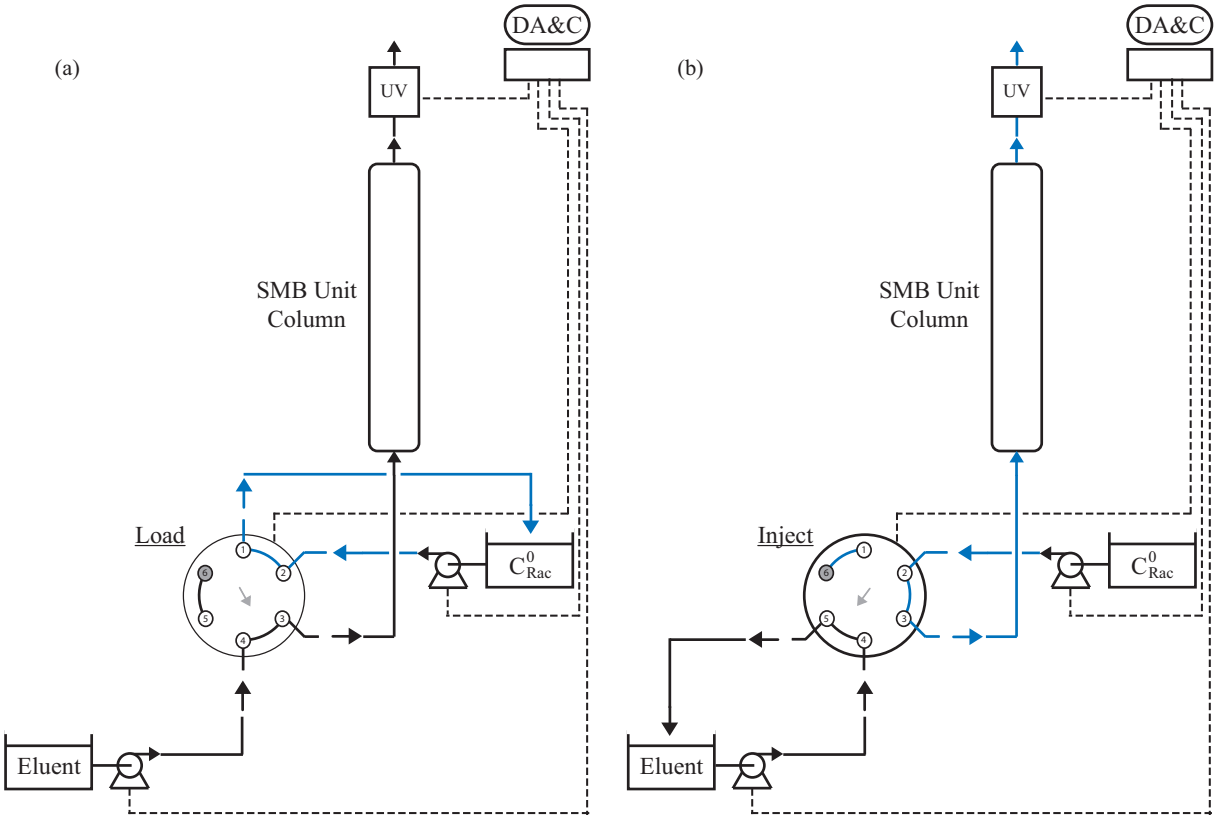

Figure 2: Schematic diagram of the experimental set-up for injecting large-size rectangular concentration pulses. The two HPLC pumps are continuously operating at prescribed flow rates, to minimize disturbances, but the direction of the two outflow streams can be diverted by means of a 2-position valve. Initially, (a) the racemic mixture is pumped in closed loop, whereas pure eluent is fed to the chromatographic column; (b) the pulse is started by commuting the valve position from load to inject; the feed solution thus is redirected to the chromatographic column, whereas the eluent stream is recirculated in closed loop; to end the pulse, the valve is returned to its original position, as shown in (a).

The HPLC pumps are continuously operated in closed loop at prescribed flow rates to minimize disturbances in their operation. The 6-port valve has two defined positions: *load* and *inject*. In the load position (Fig. 2a) the feed mixture is pumped in closed loop, through the active connection between ports 1 and 2 of the valve, whereas mobile phase is fed to the chromatographic column through the active connection between ports 3 and 4. To start the injection of the rectangular pulse, the valve is commuted to the inject position (Fig. 2b) so that the feed solution is introduced into the chromatographic column

through ports 2 and 3 of the valve, whereas the mobile phase is circulated in closed loop through the bridge between ports 4 and 5. This is an instantaneous event and, therefore, is expected to provide a very good approximation to the sharp front edge of an ideal pulse. To finalize the pulse with a sharp rear edge, the valve is commuted to the initial load position (Fig. 2a), and the column is eluted with mobile phase.

3.2 Parameter estimation

In the inverse method, parameter estimation is the process of determining values for the unknown parameters, Θ, of the prescribed adsorption isotherm model, that maximize the probability that the model will predict the values from the experiments. The steps taken in our implementation of the inverse method are the following. First, an isotherm model is selected and initial estimates are determined for its numerical parameters. Then, band profiles of the racemic mixture are calculated by solving the column model. The experimental and calculated band profiles are compared by evaluating the objective function

$$\min \int_t r^2 \, dt = \min \int_t \left[\{c^{\text{out}}(t)\}^{\text{exp}} - \{c^{\text{out}}(t)\}^{\text{sim}} \right]^2 dt, \tag{6}$$

where $\{c^{\text{out}}(t)\}^{\text{exp}}$ and $\{c^{\text{out}}(t)\}^{\text{sim}}$ are the measured and calculated profiles of total enantiomer concentration at the column outlet, respectively. Finally, the isotherm parameters are iteratively changed until the objective function is minimized.

To solve the nonlinear least-squares problem given by Eq. (6), we use the multiple-shooting implementation of gPROMS for dynamic optimization, which makes use of HQP, a solver for nonlinearly constrained, large-scale optimization problems [23]. gPROMS also provides an advanced statistical analysis tool that allows the user to further analyze the results and create several statistical plots. At this point it is worth mentioning that especially tailored algorithms have been proposed in the literature for solving the inverse problem of isotherm determination [24]; these are likely to be more efficient than HQP.

4 Reproduction of the cyclic steady state of the SMB using a single-column setup

The SMB process is a practical implementation of the true moving-bed process, where the adsorbent and the fluid phase move countercurrently. The latter is continuous and has a steady state that can be easily computed, whereas the former is intrinsically dynamic. However, the SMB attains a CSS after a sufficiently long period of operation, where the internal composition profile moves steadily in the direction of fluid flow and the outlet concentrations are time periodic.

For designing the SMB the initial transient behavior is of little interest, but only the fully established periodic state. The type and amount of minimal experimental data required for proper determination of adsorption isotherms in SMB chromatography is still an open question. Although we do not pretend to give a definite answer to this question, we put forward in this paper that it is reasonable to assume that the CSS composition profile at the inlet or outlet of one SMB column (the other columns have the same profiles, but shifted in time by multiples of the switching interval), over a complete operating cycle, will be very close to the optimal information required to design and optimize the process. However, this information is costly and time-consuming to obtain in a real SMB plant.

In the present work, the experimental CSS composition profile is conveniently and inexpensively replicated using a streamlined version of a single-column set-up [15] that reproduces the steady periodic behavior of the SMB in a minimum number of cycles. The original set-up has proven to be a simple, compact, and fast method of experimentally mimicking the CSS of an SMB process with minimal solvent and solute consumptions [25–27]. A simplified version of this scheme is employed in the present work as the basis for "polishing" or finetuning the isotherm parameters estimated by the inverse method.

The idea is simple. Using suitable optimization tools, the SMB cycle is designed (i.e., the optimal values of the switching interval and zone flow rates are determined) based on the parameters of the prescribed adsorption isotherm model estimated by the inverse method. Then, the simulated inlet composition profile, $\{c_i^{\mathrm{in}}(t)\}^{\mathrm{sim}}$, given by the CSS solution of the optimized SMB model, is used to experimentally generate the simulated inlet composition profile.

The effect of the simulated upstream column is experimentally reproduced using three

HPLC pumps to continuously manipulate three distinct flow rates, Q_i^{in}, according to

$$\begin{cases} Q_{\text{A}}^{\text{in}}(t) = \{c_{\text{A}}^{\text{in}}(t)\}^{\text{sim}}\, Q(t)/c_{\text{A}}^{\text{s}} \\ Q_{\text{B}}^{\text{in}}(t) = \{c_{\text{B}}^{\text{in}}(t)\}^{\text{sim}}\, Q(t)/c_{\text{B}}^{\text{s}} \\ Q_{\text{E}}^{\text{in}}(t) = Q(t) - Q_{\text{A}}^{\text{in}}(t) - Q_{\text{B}}^{\text{in}}(t) \end{cases}, \tag{7}$$

where c_i^{s} is a concentrated solution in pure enantiomer i and Q_{E}^{in} is the flow rate of pure mobile phase. The admixture of the three HPLC pump outlets replicates the flow rate, $Q(t)$, and inlet composition profile, $c_i^{\text{in}}(t)$, as if the column were in the SMB unit operating under CSS conditions. A schematic diagram of the single-column set-up is depicted in Fig. 3. An UV detector is placed at the column outlet to monitor the total enantiomer concentration, $\{c^{\text{out}}(t)\}^{\text{exp}}$, exiting the column.

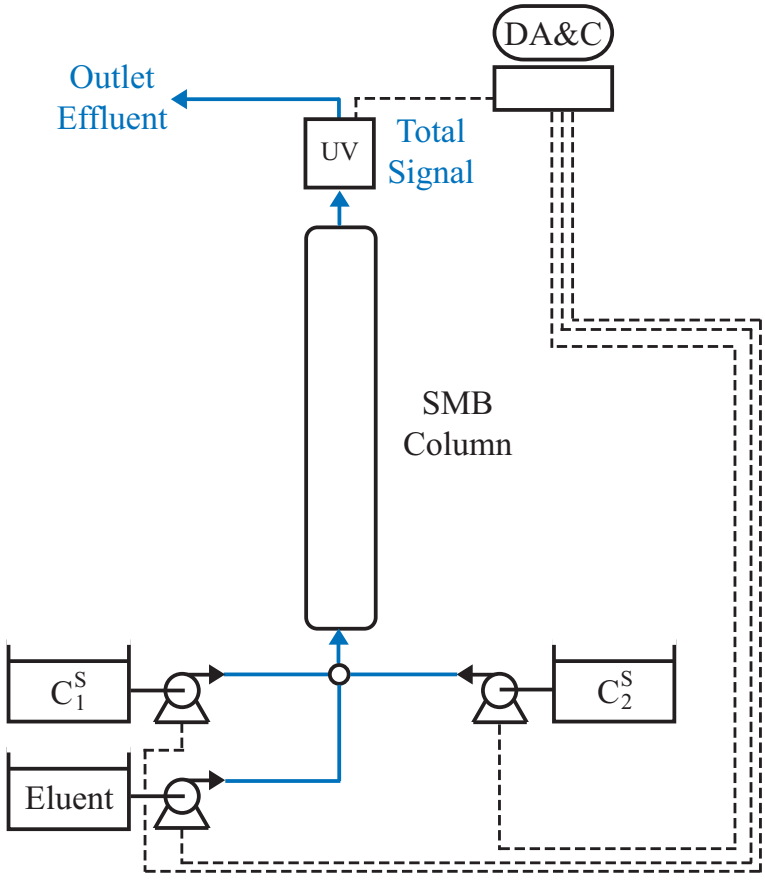

Figure 3: Schematic diagram of the single-column SMB analog chromatograph. Pumps and detector are connected to an automated data acquisition and control unit.

One final trick is employed to shorten the experiment as much as possible. The SMB cycle is shifted in time to make it end when the column is in the leftmost position of zone I of the mimicked SMB. This way the steady periodic state of the column at the start of a cycle is the closest to that of a clean column. But this is precisely the state of the column

at the start of the experiment. Under these conditions the column should approach the CSS in a minimum number of cycles. Experience has shown that this happens in 1–3 cycles.

The steady periodic solution, $\{c_i(z,t)\}^{\text{sim}}$, is obtained from the SMB model using an efficient numerical procedure described elsewhere [28]. The isotherm parameters are recomputed by fitting $\{c^{\text{out}}(t)\}^{\text{sim}}$ to the experimentally measured one, $\{c^{\text{out}}(t)\}^{\text{exp}}$, using an algorithm similar to the one described in section 3. The procedure is thus identical to the standard inverse method, but here the CSS of the SMB experiment is used instead of the series of overloaded band profiles. The objective function is that given by Eq. (6) with t varying over the duration of a SMB cycle, i.e. $N\tau$ time units (N is the number of columns in the mimicked SMB).

For convenience, the curve-fitting is not performed in gPROMS, but is instead defined as a nonlinear programming (NLP) problem in AMPL [29] and solved using the interior-point solver IPOPT [30]. The reason for this is that the NLP problem for the inverse method is only a slight modification of the NLP problem for optimal design of the SMB process [28], and both are efficiently formulated and solved using AMPL/IPOPT.

A illustration of the hybrid inverse method estimation principle, that conjugates the analysis of band profiles of the racemic mixture obtained in the overloaded elution mode and the periodic steady state of a SMB experience, is depicted in Fig. 4.

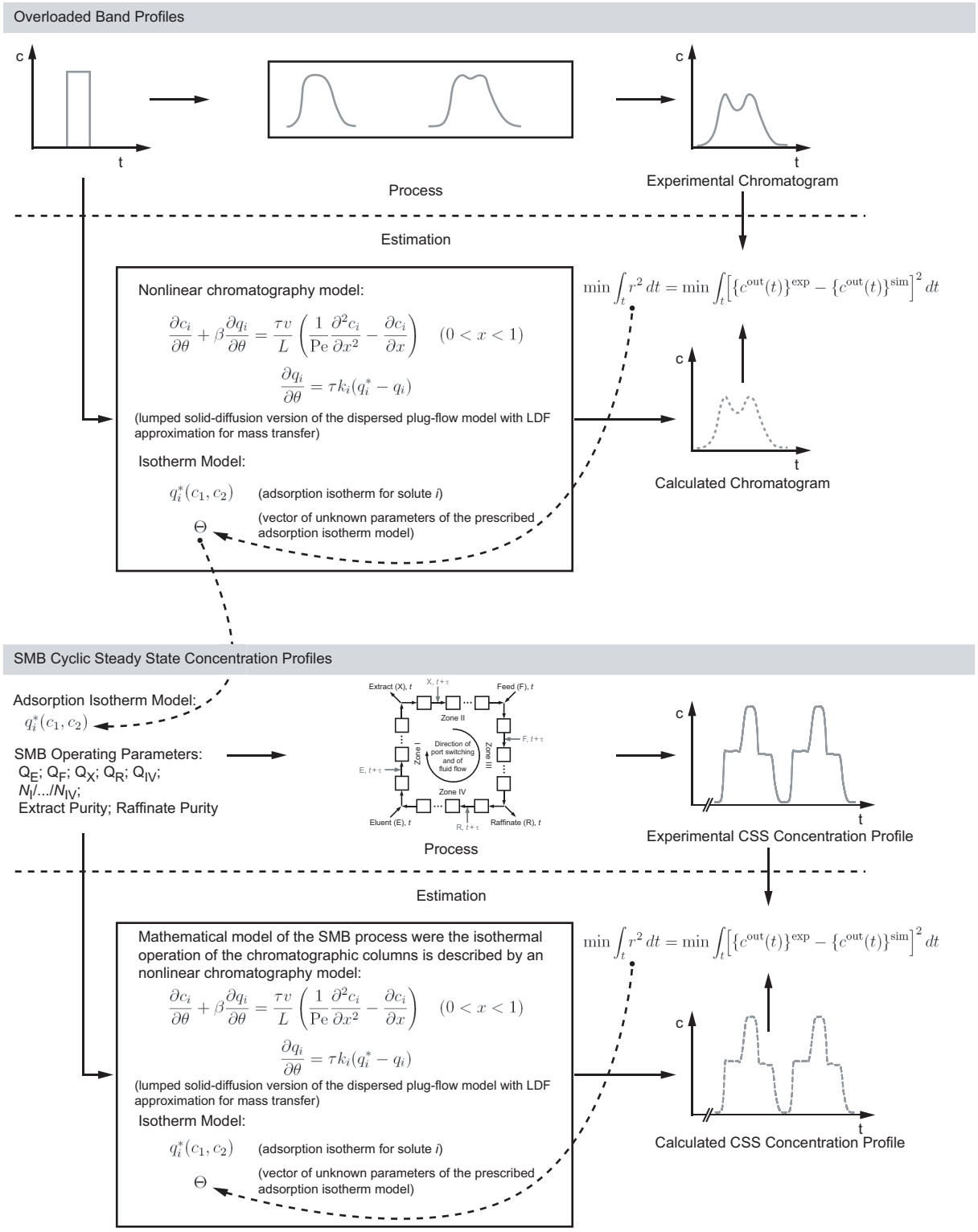

Figure 4: Hybrid inverse method estimation principle.

5 Adsorption isotherm models

The adsorption isotherm relates, at a given temperature, the equilibrium solute concentrations in the stationary (q_i^*) and mobile (c_i) phases. The nature of the adsorbate–adsorbent interactions varies from system to system, which explains why there is a large number of adsorption isotherm models.

In many cases the surface of the adsorbents used in chromatography is not homogeneous. The simplest model for an heterogeneous surface is a patchwork surface covered with two different types of adsorption sites, as is, e.g., the case for most chiral stationary phases (CSPs) [31, 32]. Part of their surface is covered by nonspecific interaction sites, type-I adsorption sites in the Kiselev classification [33]. The rest of the surface is covered with enantioselective sites (type II sites [33]), which are responsible for the chiral separation. The saturation capacity of type II sites is relatively low for most CSPs. For this reason, when the enantiomeric concentration is increased, the selective retention mechanism is rapidly overloaded and the chiral separation disappears. When a surface is covered by two different types of adsorption sites, behaving independently, the adsorption isotherm results from the addition of the independent contributions from the two types of sites [34].

Table 1 lists the various types of adsorption isotherm models considered in the present work. The simpler model, the linear isotherm, has only one adjustable parameter per solute (the Henry constant). The most complex model considered here, the competitive biLangmuir model, has four adjustable parameters per solute. It is worth mentioning that the condition for thermodynamic consistency of a Langmuirian-type isotherm imposes the restriction that the saturation capacity, q_{is}/b_i, be the same for all adsorbates [35]. However, this constraint is usually lifted in practice, since the extra degree of freedom allows for a better fitting of experimental chromatograms.

5.1 Linear isotherm

The linear isotherm is widely used in analytical chromatography, where it gives satisfactory results. However, for high values of concentration deviations from linearity take place, competitive interactions between the different solutes appear, and a more complex model becomes necessary to account for the experimental results. The linear adsorption isotherm is given by

$$q_i^* = K_i c_i, \tag{8}$$

Table 1: Adsorption isotherm models.

Isotherm	q_i^* $(i = \mathrm{A}, \mathrm{B})$	Parameters, Θ $(i = \mathrm{A}, \mathrm{B})$
Linear	$K_i c_i$	K_i
Langmuir	$\dfrac{q_{i\mathrm{s}} b_i c_i}{1 + b_\mathrm{A} c_\mathrm{A} + b_\mathrm{B} c_\mathrm{B}}$	$q_{i\mathrm{s}}$, b_i
Linear-Langmuir	$K_i c_i + \dfrac{q_{i\mathrm{s}} b_i c_i}{1 + b_\mathrm{A} c_\mathrm{A} + b_\mathrm{B} c_\mathrm{B}}$	K_i, $q_{i\mathrm{s}}$, b_i
BiLangmuir	$\displaystyle\sum_{k=\mathrm{I,II}} \frac{q_{i\mathrm{s},k} b_{i,k} c_i}{1 + b_{\mathrm{A},k} c_\mathrm{A} + b_{\mathrm{B},k} c_\mathrm{B}}$	$q_{i\mathrm{s},k}$, $b_{i,k}$ $(k = \mathrm{I}, \mathrm{II})$

where K_i is the Henry's constant for component i, i.e. the slope of the linear relation between q_i^* and c_i.

5.2 Competitive Langmuir isotherm

The competitive Langmuir isotherm is obviously the first choice to model the nonlinear region of the adsorption equilibrium. Although the experimental isotherm data often fit approximately to the ubiquitous Langmuir model, they rarely fit well to it [7].

This simple model considers that the adsorption process occurs on a surface with a fixed number of adsorption sites of equal energy, one molecule being adsorbed per given number of sites until monolayer coverage is achieved [39,40]. The Langmuir model has been widely used in the study of liquid-solid equilibria, in spite of its semi-empirical nature [21]. However, the model has been criticized because of its restrictions to homogeneous surfaces and monolayer coverage. Nevertheless, the Langmuir isotherm is convenient for quantitative analysis of adsorption processes and has a physical basis, unlike other empirical models, such as the Freundlich model, which has no significant theoretical corroboration [41]. The great advantage of the Langmuir isotherm model is the small number of parameters required and the simplicity of its derivation [42]. The competitive Langmuir isotherm for a binary mixture of two solutes, A and B, is given as

$$q_i^* = \frac{q_{i\mathrm{s}} b_i c_i}{1 + b_\mathrm{A} c_\mathrm{A} + b_\mathrm{B} c_\mathrm{B}}, \tag{9}$$

where $q_{i\mathrm{s}}/b_i$ is the saturation capacity for component i and b_i is the corresponding equilibrium constant or distribution coefficient. The condition for thermodynamic consistency of the isotherm imposes the restriction that $q_{\mathrm{As}}/b_\mathrm{A} = q_{\mathrm{Bs}}/b_\mathrm{B}$, i.e. that the saturation capacity is the same for both components [39]. However, this constraint is usually lifted

in practice, since the extra degree of freedom allows for a better fitting of experimental chromatograms.

5.3 Competitive Linear-Langmuir Isotherm

A modified Langmuir competitive isotherm, that arises from the combination of the linear adsorption isotherm (Eq. 9) and the competitive langmuir isotherm (Eq. 10), for both components takes the form

$$q_i^* = K_i c_i + \frac{q_{is} b_i c_i}{1 + b_\mathrm{A} c_\mathrm{A} + b_\mathrm{B} c_\mathrm{B}}. \tag{10}$$

The competitive adsorption behavior of racemic mixtures is frequently modeled by this isotherm, since it can take into account the adsorption on a heterogeneous surface that consists of two different types of adsorption sites: the non-chiral interaction sites (linear term), and the enantioselective sites that discriminate based on the affinity for each enantiomer (Langmuirian term). This model is based on the assumption that the non-chiral adsorption sites do note possess a saturation limit. This is true only for low concentrations; at higher concentrations, the adsorption behavior of the non-chiral sites also becomes nonlinearly dependent on the solute concentration.

5.4 Competitive BiLangmuir Isotherm

Here, the competitive Langmuir isotherm is extended to an equation with two Langmuir terms, called the competitive biLangmuir isotherm. This model assumes that the surface of the chiral stationary phase contains two different types of sites: the nonselective and the enantioselective sites, which behave independently but homogeneously. The biLangmuir isotherm is given by

$$q_i^* = \frac{q_{is,I} b_{i,I} c_i}{1 + b_{\mathrm{A,I}} c_\mathrm{A} + b_{\mathrm{B,I}} c_\mathrm{B}} + \frac{q_{is,II} b_{i,II} c_i}{1 + b_{\mathrm{A,II}} c_\mathrm{A} + b_{\mathrm{B,II}} c_\mathrm{B}}, \tag{11}$$

where the numerical subscripts refer to the type of adsorption site, $q_{is,\mathrm{I}}/b_{i,\mathrm{I}}$ and $q_{is,\mathrm{II}}/b_{i,\mathrm{II}}$ are the saturation capacity for component i in type I and type II sites, respectively, and $b_{i,\mathrm{I}}$ and $b_{i,\mathrm{II}}$ are the corresponding equilibrium constants or distribution coefficient.

6 Experimental

The selected model system for evaluating and demonstrating the feasibility of the proposed method is the separation of Tröger's base enantiomers on Chiralpak AD, using pure methanol as mobile phase, in both linear and nonlinear regions of the adsorption equilibrium. Chiralpak AD (Daicel Chemical Industries Ltd, Chiral Technologies Europe, Illkirch, France), a 20-μm silica-based packing material, coated with amylose tri-(3,5-dimethylphenyl carbamate), is convenient for the separation of aromatic enantiomers. The structure of this stationary phase is illustrated in Fig. 5 [36].

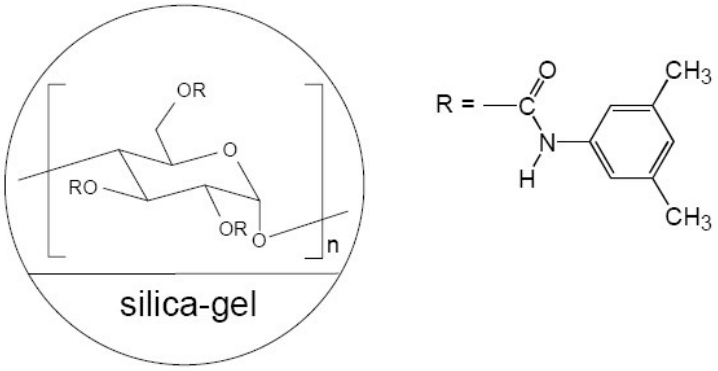

Figure 5: Chemical structure of the CSP in Chiralpak AD [36].

6.1 Equipment

The HPLC pumps employed in the experiments are model K-501 from Knauer (Berlin, Germany) with 10 ml and 50 ml pump heads, controlled by RS232 communication protocol. The whole setup is fully automated and driven by our Labview-based software system (BioCTR) for process monitoring and control of chromatographic processes [37].

A multi-wavelength UV detector (USB2000 from Ocean Optics, USA) equipped with a DH-2000-S-DUV light source (Micropack, Ostfildern, Germany), and attenuator, was employed to continuously monitor the total enantiomeric concentration profile at the column outlet. The UV detector was calibrated at two distinct wavelengths, depending on which experimental set-up it was attached to. To monitor the single-column SMB chromatograph (Fig. 3), the UV detector was calibrated at a wavelength of 264.5 nm, at which UV absorption by product impurities was small and the detector showed a linear response over the concentration range spanned by the SMB experiments. When the UV was attached to the set-up shown in Fig. 2, for producing wide plug injections, the wavelength was fixed at 300 nm. The UV detector response at this wavelength is only

slightly nonlinear over the concentration range spanned by the band profiles. In this case, the UV calibration curve was accurately fitted to a second-order polynomial.

6.2 Materials and system characterization

The pure enantiomers were purchased from Fluka (Germany), with a purity of 99%, and the racemic mixture was purchased from Sigma-Aldrich (Germany), with a purity of 98%. The stationary phase was slurry-packed into one thermojacketed Superformance 10 mm i.d. glass column (Götec Labortechnik, Germany) to a bed height of $L = 10.0$ cm. HPLC-grade methanol was used as the mobile phase; it was obtained from Sigma-Aldrih (Germany) and used after filtration. The system was operated isothermally at 30°C.

The total porosity (ϵ) of the column was measured using 1,3,5-tri-tert-butylbenzene (TTBB) from Sigma-Aldrich (Germany). This compound is not retained but has access to the pore volume of the stationary phase. Extra-column volumes in the two experimental set-ups were estimated from TTBB pulse experiments with and without the chromatographic column.

The rate parameters Pe and k_i were estimated by simultaneously fitting the chromatographic model to a series of experimental chromatograms obtained by injecting several diluted pulses of racemic mixture at different flow rates over the range 5–30 ml/min. Examples of this procedure are reproduced in Fig. 6, which compares fitted and experimental chromatograms obtained for three different flow rates. The estimated values for the rate parameters are $k_{\mathrm{A}} = 12.06\ \mathrm{s}^{-1}, k_{\mathrm{B}} = 11.98\ \mathrm{s}^{-1}$, and $\mathrm{Pe} = 1586$.

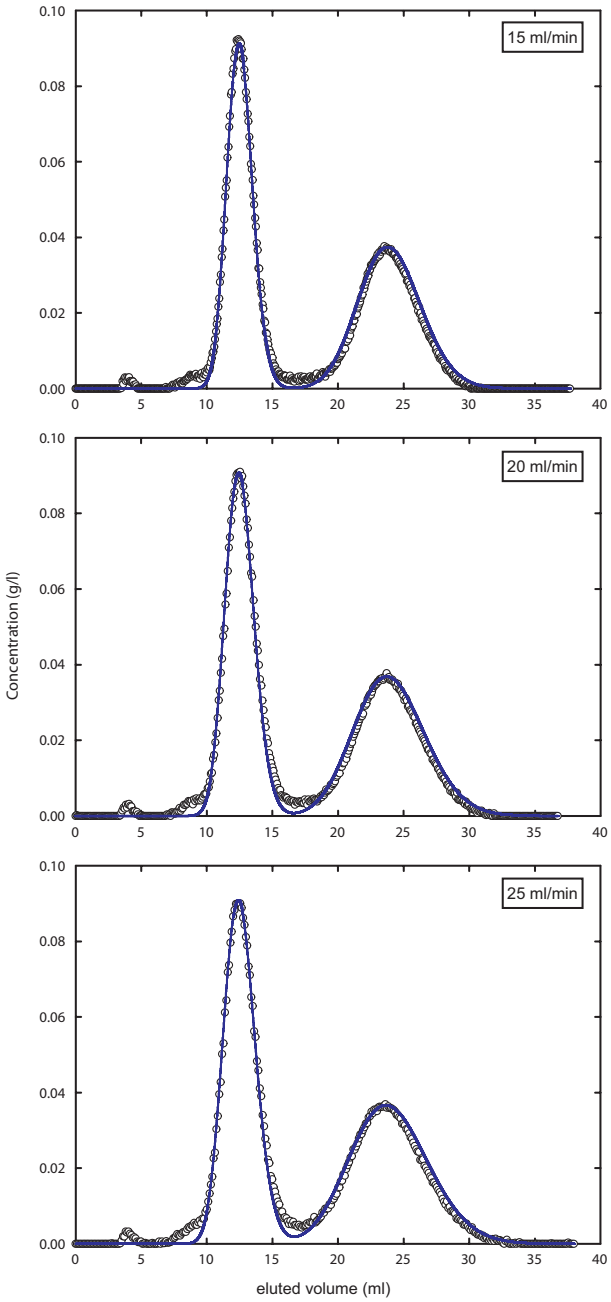

Figure 6: Examples of fitted (——) and experimental (∘) chromatograms for the injection of diluted pulses of racemic mixture at different flow rates. The rate parameters Pe and k_i were determined by simultaneously fitting Eq. (1) to 6 different chromatograms over the flow-rate range 5–30 ml/min. The obtained results are: $k_\mathrm{A} = 12.06\ \mathrm{s}^{-1}$, $k_\mathrm{B} = 11.98\ \mathrm{s}^{-1}$, and $\mathrm{Pe} = 1586$.

7 Results and discussion

The analysis is first carried out for the linear region of the adsorption equilibrium. The three chromatograms plotted in Fig. 7 were obtained using the experimental set-up depicted in Fig. 2. In every case the feed solution is 3.0 g/l of racemic mixture, and the volumetric flow rate was fixed at 25 ml/min; the pulse width was varied by changing the duration of the injection. The chromatograms show the presence of some impurities, in agreement with the 98%-purity level reported by the Sigma-Aldrich. The impurities are mostly eluted before the two enantiomeric peaks.

The linear isotherm model, $q_i^* = K_i c_i$, is firstly fitted separately to each of the six different chromatograms whose injected pulse widths are listed in Table 2. The vector of unknown parameters to be estimated comprises the Henry coefficient for each enantiomer, $\Theta = (K_\mathrm{A}, K_\mathrm{B})$. The fitted values for these coefficients are listed in Table 2. It is seen that the value of the Henry coefficient for each enantiomer decreases with increasing volume of injected sample, in agreement with the convex shape for a favorable isotherm. The decreasing trend on the estimated value of K_i is a consequence of averaging over progressively smaller isotherm slopes as the concentration range spanned by the chromatograms is increased.

Table 2: Estimated values of the Henry coefficient, K_i (l/g), for each enantiomer as a function of injected sample volume, and their average values obtained by simultaneously fitting all chromatograms. These are depicted in Fig. 7.

Sample size (μl)	K_A	K_B
125	2.428	6.107
150	2.435	6.107
250	2.401	6.047
400	2.401	5.990
600	2.348	5.865
1000	2.386	6.027
All	2.382	5.990

The bottom row of Table 2 lists the Henry coefficients obtained by simultaneously fitting the six chromatograms; the best-fit values of the isotherm parameters are $K_i = \{2.382, 5.990\}$. The solid lines plotted in Fig. 7 are the simulated band profiles for these

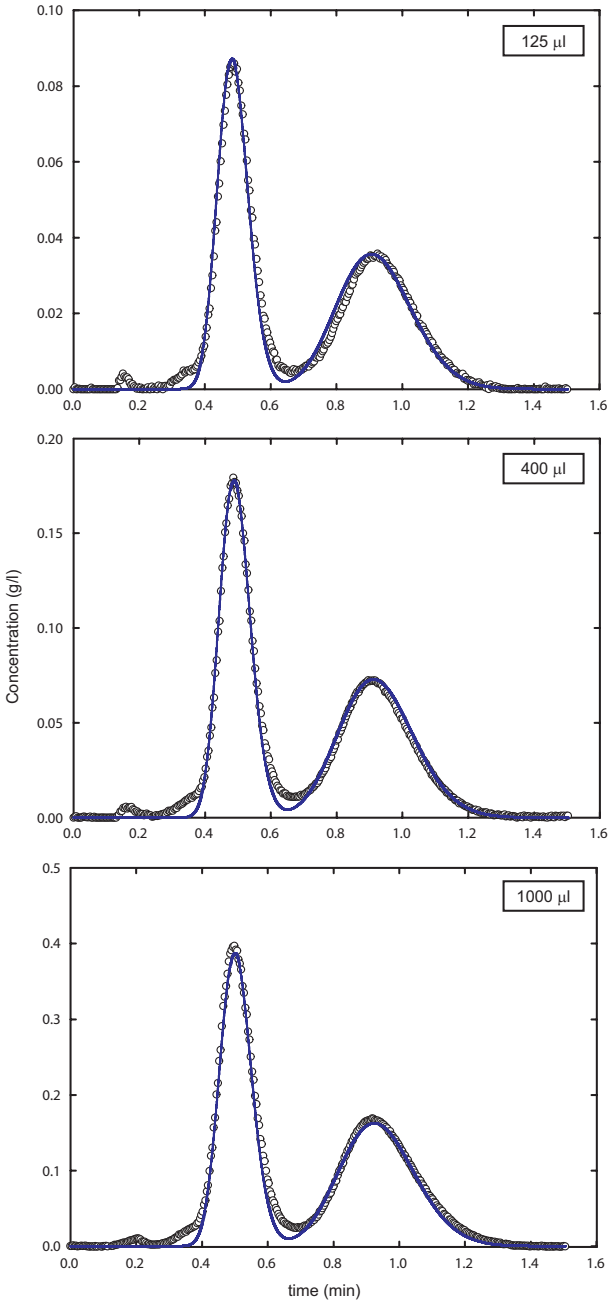

Figure 7: Comparison of experimental (○) and simulated (——) chromatograms for the linear range of the adsorption equilibrium. The latter were obtained by simultaneously fitting the linear isotherm model, $q_i^* = K_i c_i$, to the chromatograms for the six pulse widths listed in Table 2. The best-fit values of the isotherm parameters are listed in the bottom row of Table 2. For conciseness, only three chromatograms are plotted.

values of the Henry constants. The agreement between experimental and theoretical band profiles is reasonably good for all six chromatograms. This indicates that in the concentration range spanned by the chromatograms the adsorption equilibrium is only mildly nonlinear. The results from these injections are helpful as initial estimates for the isotherm parameters when the inverse method is applied to the nonlinear region of the adsorption equilibrium.

The first obvious choice to model nonlinear isotherms in chromatography is the competitive Langmuir isotherm. The condition for thermodynamic consistency of this isotherm, imposes that the saturation capacity be the same for both enantiomers. However, this constraint is dropped in the present study, since the extra degree of freedom allows for a better fitting of the experimental chromatograms.

The six overloaded chromatograms listed in Table 3 were used to obtain the isotherm parameters for the competitive Langmuir isotherm. For this isotherm model the vector of unknown parameters to be estimated is $\Theta = (q_{\mathrm{As}}, q_{\mathrm{Bs}}, b_{\mathrm{A}}, b_{\mathrm{B}})$. The first six rows of Table 3 list the estimated values obtained by fitting the competitive Langmuir isotherm to each individual chromatogram, whereas the bottom row lists the estimated values obtained by simultaneously fitting all chromatograms.

Table 3: Parameters of the competitive Langmuir isotherm model, estimated by applying the inverse method to the six overloaded band profiles listed below. $q_{i\mathrm{s}}$ is given in g/l and b_i in l/g.

Sample size (μl)	$q_{\mathrm{As}}b_{\mathrm{A}}$	$q_{\mathrm{Bs}}b_{\mathrm{B}}$	$100b_{\mathrm{A}}$	$100b_{\mathrm{B}}$
600	2.363	5.942	0.790	7.693
1500	2.481	5.857	8.655	8.600
4000	2.407	5.688	4.645	8.260
6000	2.430	5.682	4.196	8.544
10000	2.425	5.489	1.948	6.497
30000	2.447	5.537	2.540	4.869
All	2.445	5.783	3.400	8.851

The simulated band profiles for the individual and global fittings are plotted in Fig. 8 as dashed and solid lines, respectively. The agreement between experimental and simulated profiles is excellent, and the quality of the global fitting is nearly as good as that obtained by individually fitting each chromatogram.

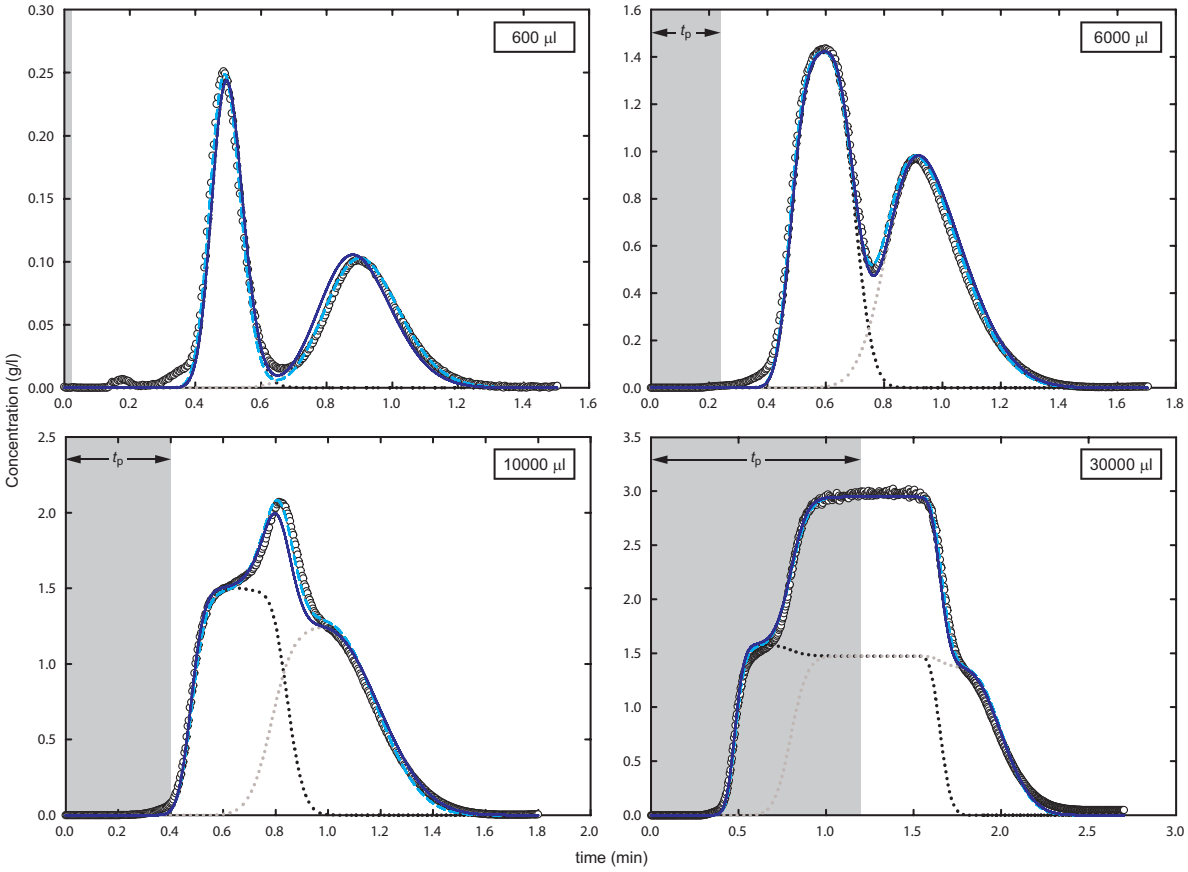

Figure 8: Comparison of experimental (∘) and simulated (——) band profiles obtained by simultaneously fitting the competitive Langmuir isotherm model, $q_i^* = q_{is}c_i/(1 + b_A c_A + b_B c_B)$, to six different chromatograms for different injection widths (Table 3). The best-fit values of the isotherm parameters are listed in Table 3. The simulated (- - -) band profiles for the individual fitting of each chromatogram are also included for comparison. For conciseness, only four chromatograms (sample size: 600 μl; 6000 μl; 10000 μl and 30000 μl) are shown. In each graph the duration of sample injection (t_p) is given by the grayed area. The rate constants are fixed at $k_A = 12.06$ s^{-1}, $k_B = 11.98$ s^{-1}, and Pe = 1586. In every case the concentration of the injected sample is 3.0 g/l of racemic mixture.

It is worth noting that the band profile in the bottom-right graph of Fig. 8 corresponds to a breakthrough experiment (sample volume of 30000 μl), which was included in an attempt to minimize the uncertainty on the estimated saturation capacities due to the dilution of the band profiles with respect to the injected concentrations. If the loading factor is too low (smaller sample sizes), the saturation capacity is estimated with large uncertainty because the concentration range sampled by the bands is very distant from the saturation plateau. Note, however, that in the present case the values of q_{is} deduced

from Table 3 indicate that the plateau of the breakthrough experiment cannot be related to the saturation capacity because the latter is still significantly distant. The isotherm parameters, listed in the bottom row of Table 3, were determined by fitting simultaneously the experimental band profiles and breakthrough curve. Using this procedure, the isotherm model is able to predict the adsorption capacity over the full concentration range, from diluted conditions up to the injected concentration.

The simulated band profiles for the fitted values of the linear isotherm (bottom row of Table 2) and Langmuir isotherm (bottom row of Table 3) parameters are compared in Fig. 9, as solid lines and dashed lines, respectively. It is clear that the linear isotherm model cannot accurately characterize the adsorption equilibrium region up to a feed concentration of 3.0 g/l of racemic mixture.

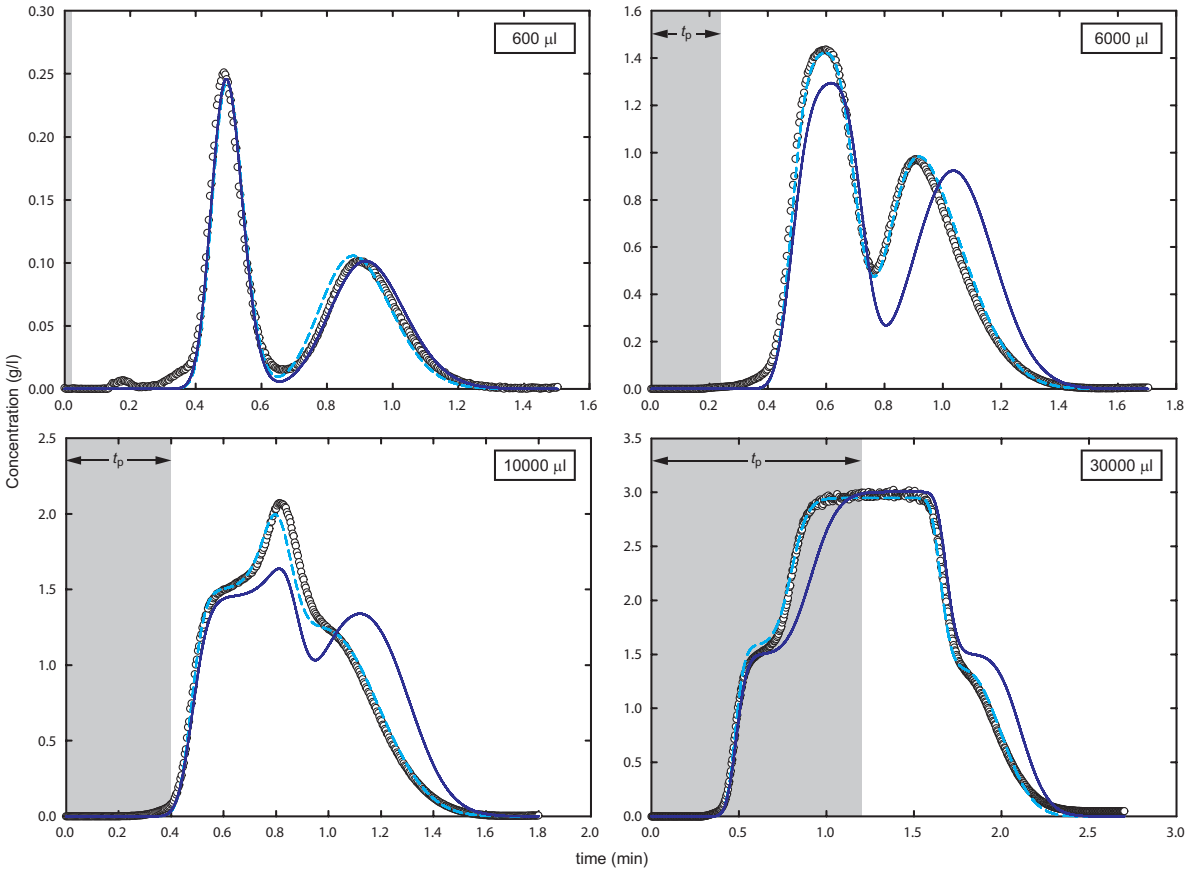

Figure 9: Comparison of experimental (○) and simulated band profiles for the linear (——, bottom row of Table 2) and Langmuir (– – –, bottom row of Table 3) isotherm models. In each graph the duration of sample injection (t_p) is given by the grayed area. The rate coefficients and feed concentration are the same as in Fig. 8.

To validate the numerical constants of the linear and Langmuir isotherm models, two SMB experiments were carried out using the single-column chromatograph. One run was carried out in the linear range of the adsorption equilibrium, and the other run under overloaded conditions. In both cases, the operating conditions were determined by maximizing the feed throughput, subject to a minimum purity requirement of 98% for both extract and raffinate streams. The operating parameters are listed in Table 4. The concentration of each enantiomer in the feed is $c_i^{\mathrm{F}} = 0.05$ g/l for the linear case, and $c_i^{\mathrm{F}} = 0.5$ g/l for overloaded operation.

Table 4: Model parameters and operating conditions for the enantiomeric separation by SMB. The column configuration is fixed at 1/1/1/1.

L (cm)	10.0		Pe	1586		
d (cm)	1.0		k_i (s^{-1})	$12.06, 11.98$		
ϵ	0.626		c_i^{F} (g/l)	0.05 / 0.5		
Isotherm	τ	Q_{IV}	Q_{E}	Q_{F}	Q_{X}	Q_{R}
Linear	4.620	2.632	2.500	2.312	2.478	2.334
Langmuir	4.121	2.963	2.500	2.284	2.536	2.248
Linear-Langmuir	4.457	2.723	3.000	2.354	3.061	2.293

Figure 10 shows that the SMB operation under linear adsorption conditions was successfully reproduced experimentally by the single-column chromatograph. This figure compares the total enantiomer concentration at the column outlet, $\{c^{\mathrm{out}}\}^{\mathrm{exp}}$, with the steady periodic solution, $\{c^{\mathrm{out}}\}^{\mathrm{sim}}$, obtained from the SMB model, for the duration of the experiment which spanned three cycles of operation. The agreement between experimental and simulated data is excellent, which indicates that the linear isotherm parameters, listed in the bottom row of Table 2, were correctly estimated. The second cycle is seen to have already attained the cyclic steady state.

Figure 11 shows a similar comparison but for overloaded operation. Although the agreement between simulated and experimental concentrations profiles is reasonably good, it is observed that during some periods of the cycle, mostly those coinciding with the highest concentration region of the total enantiomeric concentration profile, there is some misfit between simulated and measured concentrations. The observed discrepancies suggest that the estimated parameters for the Langmuir isotherm, listed in the bottom row of Table 3, may be subject to some inaccuracy and could be improved. It is worth men-

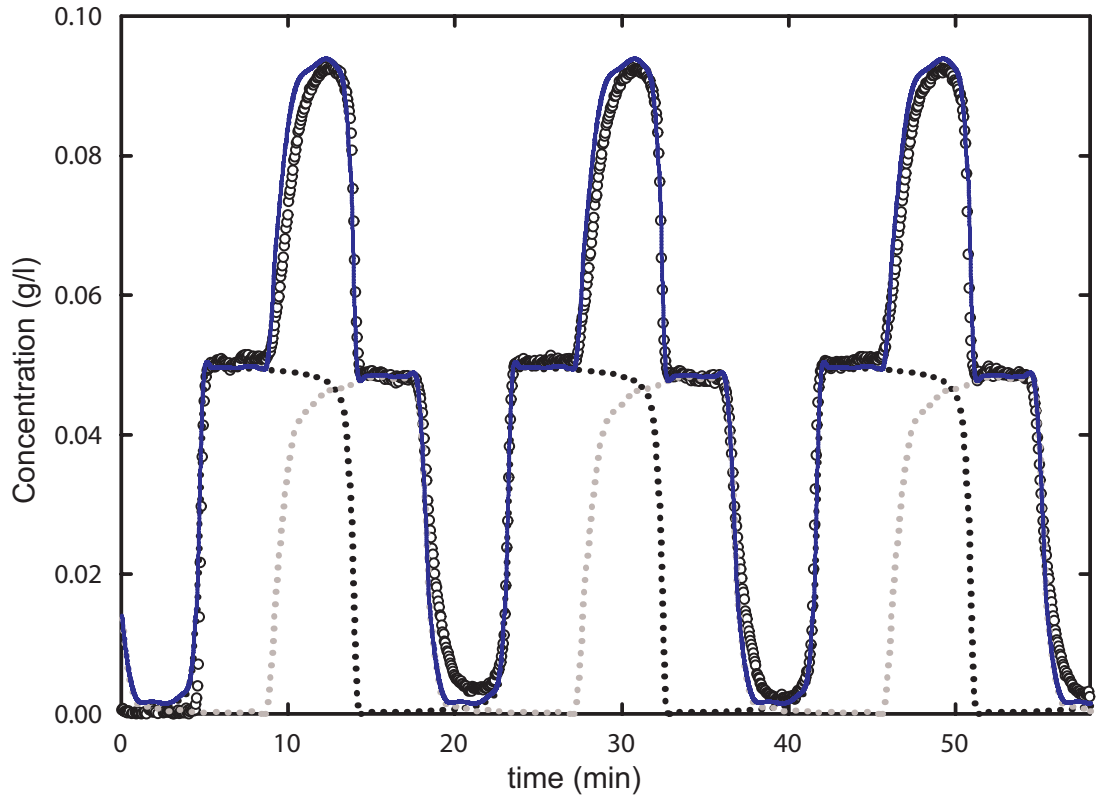

Figure 10: Total enantiomer concentration at the outlet of the single-column setup, mimicking a 4-column SMB unit operated in the linear region of the adsorption equilibrium ($c_i^{\mathrm{F}} = 0.05$ g/l), over three complete cycles of operation. The measured values ($\circ$) are compared with the steady periodic solution (——) of the SMB model for the linear isotherm parameters listed in the bottom row of Table 2. Note that by judiciously selecting the step within the cycle at which the run is started, CSS conditions are readily attained on the second cycle of the run.

tioning that Trögers base enantiomers show an unusual adsorption behavior on Chiralpak AD at high loadings [38].

In order to improve the fitting of the isotherm model in the nonlinear region of the adsorption equilibrium, the experimental concentration profiles measured over the second and third cycles of the SMB experiment are employed as fitting data to recompute a new competitive nonlinear isotherm. The isotherm models considered for this purpose are the competitive Langmuir model, the competitive Linear-Langmuir model, and the competitive BiLangmuir model. The number of unknown parameters to be estimated for each of these isotherm models is, respectively, 4, 6, and 8 (Table 1).

The results of this procedure are shown in Fig. 12, which compares the measured concentration profile with the fitted CSS solution of the SMB model, for each isotherm model. The estimated values of the isotherm parameters are listed in Table 5, which also includes the minimum value of the objective function obtained in each case.

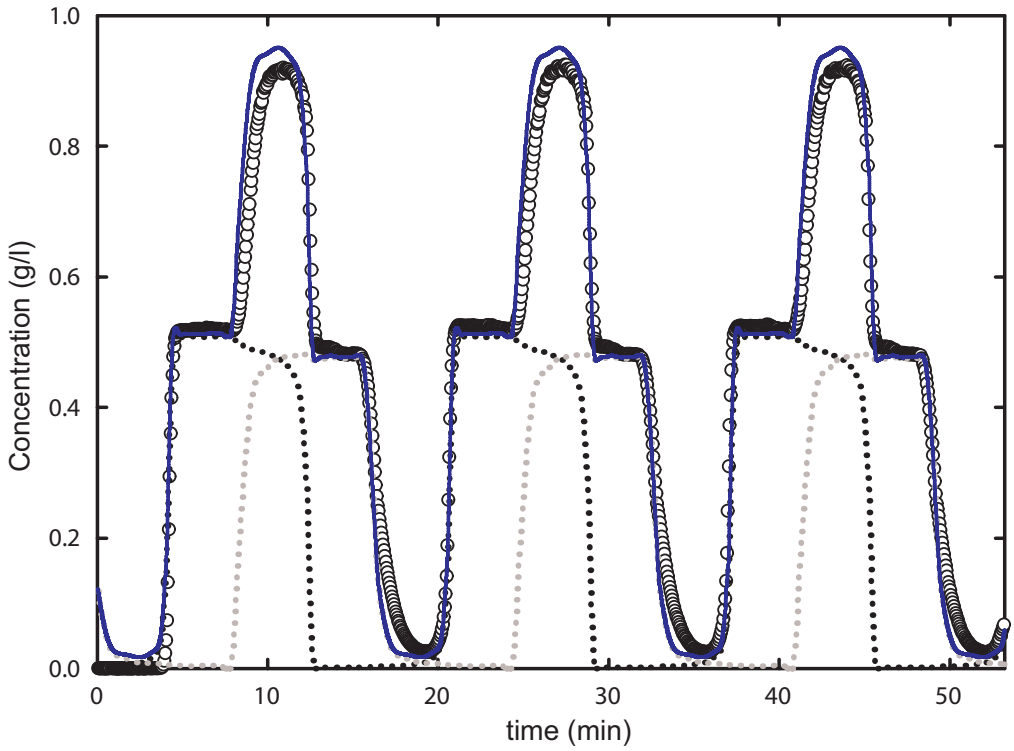

Figure 11: Total enantiomer concentration at the outlet of the single-column setup, mimicking a 4-column SMB unit operated in the nonlinear region of the adsorption equilibrium ($c_i^{\mathrm{F}} = 0.5$ g/l)), over three complete cycles of operation. The measured values ($\circ$) are compared with the steady periodic solution (——) of the SMB model for the Langmuir isotherm model given in Table 3.

The fitting of the Langmuir isotherm model has an associated error which is 35% larger than those for the other two isotherm models. The fittings shown in Fig. 12 for both the competitive linear-Langmuir and biLangmuir isotherms have the same accuracy, because the minimized values of the objective function are identical. An inspection of the isotherm parameters listed in Table 5, shows that in practice the fitted parameters of the biLangmuir isotherm are identical to those of the linear-Langmuir because the distribution coefficients for the non-chiral sites are negligible and the Langmuirian description of the enantioselective sites is the same as that given by the biLangmuir model. Therefore, for all practical purposes the linear-Langmuir isotherm model provides the best fit of the experimental CSS concentration profile.

To validate the parametrization of the linear-Langmuir isotherm model based on CSS data from the SMB experiment, a third SMB run was carried out using the single-column chromatograph. The operating conditions for the SMB cycle are based on the adsorption equilibrium defined by the newly estimated isotherm. The NLP problem is the same as that used previously for determining the operating parameters for the other SMB cycles.

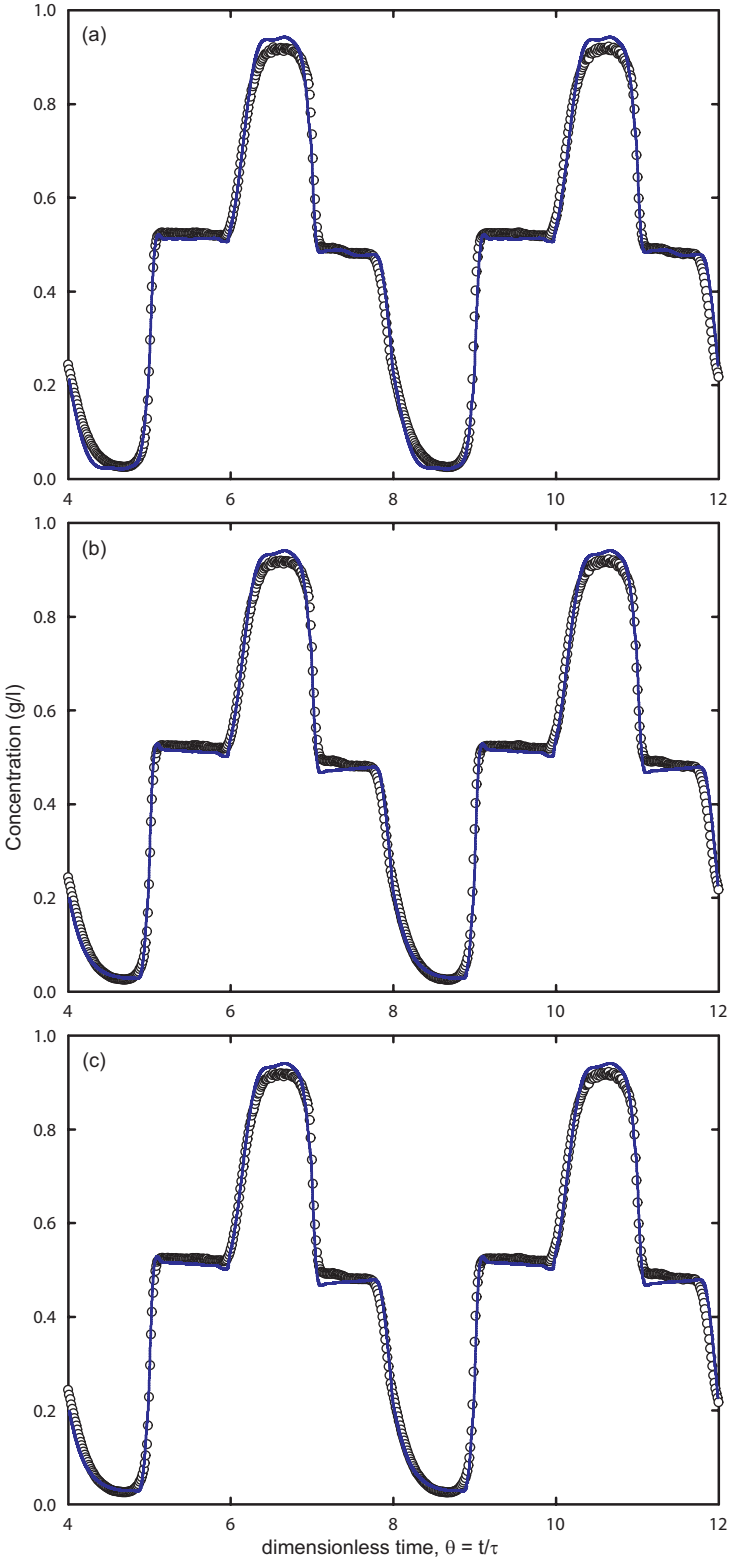

Figure 12: Determination of competitive adsorption isotherms by applying the inverse method to the experimental CSS of the single-column SMB analog under overloaded conditions. For this purpose only the 2nd and 3rd experimental cycles of the run were taken into consideration. Lines represent the simulated concentration profiles for the (a) Langmuir, (b) linear-Langmuir, and (c) biLangmuir isotherm models.

Table 5: Estimated values of the parameters for the Langmuir, Linear-Langmuir, and BiLangmuir isotherm models. The parameters for each isotherm model were estimated by applying the inverse method to the CSS of an overloaded SMB experiment, mimicked by the single-column set-up depicted in Fig. 3. The value of the minimized objective function, given by Eq. (6), is also listed for each case.

Isotherm model	q_i^* (g/l)	f_{obj}
Langmuir	$\dfrac{2.359c_{\mathrm{A}},\ 6.221c_{\mathrm{B}}}{1+7.210\times10^{-3}c_{\mathrm{A}}+0.107c_{\mathrm{B}}}$	3.34
Linear-Langmuir	$(2.212c_{\mathrm{A}},\ 5.611c_{\mathrm{B}})+\dfrac{0.621c_{\mathrm{A}},\ 2.609c_{\mathrm{B}}}{1+6.386c_{\mathrm{A}}+11.21c_{\mathrm{B}}}$	2.49
BiLangmuir	$\dfrac{2.212c_{\mathrm{A}},\ 5.611c_{\mathrm{B}}}{1+2.6\times10^{-8}c_{\mathrm{B}}}+\dfrac{0.621c_{\mathrm{A}},\ 2.609c_{\mathrm{B}}}{1+6.386c_{\mathrm{A}}+11.21c_{\mathrm{B}}}$	2.49

The operating parameters for the third SMB run are listed in the bottom row of Table 4.

Figure 13 compares the total enantiomer concentration profile at the outlet of the single-column set-up with the simulated profile from the steady periodic solution of the SMB model for the linear-Langmuir model. The duration of the experiment spans three cycles of operation. The simulated profiles of individual enantiomer concentration are also included for completeness. The agreement between experimental and simulated data is excellent, which indicates that the competitive linear-Langmuir isotherm parameters, listed in Table 4, were correctly estimated. This demonstrates that the parametrization of the linear-Langmuir isotherm model based on a previous SMB run was fully transferable to the newly optimized SMB cycle.

Before concluding, Table 6 summarizes the results of a statistical analysis of the reproducibility of the six chromatograms given in Table 3 by two different fittings of the linear-Langmuir isotherm model: the one (BP) derived from the global fitting of the six batch chromatograms and the one (CSS) derived from the experimental CSS profile of the SMB run (Table 5). To determine which fitting is the most appropriate to account for the recorded band profiles of the batch chromatograms, the sum of squares of the residuals (SSR) of the two fittings are compared. For this purpose the Fisher-test can be applied to assess whether the difference in the SSRs is statistically significant or not. Table 6 gives the Fisher-ratio, FR $= F_{\mathrm{BP}}/F_{\mathrm{CSS}}$, and its critical value, $\mathrm{CFR}_{\alpha,m,m}$, where $m = n - p$, n and p are the number of data points in the chromatograms and number of parameters in the isotherm model, respectively, and $\alpha = 0.05$ is the universally accepted value for

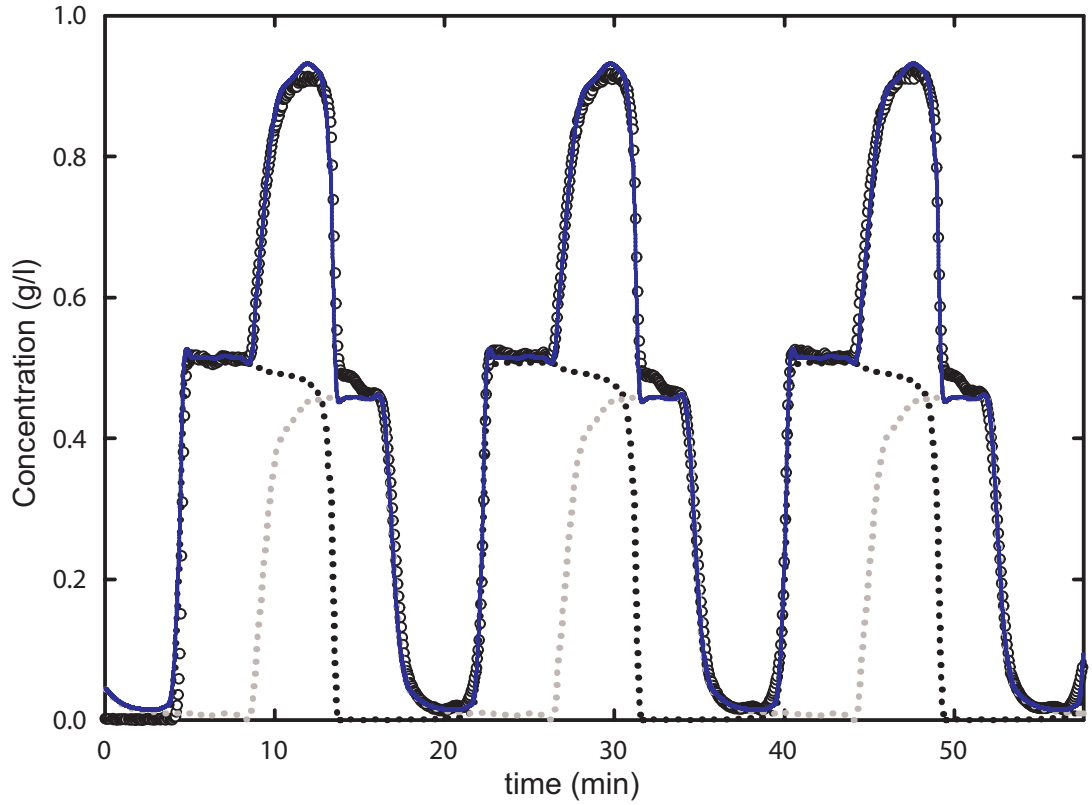

Figure 13: Individual and total enantiomer concentrations at the outlet of the single-column chromatograph, mimicking a 4-column SMB unit operated in the nonlinear region of the adsorption equilibrium, over three complete cycles of operation. The operating parameters are listed in the bottom row of Table 4. The measured values (∘) of total enantiomeric concentration are compared with the steady periodic solution (——) of the SMB model for the linear-Langmuir model given in Table 5.

statical significance. For the test to be considered statistically significant one must have $\max(\mathrm{FR}, 1/\mathrm{FR}) > \mathrm{CFR}$.

The Fisher test shows that both fittings describe equally well the band profiles for the largest loading factors (sample volumes of 10^4 and 3×10^4 μl). Although the isotherm derived from the CSS data appears to fit these chromatograms slightly better, the improvement is not statistically significant. For intermediate loading factors (sample volumes of 1500, 4000, and 6000 μl) the isotherm derived from the CSS data gives a better fitting of the experimental chromatograms; the improvement over the fitting provided by the isotherm derived from the band profiles is statistically significant. For the lowest loading factor (600 μl), however, the trend is reversed because its recorded band profile is better accounted for by the isotherm derived from the global fitting of the batch chromatograms (the test is statistically significant).

These results are somewhat surprising, particularly when considering that the SMB run was carried out with a total feed concentration $c^{\mathrm{F}} = 1$ g/l, whereas the band profiles for

Table 6: Statistical analysis of the reproducibility of the 6 chromatograms given in Table 3 by two different fittings of the linear-Langmuir isotherm model: the one (BP) derived from the global fitting of the six experimental band profiles, and the one (CSS) derived from the experimental CSS profile of the SMB run (Table 5). n is the number of data in the experimental chromatograms, $p = 6$ is the number of isotherm parameters, SSR denotes the sum of squares of the residuals, $\mathrm{FR} = F_{\mathrm{BP}}/F_{\mathrm{CSS}}$ is the Fisher ratio, and $\mathrm{CFR}_{\alpha,m,m}$ is its critical value ($\alpha = 0.05$, $m = n - p$).

Sample size (μl)	n	SSR$\times 10^3$ (BP)	SSR$\times 10^3$ (CSS)	$\mathrm{CFR}_{\alpha,m,m}$ (α, m, m)	FR
600	407	0.021	0.045	1.18	0.48
1500	431	0.190	0.160	1.17	1.19
4000	425	1.573	0.910	1.17	1.73
6000	436	1.180	0.883	1.17	1.34
10000	508	1.089	0.991	1.16	1.10
30000	788	1.393	1.246	1.12	1.11

the largest pulses and frontal analysis experiment attain total concentrations up to 3 g/l. We speculate that probably the smallest pulses introduce an unnecessary bias towards the lowest concentration range for the fit. This may be useful for correctly estimating the Henry constants, but is not relevant when designing a SMB separation under overloaded conditions. Overall, Table 6 shows that the isotherm derived from the CSS profile of the SMB experiment matches extremely well the band profiles of a series of overloaded batch chromatograms carried out independently for concentrations exceeding those spanned by the CSS profile of the SMB.

8 Conclusions

In the present work, a hybrid inverse method for isotherm determination in SMB chromatography was developed and successfully implemented experimentally. The method uses two distinct experimental sets of total enantiomer concentration profiles. On one hand, it uses overloaded band profiles of the racemic mixture. These should preferably be complemented by a breakthrough experiment carried out at the feed conditions of the SMB. On the other hand, the method also uses the periodic state of the target SMB. The numerical parameters of a prescribed competitive adsorption isotherm model are derived by applying the inverse method to the overloaded band profiles of the racemic mixture, including the recorded data from the frontal analysis. The set of estimated parameters are then validated using the periodic state of the SMB experiment, and if necessary recomputed by applying the inverse method of isotherm estimation to its cyclic steady state. This is easily and economically achieved using the single-column chromatograph described above.

The proposed method was successfully applied to determine the competitive adsorption equilibrium of Trögers base enantiomers on Chiralpak AD, using methanol as mobile phase. The competitive linear-Langmuir model was found to be the most appropriate model over the concentration range employed in the SMB experiment (total feed concentration of 1.0 g/l). It is worth noting, however, that a more complex isotherm would probably be required if the SMB unit were operated at much higher feed concentrations.

Our results indicate that the hybrid inverse method offers a reliable and quick approach to determine the competitive adsorption isotherms for a specific SMB separation, with minimum solute and solvent consumptions. The proposed procedure is adequate for conveniently designing the SMB operating conditions over the full concentration range.

Nomenclature

c	solute concentration (g/l)
D_{L}	axial dispersion coefficient ($\mathrm{cm}^2/\mathrm{min}$)
k	LDF coefficient (s^{-1})
L	column length (cm)
N	number of columns
Pe	Péclet number
q	adsorbed concentration (g/l)
Q	flow rate ($\mathrm{cm}^3/\mathrm{min}$)
t	time (min)
v	linear velocity (cm/min)
x	dimensionless axial position, z/L
z	axial position in column (cm)

Greek letters

β	phase ratio, $(1-\epsilon)/\epsilon$
ϵ	total porosity
τ	switching interval (min)
θ	dimensionless time, t/τ
Θ	unknown parameters of prescribed adsorption isotherm model

Subscripts and superscripts

A	R-(+)-Trögers base enantiomer
B	S-(-)-Trögers base enantiomer
E	eluent
exp	experimental
F	feed
i	solute index
I,...,IV	zone index
in	inlet effluent
j	column index
out	outlet effluent
R	raffinate
sim	simulated
X	extract

$\tilde{}$ filtered value

List of Tables

List of Figures

Bibliography

[1] FDA, Chirality 4 (1992) 338.

[2] R.M. Nicoud, G. Fuchs, P.Adam, M. Bailly, E. Küsters, F.D. Antia, R. Reuille, E. Schmid, Chirality 5 (1993) 267.

[3] M. Juza, M. Mazzotti, M. Morbidelli, Trends in Biotech. 18 (2000) 108.

[4] R.M. Nicoud, Pharm. Technol. Eur. 11 (1999) 28.

[5] G. Guiochon, A. Felinger, D.G. Shirazi, A.M. Katti. Fundamentals of Preparative and Nonlinear Chromatography second edition. Elsevier Academic Press, San Diego, CA, 2006.

[6] M. Juza, J.Chromatatgr. A 865 (2000) 35.

[7] C.B. Ching, W. Arlt, M. Lisso, G. Wozny, Ind. Eng.Chem. Res. 39 (2000) 4365.

[8] D. Antos, A. Seidel-Morgenstern, Chem. Eng. Sci. 56 (2001) 6667.

[9] E.V. Dose, S. Jacobson, G. Guiochon, Anal. Chem. 63 (1991) 833.

[10] F. James, M. Sepúlveda, Inverse Problems 10 (1994) 1299.

[11] G. Guiochon, F. James, M. Sepúlveda, Int. Ser. Numer. Math. 129 (1999) 423.

[12] A. Fellinger, A. Cavazzini, G. Guiochon, J. Chromatogr. A 986 (2003) 207.

[13] R. Arnell, P. Forssén, T. Fornstedt, J. Chromatogr. A 1099 (2005) 167.

[14] J.M.M. Araújo, R.C.R. Rodrigues, J.P.B. Mota, submmitted to J. Chromatogr. A 1189 (2008), 302.

[15] R.C.R. Rodrigues, J.M.M. Araújo, M.F.J. Eusébio, J.P.B. Mota, J. Chromatogr. A 1142 (2007), 69.

[16] J.M.M. Araújo, J.P.B. Mota, AIChE J. 51 (2005) 1641.

[17] J.M.M. Araújo, R.C.R. Rodrigues, J.P.B. Mota, Ind. Eng. Chem. Res. 45 (2006) 5314.

[18] D.M. Ruthven, Principles of Adsorption and Adsorption Processes, John Wiley & Sons, New York, 1984.

[19] O. Ludemann-Hombourger, M. Bailly, R.M. Nicoud, Sep. Sci. Technol. 35 (2000) 1285.

[20] P.I. Barton, C.C. Pantelides, AIChE J. 40 (1994) 966.

[21] M. Oh, C.C. Pantelides, Comput. Chem. Eng. 20 (1996) 611.

[22] I. Quiñones, J.C. Ford, G. Guiochon, Chem. Eng. Sci. 55 (2000) 909.

[23] http://www.sourceforge.net/projects/hqp, Dec. (2005).

[24] P. Forssén, R. Arnell, T. Fornstedt, Comput. Chem. Eng. 30 (2006) 1381.

[25] R.C.R. Rodrigues, J.M.M. Araújo, M.F.J. Eusébio, J.P.B. Mota, J. Chromatogr. A 1162 (2007) 14.

[26] J.P.B. Mota, I.A.A.C. Esteves, M.F.J. Eusébio, AIChE J. 53 (2007) 1192.

[27] J.P.B. Mota, I.A.A.C. Esteves, M.F.J. Eusébio, Ind. Eng. Chem. Res. 46 (2007) 6978.

[28] J.M.M. Araújo, R.C.R. Rodrigues, J.P.B. Mota, J. Chromatgr. A 1132 (2006) 76.

[29] R. Fourer, D.M. Gay, B.W. Kernigham, AMPL - a modeling language for mathematical programming, 2nd edition, Brooks/Cole ThomsonLearning, CA, 2003.

[30] A. Wachter, L.T. Bigler, Math Prog. 106 (2005) 25.

[31] T. Fornstedt, G. Guiochon, Anal. Chem. 73 (2001) 608A.

[32] G. Götmar, N. Robinat, T. Fornstedt, Anal. Chem. 74 (2002) 2950.

[33] A.V. Kiselev, Gas-solid chromatography, Plenun Press, New York, 1969.

[34] J.D. Andrade, Surface and Interfacial Aspects of Biomedical Polymers, Plenum Press, New York, Vol.2, 1985.

[35] C. Kemball, E.K. Rideal. E.A. Guggenhein, Trans. Faraday Soc. 44 (1948) 948.

[36] Instructions manual for Chiralpak AD columns, Chiral Technologies Europe, March 2003.

[37] M.F.J. Eusébio, Ph.D. Thesis, Universidade Nova de Lisboa, Lisbon, Portugal, 2006 (in Portuguese).

[38] L. Mihlhbachler, K. Kaczmarski, A. Seidel-Morgenstern, G. Guiochon, J. Chromatogr. A 955 (2002) 35.

[39] P.R. Bevington, Data Reduction and Errors Analysis for the Physical Sciences, McGraw-Hill, New York, 1969.

Chapter 5

On-line Enantiomeric Analysis using High-Performance Liquid Chromatography in Chiral Separation by Simulated Moving-Bed

1 Introduction

The Simulated moving bed (SMB) is a multicolumn, continuous, binary separation process that simulates the countercurrent contact between a mobile phase (eluent or desorbent) and a stationary phase (separating medium) [1–3]. A binary feed (A/B) may be separated by SMB into two products: an extract product containing mainly solute A (the more strongly adsorbed species, or group of species with similarly strong adsorption properties) and a raffinate containing mainly solute B (the less strongly adsorbed species or group of species). SMB chromatography increases throughput, purity, and yield relative to batch chromatography [4–7].

During the last decade, the SMB process has been increasingly applied for the separation of pure substances in the pharmaceutical, fine chemistry, and biotechnology industries, at all production scales [8]. SMB chromatography is now considered an efficient production tool for the separation of optical isomers. Daicel chemicals and UCB pharma have been reportedly operating SMB units since 1998 for the production of several tons per year of pure enantiomers of two different chiral drugs [9]. There is now a generalized interest in SMB for performing large-scale separations and several industrial developments are underway.

Two major SMB operating problems are apparent at production scale: the assessment of product quality and the maintenance of long-term stable and controlled operation. Constraints regarding product purity, dictated by pharmaceutical and food regulatory organizations (lead by the American FDA [10]), have drastically increased the demand for product quality control. The strict imposed regulations are increasing the need for developing optically-pure drugs [11].

It is current practice to install a fraction collector on the recycling line of the SMB loop to allow an internal sample to be periodically collected and analyzed by off-line HPLC. This way, the internal concentration, at either the inlet of the downstream column or outlet of the upstream column (depending on the exact placement of the collector), can be measured. As the concentration profiles circulate around the multicolumn loop, the periodic sampling of the internal concentration at that fixed position allows the measurement of the internal composition profile in the system. This profile is of major importance to optimize the SMB process [12].

Alternatively, the enantiomeric composition can be monitored with two on-line optical detectors in series [13, 14]: an UV detector to measure the absorbance of light, and a po-

larimeter to measure the rotation of polarized light. The former gives a signal proportional to the total enantiomeric concentration, whereas the latter measures the enantiomeric concentration difference. This is a straightforward detection solution for chiral analysis. However, the polarimeter is an expensive analyzer. Furthermore, it has been shown that the high sensitivity of the accuracy of the polarimeter detector to experimental factors, such as impurities in the system, or pressure fluctuation in the measuring cell, has a direct impact on the accuracy and robustness of the measurements [15–18].

The ultimate goal of this work is the development of a robust control system for chiral SMB separations, i.e. a proper feedback control scheme which guarantees the fulfillment of product and process specifications. Such a scheme invariably needs accurate enantiomeric concentration data about the system for calculation of purity and recovery. To accomplish this, the SMB unit must have an on-line monitoring scheme for determining the enantiomeric composition profile circulating around the multicolumn loop. With this objective in mind, in the present work [19] (**paper V**) we describe an on-line enantiomeric monitoring system, comprising an analytical HPLC set-up with two UV detectors, which does not require the use of a polarimeter. This system was first presented at the SPICA 2006 Symposium [20]. Our on-line monitoring scheme is in many aspects similar to the one employed by Staerk et al. [21] for monitoring the preparative-scale gas chromatographic separation of isoflurane enantiomers or to the method developed by Cavazzini et al. [22] for automated on-line fraction analysis and peak deconvolution in multicomponent HPLC. Our set-up, however, uses an extra UV detector to increase the robustness of the measurements.

The analytical HPLC column is packed with the same (or similar) stationary phase as that used in the preparative unit, though this is not mandatory, but with smaller particle size to achieve lower retention times for the same peak resolution. By selecting an appropriate particle size, the monitoring scheme can achieve a faster sampling rate than the overall dynamics of the preparative unit. In a future work, this information will be fed back to a controller, at a relatively high frequency, in order to take the appropriate control actions. The proposed chiral monitoring system has been successfully tested experimentally on the preparative resolution of Tröger's base racemate.

2 On-line monitoring system

The on-line monitoring system is illustrated in Fig. 1. It comprises an electrically-actuated 6-port 2-position valve, an analytical HPLC column, one HPLC pump, and two UV detectors sharing the same light source by means of a bifurcated optical fiber assembly.

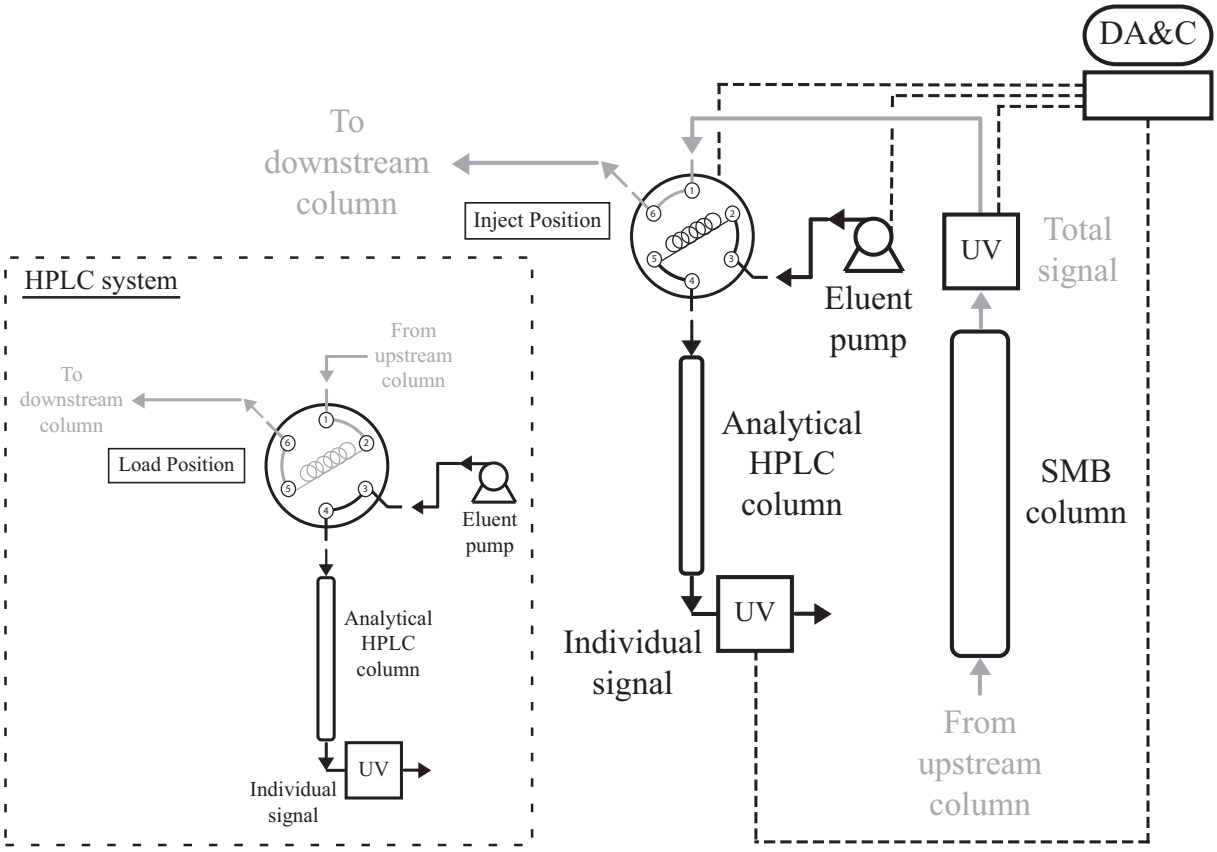

Figure 1: Schematic diagram of the on-line chiral monitoring system. The main equipment comprises an electrically-actuated 6-port 2-position valve, an analytical HPLC column, one HPLC pump, and two UV detectors sharing the same light source by means of a bifurcated optical fiber assembly. The set-up is fully automated.

One of the UV detectors is placed in the SMB loop, at the outlet of one of the columns, for measuring the total enantiomeric concentration profile at that fixed point of the multicolumn unit. The UV detector is followed by the 6-port valve, which is also positioned on the SMB line immediately downstream of the UV. Most of the time, the effluent from the column flows through the UV measuring cell and through the 6-port valve, following the gray flow path depicted in Fig. 1, and is directed to the next column.

At fixed time intervals the 6-port valve is switched to the 'load position' to divert the effluent from the column into the injection loop for collecting an internal sample. The total enantiomeric concentration in the sample is determined by averaging the measured upstream UV signal over the duration of the loop filling. Mobile phase, previously in the

loop, is pushed to the downstream SMB column while the loop is being filled. Thus, the recirculation flow rate in the SMB loop is not interrupted. Furthermore, by working with a sufficiently small injection loop, the sample volume drawn from the system will have an insignificant impact on the composition profile circulating around the SMB loop and, therefore, will not perturb its operation. When the injection loop is filled, the valve is switched back to its original position ('inject position'), and the normal recirculation flow is resumed.

When the 6-port valve is periodically switched back to 'inject position,' the injection loop is placed within the flow path of mobile phase that is being pumped into the analytical column. The sample in the injection loop is thus pushed onto the analytical column for analysis and the injection loop is washed with mobile phase. A second UV detector is placed at the outlet of the analytical HPLC column for automated analysis of the chromatographic profiles and their conversion into concentrations.

To summarize, the total enantiomeric concentration profile exiting a fixed SMB column is monitored on line and in real time by UV; this composition profile is further sampled at fixed time intervals and the on-line collected fractions are directly injected into a second high-efficiency chromatographic column, operated under analytical conditions.

3 Experimental

The feasibility and effectiveness of the proposed monitoring system were assessed experimentally on the separation of Tröger's base racemate, using Chiralpak AD as stationary phase and methanol as eluent. Daicel's Chiralpak AD (Chiral Technologies Europe, Illkirch, France), a 20-μm silica-based packing material, coated with amylose tri-(3,5-dimethylphenyl carbamate), is convenient for the separation of aromatic enantiomers.

For the purpose of experimental validation, the on-line monitoring system was connected to the outlet of a single-column set-up that was recently developed by our group [23] for mimicking the steady periodic behavior of SMB chromatography. This apparatus has proven to be a simple, compact, and fast method of experimentally reproducing the cyclic steady state of an SMB process with minimal consumptions of mobile phase and feedstock. Its purpose is not to perform a real separation (see [24] for its true counterpart), but to conveniently establish experimental data that otherwise could only be obtained from a real SMB plant. It has been extensively demonstrated [23, 25–27] that this set-up accurately reproduces the intrinsic SMB dynamics (i.e., in the absence of sec-

ondary effects, such as multi-packing variability and asymmetric extra-column volumes). It is worth emphasizing that when the proposed on-line monitoring system is attached to our single-column SMB analog it gives the same measurements and samples the same composition profile as when it is placed in the loop of the equivalent SMB unit.

3.1 Materials and system characterization

The pure enantiomers were purchased from Fluka (Germany) with a purity of 99%, and the racemic mixture was purchased from Sigma-Aldrich (Germany) with a purity of 98%. The stationary phase was slurry packed into a thermojacketed 10 mm I.D. preparative glass column (Götec Labortechnik, Germany) to a bed height $L = 10.0$ cm. HPLC-grade methanol was obtained from Sigma-Aldrih (Germany) and employed as mobile phase after filtration. The system was operated isothermally at 30°C.

The total column porosity (ϵ) was measured using 1,3,5-tri-tert-butylbenzene (TTBB) from Sigma-Aldrich (Germany). This solute is not retained but can access to the internal porosity of the stationary phase. Extra-column volumes in the experimental set-up were estimated from TTBB pulse experiments with and without the chromatographic column.

In the working range of fluid velocity used in preparative chromatography, the Van Deemter plot is well approximated by a straight line [28]. The intercept and slope for each enantiomer, expressed here in terms of the Péclet number (Pe) and linear-driving-force (LDF) coefficient for mass-transfer (k_i), were determined by fitting the experimental dependence of the plate height with flow rate for diluted pulses of racemic mixture. This procedure is detailed elsewhere [29]. The estimated values of the parameters are listed in Table 1.

The HPLC pumps employed in the experiments are model K-501 from Knauer (Berlin, Germany) with 10 ml and 50 ml pump heads, controlled by RS232 communication protocol. The whole set-up is fully automated and driven by our Labview-based software system (BioCTR) for process monitoring and control of chromatographic processes [30].

Two multi-wavelength UV detectors (USB2000/USB4000 from Ocean Optics, USA) with attenuator, sharing a DH-2000-S-DUV light source (Micropack, Ostfildern, Germany), and an electrically-driven 6-port 2-position valve from Knauer (Berlin, Germany), were employed in the on-line monitoring system. The analytical HPLC column is 150×4.6 mm I.D., packed with Chiralpak IA [amylose tri-(3,5-dimethylphenyl carbamate) immobilized on 5 μm silica gel], purchased from Daicel Chemical Industries Ltd (Chiral Technologies

Table 1: Column characterization and adsorption parameters for the binary separation of Trögers base enantiomers on Chiralpak AD, using methanol as mobile phase. Scripts 'r' and 's' denote the less- [*R*-(+)-] and more- [*S*-(-)-] retained enantiomers, respectively.

Column length, L (cm)	10.0	Péclet number, Pe	1586
Column diameter, d (cm)	1.0	LDF coeficients, k_i (s^{-1})	12.06, 11.98
Total Porosity, ϵ	0.626	Feed (linear/overloaded), c_i^F (g/l)	0.05 / 0.5
Linear isotherm, q_i^* (g/l)		$(2.382c_r,\ 5.990c_s)$	
Linear-Langmuir isotherm, q_i^* (g/l)		$(2.212c_r,\ 5.611c_s) + \dfrac{0.621c_r,\ 2.609c_s}{1 + 6.386c_r + 11.21c_s}$	

Europe, Illkirch, France). The UV detectors were calibrated at a wavelength of 264.5 nm, at which UV absorption by impurities present in the racemic mixture is small, and the detector response shows a linear response in the range of concentrations operated.

3.2 Adsorption isotherms

The experimental determination of adsorption isotherms is of utmost importance for the design and operation of any SMB process. The operating conditions of a chiral SMB process cannot be properly determined without knowledge of the competitive isotherms of the two enantiomers. The *inverse method* of isotherm determination [31] is becoming popular as a quick procedure for the estimation of the competitive isotherms necessary for designing SMB separations [32–34].

In the present work, the isotherms of the two enantiomers were estimated with good accuracy by applying the inverse method to the band profiles of the racemic mixture obtained both in linear and overloaded elution modes, without measuring any of the single-component chromatograms. To accurately determine the competitive isotherms for overloaded SMB operation, our method also incorporates breakthrough data from a single frontal analysis at the feed conditions employed in the SMB. This reduces the uncertainty of the estimation of the saturation capacity, because the concentration range sampled by the bands profiles is diluted with respect to that of the injected pulse. The procedure is described in detail elsewhere [29].

The fitted parameters of the selected adsorption isotherm model (linear-Langmuir) are listed in Table 1. An analytical profile of the racemic mixture is illustrated in Fig. 2, to

depict the elution order of the two enantiomers. The isotherms were determined on the same column in which the preparative experiments were carried out.

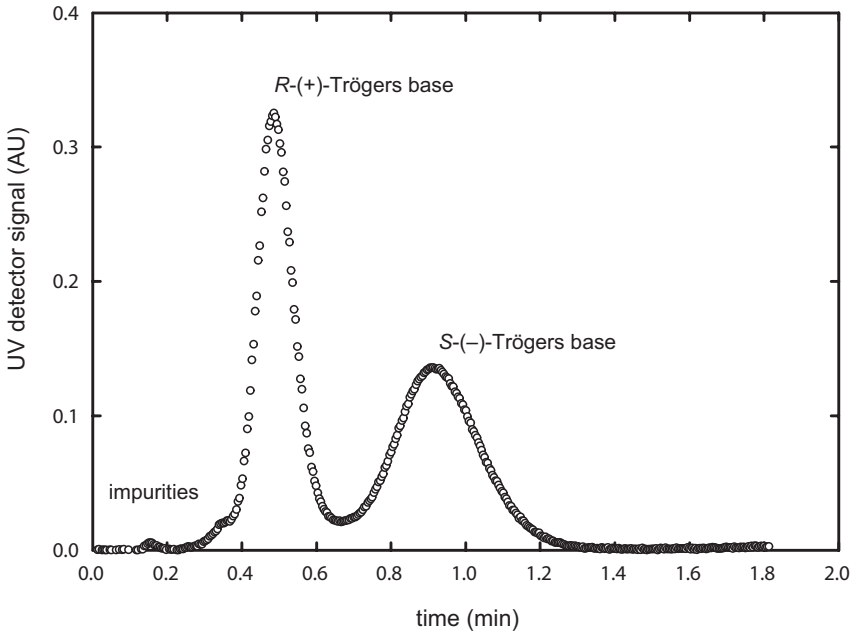

Figure 2: Analytical injection of Tröger's base racemate on Chiralpak AD, 100 mm×10 mm I.D. Mobile phase is pure methanol at 30°C and flow rate of 25 ml/min. The injected volume is 150 μl with a racemate concentration of 3.0 g/l; UV detection at 264.5 nm. The small early-eluting peak denotes the presence of some impurities, which is agreement with the 98% purity level reported by the supplier.

3.3 Experimental procedure

The automated procedure for on-line processing of the signals from the two UV detectors is detailed here. The UV detector labeled 'Total signal' in Fig. 1 monitors the total absorbance, which is proportional to the total enantiomeric concentration. The sampling interval for this UV was fixed at 0.25 s.

The second UV detector, placed at the outlet of the analytical HPLC column, monitors the individual chromatograms of the two enantiomers. The flow rate of mobile-phase pump connected to the analytical HPLC column was fixed at 2.9 ml/min to give a 10% safety margin on the pressure drop below the limit of 100 bar for the Chiralpak IA column. Figure 3 shows the influence of the mobile-phase flow rate on the enantiomeric chromatograms eluted from the high-efficiency analytical Chiralpak IA column. The chromatographic resolution, R_s, obtained at a flow rate of 3.0 ml/min is larger than one, which is considered the lower limit to correctly integrate single-component peaks [35]. This suggests that higher flow rates could be employed, if the pressure drop constraint was not

a limiting factor. Note that for a chiral separation, $R_s > 1$ is not strictly required for accurate analysis of the racemate peaks, because both enantiomers have the same UV calibration curve. Even if the peaks are moderately overlapping, they can still be properly deconvoluted at a single wavelength.

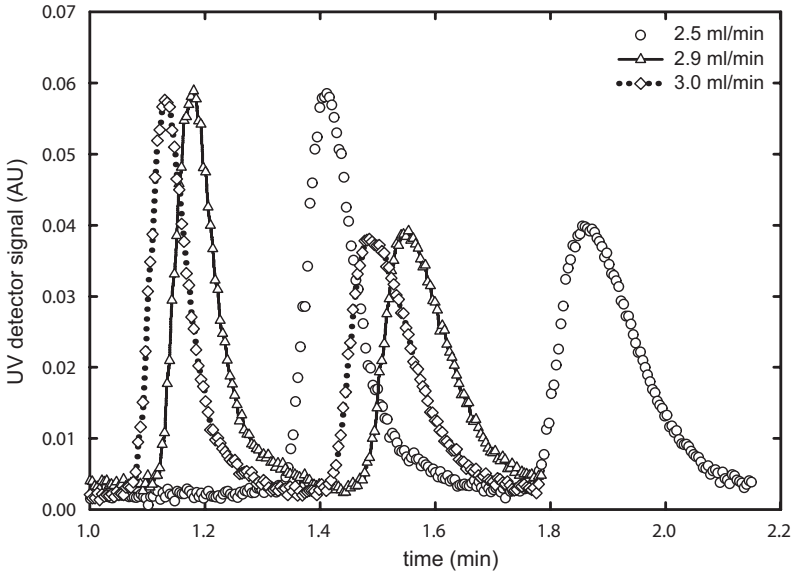

Figure 3: Analytical injections of Tröger's base racemate on Chiralpak IA, 150 mm×4.6 mm I.D. Mobile phase is pure methanol at 30°C and flow rates of 2.5 ml/min (ΔP = 72–74 bar), 2.9 ml/min (ΔP = 86–88 bar), and 3.0 ml/min (ΔP = 89–92 bar). The injected volume is 150 μl with a racemate concentration of 0.1 g/l; UV detection at 264.5 nm.

An injection loop of 150 μL was employed for accurate analysis of the chromatograms over the whole concentration range spanned by the SMB. This way, a sufficiently strong UV signal was obtained even for the more diluted samples. Note, however, that despite the relatively large volume of the sampled fractions, all injections on the Chiralpak IA column were performed under analytical or near-analytical conditions.

The maximum sampling frequency at which the tail of the more-retained peak from one injection and the front of the less-retained peak from the subsequent injection are baseline separated was determined to be 1/45 s^{-1} (i.e. one sample every 0.8 min). This is shown in Fig. 4, which reproduces typical chromatograms for successive injections. The initial delay corresponds to the retention time (at the given flow rate) on the analytical column. In practice, the sampling frequency was slightly decreased to 1/54 s^{-1} (i.e. one sample every 0.9 min). This safety margin was added to ensure robust and reproducible peak deconvolution and base-line correction.

The experimental chromatographic peaks obtained on the analytical HPLC column exhibit different shapes, i.e. symmetric or with tailing, depending on the eluted species. This

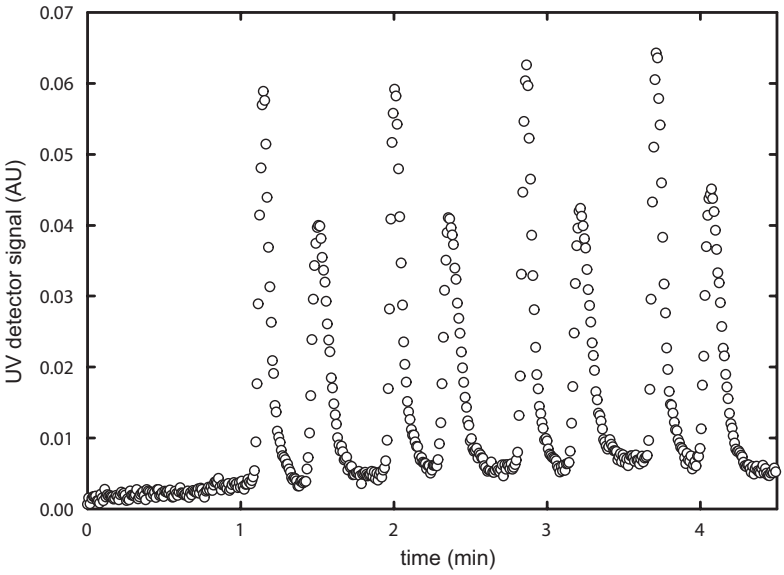

Figure 4: Chromatograms for successive injections of Tröger's base racemate on Chiralpak IA, 150 mm×4.6 mm I.D. The samples are injected with a frequency of 1/45 s^{-1} (one sample every 0.8 min). Mobile phase is pure methanol at 30°C and flow rate of 3.0 ml/min. The injected volume is 150 μl with a racemate concentration of 0.1 g/l; UV detection at 264.5 nm.

is typical in chiral chromatography even at analytical scale. The exponentially modified Gaussian (EMG) function is usually an adequate model for this type of chromatographic peaks [36], and is one of the most popular peak models [37]. The EMG function has been shown to give good agreement between theory and experiment in many real cases [38].

The EMG function results from the convolution of a Gaussian function and an exponentially decay function, and can be expressed in a variety of ways [39–41]. The specific form used here is

$$\mathrm{EMG}(t) = \frac{A}{\tau'} \exp\left[\frac{1}{2}\left(\frac{\sigma_\mathrm{G}}{\tau'}\right)^2 - \frac{t - t_\mathrm{G}}{\tau'}\right] \frac{1 + \mathrm{erf}(Z/\sqrt{2})}{2}, \tag{1}$$

where $\mathrm{erf}(\cdot)$ is the standard error function, A is the peak area, t_G and σ_G are the retention time and standard deviation of the Gaussian function, τ' is the time constant of the exponential decay function, and

$$Z = \frac{t - t_\mathrm{G}}{\sigma_\mathrm{G}} - \frac{\sigma_\mathrm{G}}{\tau'}. \tag{2}$$

Each pair of chromatographic peaks detected per injection are fitted to the sum of two EMG functions (one per peak), after adjusting for baseline drifting. To do this, the chromatographic data are first corrected by subtracting the linear interpolation of the experimental baseline in the regions before and after elution of the peaks. Then, the adjusted chromatographic data are fitted to the EMG sum by nonlinear least-squares

curve fitting. The method is automated and built into our control software. Using this procedure the area under each peak is easily determined. The peak-area information can be subsequently processed in two ways, originating two distinct methods to calculate the enantiomeric composition.

The first method uses directly the peak area to determinate the individual enantiomer concentration, c_i (g/L), by the generalized relation

$$c_i = \frac{1}{\alpha_i} \frac{(\text{peak area } i) \times (\text{volumetric flow rate})}{(\text{injection-loop volume})}, \tag{3}$$

where α_i (mAU $\times$ L/g) is the slope of the UV calibration curve, A_{bs} (mAU) $= \alpha_i c_i$.

The second method uses the areas of the two peaks to calculate the enantiomeric purity, p_i:

$$p_i = \frac{c_i}{c_1 + c_2} = \frac{(\text{peak area } i)}{(\text{peak area less-retained}) + (\text{peak area more-retained})}. \tag{4}$$

Both methods have been implemented experimentally. It is worth noting that the first method relies only on the chromatograms from the analytical HPLC column to determine the individual enantiomer concentrations, according to Eq. (3). On the other hand, the second method employs the chromatographic peaks to compute the enantiomeric purity, which is then converted to individual concentrations using the total concentration value, $c = c_1 + c_2$, measured independently by the UV detector installed in the SMB loop:

$$c_i = p_i c. \tag{5}$$

4 Results and Discussion

The automated on-line monitoring system was tested under both linear and overloaded separation conditions. In the former case the feed concentration was fixed at 0.05 g/l of each enantiomer, whereas in the latter case the feed concentration was increased to 0.5 g/l of each enantiomer. The number of columns in the SMB unit mimicked by our one-column analog was fixed at four, with one column allocated per SMB zone. The switching interval, τ, and the four SMB zone flow rates, $Q_{\text{I}}, \ldots, Q_{\text{IV}}$, were optimized for maximum feed throughput, subject to minimal raffinate and extract purities of 98%. The procedure for solving the optimal SMB design problem is described elsewhere [23, 42–44].

The eluent flow rate, Q_{E}, was fixed at 3.0 ml/min in order to obtain an optimized value of τ that allowed approximately twenty injections per SMB cycle (i.e. 4τ time units). This is a rough estimate (though a conservative one) of the number of samples

that could be injected per cycle on the analytical HPLC column if the eluent flow rate was not constrained by pressure drop or if the analytical column had a more favorable aspect ratio (i.e., a shorter column with larger diameter to reduce the linear velocity). The optimized SMB operating parameters are listed in Table 2.

Table 2: Optimized SMB operating parameters for linear and overloaded operation. In both cases, the SMB column configuration is 1/1/1/1. Flow rates are expressed in ml/min and τ in min.

Condition	τ	Q_{IV}	Q_{E}	Q_{F}	Q_{X}	Q_{R}
Linear	4.620	2.632	2.500	2.312	2.478	2.334
Overloaded	4.457	2.723	3.000	2.354	3.061	2.293

Figure 5 shows the temporal profile of the total enantiomeric concentration at the outlet of the single-column set-up, measured experimentally over three operating cycles, for both linear and overloaded conditions. For visual clarity only a subset of the measurements is plotted in Fig. 5, since including all sampled data would produce a very dense plot.

These profiles were monitored by the UV detector labeled 'total signal' in Fig. 1 (the one placed in the SMB loop). This figure compares the total enantiomeric concentration in the effluent exiting the preparative column, $\{c_{\mathrm{r}}^{\mathrm{out}} + c_{\mathrm{s}}^{\mathrm{out}}\}^{\mathrm{exp}}$, where 'r' and 's' identifies the less- [*R*-(+)-] and more- [*S*-(-)-] retained enantiomers, respectively, with the steady periodic solution, $\{c_{\mathrm{r}}^{\mathrm{out}} + c_{\mathrm{s}}^{\mathrm{out}}\}^{\mathrm{sim}}$, of the SMB model. There is excellent agreement between experimental and simulated data. It is also seen that the second cycle of operation has already attained the steady periodic state; this is one of the advantages of our single-column apparatus [23, 25–27]. In a real SMB plant it would have taken ten times more cycles.

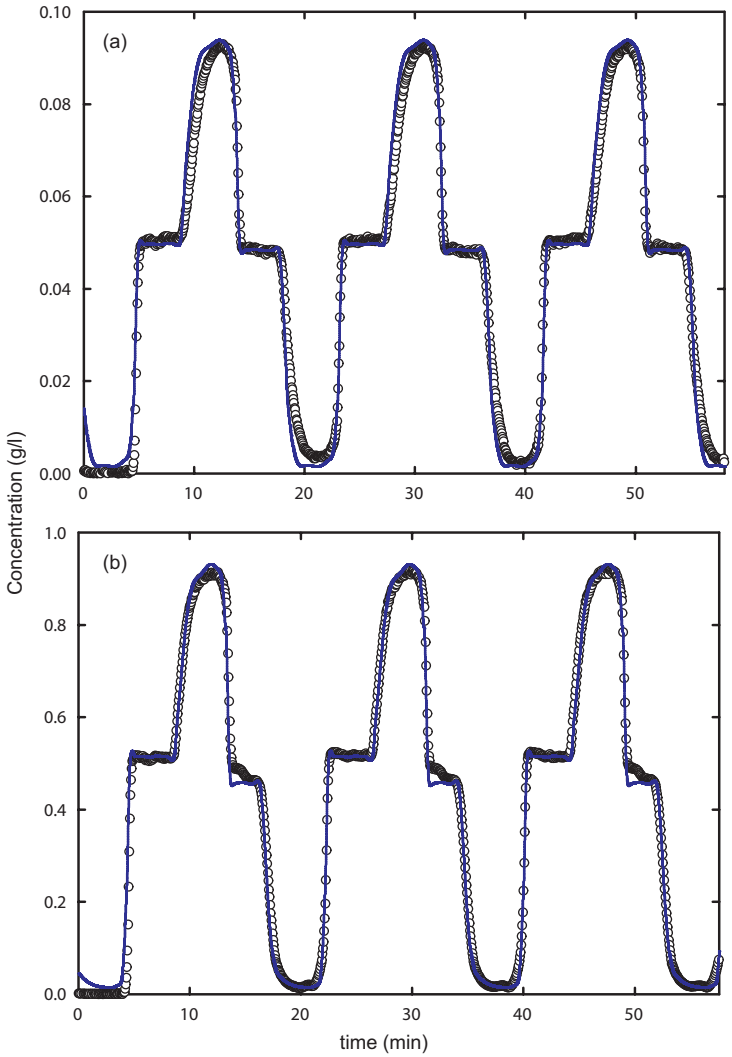

Figure 5: Temporal profile of total enantiomeric concentration at the outlet of the single-column SMB analog, over three cycles of operation ($3 \times 4\tau$ time units), for (a) linear and (b) overloaded SMB conditions. The operating parameters are those listed in Table 2. Symbols ($\circ$) represent the values measured by the UV detector labeled 'total signal' in Fig. 1. The lines represent the steady periodic solution of the SMB model. Note that the cyclic steady-state behavior is already attained on the second cycle of operation.

Figure 6 shows the raw measurements recorded by the UV detector placed at the outlet of the analytical HPLC column for the experimental run of Fig. 5. They represent the series of experimental chromatograms for the various fractions collected from the outlet effluent of the preparative column by periodic sampling through the switching valve. Baseline drifting is apparent, but this is automatically corrected in the peak analysis.

Figure 7 compares the total enantiomeric concentration in each sampled fraction (open circles), determined from the peak area of the corresponding analytical chromatogram, with the corresponding value recorded by the UV detector (filled circles) placed at the outlet of the single-column set-up (the UV labeled 'Total signal' in Fig. 1). The comparison

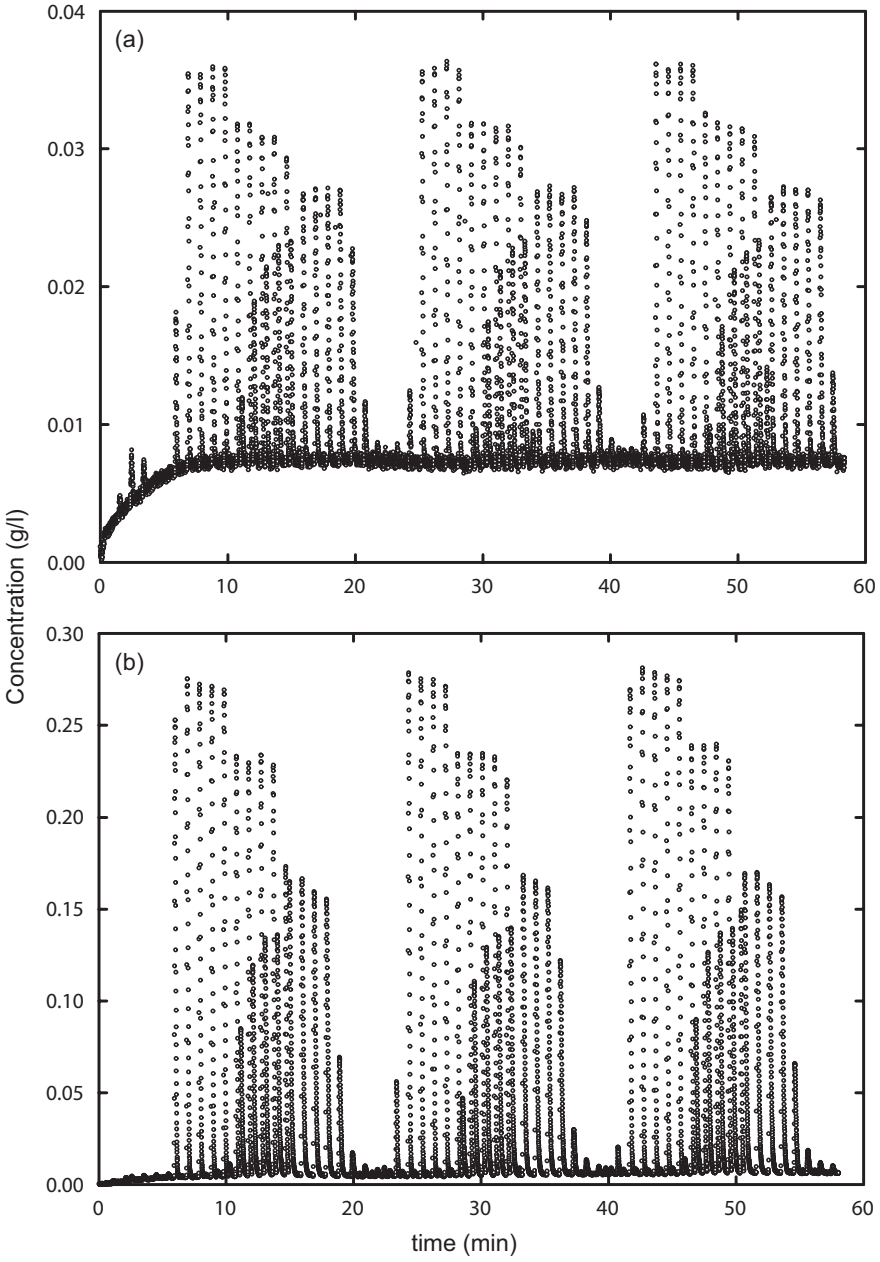

Figure 6: Experimental chromatograms for the automated on-line enantiomeric fraction analysis of the concentration profiles plotted in Fig. 5. Graphs (a) and (b) are for linear and overloaded SMB conditions, respectively.

is shown for overloaded operating conditions, but similar results were obtained for the linear case. The steady periodic solution of the SMB model (solid line) is also included for comparison. Figure 7 shows that there is some mismatch between the total UV signal of the on-line measurement and the sum of the individual concentrations of the two enantiomers determined from the analysis of the chromatogram of the corresponding sampled fraction.

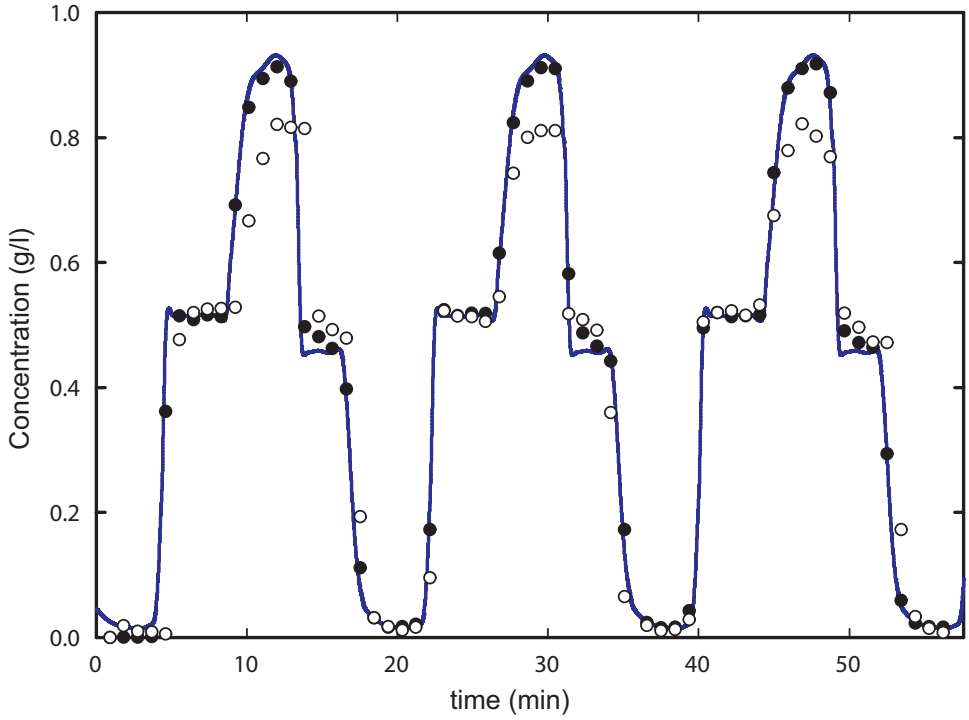

Figure 7: Temporal profile of total enantiomeric concentration at the outlet of the single-column SMB analog, over three cycles of operation, under overloaded SMB conditions. •, profile measured by the UV labeled 'total signal' in Fig. 1; ∘, automated on-line HPLC analysis of the collected fractions; line, simulated profile.

The total UV signal is more reproducible from cycle to cycle than the cumulative area under the two chromatographic peaks for each sampled fraction. However, the differences between solid and open circles appear to be consistent from cycle to cycle, which suggests that probably there was incomplete loop filling for the samples collected at the highest flow rates. Another possible reason might be a calibration problem. The two UV detectors were simultaneously calibrated at a wavelength that necessarily could not be that of maximum absorption for the enantiomers under investigation. Otherwise, saturation of the detector placed downstream the SMB column (the one labeled 'total signal' in Fig. 1) would have been unavoidable. Thus, a less sensitive calibration curve was used to analyze chromatograms recorded under diluted conditions (the signals coming from the analytical column). This might have influenced the accuracy of the signal reconstruction. Improving detector sensitivity, by operating it at a wavelength corresponding (or near) to maximum

sensitivity, would definitely improve signal reconstruction.

Overall, the most significant conclusion drawn from Figure 7 is that the total enantiomeric concentration in our set-up is more accurately and robustly determined from the total UV signal than from the HPLC analysis of the collected fraction.

Figures 8 and 9 provide a zoom over selected regions of the chromatograms plotted in Fig. 6. Four different zones of the enantiomeric composition profile are analyzed: sample 23 is taken from the region where both enantiomers are in diluted concentration, when the port switching places the column in zone IV of the SMB; samples 25–27 are collected in the raffinate withdrawal region, where the less-retained enantiomer is recovered in purified form; samples 31–33 are in the high-concentration region of both enantiomers, when the column is in zone II of the SMB; and samples 35–36 are in the extract withdrawal region, where the more-retained enantiomer is recovered in purified form. The two topmost graphs of Figs. 8 and 9 display the raw UV data; the other graphs show the chromatograms for individual samples after correction for baseline drifting, as well as the corresponding EMG curve fitting. Note that the chromatographic peaks for sample 23 are fitted to the EMG function in the very dilute concentration region, where the noise-to-signal ratio is high; the fitting is, nevertheless, reasonably good even for this extreme case. It is apparent that in all cases the EMG function provides an accurate fit of the experimental peaks. From the curve fitting, the area of each peak is easily obtained and the enantiomeric purity is readily estimated as described above.

The temporal profiles of enantiomeric purity, determined by on-line HPLC analysis of the collected fractions, are depicted in Fig. 10 and compared to the simulated steady periodic profiles. The agreement between experimental and simulated profiles is excellent. On the one hand, the good agreement between measured and predicted profiles shows that the linear-Langmuir model in Table 1 provides a fairly good description of the adsorption equilibrium over the whole composition range spanned in the SMB experiment. This is also corroborated by the good agreement between measurements and model predictions exhibited in other figures. On the other hand, Fig. 10 also shows that the enantiomeric-purity profile is accurately reconstructed from the HPLC analysis of the collected fractions, even though the total enantiomeric concentration is not always precisely determined. This is consistent with possible systematic and random error sources, such as incomplete loop filling, baseline drift, and variability of the slope of the UV calibration curve, which affect the areas under the two peaks but not their relative magnitude or ratio.

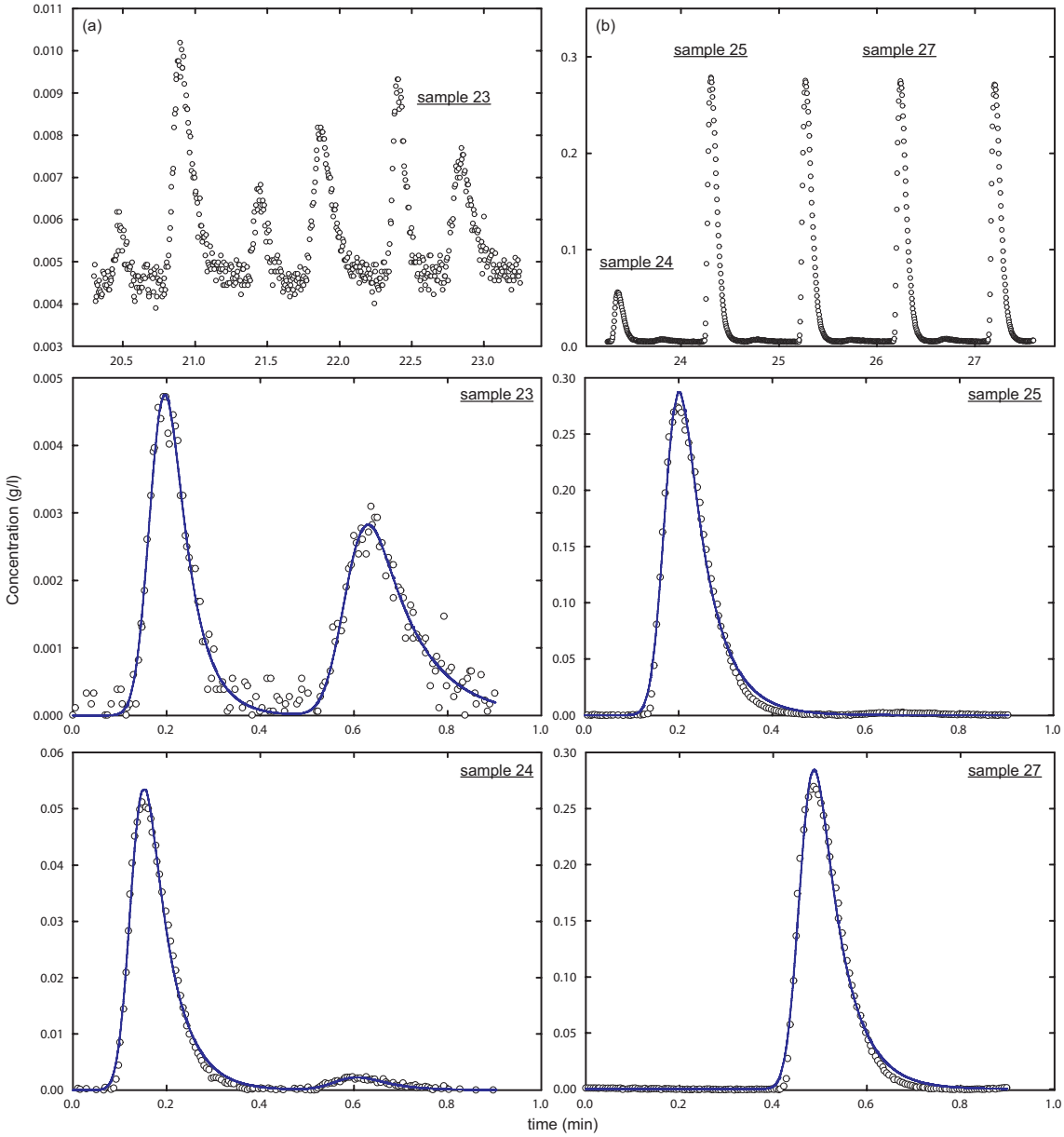

Figure 8: On-line HPLC analysis of the (a) 21st–23rd and (b) 24th–28th collected fractions from the composition profile at the outlet of the single-column SMB analog (c.f. Fig. 5). The symbols in the topmost graphs are the raw experimental UV measurements recorded at the outlet of the analytical HPLC column, whereas those in the other graphs have been adjusted for baseline drifting. The lines represent the fitting of the sum of two EMG functions.

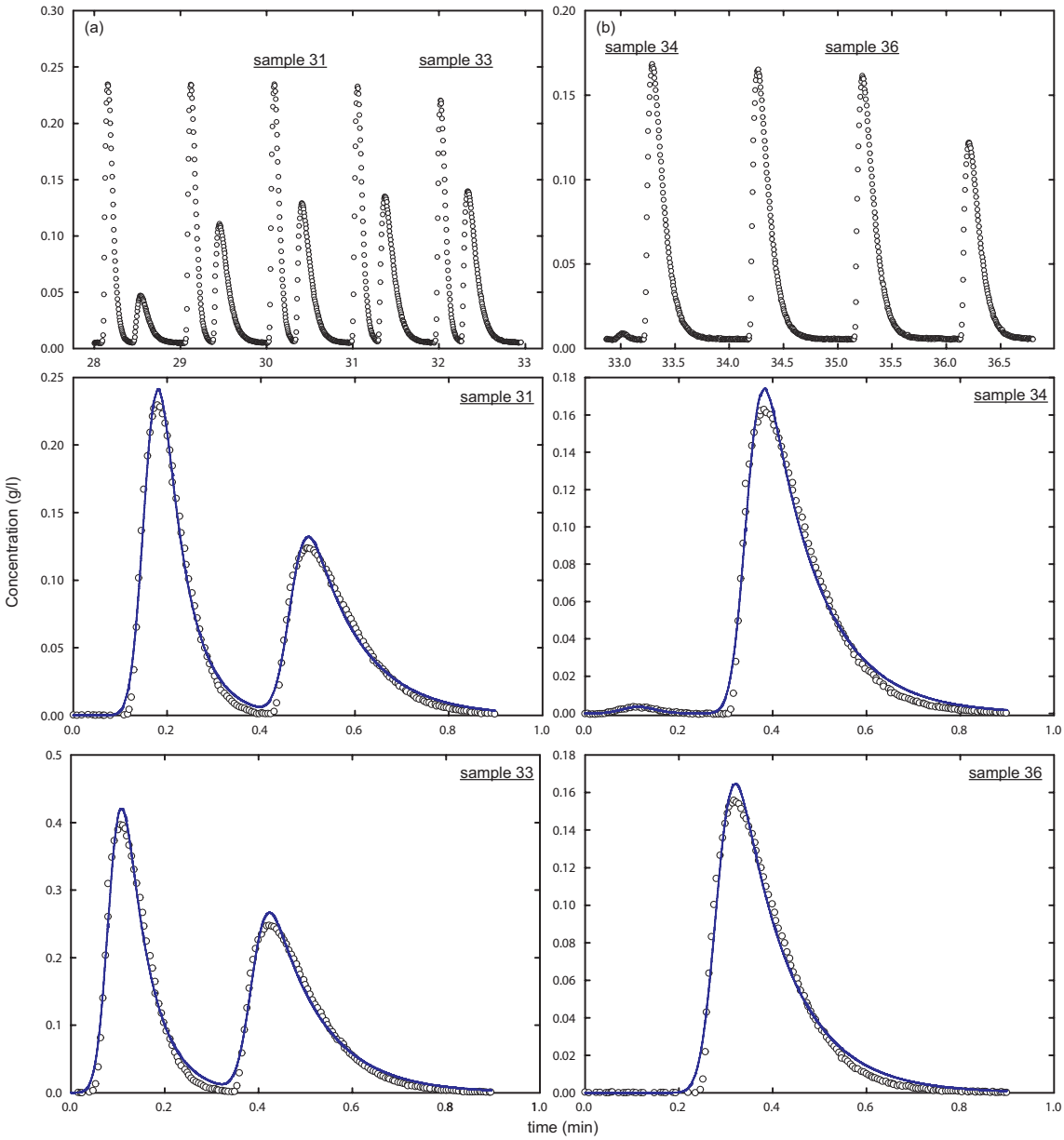

Figure 9: On-line HPLC analysis of the (a) 29st–33rd and (b) 34th–37th collected fractions from the composition profile at the outlet of the single-column SMB analog (c.f. Fig. 5). The symbols in the topmost graphs are the raw experimental UV measurements recorded at the outlet of the analytical HPLC column, whereas those in the other graphs have been adjusted for baseline drifting. The lines represent the fitting of the sum of two EMG functions.

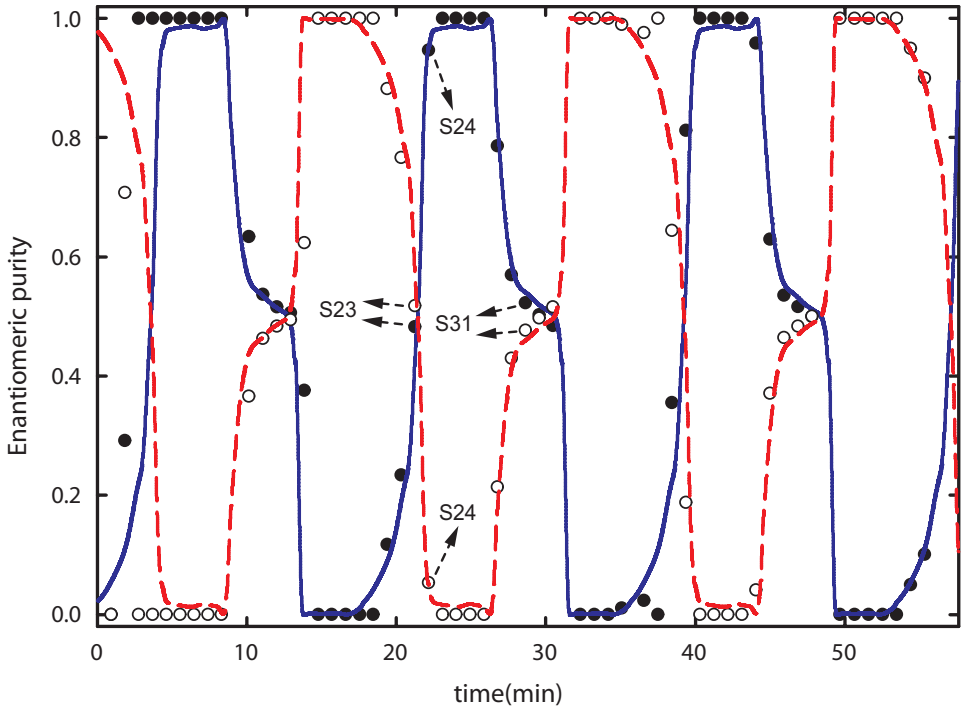

Figure 10: Temporal profile of enantiomeric purity, $p_i = c_i/(c_r + c_r)$, at the outlet of the single-column SMB analog. Lines are simulated profiles, and symbols are measured values determined by HPLC analysis of the collected fractions (less-retained enantiomer, p_r: •, ——; more-retained enantiomer, p_s: ○, - - -). Labels S23, S24, and S31 identify some of the samples shown in Fig. 8 and Fig. 9.

Finally, Fig. 11 compares the individual enantiomeric concentration profiles, determined by HPLC analysis of the collected fractions in combination with the total UV measurement, to the steady periodic solution of the SMB model. We advocate that this is the preferred method for robust on-line enantiomeric monitoring. The comparison is shown for both linear and overloaded SMB conditions. Samples 23, 24, and 31, whose chromatograms are depicted in Figs. 8 and 9, are identified in both Figs. 10 and 11 by labels S23, S24, and S31, respectively. Except for the first cycle, which experimentally has not yet attained the steady periodic state, the agreement between the discrete concentration measurements and the simulated profiles is quite good.

Overall, the results presented here support our claim that the proposed on-line chiral monitoring system allows for fast, accurate, and robust detection of the individual enantiomeric concentration profiles without the use of a polarimeter. Some of the advantages of employing the dual UV measurement strategy are apparent from the discussion above. It minimizes the impact of systematic and random error sources on the total enantiomeric concentration measurement, which is not determined from the HPLC analysis of the collected samples. On the other hand, the enantiomeric purity is much less sensitive

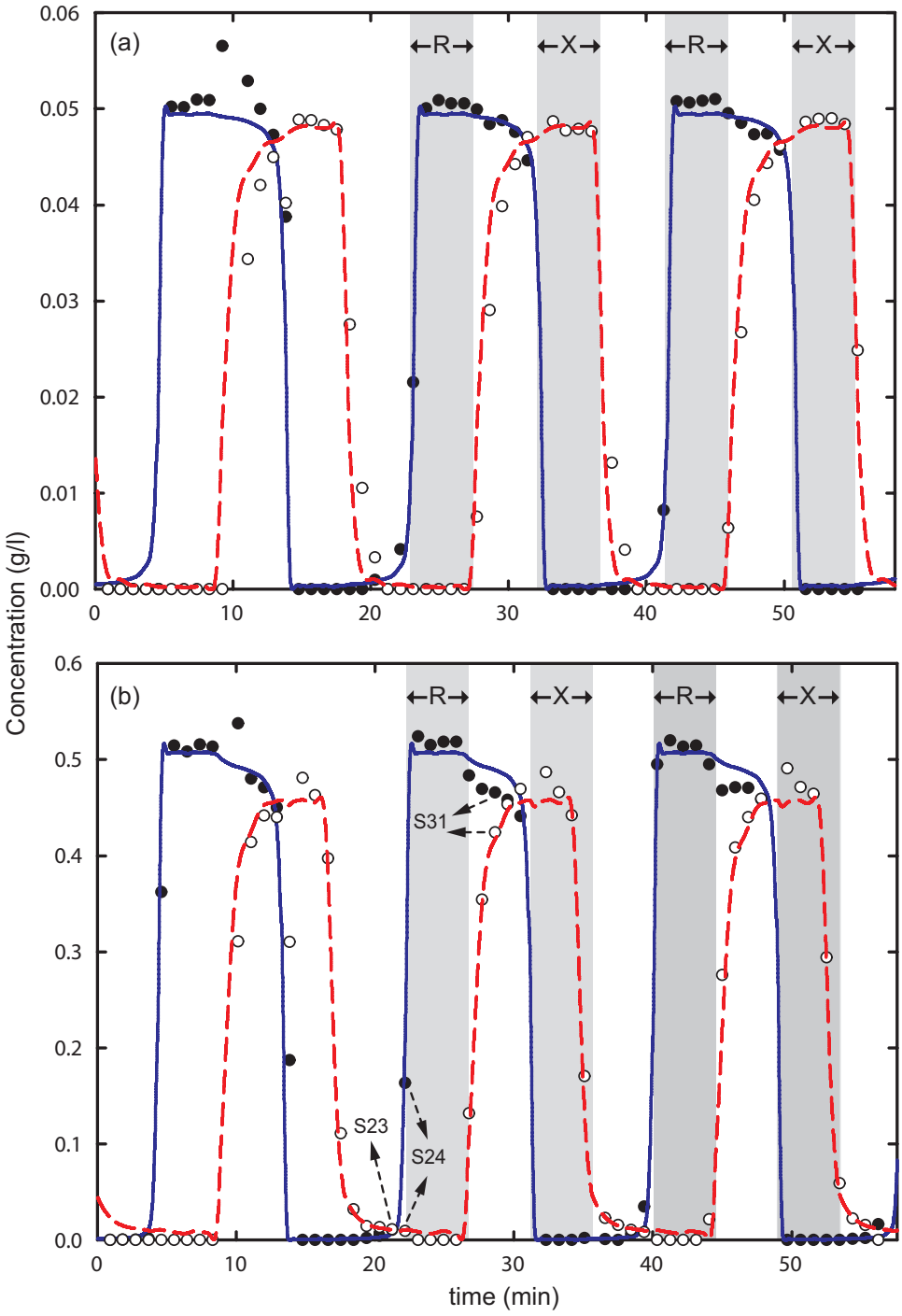

Figure 11: Experimental (symbols) temporal profiles of individual enantiomer concentration at the outlet of the single-column SMB analog, for (a) linear and (b) overloaded SMB conditions, and their comparison with the steady periodic solution (lines) of the process model. (less-retained enantiomer: •, ——; more-retained enantiomer: ○, - - -). Labels S23, S24, and S31 identify some of the samples depicted in Figs. 8 and 9. R and X denote the raffinate and extract withdrawal periods, respectively, for the 2nd and 3rd cycles of operation.

to systematic and random error sources in the HPLC analysis and can be confidently determined from the analysis of the chromatograms of the collected fractions. Furthermore, since the UV detector placed in the SMB loop is operated at a high sampling frequency (i.e. continuous monitoring) it opens up the possibility for estimation of the individual enantiomeric concentration profiles between fraction collections. This is the objective of future work.

5 Conclusions

An on-line monitoring system for enantiomeric detection in multicolumn continuous chiral chromatography has been presented and experimentally validated. The proposed on-line monitoring system has been shown to be accurate and robust, thus providing promising perspectives for process control and dynamic optimization of the SMB. The system does not use a UV detector and a polarimeter in series. The signal of the latter is very sensitive to temperature and pressure fluctuations in the measuring cell, which have a direct impact on the accuracy and robustness of the measurements [15, 16].

Our on-line monitoring system should preferably incorporate an analytical HPLC column with optimized aspect ratio and particle size of the stationary phase, to minimize the retention time and pressure drop. In many cases, the standard sizes of commercial analytical HPLC columns will require the use of low-viscosity solvents because of the pressure drop constraint. But this will, in turn, give rise to the general problem of using a different solvent for injection than for the mobile phase [45], which introduces other problems, such as undesirable effects of peak splitting [45, 46] and, less frequently, crystallization and block phenomena.

Finally, it is worth mentioning that, in most cases, the mobile phase from the analytical HPLC system can be reused in the SMB system, because it is only contaminated with trace amounts of the two enantiomers. The outlet effluent from the analytical HPLC column can either be sent to the eluent storage vessel or pumped directly to the beginning of zone I of the SMB.

Nomenclature

c	solute concentration (g/l)
D_{L}	axial dispersion coefficient (cm^2/min)
k	LDF coefficient (s^{-1})
L	column length (cm)
N	number of columns
Pe	Péclet number
q	adsorbed concentration (g/l)
Q	flow rate (cm^3/min)
t	time (min)
v	linear velocity (cm/min)
x	dimensionless axial position, z/L
z	axial position in column (cm)
A	peak area (mAU.min)
t_G	retention time of the Gaussian function (min)

Greek letters

β	phase ratio, $(1-\epsilon)/\epsilon$
ϵ	total porosity
τ	switching interval (min)
τ'	time constant of the exponential decay function (EMG)
σ_G	standard deviation of the Gaussian function
θ	dimensionless time, t/τ

Subscripts and superscripts

E	eluent
exp	experimental
F	feed
i	solute index
I,...,IV	zone index
in	inlet effluent
j	column index
out	outlet effluent
R	raffinate
sim	simulated

X	extract
˜	filtered value
r	R-(+)-Trögers base enantiomer
s	S-(-)-Trögers base enantiomer

List of Tables

List of Figures

Bibliography

[1] D.M. Ruthven, C.B. Ching, Chem. Eng. Sci. 44 (1989) 1011.

[2] R.M. Nicoud, LC-GC 5 (1992) 43.

[3] G. Storti, M. Mazzotti, M. Morbidelli, QA. Carrà, AIChE J. 39 (1993) 471.

[4] J. Strube, S. Haumreisser, H. Schmidt-Traub, M. Schulte, R. Ditz, Org. Proc. Res. Devel. 2 (1998), 305.

[5] A. Jupke, A. Epping, H. Schmidt-Traub, J. Chromatogr. A 944 (2002), 93.

[6] L. Miller, C. Grill, T. Yan, O. Dapremont, M. Juza, J. Chromatogr. A 1006 (2003) 267.

[7] C.M. Grill, L. Miller, T.Q. Yan, J. Chromatogr. A 1026 (2004) 101.

[8] M. Juza, M. Mazzotti, M. Morbidelli, Trends in Biotech. 18 (2000) 108.

[9] R.M. Nicoud, Pharm. Technol. Eur. 11 (1999) 28.

[10] FDA, Chirality 4 (1992) 338.

[11] S.C. Stinson, Chem. Eng. News 9 (1995) 44.

[12] O. Ludemann-Hombourger, R. M. Nicoud, M. Bailly, Sep. Sci. Technol. 35 (2000) 1829.

[13] K.-H. Rimbčk, F. Kastner, A. Mannschreck, J. Chromatogr. 351 (1986) 346.

[14] G. Zenoni, M.P. Pedeferri, M. Mazzotti, M. Morbidelli, J. Chromatogr. A 888 (2000) 73.

[15] C. Roussel, N. Vanthuyne, M. Serradeil-Albalat, J.-C. Vallejos, J. Chromatogr. A 995 (2003) 79.

[16] A. Ghanem, J. Chromatogr. A 1132 (2006) 329.

[17] M. Morari, Optimizing Control of Simulated Moving Beds, Presentation 287a at 2006 AIChE Annual Meeting, San Francisco, CA, November 12–17, 2006.

[18] M. Mazzotti, Optimizing Control of SMB and Varicol Processes, Presentation L-201 at PREP 2007 - 20th International Symposium on Preparative/Process Chromatography, Baltimore, MD, June 3–6, 2007.

[19] J.M.M. Araújo, R.C.R. Rodrigues, M.F.J. Eusébio, J.P.B. Mota, J. Chromatogr. A 1189 (2008) 292.

[20] J.M.M. Araújo, R.C.R. Rodrigues, M.F.J. Eusébio, J.P.B. Mota, Presentation P48 at the SPICA 2006 Symposium, Innsbruck, Austria, October 2006.

[21] D. U. Staerk, A. Shitangkoon, G. Vigh, J. Chromatogr. A 663 (1994) 79.

[22] A. Cavazzini, V. Costa, G. Nadalini, D. Dondi, J. Chromatrgr. A 1137 (2006) 36.

[23] R.C.R. Rodrigues, J.M.M. Araújo, M.F.J. Eusébio, J.P.B. Mota, J. Chromatogr. A 1142 (2007) 69.

[24] J.M.M. Araújo, J.P.B. Mota, AIChE J. 51 (2005) 1641.

[25] R.C.R. Rodrigues, J.M.M. Araújo, J.P.B. Mota, J. Chromatogr. A 1162 (2007) 14.

[26] J.P.B. Mota, I.A.A.C. Esteves, M.F.J. Eusébio, AIChE J. 53 (2007) 1192.

[27] J.P.B. Mota, I.A.A.C. Esteves, Ind. Eng. Chem. Res. (2007), doi:10.1021/ie061547a.

[28] G. Guiochon, S. Golshan-Shirazi, A. Katti, Fundamentals of Preparative and Nonlinear Chromatography, Academic Press, Boston, MA, 1994.

[29] J.M.M. Araújo, R.C.R. Rodrigues, J.P.B. Mota, submmitted to J. Chromatogr. A (2007).

[30] M.F.J. Eusébio, Development of an Universal Interface for Monitoring and Control of Chemical and Biochemical Processes, Ph.D. Thesis. Universidade Nova de Lisboa, Lisboa, Portugal, 2006 (in Portuguese).

[31] F. Attila, A. Cavazzini, G. Guiochon, J. Chromatogr. A 986 (2003) 207.

[32] C.B. Ching, W. Arlt, M. Lisso, G. Wozny, Ind. Eng. Chem. Res. 39 (2000) 4365.

[33] M. Juza, J. Chromatatgr. A 865 (2000) 35.

[34] D. Antos, A. Seidel-Morgenstern, Chem. Eng. Sci. 56 (2001) 6667.

[35] A. Felinger, Data Analysis and Signal Processing in Chromatography, Elsevier, Amsterdam, 1998.

[36] J.P. Foley, J.G. Dorsey, J. Chromatogr. Sci. 22 (1984) 40.

[37] M.S. Jeansonne, J.P. Foley, J. Chromatogr. Sci 29 (1991) 258.

[38] A.N. Papas, CRC Crit. Rev. Anal. Chem. 22 (1989) 359.

[39] R. Delley, Chromatographia 18 (1984) 374.

[40] R. Delley, Anal. Chem. 57 (1985) 388.

[41] D. Hanggi, P.W. Carr, Anal. Chem. 57 (1985) 2394.

[42] J.M.M. Araújo, R.C.R. Rodrigues, J.P.B. Mota, J. Chromatgr. A 1132 (2006) 76.

[43] J.P.B. Mota, J.M.M. Araújo, R.C.R. Rodrigues, AIChE J. 53 (2007) 2630.

[44] J.M.M. Araújo, R.C.R. Rodrigues, J.P.B. Mota, Ind. Eng. Chem. Res. 45 (2006) 5314.

[45] K. Gedicke, M. Tomusiak, D. Antos, A. Seidel-Morgenstern, J. Chromatogr. A 1092 (2005) 142.

[46] P. Janderea, G. Guiochon, J. Chromatogr. 588 (1991) 1.

Chapter 6

Chiral Separation by Compact Two-column, Open-loop Simulated Moving-Bed Chromatography

1 Introduction

The simulated moving bed technology (SMB) is a multicolumn, continuous adsorption separation process that increases throughput, purity, and yield relative to batch chromatography [1–3]. Broughton and Gerhold developed the SMB technology in the early 1960s [4], and it was primarily applied to large-scale production in the petrochemical and sugar industries [5]. Nowadays, the SMB technology has been extended to other application areas, such as the pharmaceutical and fine chemistry industries, for the separation and purification of various substances [6].

The SMB is a practical way of implementing the true moving bed (TMB) concept, in which the adsorbent and the mobile phase move counter-currently [7–9]. The driving force for mass transfer is enhanced by countercurrent operation, thus providing for a better use of he adsorbent than that of the traditional batch mode. The SMB comprises a set of identical chromatographic columns interconnected circularly to form a closed loop. The circular column arrangement is divided in four sections (or zones) of constant flow rates by the presence of four ports: two inlet ports for adding fresh eluent and feed, and two outlet ports for collecting the product streams. The periodical movement of the inlet and outlet ports, by one column ahead in the direction of the fluid flow, simulates the counter-current contact between the solid and liquid phases.

Although the continuous movement of the solid in the TMB unit is simulated in a discrete fashion, the analogy between the two processes increases as the zones are subdivided into more columns [7, 10]. Due to the circular column arrangement and the periodic port shifting, the SMB attains a cyclic steady state (CSS) in which the internal composition profile circulating around the multicolumn loop is $N\tau$-periodic and the composition profiles in the raffinate and extract streams are τ-periodic (N is the number of columns and τ is the switch interval).

The increasing use of the SMB as a multipurpose unit, mainly in the pharmaceutical industry, where SMB units can be applied to different separations in all stages of the drug-development cycle [11], has led to the development of novel cyclic operation schemes, some of which are substantially different from the classical process. Broadly speaking, the new operation schemes introduce modulations of selected control parameters into the operating cycle. Concepts such as asynchronous port switching [12–14], cyclic modulation of feed concentrations [15, 16], time-variable manipulation of the flow rates [17–21], and modulation of solvent strength during process operation [22–24], have been thoroughly

analyzed. The extra degrees of freedom available with the non-classical schemes improve the separation efficiency, thus allowing the use of units with smaller number of columns. The advantages are obvious: less stationary phase is used, the set-up is more economic, and the overall pressure drop can be reduced. Furthermore, switching from one mixture to another is easier and takes less time than with more columns.

Alternative SMB schemes with less zones than the classical SMB implementation comprising four zones, with one or more columns per zone, have also been studied. For example, the three-zone SMB configuration [7, 25, 26] takes the four-zone open-lop SMB and removes zone IV. Optimizing the amount of adsorbent allocated to each zone by means of asynchronous port switching , allows a better performance of the three-zone SMB against the four-zone SMB [27–29]. The advantages and drawbacks of the three-zone SMB have been discussed by chin and Wang [30].

A two-zone SMB with continuous feeding and partial withdrawal developed by Lee [31], for glucose-fructose separation, appears rather suitable only for enriching products than for high-purity separations [30]. Another two-zone SMB scheme uses intermittent feeding and withdrawal to achieve ternary separations [32]. More recently, two-zone SMBs for binary separation were developed by Wankat et al.[33, 34], which incorporate a storage tank to hold desorbent temporarily for later use. The results show that good separation can be achieved with their two-zone SMB systems, but with more desorbent than required by a four-zone SMB. However, partial feed was shown to improve the product purities and recoveries considerably. An upgrade to the system was achieved for ternary separations [35], and a different two-zone SMB system, which does not use a storage tank, was developed for center-cut separation from ternary mixtures [36]. For bioseparations the three-column MCSGP process is particularly suitable [37], which incorporates the principle of countercurrent operation and the possibility of using solvent gradients. One-column processes that reproduce the cyclic behavior of multicolumn SMB chromatography, by means of a recycle lag, have also been proposed [38–40].

In the present study [41] (**paper VII**), a new two-column SMB system for chiral separation is developed. Emphasis is given to the use of two columns rather than two zones, because with three or more columns it is always possible to implement a better SMB scheme which uses more zones with roughly the same ancillary equipment. In fact, running a two-zone configuration with three columns can be detrimental to the separation because the zone lengths become highly asymmetrical [33].

In the proposed two-column process, both the port switching and the flow rates are modulated over the cycle. The cycle itself is optimized and adapted to the difficulty of the separation and process specifications. Somewhere in between the SMB and batch chromatography, and in an attempt to work with the best of 'two worlds', a compact two-column open-loop SMB process for enantiomeric separation was designed, which is particularly effective when the resolution is limited.

The feasibility and effectiveness of the proposed compact two-column, open-loop SMB for enantiomeric separations are demonstrated experimentally on the direct separation of the enantiomers of reboxetine on amylose-based chiral stationary phase. Reboxetine is a selective norepinephrine reuptake inhibitor, currently approved in over 60 countries as an antidepressant, and is marketed under the trade names Edronax, Norebox, Prolifit, Vestra, and Integrex in Europe and Latin America.

1.1 Chirality and 'Chiral switch'

A recent survey [42] carried out by the Process Chemistry R&D departments of GlaxoSmithKline, AstraZeneca and Pfizer — three of the most important pharmaceutical companies — provides a pan-industry cross site analysis of the chemistry currently used in drug development, informing researchers about the needs of pharmaceutical industry and indicating significant gaps in synthetic methodologies. This overview of pharmaceutical synthesis shows that 54% of the drug substances coming from medical chemistry programmes into the Process Chemistry R&D departments of the three companies are chiral. It is important to notice that the preparation of biopharmaceuticals falls outside the scope of the review, so the percentage of chiral drugs is clearly underestimated.

The requirement to produce chiral compounds as single enantiomers/diasteroisomers for pharmaceutical applications is well understood, as demonstrated in a recent publication providing a snapshot of asymmetric methods used at process scale [43].

It is clear from the data presented in [42], that the predominant method for in-house generation of chirality is resolution. The preferred methods to generate a chiral center are relative diastereocontrol or preparation of a racemate followed by resolution [42]. It is clear from [42] that resolution remains an important and cost-effective approach to chiral molecules, especially if carried out early in the synthesis pathway. Efficient symmetric synthesis followed by resolution is usually more effective than designing a synthesis around asymmetric technology.

Over the last two/three decades, most pharmaceuticals with an asymmetric carbon (chiral center) have been commercialized as mixtures of enantiomers. The introduction and widespread use of asymmetric synthesis and chiral separation technologies have made it possible for pharmaceutical manufacturers to develop single-enantiomer drugs. Another factor has been the strict imposed regulations, dictated by pharmaceutical and food regulatory organizations (lead by the US Food and Drug Administration (FDA) [44]), which are increasing the need for developing optically-pure drugs [45]. The market share of optically-pure drugs increased from 27% in 1996 to 39% in 2002 [46, 47]. The Business Communications Company projects that revenue from chiral drug development will continue to grow at an average annual rate of 10.2% annually, from 75.0 billion in 2003 to 122.0 billion in 2008 [48].

Although enantiomers have the same reactivity toward achiral compounds, they may react differently with chiral substances. Thus, one enantiomer of a chiral drug may bind to a receptor's asymmetric active site, while the other may bind weakly or not at all. Many biological molecules (e.g., enzymes and receptors) are chiral or asymmetric. Consequently, different enantiomers often have very different pharmacologic properties. If the nontherapeutic enantiomer has undesirable reactivity, there is a potential for serious, even tragic consequences. The marketing and subsequent withdrawal of thalidomide in Europe is the classic example [49–51]. Drug stereochemistry has become an issue for the pharmaceutical industry an the regulatory authorities [52–55], due to technological developments and the potential benefits of single enantiomer drugs, summarized in Table 1.

A racemic or chiral switch may be defined as the development of a single enantiomer from a previously marketed racemate [57]. The chiral switch process has resulted in a number of agents being re-marketed as single enantiomer products; examples are given in Table 2.

When a pharmaceutical manufacturer develops a single-enantiomer product from a

Table 1: Potencial advantages of single enantiomer products [56].

Less complex, more selective pharmacodynamic profile
Potential for an improved therapeutic index
Less complex pharmacokinetic profile
Reduced potential for complex drug interactions
Less complex relationship between plasma concentration and effect

Table 2: Commonly prescribed drugs and their enantiomeric switches [59–62].

Product	**Chiral Switch**
citalopram (Celexa)	escitalopram (Lexapro)
omeprazole (Prilosec)	esomeprazole (Nexium)
oxybutynin (Detropan)	esoxybutynin (Phase III)
amlodipine (Norvasc)	(S)-amlodipine (Phase II)
budesonide (Rhinocort)	dexbudesonide (Biological testing)
sotalol (Betaspace)	dexsotalol (Phase III)
ketoprofen (Actron, Orudis)	dexketoprofen (Trometamol)
methylphenidate (Ritalin)	dexmethylphenidate (Focalin)
lansoprazole (Prevacid)	dexlansoprazole (status unknown)
venlafaxine (Effexor)	desvenlafaxine (Phase III)
formoterol (Foradil)	arformoterol (Phase III)
albuterol	levalbuterol (Xopenex)
zopiclone (Imovane in Canada)	eszopiclone (Lunesta)
cetirizine (Zyrtec)	levocetirizine (Xyzal/Zuzal)
modafinil (Provigil, Alertec, etc.)	armodafinil (Nuvigil)

drug marketed as a racemic mixture, that is called a chiral switch. The single-enantiomer product receives additional patent protection and a new generic name based on the rules for naming enantiomers (e.g., USAN-United States Adopted Names, WHO-World Health Organization). The manufacturer markets the single-enantiomer drug as a new product, with a different trade name. Chiral switches have been used by manufacturers to extend the life of blockbuster (bestsellers) drugs [58, 59], and this has been cited as an important factor in their development of chiral switches [59–62]. When the original developer of a blockbuster did not patent individual enantiomers, third-party companies, such as the specialist chiral chemical company Sepracor (`http://www.sepracor.com`), have been able to develop the single isomer and enter into licensing agreements with the company that marketed the racemic mixture. Pharmaceutical-industry analysts and journalists have suggested that manufacturers will increasingly rely on chiral switches to fuel growth [47, 48].

There is evidence that that the rate of development of new agents is declining [63–65]; for example, the US FDA approved only 28 new chemical entities in 2001 which is reported

to be the lowest nunber for 30 years [63]. This situation is compounded by the fact that research and development coast are increasing, having double over the last fifteen years [64]. Additionally, drug development time is now so long that the average effective patent life of a new agent is only $10 - 12$ years [63].

As a number of commercially highly successful drugs are chiral, the economic significance of stereochemistry to the pharmaceutical industry is obvious. The chiral switch process provides a strategy to extend the profitable life of a pharmaceutical bestseller, and may result in extended patent protection and provide an advantage against generic competition. Re-evaluation of the enantiomers of racemic drugs will undoubtedly continue and, in some instances, result in the introduction of single enantiomer versions of established drugs. Hopefully, such re-evaluations will provide agents with a cleaner pharmacological profile, improved safety and efficacy, and ultimately therapeutic benefits in addition to commercial advantages.

In the context of chiral considerations and chiral switches, the preparative separation of enantiomers by chromatography on chiral stationary phases (CSPs) has been recognized as being a useful alternative to the more conventional approaches, such as crystallization, enantioselective synthesis, and enzymatically catalyzed transformations [66–69]. SMB chromatography has largely contributed to radically changing the level of acceptance of chromatography as a real and powerful alternative for the preparative isolation of enantiomerically pure compounds, at all production scales, from laboratory to pilot to production scale [11]. The technical feasibility of scaling-up the technology, and its relatively low running costs, have rendered this technique great attraction from the pharmaceutical industry. Compared to an enantioselective synthesis approach, chromatography will be all the more attractive since the number or reaction steps for preparing the racemate (for chromatography) is considerably reduced compared to the number of steps needed for the asymmetric synthetic route [70].

2 Two-column SMB process for enantioseparations

In the design of a two-column SMB process, due to its particular nature, there are multiple aspects that must be taken into account. Firstly, the versatility of the valves — the portion of the equipment that controls the port switching — must be accomplished to accommodate various port configurations. This implies that the system must be able to operate without some of the standard zones of an SMB, particularly zones II and IV.

Secondly, since the proposed scheme relies on a time-variable flow-rate policy, a robust pump configuration is critical for a successful implementation of the system in practice.

The schematic depicted in Fig. 1 shows the position of the intlet/outlet lines when all four zones are brought together between two adjacent columns. A duplication of the inlet line for the eluent stream is verified, because it precedes de extract outlet port when zone I is suppressed, but follows the raffinate withdrawal port when zone IV is temporarily or permanently removed. It is important to discern, that not all port configurations have to be realized in practise. For example, since the feed inlet port and the raffinate outlet port are never active at the same node, the inlet line for the feed stream does not have to precede the raffinate line. In the implementation developed, the eluent port is placed downstream of the raffinate port, to allow the suppression of zone IV by having both ports opened at the same node. This is not replicated upstream of the extract port. The resulting node configuration is depicted in Fig. 2.

In the implemented two-column SMB process, we use a distributed valve design based on two-way valve, since they allow independent port switching and are quite versatile. Two-way valves allow the flow either to go through or not to go through. Each valve is attached to the transfer line between columns by a tee. A two-way valve is placed immediately downstream of the two outlet ports of each column, but preceding the two inlet ports, to control the flow rate of liquid from the column that is directed to the next. The flow rate of liquid that is withdrawn at each node is controlled by material balance. The two internal recirculating pumps considered in the two-column implementation previously analyzed by the group [71] are suppressed, to reduce the ancillary equipment to a minimum and to maximize the potentialities of a simpler process closer to a batch system. Since the proposed two-column SMB process is target at chiral separations at all production scales, cost is a major factor that will determine if this chromatographic method is applied for the preparation of optically pure compounds. It is important to remark that

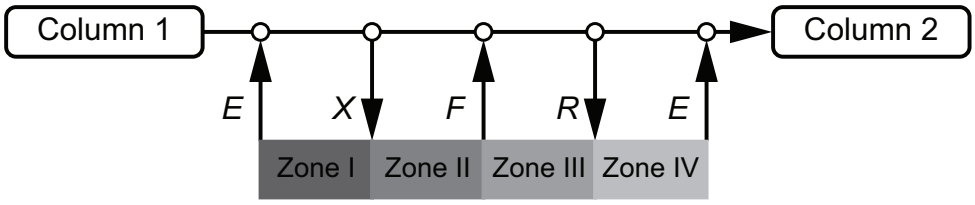

Figure 1: Schematic of inlet/outlet lines when all four zones are brought together onto the junction between two adjacent columns. Notation is as follows: E, eluent inlet; X, extract outlet; F, feed inlet; R, raffinate outlet.

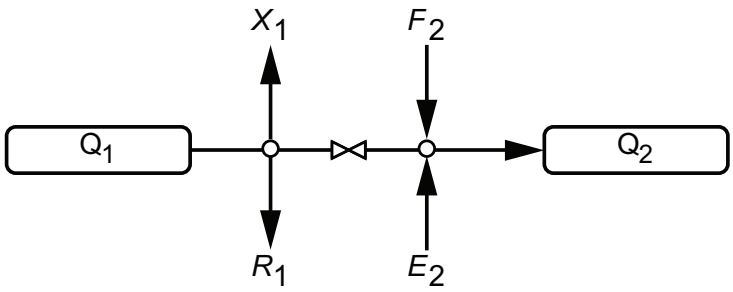

Figure 2: Schematic of node design for the proposed two-column process. An on/off valve is placed between the outlet and inlet lines. Notation is as follows: E, eluent inlet; X, extract outlet; F, feed inlet; R, raffinate outlet; Q, internal flow rate.

the proposed two-column SMB process employs as ancillary equipment only two inlet pumps for supplying feed and eluent to the system, and ten two-way valves two control the port switching.

The node design is flexible enough to allow for open-loop operation, where the effluents from zone I or III are totally removed as products without partially flowing to the next zone. The two-way valve, placed immediately downstream of the two outlet ports of each column, is normally open and is only actuated when the effluent from the column is totally withdrawn as product or the fluid in the column needs to be temporarily frozen.

The different port configurations allowed with the proposed node design are depicted in Fig. 3. These port configurations can be thought of as the building blocks for establishing the cyclic operation scheme for the implemented two-column process. Due to the suppression of the two internal recirculating pumps, some of the port configurations outlined in [71] cannot be implemented, such as partial withdrawal and partial withdrawal and flow addition at the same node. Despite of the reduction of the port configuration options, it is important to emphasize that this is not a limiting step for an optimal cycle design of the enantioselective two-column system.

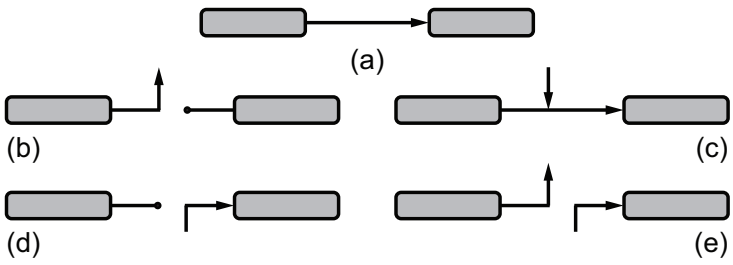

Figure 3: Flow diagram for the different types of port configuration that can be implemented with the proposed node design: (a)complete direction of flow to the next column, (b) downstream frozen bed, (c) flow addition to circulating stream, (d) upstream frozen bed, and (e) complete withdrawal and flow injection on the same node. Steps b, d, and e, allow for open-loop operation.

A schematic diagram of the proposed setup is illustrated in Fig. 4. Overall, our system employs two inlet pumps for supplying feed and eluent to the system, and ten two-way valves to control the port switching. The HPLC pumps are model K-501 from Knauer (Berlin, Germany) with 10 ml pump heads, and are controlled via RS232 communication protocol. The two-way valves are model SFVO from valco International (Schenkon, Switzerland) with pneumatic actuation. Each valve is automated by means of a single computer-controlled three-way solenoid: application of 50 psi opens the valve; venting the air allows the spring to return the valve to the closed position. The experimental setup is fully automated and driven by an in-house developed automation system [72] using LabView software (National Instruments). Figure 4 also depicts the use of the on-line monitoring analysis system, which is discussed in Chapter 5 and elsewhere [73], to monitor the internal composition profile. Accurate and robust online monitoring is important, as the two-column SMB process is designed for the production of optically pure compounds.

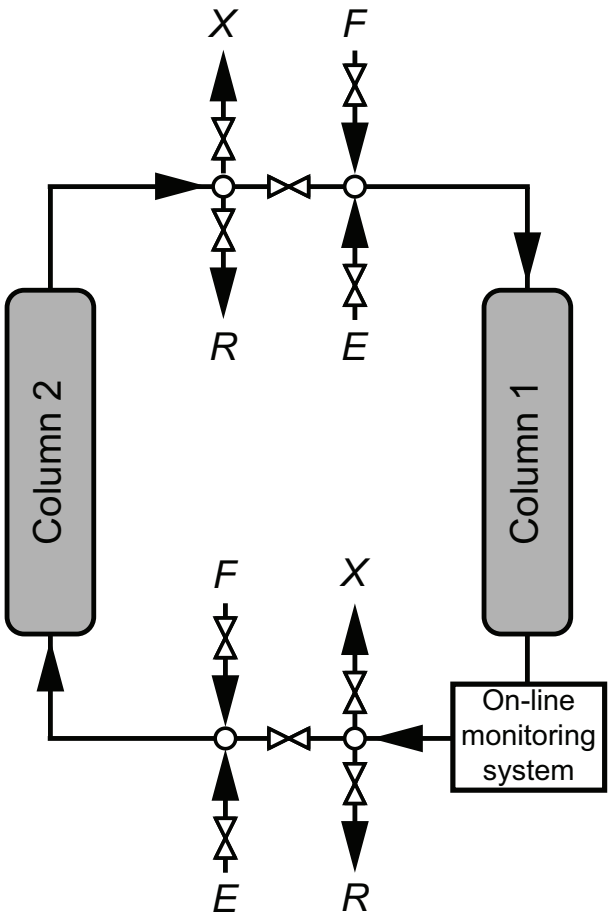

Figure 4: Schematic diagram of the enantioselective two-column SMB unit. The use of an automated on-line enantiomeric analysis system [73], employed to monitor the internal composition profile, is also shown.

3 Procedure for optimal cycle design

The periodically moving of the input and withdrawal ports one column ahead, each τ time units (τ is the switching interval), in the direction of the fluid low, that occurs in the standard SMB, to simulate the counter-current contact between the solid and the liquid, is also implemented in the new two-column process. Because the two columns are assumed to be identical, the cycle can be divided into two steps of equal length, τ, where τ is equivalent to the switching interval of a standard SMB. At the end of each step, i.e. every τ time units, the inlet/outlet ports are switched, and the columns reverse roles.

The feed and eluent flow rates are fully modulated in time to achieve maximum process performance. An optimized time-variable flow rate policy usually gives better productivity and less eluent consumption than the simpler partial-feed strategy. For simplicity, the τ-periodic modulations implemented in the present work are piecewise constant. In practise, each step of the cycle is divided into a given number n_{Q} of subintervals of equal length, and the flow rates are kept constant over each subinterval before jumping discretely to different values over the next subinterval. The same assumption applies to the port configuration.

A rigorous model-based optimization approach [27] is employed to determine the optimal operating scheme. The purpose of the optimization procedure is to guarantee the fulfillment of product and process specifications, such as minimum purities and maximum operating flow rates, while optimizing process performance in terms of productivity and eluent consumption.

The adopted formulation does not explicitly track the port switching over the cycle; instead, the status of the two-way valves is inferred from the piecewise-constant flow-rate profiles. If in Fig. 2, for example, $E_j = 0$ over a subinterval of the step, then the two-way valve that connects the eluent pump to the inlet of column j is closed, otherwise is open. Similarly, if $Q_j = 0$ or $X_j + R_j = Q_j$ then the two-way valve located between the inlet/outlet ports downstream of column j is closed, otherwise it is open. This formulation is highly flexible and has the advantage of eliminating the integer nature of the design problem, since the only remaining degrees of freedom are the switching interval and the time-variable flow rates.

At each step of the flow-rate modulation, the following basic conditions must be fulfilled:

$$0 \leq E_j \leq Q_{\max}, \qquad X_j \geq 0,$$

$$0 \leq F_j \leq Q_{\max}, \qquad R_j \geq 0, \tag{1}$$

$$Q_j - X_j - R_j \geq 0, \tag{2}$$

$$(X_j + R_j) \times (Q_j - X_j - R_j) = 0, \tag{3}$$

where $Q_{\max}$ is the capacity of the installed HPLC pumps. These constrains guarantee that the solution is physically realizable with our experimental setup. Eq. 2 prevents the product from being withdrawn at a higher flow rate than that provided by the column. Eq. 3 ensures that product withdrawal can be implemented with on-off valves: nothing is withdrawn from column j ($X_j + R_j = 0$) and the flow is totally directed to the next column, or the effluent from column j is totally withdrawn as product ($Q_j - X_j - R_j = 0$).

Product purity and recovery are enforced through the following constrains:

$$P_R \geq P_R^{\min}, \qquad P_X \geq P_X^{\min}, \tag{4}$$

$$R_R \geq R_R^{\min}, \qquad R_x \geq R_x^{\min}, \tag{5}$$

where P and R denote product purity and recovery, respectively, and the 'min' script their minimal admissible values; these performance parameters are defined in Fig. 5. In a first instance the objective function, f_{obj}, is chosen to be the maximization of productivity, or feed throughput:

$$f_{\text{obj}} = \max(\overline{F}), \qquad \overline{F} = \int_0^1 (F_1 + F_2)\, d\theta = \int_0^2 F_j\, d\theta, \tag{6}$$

where $\theta = t/\tau$ is a dimensionless time coordinate and $\overline{F}$ is the average feed flow rate per cycle. We note, however, that in general the optimization of a chromatographic process is a multi-objective optimization problem in which productivity is to be maximized and eluent consumption is to be minimized.

To enforce the use of a single eluent pump and a single feed pump, the flow rates are also subjected to the following additional constrains:

$$E_1(\theta)E_2(\theta) = 0, \qquad F_1(\theta)F_2(\theta) = 0. \tag{7}$$

The optimization problem is formulated with a single-column analog model that reproduces the cyclic steady state of the two-column unit [38, 74], together with a full-discretization approach for steady period dynamics. For this purpose, a full-discretization method is applied to the single-column model in which the time coordinate is discretized over a full cycle (2τ time units) and the CSS conditions are directly imposed [28, 75].

The computational domain and governing equations are shown in Fig. 5, together with a schematic diagram of the single-column model.

Discretization is handled via collocation, using 15 cubic Hermite elements [76] for the spatial domain and $10N = 20$ Radau elements (with two interior points) for the time domain. The latter type of collocation elements is suitable especially for handling process dynamics with frequent discontinuities in time [77]. The flow rates remain constant over each Radau element, but are allowed to change discretely to different values across elements. This means that the largest number of subintervals that can be allocated per step for the piecewise-constant flow rate modulation is $n_{\mathrm{Q}} = 10$. This is perfectly adequate for every practical application, since higher resolutions have little impact on process performance.

As proposed by Biegler et al. [27, 77], the nonlinear programming problem obtained after discretization is formulated in AMPL [78] and solved using IPOPT 3.2.3 [79]. This solution strategy has been previously employed with success by our group on a broad class of SMB problems [28, 29, 80]. IPOPT implements a primal-dual interior-point method, and uses line searches based on filter methods. It directly exploits the first and second derivative (Hessians) information provided by AMPL via automatic differentiation.

4 Chromatographic column model

The isothermal operation of a chromatographic column is adequately described by a dispersed plug-flow model with linear-driving-force approximation for mass transfer. These assumptions are standard practice in preparative chromatography and SMB modeling [83]. The lumped solid-diffusion version of the model can be written as

$$\frac{\partial c_i}{\partial \theta} + \beta \frac{\partial q_i}{\partial \theta} = \frac{\tau v}{L} \quad \frac{1}{\mathrm{Pe}} \frac{\partial^2 c_i}{\partial x^2} - \frac{\partial c_i}{\partial x} \Bigg) \quad (0 < x < 1), \tag{8}$$

$$\frac{\partial q_i}{\partial \theta} = \tau k_i (q_i^* - q_i), \tag{9}$$

where subscript i is the solute index, $\theta = t/\tau$ and $x = z/L$ are the dimensionless temporal and axial coordinates, respectively, $\beta = (1 - \epsilon)/\epsilon$ is the phase ratio, L is the column length, v is the linear velocity of the mobile phase, $\mathrm{Pe} = vL/D_{\mathrm{L}}$ is the Péclet number, D_{L} is the axial dispersion coefficient, $q_i^*(c_1, c_2)$ is the adsorption isotherm for solute i, and k_i is the linear-driving-force (LDF) coefficient for mass transfer. The reference time, τ, to render the time coordinate dimensionless, is chosen to be equal to the switching interval of the two-column SMB process.

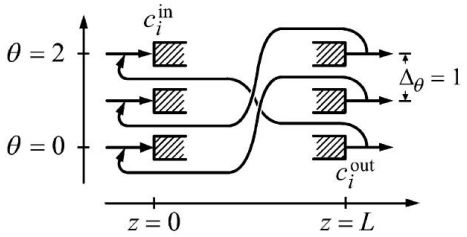

Dimensionless time coordinate:

$$\theta = t/\tau, \quad \theta^+ = \begin{cases} \theta + 1, & \theta < 1 \\ \theta - 1, & \theta > 1 \end{cases}$$

Computational domain:

$$\Omega = \Omega_z \times \Omega_\theta, \quad \Omega_\theta = [0, 2], \ \ \Omega_z = [0, L]$$

Formulate chromatographic column model with cyclic condition:

$$c_i(z, 2) = c_i(z, 0), \ \ q_i(z, 2) = q_i(z, 0), \ \ \forall z \in \Omega_z$$

Condition for simulated countercurrent (SCC) flow:

$$c_i(z, \theta^+) = c_i(z, \theta), \ \ q_i(z, \theta^+) = q_i(z, \theta), \ \ \forall z \times \theta \in \Omega$$

Node balances with embedded SCC condition:

$$\big(Q - X - R\big)_\theta = \big(Q - E - F\big)_{\theta^+}$$

$$\big[(Q - X - R)c_i^{\text{out}}\big]_\theta = \big(Qc_i^{\text{in}} - Fc_i^{\text{F}}\big)_{\theta^+},$$

Purities:

$$P_{\text{X}} = \frac{\int_{\Omega_\theta} c_2^{\text{out}} X \, d\theta}{\int_{\Omega_\theta} (c_1^{\text{out}} + c_2^{\text{out}}) X \, d\theta}, \quad P_{\text{R}} = \frac{\int_{\Omega_\theta} c_1^{\text{out}} R \, d\theta}{\int_{\Omega_\theta} (c_1^{\text{out}} + c_2^{\text{out}}) R \, d\theta}$$

Recoveries:

$$R_{\text{X}} = \frac{\int_{\Omega_\theta} c_2^{\text{out}} X \, d\theta}{c_2^{\text{F}} \int_{\Omega_\theta} F \, d\theta}, \quad R_{\text{R}} = \frac{\int_{\Omega_\theta} c_1^{\text{out}} R \, d\theta}{c_1^{\text{F}} \int_{\Omega_\theta} F \, d\theta}$$

Conversion from single- to two-column formulation:

$$\phi_1(\theta) = \phi(\theta), \ \ \phi_2(\theta) = \phi(\theta + 1), \quad \forall \phi \equiv E, X, F, R, Q, c, q$$

Figure 5: Schematic diagram and main governing equations of single-column model that replicates the cyclic steady state of the two-column SMB process. The design problem can be formulated with one column operating over 2τ time units [74, 75], as described above, or two columns operating over τ time units [27, 77]. The chromatographic column model is given by Eqs. (8)-(10).

Equation (8) is subject to the usual boundary conditions

$$c_i - \frac{1}{\mathrm{Pe}}\frac{\partial c_i}{\partial x} = c_i^{\mathrm{in}} \quad \text{for} \quad x = 0, \tag{10}$$

$$\frac{\partial c_i}{\partial x} = 0 \quad \text{for} \quad x = 1, \tag{11}$$

where c_i^{in} is the inlet concentration of solute i.

In the working range of fluid velocity used in preparative chromatography, the Van Deemter plot is well approximated by a straight line [84]. The intercept and slope for each enantiomer, expressed here in terms of the Péclet number (Pe) and linear-driving-force (LDF) coefficient for mass-transfer (k_i), were determined by fitting the experimental dependence of the plate height with flow rate for diluted pulses of racemic mixture. This procedure is detailed in Chapter 4 and elsewhere [85].

5 Experimental

The feasibility and effectiveness of the proposed enantioselective two-column SMB were assessed experimentally on the separation of reboxetine racemate, using Chiralpak AD as stationary phase and a mixture of 90:10 hexane/ethanol with 0.2% DEA (basic modifier) as eluent. Daicel's Chiralpak AD (Chiral Technologies Europe, Illkirch, France), a 20-μm silica-based packing material, coated with amylose tri-(3,5-dimethylphenyl carbamate), is convenient for the separation of aromatic enantiomers (see Fig. 6 for chemical structure).

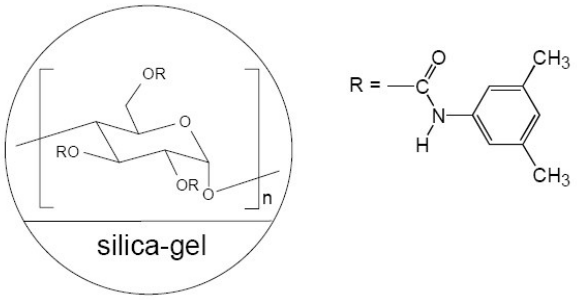

Figure 6: Chemical structure of the CSP in Chiralpak AD [81].

This system is one in which there is clearly a lack of resolution between the two components. It is thus difficult to obtain both products with high purity and yield by HPLC for the chosen chromatographic conditions.

5.1 Materials, characterization of adsorption equilibrium and band broadening

Racemic reboxetine was kindly supplied by Pfizer (Compound Control Center, Pfizer Global Research and Development). The chromatographic columns are Superformance 10 mm ID thermojacketed glass columns (Götec Labortechnik, Germany). The stationary phase was slurry packed into each column to a bed height of $L = 10.0$ cm. The solvents used were HPLC-grade n-hexane (Sigma-Aldrich, Germany), and ethanol (Panreac, Spain), and employed as mobile phase after filtration. Diethylamine (DEA), a basic modifier, was obtained from Sigma-Aldrich (Germany). The system was operated isothermally at 25°C.

The HPLC pumps employed in the experiments are model K-501 from Knauer (Berlin, Germany) with 10 ml pump heads, controlled by RS232 communication protocol. The whole set-up is fully automated and driven by our Labview-based software system (BioCTR) for process monitoring and control of chromatographic processes [72].

Two multi-wavelength UV detectors (USB2000/USB4000 from Ocean Optics, USA) with attenuator, sharing a DH-2000-S-DUV light source (Micropack, Ostfildern, Germany), and an electrically-driven 6-port 2-position valve from Knauer (Berlin, Germany), were employed in the on-line monitoring system. The analytical HPLC column is 150× 4.6 mm I.D., packed with Chiralpak IA [amylose tri-(3,5-dimethylphenyl carbamate) immobilized on 5 μm silica gel], purchased from Daicel Chemical Industries Ltd (Chiral Technologies Europe, Illkirch, France). The UV detector placed in the SMB loop (labeled as 'Total signal' in Fig. 7), at the outlet of column 1, was calibrated at the wavelength of 276 nm. The second UV detector, placed at the outlet of the analytical HPLC column, was calibrated at a wavelength of 230 nm.

The total column porosity (ϵ) was measured using 1,3,5-tri-tert-butylbenzene (TTBB) from Sigma-Aldrich (Germany). This solute is not retained but can access the internal porosity of the stationary phase. The packing reproducibility was assessed by comparing the peak shapes and retention times of the chromatograms obtained with the two columns; both columns were identically, and reasonably well, packed. Extra-column volumes in the experimental set-up were estimated from TTBB pulse experiments with and without the chromatographic columns.

The procedure to determine the Péclet number (Pe) and the linear-driving-force (LDF) coefficient for mass-transfer (k_i), is discussed in Section 4. The estimated values of the

parameters are listed in Table 3.

The experimental determination of adsorption isotherms is of utmost importance for the design and operation of any SMB process. The operating conditions of a chiral SMB process cannot be properly determined without knowledge of the competitive isotherms of the two enantiomers. In the present work, the competitive isotherm of the two enantiomers of reboxetine for overloaded SMB operation, was estimated with good accuracy by applying the hybrid inverse method detailed in Chapter 4 and in the correspondent paper [85]. The fitted parameters of the selected adsorption isotherm model (Linear-Langmuir) are listed in Table 3.

An analytical profile of the racemic mixture is illustrated in Fig. 9 and detailed in Section 6, to depict the elution order of the two enantiomers. The isotherm was determined on the same columns in which the preparative experiments were carried out. The parameters listed in Table 3 were then used in the design and optimization of the cycle for the two-column chiral SMB process.

Table 3: Column characterization and adsorption parameters for the binary separation of reboxetine enantiomers on Chiralpak AD, using a mixture of 90:10 hexane/ethanol with 0.2% DEA (basic modifier) as mobile phase. Scripts '1' and '2' denote the less- [(-)-*R,R*-] and more- [(+)-*S,S*-] retained enantiomers, respectively.

Column length, L (cm)	10.0	Péclet number, Pe	539.1
Column diameter, d (cm)	1.0	LDF coeficients, k_i (s^{-1})	$8.715, 8.715$
Total Porosity, ϵ	0.568	Feed (linear/overloaded), c^F (g/l)	0.1 / 1.10
Linear isotherm, q_i^* (g/l)		$(4.929c_1,\ 5.479c_2)$	
Linear-Langmuir isotherm, q_i^* (g/l)		$(4.452c_1,\ 5.031c_2) + \dfrac{0.443c_1,\ 1.273c_2}{1 + 10.79c_1 + 15.44c_2}$	

5.2 On-line monitoring system

Since the two-column SMB process is designed for the production of optically pure compounds, Fig. 4 shows the use of the on-line monitoring analysis system, to monitor the internal composition profile, which is discussed in Chapter 5 and in [73]. The on-line monitoring system is illustrated in Fig. 7. It comprises an electrically-actuated 6-port 2-position valve, an analytical HPLC column, one HPLC pump, and two UV detectors

sharing the same light source by means of a bifurcated optical fiber assembly.

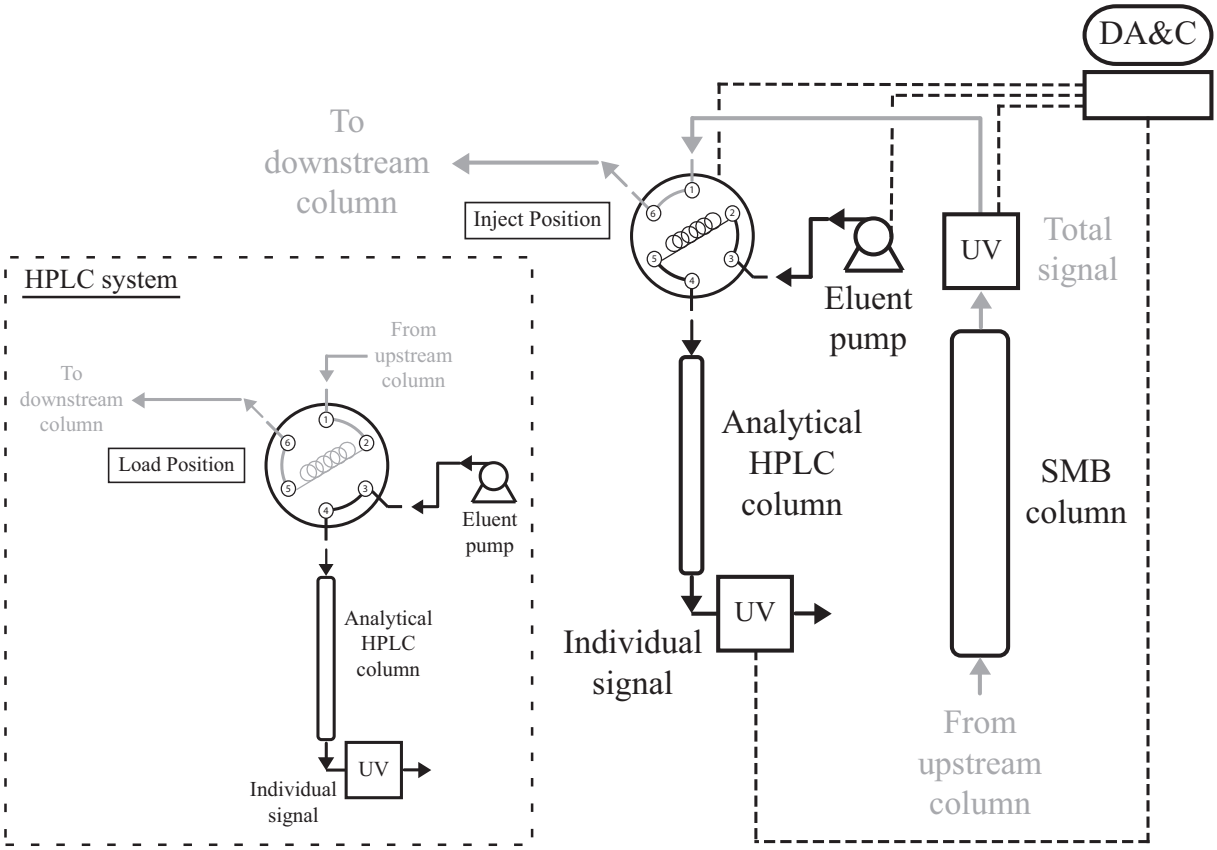

Figure 7: Schematic diagram of the on-line chiral monitoring system. The main equipment comprises an electrically-actuated 6-port 2-position valve, an analytical HPLC column, one HPLC pump, and two UV detectors sharing the same light source by means of a bifurcated optical fiber assembly. The set-up is fully automated.

The on-line monitoring system for enantiomeric detection in multicolumn continuous chiral chromatography, discussed in Chapter 5 and in [73], implements an automated procedure for on-line processing of the signals from the two UV detectors depicted in Fig. 7. The UV detector labeled 'Total signal' monitors the total absorbance, which is proportional to the total enantiomeric concentration. The sampling interval for this UV was fixed at 0.25 s^{-1}. The second UV detector, placed at the outlet of the analytical HPLC column, monitors the individual chromatograms of the two enantiomers.

The method implemented to calculate the enantiomeric composition, relies on the chromatograms from the analytical HPLC column to compute the enantiomeric purity, which is then converted to individual concentrations using the total concentration value, measured independently by the UV detector installed in the SMB loop. Each pair of chromatographic peaks detected per injection are fitted to the sum of two EMG functions (one per peak), by nonlinear least-squares curve fitting, to estimate the area under each

peak. The peak-area information is used to calculate the enantiomeric purity which is then converted to individual concentrations using the total concentration value, measured independently by the UV detector installed in the SMB loop. A more comprehensively discussion of the method implemented can be found elsewhere (Chapter 5 and [73]).

6 Direct separation of the enantiomers of reboxetine by HPLC

Reboxetine, (*RS*)-2-[(*RS*)-α-(2-ethoxyphenoxy)benzyl]-morpholine (chemical structure depicted in Fig. 8) is a noradrenaline re-uptake inhibitor used to treat depressive syndromes [86]. Only the (*R,R*)-, (*S,S*)-pair is present as a racemic mixture in the active principle and in commercial formulations [87], due to the stereoselectivity of the synthesis. Pharmacological tests have shown that the enantiomers have different pharmacological efficacy; the (*S,S*)-enantiomer is more potent as antidepressant [88] and is responsible for the vasomotor and cardiac side effects of reboxetine [89].

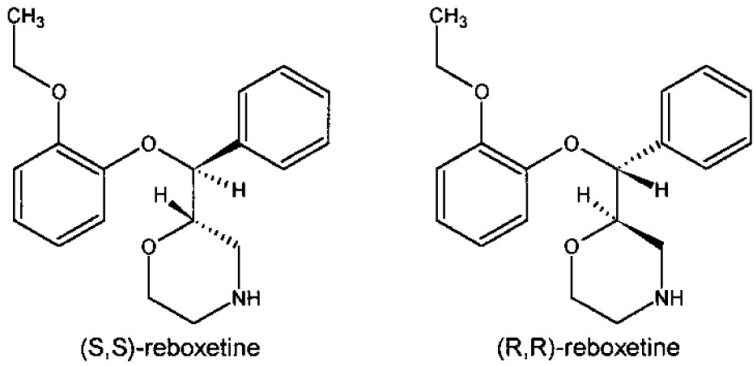

Figure 8: Chemical structure of reboxetine enantiomers.

The elution order of the two enantiomers (Fig. 9) by direct phase-HPLC and the assignment of the absolute configuration of the resolved enantiomers, according to the literature [87, 90], is as follow: the first-eluting enantiomer was identified as (-)-*R,R*-reboxetine and the second-eluting enantiomer as (+)-*S,S*-reboxetine.

Figure 9 shows an analytical profile of the racemic mixture. It is clear that the chromatographic conditions are not favorable for HPLC separation due to the low selectivity and poor resolution of the enantiomers.

Although the difficulty of separation is generally classified by the value of its selectivity, $\alpha = K_2/K_1$, this measure does not properly represent the difficulty for small K_i. A better

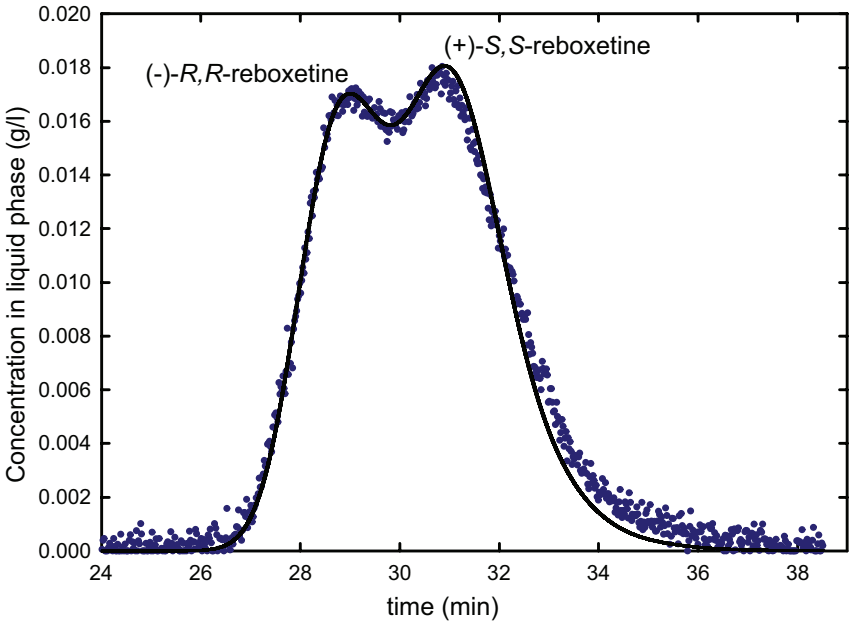

Figure 9: Analytical injection of reboxetine racemate on Chiralpak AD (20 μm), 100 mm×10 mm I.D. Mobile phase is 90:10 hexane/ethanol with 0.2% DEA (basic modifier) at 25°C and flow rate of 0.8 ml/min. The injected volume is 75 μl with a racemate concentration of 1.1 g/l; UV detection at 276 nm.

measure is α' [35], which is defined as

$$\alpha' = \frac{1 + \beta K_2}{1 + \beta K_1}. \tag{12}$$

This parameter represents the ratio of the factors by which the solute velocities are reduced with respect to the fluid velocity. The separation is somewhat arbitrarily classified as hard for $\alpha' \approx 1.1$, moderate for $\alpha' \approx 1.5$, and easy for $\alpha' \geq 4$ [82]. For the separation under consideration, $\alpha' = 1.088$, which certainly can be considered as a very difficult separation. It is thus difficult to obtain both products with high purity and yield by HPLC for the chosen chromatographic conditions. Traditional solutions to this problem would be to increase the column length or to implement a recycling strategy (e.g., steady-state recycling). These modifications lead to a reduction of the specific productivity.

A productive approach to obtain high purities for each of the components in this case, is the use of the streamlined two-column SMB process. Using the hard separation of the enantiomers of reboxetine, we shall demonstrate that, just by adding one column and applying the SMB concept, a very difficult separation on a batch process becomes quite easy and leads to very interesting results. Here we allow for open-loop operation only, since these schemes look more promising, as they generate compact schemes using only two HPLC pumps and are easily ported to supercritical fluid chromatography.

7 Two-column chiral SMB: Results and discussion

Following the work presented at the 2007 AIChE Annual Meeting [91], an upgrade from linear conditions to overloaded conditions, with an increment in the purity of the target product — the more-retained enantiomer (+)-*S,S*-reboxetine — from $P_X = 96.0\%$ to $P_X = 98.8\%$ has been accomplished in the present work.

The optimal cycle for the two-column process was determined by solving the design problem with the chromatographic parameters listed in Table 3, subject to minimal extract and raffinate requirements, $P_X^{min} = 98.8\%$ and $P_R^{min} = 90.0\%$. Five sub-divisions per step were allocated for the piecewise constant modulation of the flow rates ($n_{\mathrm{Q}} = 5$), and $Q_{\max}$ was fixed at 9.5 ml/min, which is only 5% lower than the maximum capacity of the installed HPLC pumps. The optimized operating parameters are listed in Table 4, in which the flow rates are reported in terms of the standard four zones of an SMB.

Table 4: Optimal operating cycle for the two-column process for overloaded SMB operation. Flow rates are expressed in ml/mim. The parameters values for the NLP problem ($f\mathrm{obj} = max\ \bar{F}$) are: $n_{\mathrm{Q}} = 5$, $Q_{\max} = 9.5\mathrm{ml/min}$, $P_X^{min} = 0.988$ and $P_R^{min} = 0.900$.

$N_I/\ldots/N_{IV}$						1.6/0/0.4/0
τ (min)						4.226
P_X						0.988
P_R						0.900
Step	Q_1	Q_2	Q_3	Q_4	F	E
1	0.6179	0.6179	1.2602	0.0000	0.6423	0.6179
2	3.0911	3.0911	3.0911	0.0000	0.0000	3.0911
3	1.5530	0.0000	0.0000	0.0000	0.0000	1.5530
4	1.6177	0.0000	0.0000	0.0000	0.0000	1.6177
5	1.6787	0.0000	0.0000	0.0000	0.0000	1.6787
Average					0.1285	1.7117

As shown in Table 4, the cycle can be broadly classified as an open-loop 1.6/0/0.4/0 column configuration with partial feed and selective product withdrawal. This is clearly depicted in Fig. 10, which illustrates the port switching schedule for the proposed two-column chiral SMB over the first step of the cycle (τ time-units). The second step of the cycle is identical but with the two columns exchanged. During the first and second sub-

intervals of the first step of the cycle — $\frac{1}{5}\,\tau$ and $\frac{2}{5}\,\tau$ time-units, respectively — column 2 plays the role of zone I of a classical SMB, whereas column 1 plays the role of zone III. During the remaining three sub-intervals — $\frac{3}{5}\,\tau$, $\frac{4}{5}\,\tau$, and $\frac{5}{5}\,\tau$ time-units — both columns plays the role of zone I of a classical SMB. The material balance between columns provides the flow rates for zone II and zone IV. During the second step of the cycle the two columns exchanged zones. It should be emphasized that the 1.6/0/0.4/0 port configuration is specific for the particular separation under study. The optimal port configuration is tightly coupled to the flow-rate modulation, and changes whenever the process specifications or the difficulty of separation change. This is different from the often employed basic SMB design strategy, in which the column configuration is fixed in advance and the chosen parameters to achieve given process specifications are the switching interval and the four internal flow rates.

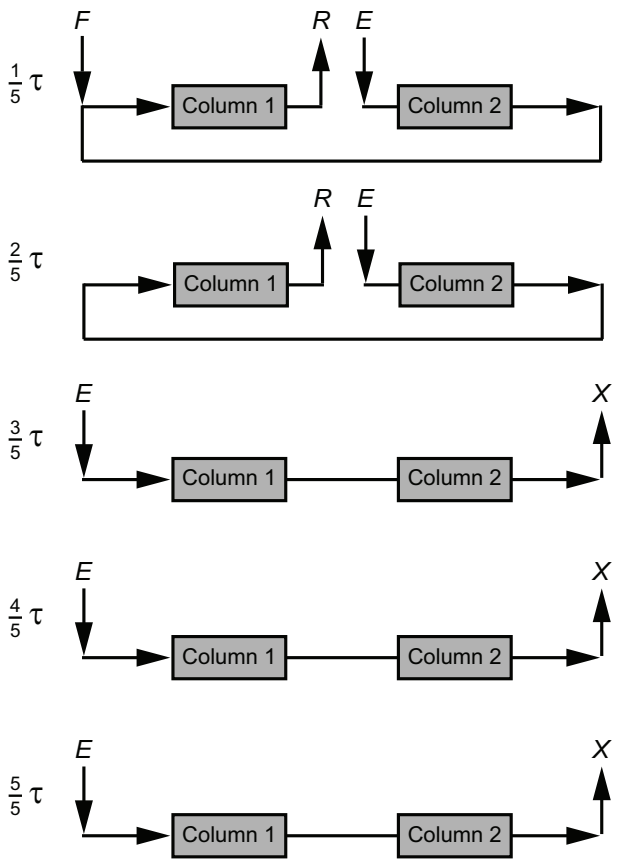

Figure 10: Port switching schedule for the proposed two-column chiral SMB over the first step of the cycle, τ time-units, for the optimized scheme listed in Table 4. The second step of the cycle is identical, but the two columns are exchanged. Symbols *F, R, E, X*, denote feed, raffinate, eluent, and extract, respectively.

Figure 11 shows the solute concentration profiles (steady periodic solution of the process model) of the two enantiomers at the outlet of column 1 and column 2 over the

first step of the cycle for the optimized scheme listed in Table 4, as well as the product withdrawal periods. The steady periodic solution of the process model for the solute concentration profiles at the outlet of column 1 over the two steps of the cycle is depicted in Fig. 12, which shows not only the solute concentration profiles of the two enantiomers, but also the total enantiomeric concentration, as well as the raffinate and extract withdrawal periods.

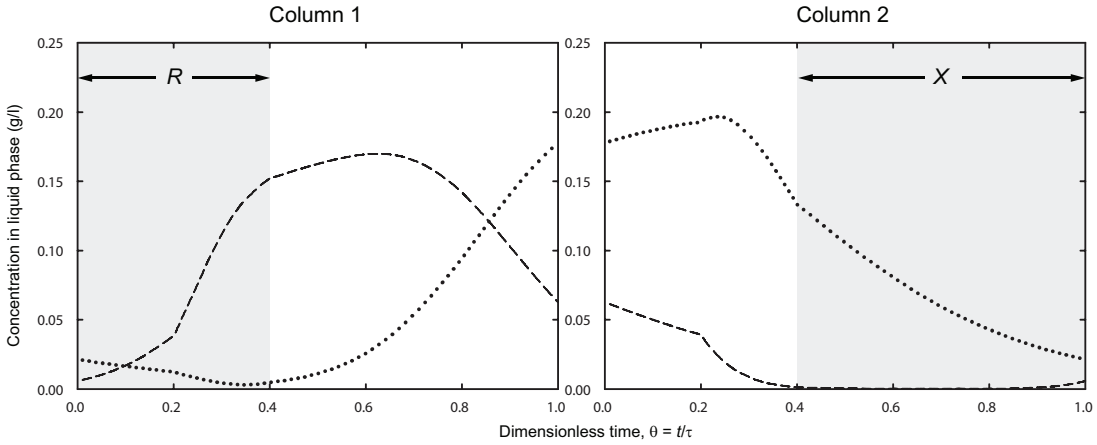

Figure 11: Solute concentration profiles at the outlet of column 1 and column 2 over the first step of the cycle for the optimized scheme listed in Table 4. Lines represent the steady periodic solution of the process model (less-retained enantiomer: – – –; more-retained enantiomer: ···). Symbols *R, X*, denote raffinate and extract withdrawal periods, respectively.

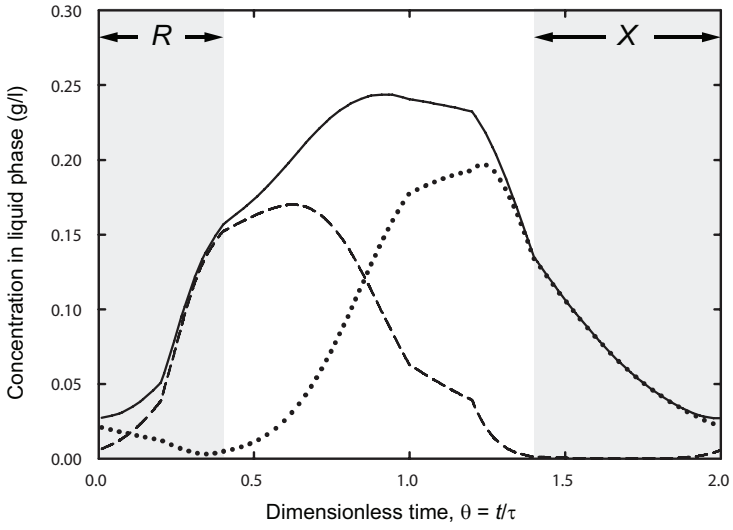

Figure 12: Solute concentration profiles at the outlet of column 1 over the two steps of the cycle for the optimized scheme listed in Table 4. Lines represent the steady periodic solution of the process model (total enantiomeric concentration: ——; less-retained enantiomer: – – –; more-retained enantiomer: ···). Symbols *R, X*, denote raffinate and extract withdrawal periods, respectively.

The optimal two-column SMB scheme reported in Table 4 was reproduced experimen-

tally over 14 operating cycles. The cyclic steady state was attained in ten to eleven cycles. The on-line monitoring system implemented to calculate the enantiomeric composition, depicted in Fig. 7, relies on the chromatograms from the analytical HPLC column to compute the enantiomeric purity, which is then converted to individual concentrations using the total concentration value, measured independently by the UV detector installed in the SMB loop. The method implement is briefly discuss in sub-section 5.2, and discuss more comprehensively elsewhere (Chapter 5 and [73]).

Figure 13 compares the experimental total enantiomeric concentration profile at the outlet of column 1, measured during the 11th, 13th, and 14th cycle of operation, with that predicted by process simulation. The symbols are the experimental profile measured by the UV labeled 'total signal' in Fig. 7 (the one placed in the SMB loop) at each sampling time of the HPLC system. There is excellent agreement between experimental and simulation profiles, they are quantitatively and qualitatively similar.

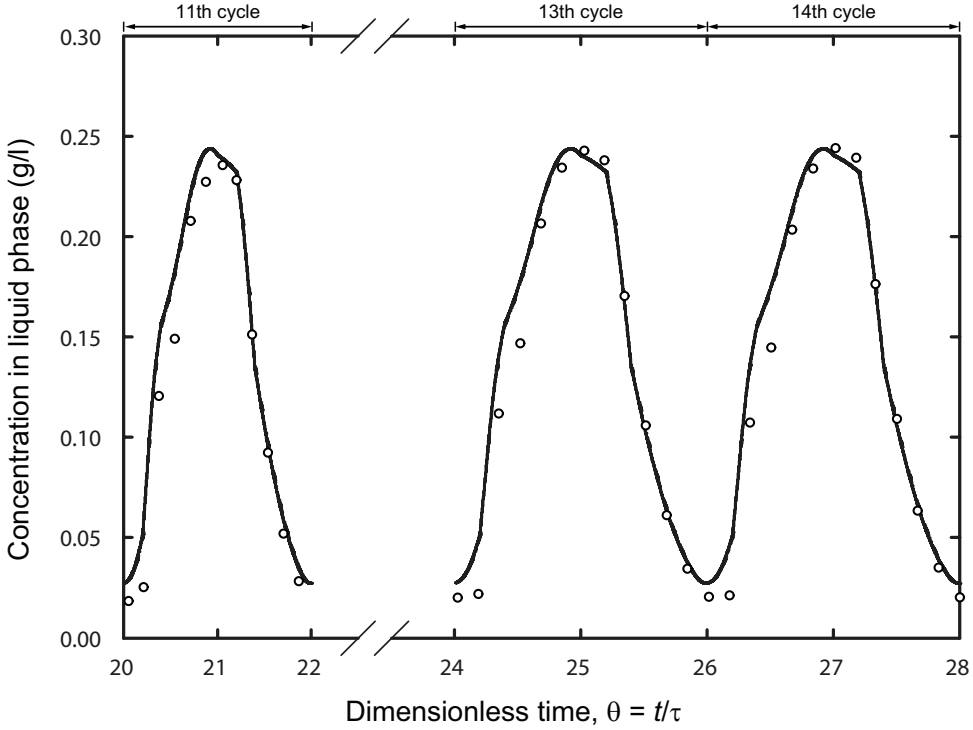

Figure 13: Temporal profile of total enantiomeric concentration at the outlet of column 1, measured over the 11th, 13th, and 14th cycle of operation, for the optimized scheme listed in Table 4. ∘, profile measured by the UV labeled 'total signal' in Fig. 7 at each sampling time of the HPLC system; ——, steady periodic solution of the process model.

Finally, Fig. 14 compares the individual enantiomeric concentration profiles at the at the outlet of column 1, measured during the 11th, 13th, and 14th cycle of operation, with those predicted by process simulation. The symbols are the experimental profiles determined by HPLC analysis of the collected fractions in combination with the total UV measurement. There is a clear match between the discrete concentration measurements and the simulated profiles, they are quantitatively and qualitatively similar.

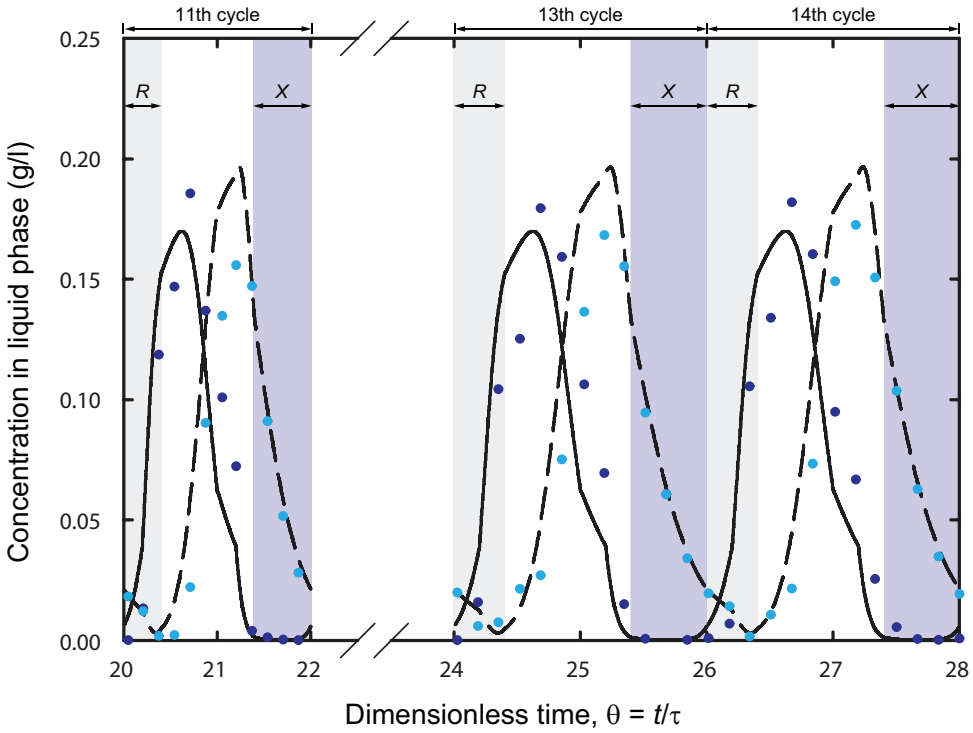

Figure 14: Experimental (symbols) temporal profiles of individual enantiomer concentration at the outlet of column 1, measured over the 10th, 13th, and 14th cycle of operation, for the optimized scheme listed in Table 4, and their comparison with the steady periodic solution (lines) of the process model. (less-retained enantiomer: ●, ——; more-retained enantiomer: ●, - - -). R and X denote the raffinate and extract withdrawal periods, respectively.

The productivity achieved by the optimized scheme listed in Table 4 is 13.0 g/(L × day), while keeping the extract purity (where the desired product is collected) within the desired specifications ($P_X^{min} = 98.8\%$), and the raffinate purity also within the desired specifications ($P_R^{min} = 90.0\%$), to guarantee a good recovery of the desired product. The productivity is expressed as

$$Productivity\ [\ \mathrm{g/(L \times day)}\ ] = \frac{c^{\mathrm{F}}\ \overline{F}}{V_{\mathrm{solid}}}, \tag{13}$$

where $\overline{F}$ is the average feed flow rate per cycle, c^{F} is the total feed concentration (racemic mixture) and V_{solid} is total volume of the stationary phase (2×column volume).

As mentioned above, the experimental setup is fully automated and driven by an in-house developed automation system [72] using LabView software (National Instruments). Figures 15, 16 and 17 show snapshots of the monitoring window of the process automation system, spanning three different zones of the enantiomeric composition profile. Figuer 15 depicts the high concentration region of both enantiomers for the 13th cycle of operation. In Fig. 16 the raffinate withdrawal region for the 15th cycle of operation is displayed, where the lees-retained enantiomer is recovered subject to minimal raffinate requirements, $P_R^{min} = 90.0\%$. Figure 17 exhibits the extract withdrawal region, where the more-retained enantiomer is recovered subject to minimal extract requirements, $P_X^{min} = 98.8\%$. In all three figures, the top-left window monitors the flow rates of the feed and eluent inlets. The top-right window monitors the total absorbance, which is proportional to the total enantiomeric concentration, acquired by the UV detector labeled 'Total signal' (Fig. 7) and installed in the SMB loop. The down-left window monitors the individual chromatograms of the two enantiomers, acquired by the second UV detector, placed at the outlet of the analytical HPLC column (Fig. 7). The down-right window monitors the position of the 6-port 2-position valve; Most of the time, the 6-port valve is in 'inject position' (value 0), so the effluent from the column flows through the UV measuring cell and through the 6-port valve, following the gray flow path depicted in Fig. 7, and is directed to the next column. At fixed time intervals the 6-port valve is switched to the 'load position' (value 1) to divert the effluent from the column into the injection loop for collecting an internal sample.

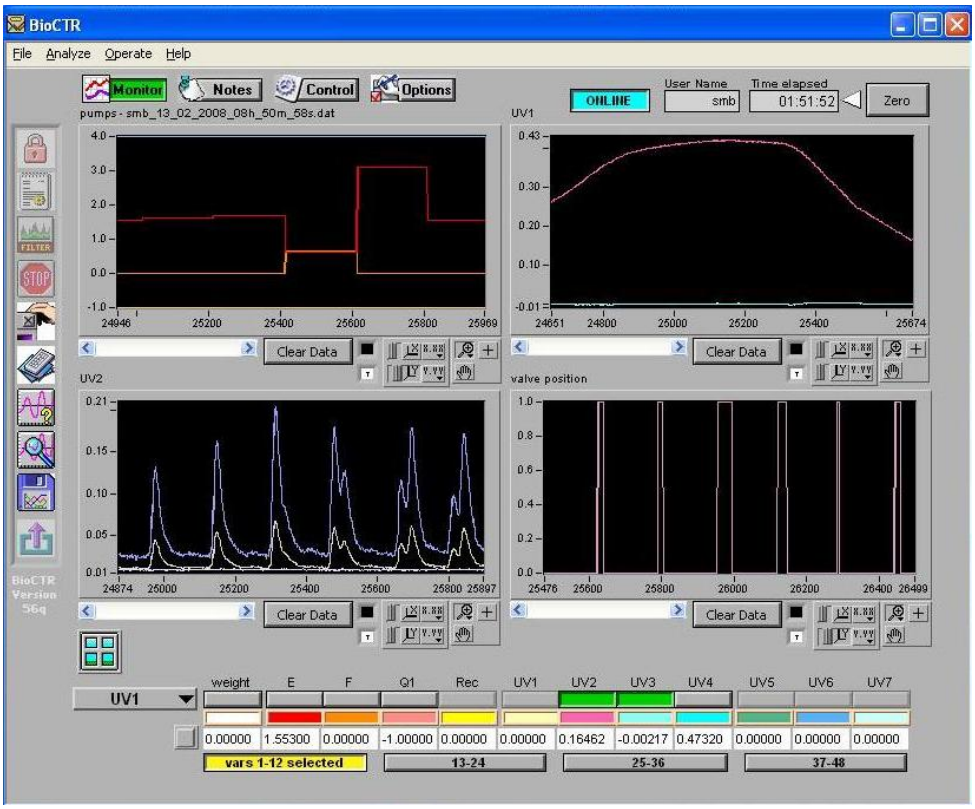

Figure 15: Snapshot of the monitoring window of process automation system for the 13th cycle of operation, spanning the region of high concentration of both enantiomers.

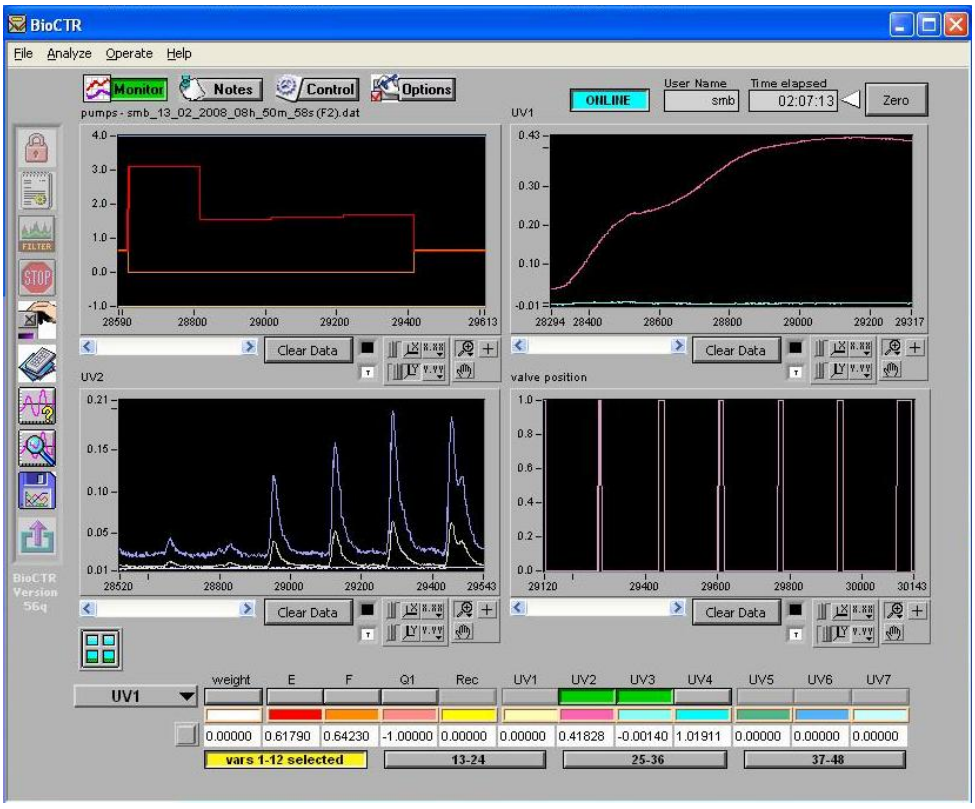

Figure 16: Snapshot of the monitoring window of process automation system for the 15th cycle of operation, spanning the raffinate withdrawal region, where the lees-retained enantiomer is recovered subject to minimal raffinate requirements, $P_R^{min} = 90.0\%$.

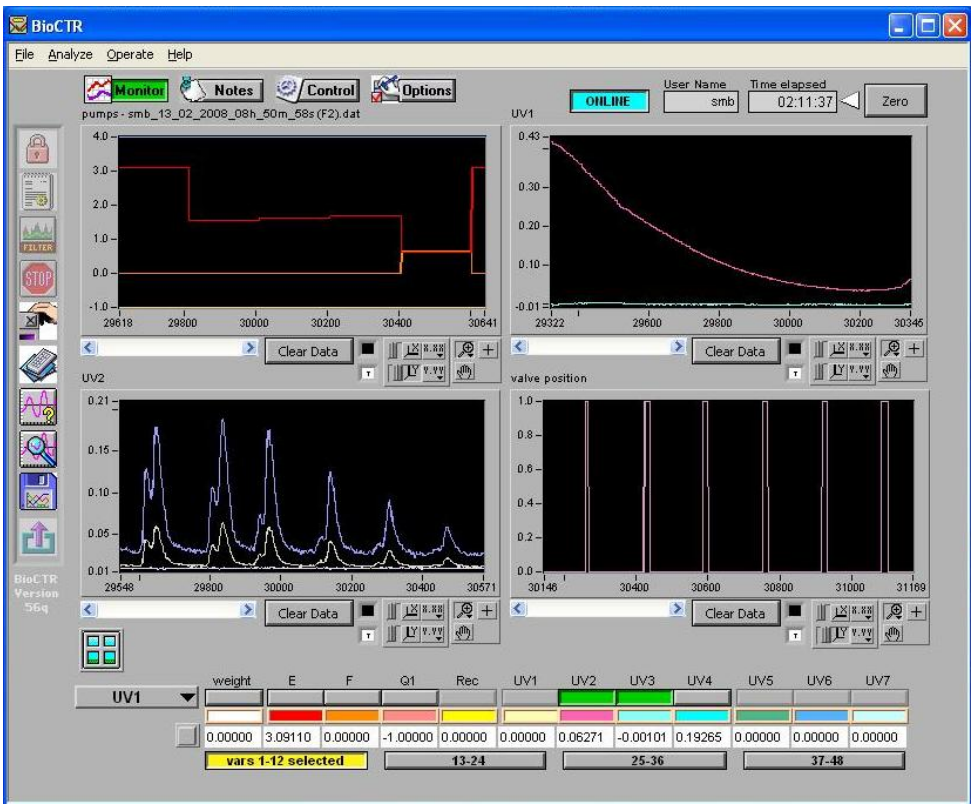

Figure 17: Snapshot of the monitoring window of process automation system for the 15th cycle of operation, spanning the extract withdrawal region, where the more-retained enantiomer is recovered subject to minimal extract requirements, $P_X^{min} = 98.8\%$.

A final experimental validation of the enantioseparation of reboxetine using the two-column SMB scheme developed, was accomplished by post-processing the purity of the extract and raffinate withdrawals for the entire 11th and 14th cycle of operation. The results depicted in Fig. 18, shows that the experimental purities are within the desired specifications ($P_X^{min} = 98.8\%$ and $P_R^{min} = 90.0\%$). The enantiomeric purity is calculated by fitting the sum of two exponentially modified Gaussian (EMG) functions to the experimental chromatograms, similarly to the method implemented to calculate the enantiomeric composition of the two-column scheme discussed above.

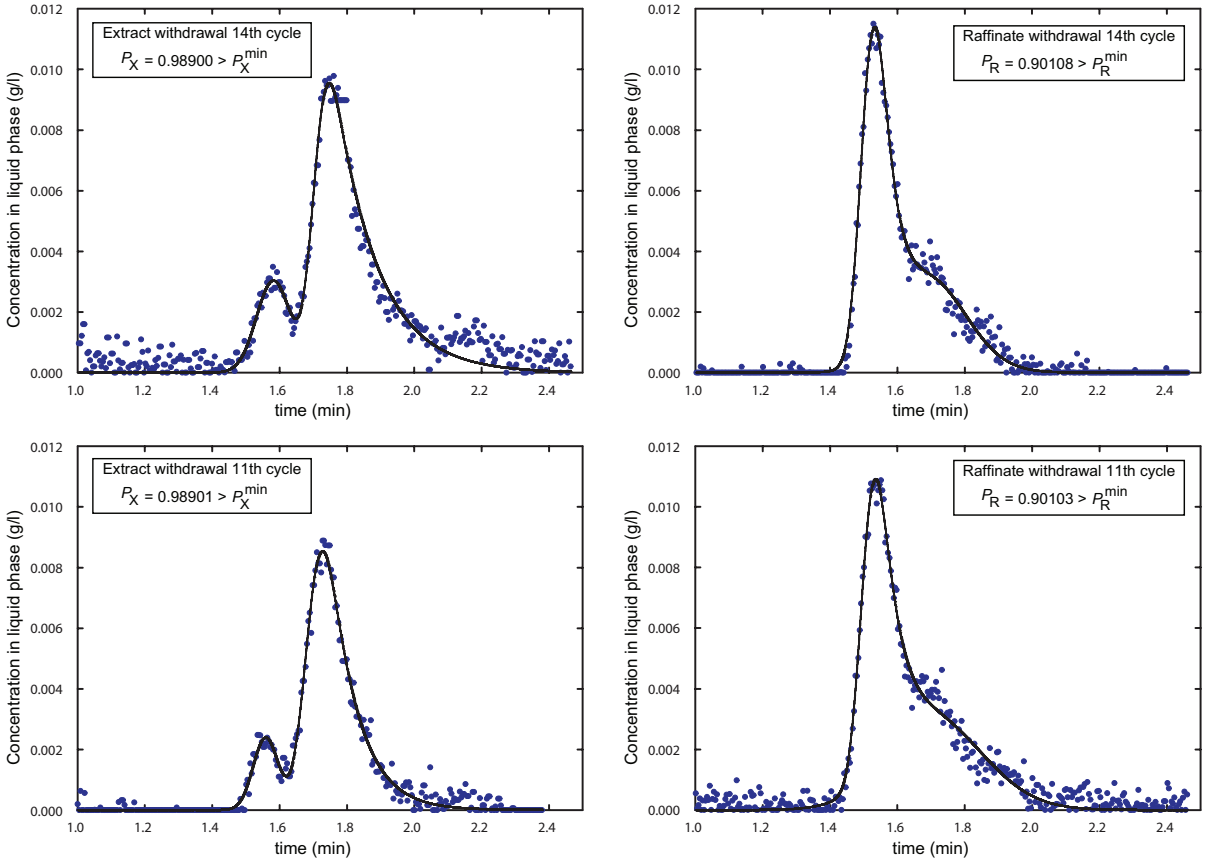

Figure 18: HPLC analysis of the extract and raffinate withdrawals for the 11th and 14th cycle of operation. The product purity values clearly fulfil the intended process specification, $P_X^{min} = 98.8\%$ and $P_R^{min} = 90.0\%$. The symbols are the analytical injection on Chiralpak IA (5 μm), 150 mm×4.6 mm I.D. Mobile phase is 90:10 hexane/ethanol with 0.2% DEA (basic modifier) and flow rate of 3.3 ml/min. The injected volume is 100 μl; UV detection at 276 nm. The lines represent the fitting of the sum of two exponentially modified Gaussian (EMG) functions, similarly to the method implemented to calculate the enantiomeric composition and discussed elsewhere (Chapter 5 and paper [73]).

8 Conclusions

In the present work, a two-column SMB process for enantiomeric separation with no internal recirculating pumps, which is particularly effective when the resolution is limited, was developed. This compact system relies on a flexible node design, and optimized flow-rate modulation. The system was implemented and experimentally validated on the direct separation of the enantiomers of reboxetine under overloaded conditions.

The two-column enantioselective SMB process proved to be a very interesting process for low resolution chromatographic separations. The two-column process is a compromise between continuous multi-column processes and traditional HPLC units, it combines the simplicity and flexibility of batch units and the higher product purity, less solvent consumption, and higher productivity per unit stationary phase of SMB chromatography. Applied to the unfavorable chiral separation of reboxetine enantiomers, it allowed to reach good purities and yields just by adding one more column. Thus a significant improvement in terms of productivity and laboratory costs is achieved.

In the context of chiral considerations and chiral switches, compact two-column, open-loop chromatography is very attractive due to its low running costs and the technical feasibility of scaling-up the technology. It is evident from the chiral switch of reboxetine accomplished using the two-column SMB process, that the developed compact process is an interesting alternative and cost-effective approach to chiral molecules.

Nomenclature

c	solute concentration (g/l)
D_{L}	axial dispersion coefficient ($\mathrm{cm}^2/\mathrm{min}$)
k	LDF coefficient (s^{-1})
K	Henry constant
L	column length (cm)
n_{Q}	number of intervals for piecewise-constant modulation
N	number of columns
Pe	Péclet number
q	adsorbed concentration (g/l)
Q	flow rate ($\mathrm{cm}^3/\mathrm{min}$)
t	time (min)
v	linear velocity (cm/min)
x	dimensionless axial position, z/L

Greek letters

α	selectivity, K_2/K_1
α'	modified selectivity, $(1+\beta K_2)/(1+\beta K_1)$
β	phase ratio, $(1-\epsilon)/\epsilon$
ϵ	total porosity
τ	switching interval (min)
θ	dimensionless time, t/τ

Subscripts and superscripts

E	eluent
F	feed
i	solute index
I,. . . ,IV	zone index
in	inlet effluent
j	column index
out	outlet effluent
R	raffinate
X	extract
1	(-)-*R,R*-reboxetine enantiomer
2	(+)-*S,S*-reboxetine enantiomer

List of Tables

List of Figures

Bibliography

[1] J. Strube, S. Haumreisser, H. Schmidt-Traub, M. Schulte, R. Ditz, Proc. Res. Dev. 2 (1998) 305.

[2] L. Miller, C. Grill, T. Yan, O. Dapremont, M. Juza, J. Chromatogr. A 1006 (2003) 267.

[3] C.M. Grill, L. Miller, T.Q. Yan, J. Chromatogr. A 1026 (2004) 101.

[4] D.B. Broughton, C.G. Gerhold, US Patent 2, 985, 589 (1961).

[5] R.M. Nicoud, LC-GC 5 (1992) 43.

[6] M. Juza, M. Mazzotti, M. Morbidelli, Trends Biotechnol 18 (2000) 108.

[7] D.M. Ruthven, C.B. Ching, Chem. Eng. Sci. 44 (1989) 1011.

[8] G. Storti, M. Mazzotti, M. Morbidelli, A. Carrà AIChE J. 39 (1993) 471.

[9] M. Mazzotti, G. Storti, M. Morbidelli, J. Chromatogr. A 769 (1997) 3.

[10] F. Charton, R.M. Nicoud, J. Chromatogr. A 702 (1995) 97.

[11] M. Juza, M. Mazzotti, M. Morbidelli, Trends in Biotech.18 (2000) 108.

[12] P. Adam, R.M. Nicoud, M. Bailly, O. Ludemann-Hombourger, US Patent 6, 136, 198 (2000).

[13] O. Ludemann-Hombourger, R.M. Nicoud, M. Bailly, Sep. Sci. Technol. 35 (2000) 1829.

[14] A. Toumi, F. Hanisch, S. Engell, Ind. Chem. Res. 41 (2002) 4328.

[15] H. Schramm, M. Kaspereit, A. Kienle, A. Seidel-Morgenstern, Chem. Eng. Technol. 25 (2002) 1151.

[16] H. Schramm, A. Kienle, M. Kaspereit, A. Seidel-Morgenstern, Chem. Eng. Sci. 58 (2003) 5217.

[17] M.M. Kearney, K.L. Hieb, US Patent 5, 102, 553 (1992).

[18] E. Kloppenburg, E.D. Gilles, Chem. Eng. Technol. 22 (1999) 813.

[19] Z.Y. Zhang, M. Mazzotti, M. Morbidelli, J. Chromatogr. A 1006 (2003) 87.

[20] Z. Zhang, M. Mazzotti, M. Morbidelli, AIChE J. 50 (2004) 3.

[21] Y.F. Zang, P.C. Wankat, Ind. Eng. Chem. Res. 41 (2002) 2504.

[22] T.B. Jensen, T.G.P. Reijns, H.A.H. Billiet, L.A.M. van der Wielen, J. Chromatogr. A 863 (2000) 149.

[23] D. Antos, A. Seidel-Morgenstern, J. Chromatogr. A 944 (2002) 77.

[24] S. Abel, M. Mazzotti, M. Morbidelli, J. Chromatogr. A 994 (2002) 23.

[25] J.P. Meissner, G. Carta, Ind. Eng. Chem. Res. 41 (2002) 4722.

[26] Y. Zang, P.C. Wankat, Ind. Eng. Chem. Res. 41 (2002) 5283.

[27] Y. Kawajiri, L.T. Biegler, Ind. Eng. Chem. Res. 45 (2006) 8503.

[28] R.C.R. Rodrigues, J.M.M. Araújo, J.P.B. Mota, J. Chromatogr. A 1162 (2007) 14.

[29] J.P.B. Mota, I.A.A.C. Esteves, M.F.J. Eusébio, AIChE J. 53 (2007) 1192.

[30] C.Y. Chin, N.H.L. Wang, Sep. Purif. Rev. 33 (2004) 77.

[31] K. Lee, Sep. Sci. Technol. 35 (2000) 519.

[32] M. Ando, M. Tanimura, M.Tamura, US PAtent 4, 970, 002 (1990).

[33] W. Jin, P.C. Wankat, Ind.Eng. Chem. Res. 44 (2005) 1565.

[34] W. Jin, P.C. Wankat, Ind.Eng. Chem. Res. 45 (2006) 2793.

[35] J.S. Hur, P.C. Wankat, Ind.Eng. Chem. Res. 44 (2005) 1906.

[36] J.S. Hur, P.C. Wankat, Ind.Eng. Chem. Res. 45 (2006) 1426.

[37] G. Stöhlein, L. Aumann, T. Müller-Späth, A. Tarafder, M. Morbidelli, Biopharm. Int. (Suppl.S) (2007) 42.

[38] J.P.B. Mota, J.M.M. Araújo, AIChE J. 51 (2005) 1641.

[39] N. Abunasser, P.C. Wankat, Ind.Eng. Chem. Res. 43 (2004) 5291.

[40] J.M.M. Araújo, R.C.R. Rodrigues, J.P.B. Mota, Ads. Sci. Tech. 25 (2007) 647.

[41] J.M.M. Araújo, R.C.R. Rodrigues, M.F.J. Eusébio, J.P.B. Mota, J. Chromatogr. A (submitted for publication).

[42] J.S. Carey, D. Laffan, C. Thomson, M.T. Williams, Org. Biomol. Chem. 4 (2006) 2337.

[43] J.D. Armstrong, III, M.J. Martinelli, C.H. Senanayake, Tetrahedron: Asymmetry 14 (2003) 3425.

[44] FDA, Chirality 4 (1992) 338.

[45] S.C. Stinson, Chem. Eng. News 9 (1995) 44.

[46] S.C. Stinson, Chem. Eng. News 76 (2000) 83.

[47] A.M. Rouhi, Chem. Eng. News 81 (2003) 45.

[48] RB-188 US Prescription Drug Market: Strategies for Sustained Growth. Norwalk, CT: Business Communications Company Inc. 2004 (Available at `www.bccresearch.com`).

[49] W. Lenz, Lancet. 1 (1962) 45.

[50] S. Tseng, G. Pak, K. Washenik, et al., J. Am. Acad. Dermatol. 35 (1996) 969.

[51] D.I. Stirling, Semin. Hematol. 37 1 suppl 3 (2000) 5.

[52] W.H. De Camp, Chirality 1 (1989) 2.

[53] M.N. Cayen, Chirality 3 (1991) 94.

[54] R.L. Nation, Clin. Pharmacokin. 27 (1994) 249.

[55] A.G. Rauws, K. Groen, Chirality 6 (1994) 72.

[56] A. Slovakova, A.J. Hutt Ces. a Slov. Farm. 48 (1999) 107.

[57] G. Tucker, Lancet. 355 (2000) 1085.

[58] I. Agranat, H. Caner, Nat. Rev. Drug Discov. 1 (2002) 753.

[59] I. Agranat, H. Caner, Drug Disc. Today 4 (1999) 313.

[60] Racemic Switch Update. World Market and Technology Assessment: Optically Active Chemical Compound Report. 11th ed. Technology Catalyst Interantional Corp. Falls Church, VA, 2001.

[61] D.A. Handley, Pharm. News 6 (1999) 11.

[62] M.J. Cannarsa, Chem. Oggi / Chem. Today 17 (1999) 28.

[63] B. Leger, Drug Plus International 1 (2002) 4.

[64] Anonymous, Nature 418 (2002) 353.

[65] A.M. Rouhi, Chem. Eng. News 80 (2002) 43.

[66] E.R. Francotte, J. Chromatogr. A 666 (1994) 565.

[67] E.R. Francotte, Preparation of drug enantiomers by chromatographic resolution on chiral stationary phases, in: H.Y. Aboul-Enein, I.W. Wainer (Eds.), The Impact of Stereochemistry On Drug Development and Use, Chemical Analysis Series, Vol. 142, John Wiley, New York, 1997, Chapter 23.

[68] E.R. Francotte, Chromatography as a separation tool for the preparative resolution of racemic compounds, in: S. Ahuja (Ed.), Chiral Separations: Applications and Technology, ACS, New York, 1996.

[69] E.R. Francotte, A. Junker-Buchheit, J. Chromatogr. A 576 (1992) 1.

[70] E.R. Francotte, J. Chromatogr. A 906 (2001) 379.

[71] R.C.R. Rodrigues, T.J.S.B Canhoto, J.M.M. Araújo, J.P.B. Mota, J. Chromatogr. A 1180 (2008) 42.

[72] M.F.J. Eusébio, Development of an Universal Interface for Monitoring and Control of Chemical and Biochemical Processes, Ph.D. Thesis. Universidade Nova de Lisboa, Lisboa, Portugal, 2006 (in Portuguese).

[73] J.M.M. Araújo, R.C.R. Rodrigues, M.F.J. Eusébio, J.P.B. Mota, J. Chromatogr. A 1189 (2008) 292.

[74] J.M.M. Araújo, R.C.R. Rodrigues, J.P.B. Mota, Ind. Eng. Chem. Res. 45 (2006) 5314.

[75] J.M.M. Araújo, R.C.R. Rodrigues, J.P.B. Mota, J. Chromatogr. A 1132 (2006) 76.

[76] J.P.B. Mota, E. Saatdjian, D. Tondeur, A.E. Rodrigues, Comp. Chem. Eng. 21 (1997) 387.

[77] Y. Kawajiri, L.T. Biegler, AIChE J. 52 (2006) 1343.

[78] R. Fourer, D.M. Gay, B.W. Kernighan, AMP: A Modeling Language for Mathematical Programming, 2nd edition, Brooks/Cole-Thomson Learning, Pacific Grove, CA, 2003

[79] A. Wachter, L.T. Biegler, Math. Prog. 106 (2005) 25.

[80] R.C.R. Rodrigues, J.M.M. Araújo, M.F.J. Eusébio, J.P.B. Mota, J. Chromatogr. A 1142 (2006) 69.

[81] Instructions manual for Chiralpak AD columns, Chiral Technologies Europe, March 2003.

[82] P.C. Wankat, Ind. Eng. Chem. Res. 40 (2001) 6185.

[83] D.M. Ruthven, Principles of Adsorption and Adsorption Processes, John Wiley & Sons, New York, 1984.

[84] G. Guiochon, S. Golshan-Shirazi, A. Katti, Fundamentals of Preparative and Nonlinear Chromatography, Academic Press, Boston, MA, 1994.

[85] J.M.M. Araújo, R.C.R. Rodrigues, J.P.B. Mota, J. Chromatogr. A 1189 (2008) 302.

[86] P. Dostert, M.S. Benedetti, I. Poggesi, Eur. Neuropsychopharm. 7 (1997) 23.

[87] P. Melloni, A. Delia Torre, E. Lazzari, G. Mazzini, M. Meroni, Tetrahedron 41 (1985) 1393.

[88] M.S. Benedetti, E. Frigerio, P. Tocchetti, G. Brianceschi, M.G. Castelli, C. Pellizzoni, P. Dostert, Chirality 7 (1995) 285.

[89] T. Denolle, C. Pellizzoni, M.G. Jannusso, I. Poggesi, Clin. Pharmacol. Ther. 66 (1999) 282.

[90] M.A. Raggi, R. Mandrioli, C. Sabbioni, C. Parenti, G. Cannazza, S. Fanali Electrophoresis 23 (2002) 1870.

[91] J.M.M. Araújo, R.C.R. Rodrigues, J.P.B. Mota, Presentation 85b at the AIChE 2007 Annual Meeting, Salt Lake City, USA, November 2007.

Conclusions

Preparative chromatography is now a key technology as a separation and purification process in the agrochemical, biotechnological, food and pharmaceutical industries. Classical single-column preparative chromatography is currently complemented by alternative operating modes that provide significant improvements in terms of productivity and solvent consumption, particularly when the process is scaled up. The most noteworthy technology available is the Simulated Moving Bed (SMB), that is a continuous multi-column chromatographic technology that allows splitting mixtures in two fractions (e.g two pure species). Both traditional HPLC units and multi-column processes have gone through tremendous improvements over the last few years, particularly in the field of fine chemical and chiral separations. In the field of chiral separations the challenges to be faced are related to the use of units with smaller number of columns, because less stationary phase is used and the setup is more economical; this is especially important for the pharmaceutical industry, where SMBs are seen as multipurpose units that can be applied to different separations in all stages of the drug-development cycle.

The majority of SMB applications are binary separations in the liquid phase using a standard four section SMB, with at least four-columns, in isocratic mode. In this work, two new SMB paradigms have been realized to broaden the SMB concept and to bridge SMB and batch chromatography in an attempt to work with the best of 'two worlds.' In this context, two new SMB paradigms have been realized: a single-column SMB process with recycle-lag (single-column SMB analog) and a streamlined two-column SMB for chiral separation (two-column open-loop SMB process).

For the first SMB paradigm mentioned above – the single-column SMB analog – we have reported conceptual and numerical results for a single-column chromatograph analogous to an SMB with classical synchronous port switching, and asynchronous port switching. It is shown that to reproduce the periodic state of a multi-column unit by a one-column chromatograph, the requirement of recycling the outlet stream that is not recovered as product back to the column with a lag of $(N-1)\tau$ time units, holds true regardless of the port configuration, or operating scheme, of the analogous multi-column unit. To implement the recycle lag in practice, a special type of plug-flow tube has been designed. It includes internal elements to provide a flow which is as close as possible to plug flow, and a piston to compensate for the difference between the inlet and outlet flow rates. The designed system is a more compact, less expensive and simpler-to-operate alternative

to the SMB that can potentially achieve the same purities while keeping the specific productivity constant. By upgrading the operation of the single-column chromatograph from the classical synchronous port switching to an optimized asynchronous Varicol mode, it is shown that one can easily compensate for a less perfect operation the recycle tube.

The second paradigm is compact two-column, open-loop SMB chromatography. The two-column enantioselective SMB process proved to be a very interesting process for low-resolution chromatographic separations. This compact system relies on a flexible node design, and optimized flow-rate modulation. The two-column process is a compromise between continuous multi-column processes and traditional HPLC units, it combines the simplicity and flexibility of batch units and the higher product purity, less solvent consumption, and higher productivity per unit stationary phase of SMB chromatography. When applied to the unfavorable chiral separation of reboxetine enantiomers, good purities and yields were attained by working with just two columns. Thus a significant improvement in terms of productivity and laboratory costs is achieved.

In the context of chiral considerations and chiral switches, compact two-column, open-loop chromatography is very attractive due to its low running costs and the technical feasibility of scaling-up the technology. It is evident from the chiral switch of reboxetine accomplished using the two-column SMB process, that the developed process is an interesting alternative and cost-effective approach for chiral molecules. It has been demonstrated that, just by adding one column and applying the SMB concept, a very difficult separation on a batch process becomes quite easy and leads to very interesting results. Here we allow for open-loop operation only, since these schemes look more promising, as they generate compact schemes using only two HPLC pumps and are easily ported to supercritical fluid chromatography (SFC). The use of supercritical fluids as chromatographic driving force is the most promising alternative to liquid chromatography. Under SFC conditions it is possible to apply a pressure gradient throughout certain zones of the SMB. In SFC the adsorption is depending not only on the mobile phase composition but also on the applied pressure. The adsorption strength of the mobile phase in the SMB zones can be changed by varying the pressure. In a classical four-section SMB, by applying the highest pressure in zone I (where the most-retained compound is desorbed) and the lowest in zone IV (where the less-retained compound is desorbed) much steeper fronts of the internal concentration profile can be attained. As a consequence the feed inlet can be increased and consequently the productivity is increased.

Moreover, a general procedure for the determination of the adsorption isotherms has been developed and validated in which the inverse method is applied directly to the cyclic steady-state (CSS) concentration profiles of the running SMB process to update the parameters of the prescribed adsorption isotherm model, estimated by applying the inverse method to the overloaded band profiles of the racemic mixture. The obtain results indicate that the hybrid inverse method offers a reliable and quick approach to determine the competitive adsorption isotherms for a specific SMB separation, with minimum solute and solvent consumptions. The proposed procedure is adequate for conveniently designing the SMB operating conditions over the full concentration range.

To provide a tool to implement a properly process control and dynamic optimization of the SMB, an automated on-line enantiomeric analysis system comprising an analytical HPLC set-up with two UV detectors sharing the same light source has been developed and experimentally validated. The system does not use a UV detector and a polarimeter in series. The signal of the latter is very sensitive to temperature and pressure fluctuations in the measuring cell, which have a direct impact on the accuracy and robustness of the measurements. Using a sampling interface placed between two SMB columns, effluent samples are directed onto a high-efficiency analytical column at a sampling rate faster than the overall dynamics of the preparative unit to achieve on-line enantiomeric analysis of the composition profile. The other UV detector is placed in the SMB loop before the fraction collector to provide instantaneous measurement of the total enantiomeric concentration. It is worth mentioning that, in most cases, the mobile phase from the analytical HPLC system can be reused in the SMB system, because it is only contaminated with trace amounts of the two enantiomers. The outlet effluent from the analytical HPLC column can either be sent to the eluent storage vessel or pumped directly to the beginning of zone I of the SMB.

The investigated technical innovations explore in this work disclose the way for many potential SMB applications and provide efficient tools for improved state-of-the-art production, especially in fields with rather scientific progress, e.g. chiral separations in pharmaceutical and fine chemical industries, and biotechnology, where appropriate separation processes are urgently needed.